INVESTIGATION OF ROUGH SURFACE SCATTERING OF ELECTROMAGNETIC WAVES USING FINITE ELEMENT METHOD

A THESIS SUBMITTED TO
THE GRADUATE SCHOOL OF NATURAL AND APPLIED SCIENCES
OF
MIDDLE EAST TECHNICAL UNIVERSITY

BY

ÖZÜM EMRE AŞIRIM

IN PARTIAL FULFILLMENT OF THE REQUIREMENTS
FOR
THE DEGREE OF MASTER OF SCIENCE
IN
ELECTRICAL AND ELECTRONICS ENGINEERING

JULY 2013

Approval of the thesis:

INVESTIGATION OF ROUGH SURFACE SCATTERING OF ELECTROMAGNETIC WAVES USING FINITE ELEMENT METHOD

submitted by **Özüm Emre Aşırım** in partial fulfillment of the requirements for the degree of **Master of Science in Electrical and Electronics Engineering Department, Middle East Technical University** by,

Prof. Dr. Canan Özgen
Dean, Graduate School of **Natural and Applied Sciences** _____

Prof. Dr. Gönül Turhan Sayan
Head of Department, **Electrical and Electronics Engineering** _____

Prof. Dr. Mustafa Kuzuoğlu
Supervisor, **Electrical and Electronics Engineering Dept., METU** _____

Assoc. Prof. Dr. Özlem Özgün
Co-supervisor, **Electrical and Electronics Engineering Dept., TEDU** _____

Examining Committee Members

Prof. Dr. Gönül Turhan Sayan
Electrical and Electronics Engineering Dept., METU _____

Prof. Dr. Mustafa Kuzuoğlu
Electrical and Electronics Engineering Dept., METU _____

Prof. Dr. Gülbin Dural
Electrical and Electronics Engineering Dept., METU _____

Assoc. Prof. Dr. Lale Alatan
Electrical and Electronics Engineering Dept., METU _____

Assoc. Prof. Dr. Özlem Özgün
Electrical and Electronics Engineering Dept., TEDU _____

Date: 23.07.2013

I hereby declare that all information in this document has been obtained and presented in accordance with academic rules and ethical conduct. I also declare that, as required by these rules and conduct, I have fully cited and referenced all material and results that are not original to this work.

Name, Last name :

Signature :

ABSTRACT

INVESTIGATION OF ROUGH SURFACE SCATTERING OF ELECTROMAGNETIC WAVES USING FINITE ELEMENT METHOD

Aşırım, Özüm Emre
M.S. Department of Electrical and Electronics Engineering
Supervisor : Prof. Dr. Mustafa Kuzuoğlu
Co-Supervisor : Assoc. Prof. Dr. Özlem Özgün

July 2013, 152 pages

This thesis analyzes the problem of electromagnetic wave scattering from rough surfaces using finite element method. Concepts like mesh generation and random rough surface generation will be discussed firstly. Then the fundamental concepts of the finite element method which are the functional form of a given partial differential equation, implementation of the element coefficient matrices, and the assemblage of elements will be discussed in detail. The rough surface and the overall mesh geometry will be implemented with the functional form of the wave equation, in the form of a global coefficient matrix using finite element method. Along with an incident wave, boundary conditions on the rough surface will be imposed and the scattering from different rough surfaces will be analyzed by solving the resulting linear system of equations that is yielded by the finite element method. The issues of wave resolution, required mesh size, and the required computation time will also be discussed as part of the analysis.

Keywords: Rough Surface, Finite Element Method, Scattering

ÖZ

BOZUK YÜZEYLERDEN ELEKTROMANYETİK DALGA SAÇILIMININ SONLU ELEMANLAR YÖNTEMİ KULLANILARAK İNCELENMESİ

Aşırım, Özüm Emre
Yüksek Lisans, Elektrik Elektronik Mühendisliği Bölümü
Tez Yöneticisi: Prof. Dr. Mustafa Kuzuoğlu
Ortak Tez Yöneticisi: Doç. Dr. Özlem Özgün

Temmuz 2013, 152 sayfa

Bu tezde bozuk yüzeylerden saçılım problemi sonlu elemanlar yöntemi kullanılarak incelenmektedir. Anlatımda öncelikle bozuk yüzey modellenmesi ve örgü modellenmesi incelenecektir. Daha sonra, sonlu elemanlar yönteminin temel içerikleri olan eleman katsayı matrisleri ve eleman birleştirilmesi gibi konular detaylıca anlatılacaktır. Dalga denkleminin fonksiyonel formu bozuk yüzeyi içeren örgü geometrisi ile birlikte sonlu elemanlar yöntemi kullanılarak katsayı matrisine çevrilecektir. Bunu takiben, bozuk yüzeye gelen dalga ile birlikte bozuk yüzey üzerindeki sınır değer problemi tanımlanacak ve bozuk yüzeyden saçılım problemi sonlu elemanlar tekniği ile elde edilen lineer denklem sisteminin çözümü ile analiz edilecektir. Dalga çözünürlüğü, analiz için gereken örgü boyutu, ve analiz için gereken işlem zamanı gibi problemlerde analizde yer alacaktır.

Anahtar Kelimeler: Bozuk Yüzeyler, Sonlu Elemanlar Yöntemi, Saçılım

To My Parents

ACKNOWLEDGMENTS

I would like to express my deepest gratitude to my supervisor Prof. Dr. Mustafa Kuzuoğlu and co-supervisor Assoc. Prof. Dr. Özlem Özgün for their guidance, advice, criticism, encouragements and tolerance throughout the research. Without their support this thesis would not have been completed.

I would also like to thank my friend Mr. Mustafa Gökhan Şanal for his suggestions and comments.

TABLE OF CONTENTS

This page is intentionally left blank.

CHAPTER 1

INTRODUCTION

Electromagnetic waves propagate in space as stated by Maxwell's equations. Based on the characteristics of the medium of propagation, we may simplify the formulation of Maxwell's equations. The propagation of electromagnetic waves can be described in a much simpler form when the medium of propagation is an unbounded medium that has no scatterers in it. However this is usually not the case and we may have many scatterers in a given medium. Therefore the propagation of electromagnetic waves in a medium that contains scattering objects requires more detailed analysis and discussion.

The analysis and discussion of electromagnetic wave propagation in a bounded media that contains scattering objects involves the determination of the scattered wave given an incident wave. To determine the scattered wave from an incident wave, we focus our interest on the shape and the structure of the scatterer. Using Maxwell's equations based on the shape and the constitutive parameters of the scatterer, we can determine the scattered wave.

In this thesis, we are interested in the determination of the scattered field in a media that is bounded by another media which has a rough boundary. Therefore we are interested in a rough surface scattering problem. In other words, our aim is to determine the scattered field from the rough surface boundary by applying Maxwell's equations given an incident field. The determination of the scattered field allows us to examine its far field pattern and to discuss the effects of surface roughness on the scattering of a given incident wave.

The effect of surface roughness on the scattered field pattern has been studied by many scientists. It is found that as the roughness of the scattering surface increases, the far field peak amplitude of the scattered field decreases. However there are no exact analytical formulations that give the relation between surface roughness and the far field peak scattered field amplitude. Furthermore, the critical roughness levels of a surface that may cause significant or complete distortion in the far field scattered field pattern for a given incidence angle are not very well known and there is still considerable ambiguity about " How rough a given rough surface really is? ". In this thesis, our aim is to determine the amount of distortion of a scattered field pattern for a given surface roughness and an incidence angle.

In literature, there are two approximate formulas that are called "Ament's formula" and "Boithias' formula", both of these formulas gives an idea about the relation between surface roughness and the far field peak scattered field amplitude. However, it is still not clear which of these two formulas is more accurate. The amount of error yielded by these two formulas is not negligible for all incidence angles and it changes with respect to the angle of incidence. Especially for grazing incidence angles, the amount of error increases significantly.

One purpose of this thesis is to determine the amount of distortion in the scattered field pattern for different surface roughness levels and for different angles of incidence by measuring the correlation coefficient of the rough surface scattered field patterns with that of a flat surface scattered field pattern.

The second and the main purpose of this thesis is to numerically determine an accurate relation between the peak amplitude of the scattered field and surface roughness. Afterwards, our goal is to compare the determined relation with Ament's formula and Boithias' formula to decide which of the two formulas is more accurate for a given surface roughness at a specific incidence angle. We produce a table of results that will give the reader a firm idea about the relation between the peak scattered field amplitude decay and surface roughness. By looking at this table, one can have a better understanding of the effect of different surface roughness levels on the far field scattered field pattern.

All of the computations in this thesis are performed by employing *Finite Element Method* (FEM), which is often used for solving partial differential equations. We will utilize Maxwell's equations to get a second order wave equation and we will solve for a scalar second order wave equation for the TM_z case. The solution of a second order partial differential equation in a domain that has an arbitrary boundary can be very accurately obtained by using FEM. In order to solve a 2D rough surface scattering problem using FEM, one has to deal with the problem of mesh generation. Generating meshes for regions with arbitrary boundaries will be discussed in detail. Since the scattering problem is an open boundary problem, the domain of interest must be limited to a manageable size. This requires the use of an absorbing boundary condition. As an absorbing boundary condition, we will use a *Perfectly Matched Layer* (PML) for absorbing the outgoing waves without reflection.

Our rough surface boundary will be lossy, which indicates that the scattering media is conductive, therefore an impedance boundary condition on the rough surface will be imposed by the FEM formulation. Since we are interested in the scattered field only, the transmitted wave in the conductive medium will not be investigated.

The scattered field plots are given for different surface roughness levels and different incidence angles for the purpose of illustration in chapter 6.

Along with the main purpose of this thesis, the necessary background for the application of FEM on a rough surface scattering problem is discussed in very detail. If the reader is already familiar with the FEM concept, chapter 6 and chapter 7 should be of more interest. The essence of this thesis is mostly given in chapter 7, which discusses and illustrates the effect of surface roughness on the far field scattered field pattern. Our computational results are compared with Ament's formula and Boithias' formula and the accuracy of each formula is tested for different surface roughness levels and for different angles of incidence.

In the conclusion chapter, the obtained results in chapter 7 are analyzed and discussed. Based on these results, the potential for future investigations is established.

CHAPTER 2

MAXWELL'S EQUATIONS AND SURFACE BOUNDARY CONDITIONS

Maxwell's equations simply describe field behaviour according to the properties of the medium of interest. They are the summary of electromagnetic theory and are considered as physical laws describing the relation between electric fields, magnetic fields, charge densities and current densities. These equations were seperately found as the result of many experiments and they are summarized by James Clerk Maxwell. Since the electric and magnetic fields are vector quantities, these equations are also vector equations which can be decoupled into their scalar forms for each dimension. Maxwell's equations can be stated in differential or integral form, here we are more interested in their differential form, therefore only the differential forms are stated here.

The differential form of Maxwell's equations are stated below

$$\boldsymbol{\nabla} \times \boldsymbol{E} = -\boldsymbol{M_i} - \frac{\partial \boldsymbol{B}}{\partial \mathrm{t}} = -\boldsymbol{M_i} - \boldsymbol{M_d}$$

$$\boldsymbol{\nabla} \times \boldsymbol{H} = \boldsymbol{J_i} + \boldsymbol{J_c} + \frac{\partial \boldsymbol{D}}{\partial \mathrm{t}} = \boldsymbol{J_i} + \boldsymbol{J_c} + \boldsymbol{J_d}$$

$$\boldsymbol{\nabla}.\boldsymbol{D} = q_{ev}$$

$$\boldsymbol{\nabla}.\boldsymbol{B} = q_{mv}$$

All of the quantities written in bold are vectors and q_{ev} and q_{mv} are scalar quantities. The description of all quantities are given below

E = Electric field intensity (volts/meter)

H = Magnetic field intensity (amperes/meter)

D= Electric flux density (coulombs/square meter)

B= Magnetic flux density (webers/square meter)

$\mathbf{J_i}$ = Impressed electric current density (amperes/square meter)

$\mathbf{J_c}$ = Conduction electric current density (amperes/square meter)

$\mathbf{J_d}$ = Displacement electric current density (amperes/square meter)

M_i = Impressed magnetic current density (volts/square meter)

M_d = Displacement magnetic current density (volts/square meter)

q_{ev} **= Electric charge density (coulombs/cubic meter)**

q_{mv} **= Magnetic charge density (webers/cubic meter)**

The equation of continuity can be derived directly from the Maxwell's equations, as follows:

$$\nabla.(\boldsymbol{J_i} + \boldsymbol{J_c}) = -\frac{\partial q_{ev}}{\partial t} \quad , \quad \nabla.\boldsymbol{J_{ic}} = -\frac{\partial q_{ev}}{\partial t} \quad (equation\ of\ continuity)$$

The quantities $\boldsymbol{E}, \boldsymbol{H}, \boldsymbol{D}, \boldsymbol{B},$ and $\boldsymbol{J_c}$ are related through the constitutive parameters of the media of interest. These constitutive parameters are different for each media, and they are related with the physical properties of the material that forms the media of interest. The constitutive relations are listed below for isotropic media

$$\boldsymbol{D} = \epsilon \boldsymbol{E} \quad , \quad \boldsymbol{B} = \mu \boldsymbol{H} \quad , \quad \boldsymbol{J_c} = \sigma \boldsymbol{E}$$

$\boldsymbol{\epsilon}$: ***Permittivity of the medium (Farad/meter)***

$\boldsymbol{\mu}$: ***Permeability of the medium (Henry/meter)***

$\boldsymbol{\sigma}$: ***Conductivity of the medium (Siemens/meter)***

Since the curl operator is a first order vector differential operator, Maxwell's equations are first order, vector differential equations. In order to have a unique solution, differential equations require boundary conditions. In electromagnetics, the field values of interest must be specified across the boundaries of the solution region in order to determine a unique solution for that region. Boundary conditions for finitely conductive media and infinitely conductive media will be considered respectively and then they will be modified when there are source currents or source charges at the boundaries.

2.1 Boundary conditions for a media with finite conductivity

The relationship between the two electric field intensities at the interface between two different media is related with the unit normal vector of the interface as follows

$$\boldsymbol{n} \times (\boldsymbol{E_2} - \boldsymbol{E_1}) = \boldsymbol{0} \quad , \quad \boldsymbol{\sigma_1} \neq \boldsymbol{0} \ , \ \boldsymbol{\sigma_2} \neq \boldsymbol{0}$$

Where $\boldsymbol{E_2}$ is the electric field intensity at media 2 and $\boldsymbol{E_1}$ is the electric field intensity at media 1 and if we consider the interface between the two media as a two dimensional surface, $\boldsymbol{n}$ is the unit normal vector pointing towards media 2.

The conductivities of media 1 and media 2 are $\boldsymbol{\sigma_1}$ and $\boldsymbol{\sigma_2}$ respectively, where $\boldsymbol{\sigma_1 \neq 0}$, $\boldsymbol{\sigma_2 \neq 0}$ implies that both of the two media have finite conductivity.

An identical relationship is valid for the magnetic field intensities at the interface between two finitely conductive media

$$\boldsymbol{n \times (H_2 - H_1) = 0} \quad , \quad \boldsymbol{\sigma_1 \neq 0} \ , \ \boldsymbol{\sigma_2 \neq 0}$$

Both of the equations for electric and magnetic fields imply that the tangential components of the electric and magnetic fields are continuous at an interface between two media with finite conductivities. However if there are source charges or currents at the interface between the two media or if either of the two media is a perfect conductor these two equations do not hold and they must be modified. Boundary conditions for electric and magnetic fields at perfectly conducting interfaces and for source containing interfaces will be discussed here respectively.

The boundary condition for the electric flux densities at an interface between two finitely conductive media is stated below

$$\boldsymbol{n \,.\, (D_2 - D_1) = 0} \quad , \quad \boldsymbol{\sigma_1 \neq 0} \ , \ \boldsymbol{\sigma_2 \neq 0}$$

This equation states that the normal components of the electric flux densities at an interface between two finitely conductive media which have no source charges or source currents are continuous. The same equation can be written in terms of the electric field intensities and permittivities of the two media as

$$\boldsymbol{n \,.\, (\epsilon_2 E_2 - \epsilon_1 E_1) = 0} \quad , \quad \boldsymbol{\sigma_1 \neq 0} \ , \ \boldsymbol{\sigma_2 \neq 0}$$

Which states that the normal components of the electric field intensities at an interface between two finitely conductive media which have no source charges or source currents are discontinuous. This is expected since their tangential components are continuous.

Similarly the boundary condition for the magnetic flux densities at an interface between two finitely conductive media is stated as

$$\boldsymbol{n \,.\, (B_2 - B_1) = 0} \quad , \quad \boldsymbol{\sigma_1 \neq 0} \ , \ \boldsymbol{\sigma_2 \neq 0}$$

This equation states that the normal components of the magnetic flux densities at an interface between two finitely conductive media which have no source charges or source currents are continuous. The same equation can be written in terms of the magnetic field intensities and permeabilities of the two media as

$$\boldsymbol{n \,.\, (\mu_2 H_2 - \mu_1 H_1) = 0} \quad , \quad \boldsymbol{\sigma_1 \neq 0} \ , \ \boldsymbol{\sigma_2 \neq 0}$$

Which states that the normal components of the magnetic field intensities at an interface between two finitely conductive media which have no source charges or source currents are discontinuous. This is expected since their tangential components are continuous.

2.2 Boundary conditions for a media with infinite conductivity

The previously-stated four boundary conditions which are given for a finitely conductive media must be modified if one of the media is of infinite conductivity or if there are source charges or currents at the interface between the two media. Assume that media 1 has infinite conductivity, this implies that $\boldsymbol{E_1}$**=0,** so the boundary condition for the electric field intensities is modified as

$$\boldsymbol{n \times E_2 = 0} \quad , \quad \boldsymbol{\sigma_1 = \infty} \quad , \quad \boldsymbol{E_1 = 0}$$

Which states that the tangential component of the total electric field intensity $\boldsymbol{E_2}$, is zero at the interface given that media 1 is a perfect electric conductor and $\boldsymbol{E_1 = 0}$.

From the first equation of Maxwell, we can find that $\boldsymbol{H_1 = 0}$ also, since $\boldsymbol{M_i = 0}$

$$\boldsymbol{\nabla \times E_1} = -\frac{\partial \boldsymbol{B_1}}{\partial \mathrm{t}} = \boldsymbol{0} \quad , \qquad \boldsymbol{then\ B_1 = 0}\ ,\ \boldsymbol{thus}\ \ \boldsymbol{H_1 = 0}$$

Since medium1 is a perfect electric conductor, there will be an induced electric current density and an induced electric charge density along the interface between media 1 and media 2, in that case the boundary condition for the magnetic field intensities must be modified to account for the induced charges as stated below

$$\boldsymbol{n \times (H_2 - H_1) = J_s} \quad , \quad \boldsymbol{\sigma_1 = \infty} \quad , \quad \boldsymbol{H_1 = 0}$$

$$\boldsymbol{thus} \qquad \boldsymbol{n \times H_2 = J_s} \quad , \quad \boldsymbol{\sigma_1 = \infty}$$

$\boldsymbol{J_s}$ ***= Induced electric current density (amperes/square meter)***

Which states that the tangential component of the total magnetic field intensity $\boldsymbol{H_2}$, is equal to the induced electric current density along the interface given that media 1 is a perfect electric conductor and $\boldsymbol{H_1 = 0}$.

The boundary condition for the electric flux densities at a perfectly conductive interface between two media, where media 1 is a perfect electric conductor is given as

$$\boldsymbol{n}\,.\,(\boldsymbol{D_2 - D_1}) = \mathrm{q}_{\boldsymbol{es}} \quad , \quad \boldsymbol{\sigma_1 = \infty} \quad , \quad \boldsymbol{D_1 = 0}\ ,\ \boldsymbol{since}\ \ \boldsymbol{E_1 = 0}$$

$$\boldsymbol{n}\,.\,\boldsymbol{D_2} = \mathrm{q}_{\boldsymbol{es}} \quad , \quad \boldsymbol{\sigma_1 = \infty}$$

$$\boldsymbol{n}\,.\,\boldsymbol{E_2} = \frac{\mathrm{q}_{\boldsymbol{es}}}{\epsilon} \qquad , \quad \boldsymbol{\sigma_1 = \infty}$$

$\mathrm{q}_{\boldsymbol{es}}$ ***= Surface electric charge density (coulombs/square meter)***

These equations state that the normal components of the electric flux density and electric field intensity are discontinuous at a perfectly conducting interface, where an induced surface charge density exists.

2.3 Boundary conditions when there is a source along the interface (General case)

If none of the two media is a perfect electric conductor, and if there are electric and magnetic sources existing at the boundary (or interface) , the four boundary conditions are modified to include the impressed (source) current and charge densities as

$$-\boldsymbol{n} \times (\boldsymbol{E_2} - \boldsymbol{E_1}) = \boldsymbol{M_s}$$

$$\boldsymbol{n} \times (\boldsymbol{H_2} - \boldsymbol{H_1}) = \boldsymbol{J_s}$$

$$\boldsymbol{n}.(\boldsymbol{D_2} - \boldsymbol{D_1}) = q_{es}$$

$$\boldsymbol{n}.(\boldsymbol{B_2} - \boldsymbol{B_1}) = q_{ms}$$

$$\boldsymbol{M_s} : \boldsymbol{Surface\ magnetic\ current\ density}\ \left(\frac{\boldsymbol{volts}}{\boldsymbol{meter}}\right)$$

$$\boldsymbol{J_s} : \boldsymbol{Surface\ electric\ current\ density}\ \left(\frac{\boldsymbol{amperes}}{\boldsymbol{meter}}\right)$$

$$q_{ms} : \boldsymbol{Surface\ magnetic\ charge\ density}\ \left(\frac{\boldsymbol{webers}}{\boldsymbol{square\ meter}}\right)$$

$$q_{es} : \boldsymbol{Surface\ electric\ charge\ density}\ \left(\frac{\boldsymbol{coulombs}}{\boldsymbol{square\ meter}}\right)$$

2.4 Summary of the boundary conditions

Finitely conductive media

$$\boldsymbol{n} \times (\boldsymbol{E_2} - \boldsymbol{E_1}) = \boldsymbol{0}$$

$$\boldsymbol{n} \times (\boldsymbol{H_2} - \boldsymbol{H_1}) = \boldsymbol{0}$$

$$\boldsymbol{n}\ .\ (\boldsymbol{D_2} - \boldsymbol{D_1}) = \boldsymbol{0}$$

$$\boldsymbol{n}\ .\ (\boldsymbol{B_2} - \boldsymbol{B_1}) = \boldsymbol{0}$$

Infinitely conductive media

$$\boldsymbol{n} \times \boldsymbol{E_2} = \boldsymbol{0}$$

$$\boldsymbol{n} \times \boldsymbol{H_2} = \boldsymbol{J_s}$$

$$\boldsymbol{n}\ .\ \boldsymbol{D_2} = q_{es}$$

$$\boldsymbol{n}\ .\ \boldsymbol{B_2} = \boldsymbol{0}$$

General case

$$-\boldsymbol{n} \times (\boldsymbol{E_2} - \boldsymbol{E_1}) = \boldsymbol{M_s}$$

$$\boldsymbol{n} \times (\boldsymbol{H_2} - \boldsymbol{H_1}) = \boldsymbol{J_s}$$

$$\boldsymbol{n}.(\boldsymbol{D_2} - \boldsymbol{D_1}) = q_{es}$$

$$\boldsymbol{n}.(\boldsymbol{B_2} - \boldsymbol{B_1}) = q_{ms}$$

2.5 Maxwell's equations in anisotropic media

Maxwell's equations for isotropic media are

$$\boldsymbol{\nabla} \times \boldsymbol{E} = -\boldsymbol{M_i} - \boldsymbol{M_c} - \mu \frac{\partial \boldsymbol{H}}{\partial \mathrm{t}} \quad , \quad \boldsymbol{M_c} = \sigma^* \boldsymbol{H}$$

$$\boldsymbol{\nabla} \times \boldsymbol{H} = \boldsymbol{J_i} + \boldsymbol{J_c} + \epsilon \frac{\partial \boldsymbol{E}}{\partial t} \quad , \quad \boldsymbol{J_c} = \sigma \boldsymbol{E}$$

$$\boldsymbol{\nabla}.\boldsymbol{D} = q_{ev}$$

$$\boldsymbol{\nabla}.\boldsymbol{B} = q_{mv}$$

$\boldsymbol{M_c}$: ***Magnetic conductivity***

Substituting $\boldsymbol{M_c} = \sigma^* \boldsymbol{H}$ into the first equation and $\boldsymbol{J_c} = \sigma \boldsymbol{E}$ into the second equation we get

$$\boldsymbol{\nabla} \times \boldsymbol{E} = -\boldsymbol{M_i} - \sigma^* \boldsymbol{H} - \mu \frac{\partial \boldsymbol{H}}{\partial t}$$

$$\boldsymbol{\nabla} \times \boldsymbol{H} = \boldsymbol{J_i} + \sigma \boldsymbol{E} + \epsilon \frac{\partial \boldsymbol{E}}{\partial t}$$

Since these two equations are 3 dimensional vector differential equations, each of them can be decoupled into 3 scalar differential equations as follows

$$\boldsymbol{\nabla} = \boldsymbol{a_x} \frac{\partial}{\partial \mathrm{x}} + \boldsymbol{a_y} \frac{\partial}{\partial \mathrm{y}} + \boldsymbol{a_z} \frac{\partial}{\partial \mathrm{z}}$$

$$\boldsymbol{E} = \boldsymbol{a_x} \mathrm{E_x} + \boldsymbol{a_y} \mathrm{E_y} + \boldsymbol{a_z} \mathrm{E_z}$$

$$\boldsymbol{H} = \boldsymbol{a_x} \mathrm{H_x} + \boldsymbol{a_y} \mathrm{H_y} + \boldsymbol{a_z} \mathrm{H_z}$$

$$\boldsymbol{\nabla} \times \boldsymbol{E} = \boldsymbol{a_x} \left(\frac{\partial \mathrm{E_y}}{\partial \mathrm{z}} - \frac{\partial \mathrm{E_z}}{\partial \mathrm{y}} \right) + \boldsymbol{a_y} \left(\frac{\partial \mathrm{E_z}}{\partial \mathrm{x}} - \frac{\partial \mathrm{E_x}}{\partial \mathrm{z}} \right) + \boldsymbol{a_z} \left(\frac{\partial \mathrm{E_x}}{\partial \mathrm{y}} - \frac{\partial \mathrm{E_y}}{\partial \mathrm{x}} \right)$$

$$\boldsymbol{\nabla} \times \boldsymbol{H} = \boldsymbol{a_x} \left(\frac{\partial \mathrm{H_y}}{\partial \mathrm{z}} - \frac{\partial \mathrm{H_z}}{\partial \mathrm{y}} \right) + \boldsymbol{a_y} \left(\frac{\partial \mathrm{H_z}}{\partial \mathrm{x}} - \frac{\partial \mathrm{H_x}}{\partial \mathrm{z}} \right) + \boldsymbol{a_z} \left(\frac{\partial \mathrm{H_x}}{\partial \mathrm{y}} - \frac{\partial \mathrm{H_y}}{\partial \mathrm{x}} \right)$$

Therefore, we seperate each vector to its {x,y,z} components

$$\frac{\partial \mathrm{E_y}}{\partial \mathrm{z}} - \frac{\partial \mathrm{E_z}}{\partial \mathrm{y}} = -\mathrm{M_{ix}} - \sigma^* \mathrm{H_x} - \mu \frac{\partial \mathrm{H_x}}{\partial \mathrm{t}}$$

$$\frac{\partial \mathrm{E_z}}{\partial \mathrm{x}} - \frac{\partial \mathrm{E_x}}{\partial \mathrm{z}} = -\mathrm{M_{iy}} - \sigma^* \mathrm{H_y} - \mu \frac{\partial \mathrm{H_y}}{\partial \mathrm{t}}$$

$$\frac{\partial \mathrm{E_x}}{\partial \mathrm{y}} - \frac{\partial \mathrm{E_y}}{\partial \mathrm{x}} = -\mathrm{M_{iz}} - \sigma^* \mathrm{H_z} - \mu \frac{\partial \mathrm{H_z}}{\partial \mathrm{t}}$$

$$\frac{\partial \mathrm{H_y}}{\partial \mathrm{z}} - \frac{\partial \mathrm{H_z}}{\partial \mathrm{y}} = \mathrm{J_{ix}} + \sigma \mathrm{E_x} + \epsilon \frac{\partial \mathrm{E_x}}{\partial \mathrm{t}}$$

$$\frac{\partial \mathrm{H_z}}{\partial \mathrm{x}} - \frac{\partial \mathrm{H_x}}{\partial \mathrm{z}} = \mathrm{J_{iy}} + \sigma \mathrm{E_y} + \epsilon \frac{\partial \mathrm{E_y}}{\partial \mathrm{t}}$$

$$\frac{\partial \mathrm{H_x}}{\partial \mathrm{y}} - \frac{\partial \mathrm{H_y}}{\partial \mathrm{x}} = \mathrm{J_{iz}} + \sigma \mathrm{E_z} + \epsilon \frac{\partial \mathrm{E_z}}{\partial \mathrm{t}}$$

Where σ , μ, and ϵ are scalars. However, for anisotropic media σ , μ, and ϵ are not scalars but they are expressed as direction dependent tensors, therefore the last 6 equations must be modified since σ , μ, and ϵ are not scalar quantities anymore and behave differently for each component of $\boldsymbol{E}$ and $\boldsymbol{H}$.

For anisotropic media σ , μ, and ϵ are expressed as

$$\boldsymbol{\sigma} = \begin{bmatrix} \sigma_{xx} & \sigma_{xy} & \sigma_{xz} \\ \sigma_{yx} & \sigma_{yy} & \sigma_{yz} \\ \sigma_{zx} & \sigma_{zy} & \sigma_{zz} \end{bmatrix} \quad , \quad \boldsymbol{\mu} = \begin{bmatrix} \mu_{xx} & \mu_{xy} & \mu_{xz} \\ \mu_{yx} & \mu_{yy} & \mu_{yz} \\ \mu_{zx} & \mu_{zy} & \mu_{zz} \end{bmatrix} \quad , \quad \boldsymbol{\epsilon} = \begin{bmatrix} \epsilon_{xx} & \epsilon_{xy} & \epsilon_{xz} \\ \epsilon_{yx} & \epsilon_{yy} & \epsilon_{yz} \\ \epsilon_{zx} & \epsilon_{zy} & \epsilon_{zz} \end{bmatrix}$$

Therefore $\boldsymbol{\sigma}$, $\boldsymbol{\epsilon}$, and $\boldsymbol{\mu}$ in anisotropic media are related to $\boldsymbol{E}$ and $\boldsymbol{H}$ by dot product operation

$$\boldsymbol{J_c} = \boldsymbol{\sigma}.\boldsymbol{E} \quad , \quad \boldsymbol{M_c} = \boldsymbol{\sigma}^*.\boldsymbol{H} \quad , \quad \boldsymbol{D} = \boldsymbol{\epsilon}.\boldsymbol{E} \quad , \quad \boldsymbol{B} = \boldsymbol{\mu}.\boldsymbol{H}$$

$$\boldsymbol{\nabla} \times \boldsymbol{E} = -\boldsymbol{M_i} - \boldsymbol{\sigma}^*.\boldsymbol{H} - \frac{\partial(\boldsymbol{\mu}.\boldsymbol{H})}{\partial \mathrm{t}} \qquad , \qquad \boldsymbol{\nabla}.(\boldsymbol{\epsilon}.\boldsymbol{E}) = q_{ev}$$

$$\boldsymbol{\nabla} \times \boldsymbol{H} = \boldsymbol{J_i} + \boldsymbol{\sigma}.\boldsymbol{E} + \frac{\partial(\boldsymbol{\epsilon}.\boldsymbol{E})}{\partial \mathrm{t}} \qquad , \qquad \boldsymbol{\nabla}.(\boldsymbol{\mu}.\boldsymbol{H}) = q_{mv}$$

Therefore the corresponding scalar equations for field components in anisotropic media are

$$\frac{\partial \mathrm{E_y}}{\partial \mathrm{z}} - \frac{\partial \mathrm{E_z}}{\partial \mathrm{y}} = -\mathrm{M_{ix}} - (\sigma_{\boldsymbol{xx}}{}^* \mathrm{H_x} + \sigma_{\boldsymbol{xy}}{}^* \mathrm{H_y} + \sigma_{\boldsymbol{xz}}{}^* \mathrm{H_z}) - \frac{\partial}{\partial \mathrm{t}} (\boldsymbol{\mu_{xx}} \mathrm{H_x} + \boldsymbol{\mu_{xy}} \mathrm{H_y} + \boldsymbol{\mu_{xz}} \mathrm{H_z})$$

$$\frac{\partial \mathrm{E_z}}{\partial \mathrm{x}} - \frac{\partial \mathrm{E_x}}{\partial \mathrm{z}} = -\mathrm{M_{iy}} - (\sigma_{\boldsymbol{yx}}{}^* \mathrm{H_x} + \sigma_{\boldsymbol{yy}}{}^* \mathrm{H_y} + \sigma_{\boldsymbol{yz}}{}^* \mathrm{H_z}) - \frac{\partial}{\partial \mathrm{t}} (\mu_{\boldsymbol{yx}} \mathrm{H_x} + \mu_{\boldsymbol{yy}} \mathrm{H_y} + \mu_{\boldsymbol{yz}} \mathrm{H_z})$$

$$\frac{\partial \mathrm{E_x}}{\partial \mathrm{y}} - \frac{\partial \mathrm{E_y}}{\partial \mathrm{x}} = -\mathrm{M_{iz}} - (\sigma_{\boldsymbol{zx}}{}^* \mathrm{H_x} + \sigma_{\boldsymbol{zy}}{}^* \mathrm{H_y} + \sigma_{\boldsymbol{zz}}{}^* \mathrm{H_z}) - \frac{\partial}{\partial \mathrm{t}} (\mu_{\boldsymbol{zx}} \mathrm{H_x} + \mu_{\boldsymbol{zy}} \mathrm{H_y} + \mu_{\boldsymbol{zz}} \mathrm{H_z})$$

$$\frac{\partial H_y}{\partial z} - \frac{\partial H_z}{\partial y} = J_{ix} + \left(\sigma_{xx}E_x + \sigma_{xy}E_y + \sigma_{xz}E_z\right) + \frac{\partial}{\partial t}\left(\epsilon_{xx}E_x + \epsilon_{xy}E_y + \epsilon_{xz}E_z\right)$$

$$\frac{\partial H_z}{\partial x} - \frac{\partial H_x}{\partial z} = J_{iy} + \left(\sigma_{yx}E_x + \sigma_{yy}E_y + \sigma_{yz}E_z\right) + \frac{\partial}{\partial t}\left(\epsilon_{yx}E_x + \epsilon_{yy}E_y + \epsilon_{yz}E_z\right)$$

$$\frac{\partial H_x}{\partial y} - \frac{\partial H_y}{\partial x} = J_{iz} + \left(\sigma_{zx}E_x + \sigma_{zy}E_y + \sigma_{zz}E_z\right) + \frac{\partial}{\partial t}\left(\epsilon_{zx}E_x + \epsilon_{zy}E_y + \epsilon_{zz}E_z\right)$$

Now let us consider the case of an anisotropic media where μ and ϵ are scalars and conductivity is diagonally direction dependent

$$\boldsymbol{\mu} = \begin{bmatrix} \mu & 0 & 0 \\ 0 & \mu & 0 \\ 0 & 0 & \mu \end{bmatrix} = \mu \quad , \quad \boldsymbol{\epsilon} = \begin{bmatrix} \epsilon & 0 & 0 \\ 0 & \epsilon & 0 \\ 0 & 0 & \epsilon \end{bmatrix} = \epsilon \quad , \quad \boldsymbol{\sigma} = \begin{bmatrix} \sigma_x & 0 & 0 \\ 0 & \sigma_y & 0 \\ 0 & 0 & \sigma_z \end{bmatrix}$$

where $\boldsymbol{\sigma}$ is not a scalar but a diagonal tensor with , $\sigma_x \neq \sigma_y$, $\sigma_y \neq \sigma_z$, $\sigma_x \neq \sigma_z$, in that case, the corresponding scalar equations for field components become

$$\frac{\partial E_y}{\partial z} - \frac{\partial E_z}{\partial y} = -M_{ix} - {\sigma_x}^* H_x - \mu\frac{\partial H_x}{\partial t}$$

$$\frac{\partial E_z}{\partial x} - \frac{\partial E_x}{\partial z} = -M_{iy} - {\sigma_y}^* H_y - \mu\frac{\partial H_y}{\partial t}$$

$$\frac{\partial E_x}{\partial y} - \frac{\partial E_y}{\partial x} = -M_{iz} - {\sigma_z}^* H_z - \mu\frac{\partial H_z}{\partial t}$$

$$\frac{\partial H_y}{\partial z} - \frac{\partial H_z}{\partial y} = J_{ix} + \sigma_x E_x + \epsilon\frac{\partial E_x}{\partial t}$$

$$\frac{\partial H_z}{\partial x} - \frac{\partial H_x}{\partial z} = J_{iy} + \sigma_y E_y + \epsilon\frac{\partial E_y}{\partial t}$$

$$\frac{\partial H_x}{\partial y} - \frac{\partial H_y}{\partial x} = J_{iz} + \sigma_z E_z + \epsilon\frac{\partial E_z}{\partial t}$$

The two examples of anisotropic media are the ionosphere and the artifical PML medium.

2.6 Impedance boundary conditions

There may be infinitely many solutions that satisfy a given differential equation, but we are usually interested in the unique solution. For a differential equation to have a unique solution over a given solution region, the boundary conditions of the differential equation over the boundary of the solution region must be specified. An electromagnetic problem is

said to be completely described if the associated Maxwell's equation is given along with its boundary conditions. If we consider two different media that are seperated by an interface, we know that in order to solve the fields in both media, we need to know the boundary conditions along the interface.

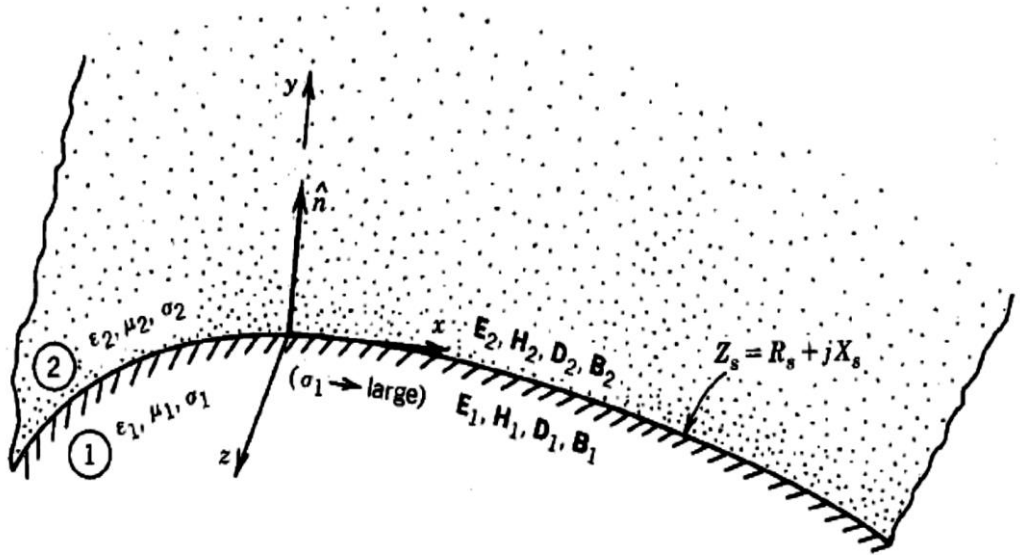

Figure2.1:Interface between two different media [1]

If the first medium is a perfect electric conductor, we do not need to use an impedance boundary condition, because since the first medium has infinite conductivity, all fields in the first medium will become zero. Therefore we only have to deal with the tangential component of the total field in the second medium, where the total field contains the incident field and the scattered field. This case results in an easy way of solving the scattered fields with the use of the general boundary conditions. However if the first medium and thus the interface is an imperfect conductor, some of the incident field in the second medium is transmitted into the first medium and some of it is scattered back into the first medium. In that case the determination of the boundary conditions and therefore the solution of the transmitted and the scattered fields is available with the use of the impedance boundary conditions.

When medium 1 is an imperfect conductor, it can be shown that the electric and magnetic fields at the surface of the conductor are approximately related by

$$\boldsymbol{E} - (\boldsymbol{n}.\boldsymbol{E})\boldsymbol{n} = Z_s(\boldsymbol{n} \times \boldsymbol{H}) \qquad (\mathbf{1})$$

$$\boldsymbol{n} \times \boldsymbol{E} = Z_s[(\boldsymbol{n}.\boldsymbol{H})\boldsymbol{n} - \boldsymbol{H}] \qquad (\mathbf{2})$$

$$Z_s : Surface\ impedance$$

Equation (2) can be directly found from equation (1) by using the principle of duality.

$$[\boldsymbol{E} - (\boldsymbol{n}.\boldsymbol{E})\boldsymbol{n}] = Z_s(\boldsymbol{n} \times \boldsymbol{H})$$

$$[\boldsymbol{H} - (\boldsymbol{n}.\boldsymbol{H})\boldsymbol{n}] = -\frac{1}{Z_s}(\boldsymbol{n} \times \boldsymbol{E})$$

Or, by applying cross product operation on both sides of equation (1) , we can get (2)

$$\boldsymbol{n} \times [\boldsymbol{E} - (\boldsymbol{n}.\boldsymbol{E})\boldsymbol{n}] = Z_s[\boldsymbol{n} \times \boldsymbol{n} \times \boldsymbol{H}]$$

$$\boldsymbol{n} \times \boldsymbol{E} = Z_s[\boldsymbol{n}(\boldsymbol{n}.\boldsymbol{H}) - \boldsymbol{H}]$$

The terms $\boldsymbol{E} - (\boldsymbol{n}.\boldsymbol{E})\boldsymbol{n}$ and $\boldsymbol{n} \times \boldsymbol{H}$ can be expressed in terms of their components as

$$\boldsymbol{E} - (\boldsymbol{n}.\boldsymbol{E})\boldsymbol{n} = \boldsymbol{a_x}\left[(1 - {n_x}^2)E_x - n_x n_y E_y - n_x n_z E_z\right] + \boldsymbol{a_y}\left[-n_x n_y E_x + \left(1 - {n_y}^2\right)E_y - n_y n_z E_z\right] + \boldsymbol{a_z}[-n_x n_z E_x - n_y n_z E_y + (1 - {n_z}^2)E_z]$$

$$\boldsymbol{n} \times \boldsymbol{H} = \boldsymbol{a_z}\left[n_x H_y - n_y H_x\right] + \boldsymbol{a_y}[n_z H_x - n_x H_z] + \boldsymbol{a_x}\left[n_y H_z - n_z H_y\right]$$

Therefore we can express the first equation in terms of a 3× 3 linear system

$$\boldsymbol{E} - (\boldsymbol{n}.\boldsymbol{E})\boldsymbol{n} = Z_s(\boldsymbol{n} \times \boldsymbol{H})$$

$$\begin{bmatrix} (1 - {n_x}^2) & -n_x n_y & -n_x n_z \\ -n_x n_y & \left(1 - {n_y}^2\right) & -n_y n_z \\ -n_x n_z & -n_y n_z & (1 - {n_z}^2) \end{bmatrix} \begin{bmatrix} E_x \\ E_y \\ E_z \end{bmatrix} = \begin{bmatrix} Z_s(n_y H_z - n_z H_y) \\ Z_s(n_z H_x - n_x H_z) \\ Z_s(n_x H_y - n_y H_x) \end{bmatrix}$$

$$\begin{bmatrix} (1 - {n_x}^2) & -n_x n_y & -n_x n_z \\ -n_x n_y & \left(1 - {n_y}^2\right) & -n_y n_z \\ -n_x n_z & -n_y n_z & (1 - {n_z}^2) \end{bmatrix} \begin{bmatrix} {E_x}^i + {E_x}^s \\ {E_y}^i + {E_y}^s \\ {E_z}^i + {E_z}^s \end{bmatrix} = \begin{bmatrix} Z_s\left(n_y {H_z}^i - n_z {H_y}^i\right) \\ Z_s\left(n_z {H_x}^i - n_x {H_z}^i\right) \\ Z_s\left(n_x {H_y}^i - n_y {H_x}^i\right) \end{bmatrix} + \begin{bmatrix} Z_s\left(n_y {H_z}^s - n_z {H_y}^s\right) \\ Z_s\left(n_z {H_x}^s - n_x {H_z}^s\right) \\ Z_s\left(n_x {H_y}^s - n_y {H_x}^s\right) \end{bmatrix}$$

$$\begin{bmatrix} (1 - {n_x}^2) & -n_x n_y & -n_x n_z \\ -n_x n_y & \left(1 - {n_y}^2\right) & -n_y n_z \\ -n_x n_z & -n_y n_z & (1 - {n_z}^2) \end{bmatrix} \begin{bmatrix} {E_x}^s - Z_s\left(n_y {H_z}^s - n_z {H_y}^s\right) \\ {E_y}^s - Z_s(n_z {H_x}^s - n_x {H_z}^s) \\ {E_z}^s - Z_s\left(n_x {H_y}^s - n_y {H_x}^s\right) \end{bmatrix} = \begin{bmatrix} Z_s\left(n_y {H_z}^i - n_z {H_y}^i\right) - {E_x}^i \\ Z_s\left(n_z {H_x}^i - n_x {H_z}^i\right) - {E_y}^i \\ Z_s\left(n_x {H_y}^i - n_y {H_x}^i\right) - {E_z}^i \end{bmatrix}$$

Similarly, the second equation can be expressed as a 3× 3 linear system

$$\boldsymbol{n} \times \boldsymbol{E} = Z_s[(\boldsymbol{n}.\boldsymbol{H})\boldsymbol{n} - \boldsymbol{H}]$$

$$\begin{bmatrix} ({n_x}^2 - 1) & n_x n_y & n_x n_z \\ n_x n_y & \left({n_y}^2 - 1\right) & n_y n_z \\ n_x n_z & n_y n_z & ({n_z}^2 - 1) \end{bmatrix} \begin{bmatrix} H_x \\ H_y \\ H_z \end{bmatrix} = \begin{bmatrix} \frac{1}{\mathrm{Z_s}}(n_y E_z - n_z E_y) \\ \frac{1}{\mathrm{Z_s}}(n_z E_x - n_x E_z) \\ \frac{1}{\mathrm{Z_s}}(n_x E_y - n_y E_x) \end{bmatrix}$$

$$\begin{bmatrix} ({n_x}^2 - 1) & n_x n_y & n_x n_z \\ n_x n_y & \left({n_y}^2 - 1\right) & n_y n_z \\ n_x n_z & n_y n_z & ({n_z}^2 - 1) \end{bmatrix} \begin{bmatrix} {H_x}^i + {H_x}^s \\ {H_y}^i + {H_y}^s \\ {H_z}^i + {H_z}^s \end{bmatrix} = \begin{bmatrix} \frac{1}{\mathrm{Z_s}}\left(n_y {E_z}^i - n_z {E_y}^i\right) \\ \frac{1}{\mathrm{Z_s}}\left(n_z {E_x}^i - n_x {E_z}^i\right) \\ \frac{1}{\mathrm{Z_s}}\left(n_x {E_y}^i - n_y {E_x}^i\right) \end{bmatrix} + \begin{bmatrix} \frac{1}{\mathrm{Z_s}}\left(n_y {E_z}^s - n_z {E_y}^s\right) \\ \frac{1}{\mathrm{Z_s}}(n_z {E_x}^s - n_x {E_z}^s) \\ \frac{1}{\mathrm{Z_s}}\left(n_x {E_y}^s - n_y {E_x}^s\right) \end{bmatrix}$$

$$\begin{bmatrix} ({n_x}^2 - 1) & n_x n_y & n_x n_z \\ n_x n_y & \left({n_y}^2 - 1\right) & n_y n_z \\ n_x n_z & n_y n_z & ({n_z}^2 - 1) \end{bmatrix} \begin{bmatrix} {H_x}^s - \frac{1}{\mathrm{Z_s}}\left(n_y {E_z}^s - n_z {E_y}^s\right) \\ {H_y}^s - \frac{1}{\mathrm{Z_s}}(n_z {E_x}^s - n_x {E_z}^s) \\ {H_z}^s - \frac{1}{\mathrm{Z_s}}\left(n_x {E_y}^s - n_y {E_x}^s\right) \end{bmatrix} = \begin{bmatrix} \frac{1}{\mathrm{Z_s}}\left(n_y {E_z}^i - n_z {E_y}^i\right) - {H_x}^i \\ \frac{1}{\mathrm{Z_s}}\left(n_z {E_x}^i - n_x {E_z}^i\right) - {H_y}^i \\ \frac{1}{\mathrm{Z_s}}\left(n_x {E_y}^i - n_y {E_x}^i\right) - {H_z}^i \end{bmatrix}$$

So there are 6 equations and 6 unknowns, therefore the systems can be easily solved to yield the values of $\{ {E_x}^s , {E_y}^s, {E_z}^s, {H_x}^s, {H_y}^s, {H_z}^s\}$ given the surface impedance and the surface normal.

Note that each of the field components consists of the incident and scattered fields in medium 2, but in medium 1, they are equal to the absorbed (transmitted) field.

The fields $\{ E_x , E_y , E_z , H_x , H_y , H_z \}$ in medium 2 can be expressed as

$$E_x = {E_x}^i + {E_x}^s \quad , \quad E_y = {E_y}^i + {E_y}^s \quad , \quad E_z = {E_z}^i + {E_z}^s$$

$$H_x = {H_x}^i + {H_x}^s \quad , \quad H_y = {H_y}^i + {H_y}^s \quad , \quad H_z = {H_z}^i + {H_z}^s$$

The incident field components are known, therefore we have only the scattered components as unknowns

$$\{ {E_x}^s , {E_y}^s , {E_z}^s , {H_x}^s , {H_y}^s , {H_z}^s\}$$

Since we have 6 equations at hand, all the scattered field components can be solved, we can also solve the transmitted field components using the general boundary conditions on the same imperfectly conducting surface

$$Transmitted\ field\ components \ : \ \{ {E_x}^t , {E_y}^t , {E_z}^t , {H_x}^t , {H_y}^t , {H_z}^t\}$$

$$\boldsymbol{n} \times (\boldsymbol{E_2} - \boldsymbol{E_1}) = -\boldsymbol{M_s} \quad , \quad \boldsymbol{n} \times (\boldsymbol{H_2} - \boldsymbol{H_1}) = \boldsymbol{J_s}$$

$$E_1 = E^i + E^s \quad , \quad E_2 = E^t \quad , \quad H_1 = H^i + H^s \quad , \quad H_2 = H^t$$

$$\boldsymbol{n} \times \left(\boldsymbol{E^i} + \boldsymbol{E^s} - \boldsymbol{E^t}\right) = -\boldsymbol{M_s} \quad , \quad \boldsymbol{n} \times \left(\boldsymbol{H^i} + \boldsymbol{H^s} - \boldsymbol{H^t}\right) = \boldsymbol{J_s}$$

i) There are 3 unknown components of $\boldsymbol{E^t}$ which are $\{ {E_x}^t , {E_y}^t , {E_z}^t \}$ and we have 3 equations from $\boldsymbol{n} \times \left(\boldsymbol{E^i} + \boldsymbol{E^s} - \boldsymbol{E^t}\right) = -\boldsymbol{M_s}$, therefore $\{ {E_x}^t , {E_y}^t , {E_z}^t \}$ can be solved.

ii) There are 3 unknown components of $\boldsymbol{H^t}$ which are $\{ {H_x}^t , {H_y}^t , {H_z}^t \}$ and we have 3 equations from $\boldsymbol{n} \times \left(\boldsymbol{H^i} + \boldsymbol{H^s} - \boldsymbol{H^t}\right) = \boldsymbol{J_s}$, therefore $\{ {H_x}^t , {H_y}^t , {H_z}^t \}$ can be solved.

CHAPTER 3

WAVE EQUATION

3.1 Wave equation for isotropic media

Although Maxwell's four equations simply describe the field behaviour in general, the first two equations involving $\boldsymbol{E}$ and $\boldsymbol{H}$ are coupled to each other which makes it hard to understand the field behaviour. Instead we use some vector algebra to obtain single variable field intensity equations for both $\boldsymbol{E}$ and $\boldsymbol{H}$ at the expense of increased order, but the equations then become uncoupled and it becomes much easier to understand the behaviour of the field intensities $\boldsymbol{E}$ and $\boldsymbol{H}$. In other words we simply convert the two first-order coupled vector differential equations into two second-order vector differential equations each of which has a single variable and therefore not coupled to each other. To get these single variable equations, we start with the first two of Maxwell's equations

$$\boldsymbol{\nabla} \times \boldsymbol{E} = -\boldsymbol{M_i} - \mu \frac{\partial \boldsymbol{H}}{\partial t} \qquad (\mathbf{1})$$

$$\boldsymbol{\nabla} \times \boldsymbol{H} = \boldsymbol{J_i} + \sigma \boldsymbol{E} + \epsilon \frac{\partial \boldsymbol{E}}{\partial t} \qquad (\mathbf{2})$$

Taking the curl of both sides of these equations and assuming a homogenous medium, we can write that

$$\boldsymbol{\nabla} \times \boldsymbol{\nabla} \times \boldsymbol{E} = -\boldsymbol{\nabla} \times \boldsymbol{M_i} - \mu \left[\boldsymbol{\nabla} \times \frac{\partial \boldsymbol{H}}{\partial t}\right] = -\boldsymbol{\nabla} \times \boldsymbol{M_i} - \mu \frac{\partial}{\partial t}[\boldsymbol{\nabla} \times \boldsymbol{H}] \qquad (\mathbf{3})$$

$$\boldsymbol{\nabla} \times \boldsymbol{\nabla} \times \boldsymbol{H} = \boldsymbol{\nabla} \times \boldsymbol{J_i} + \sigma[\boldsymbol{\nabla} \times \boldsymbol{E}] + \epsilon \left[\boldsymbol{\nabla} \times \frac{\partial \boldsymbol{E}}{\partial t}\right] = \boldsymbol{\nabla} \times \boldsymbol{J_i} + \sigma[\boldsymbol{\nabla} \times \boldsymbol{E}] + \epsilon \frac{\partial}{\partial t}[\boldsymbol{\nabla} \times \boldsymbol{E}] \qquad (\mathbf{4})$$

Substituting (2) into the right side of (3) and using the vector identity (5) at the left side

$$\boldsymbol{\nabla} \times \boldsymbol{\nabla} \times \boldsymbol{F} = \boldsymbol{\nabla}(\boldsymbol{\nabla}.\boldsymbol{F}) - \boldsymbol{\nabla^2 F} \qquad (\mathbf{5})$$

We get (6) and (7) as

$$\boldsymbol{\nabla}(\boldsymbol{\nabla}.\boldsymbol{E}) - \boldsymbol{\nabla^2 E} = -\boldsymbol{\nabla} \times \boldsymbol{M_i} - \mu \frac{\partial}{\partial \mathrm{t}} \left[\boldsymbol{J_i} + \sigma \boldsymbol{E} + \epsilon \frac{\partial \boldsymbol{E}}{\partial t}\right] \qquad (\mathbf{6})$$

$$\boldsymbol{\nabla}(\boldsymbol{\nabla}.\boldsymbol{E}) - \boldsymbol{\nabla^2 E} = -\boldsymbol{\nabla} \times \boldsymbol{M_i} - \mu \frac{\partial \boldsymbol{J}_\mathrm{i}}{\partial \mathrm{t}} - \mu\sigma \frac{\partial \boldsymbol{E}}{\partial \mathrm{t}} - \mu\epsilon \frac{\partial^2 \boldsymbol{E}}{\partial \mathrm{t}^2} \qquad (\mathbf{7})$$

Substituting Maxwell's third equation $\boldsymbol{\nabla}.\boldsymbol{D} = \epsilon(\boldsymbol{\nabla}.\boldsymbol{E}) = \mathrm{q_{ve}}$ into equation $(\mathbf{7})$ and rearranging terms, we get

$$\boldsymbol{\nabla^2 E} = \boldsymbol{\nabla} \times \boldsymbol{M_i} + \mu \frac{\partial \boldsymbol{J}_\mathrm{i}}{\partial \mathrm{t}} + \mu\sigma \frac{\partial \boldsymbol{E}}{\partial \mathrm{t}} + \mu\epsilon \frac{\partial^2 \boldsymbol{E}}{\partial \mathrm{t}^2} + \frac{\boldsymbol{\nabla} \mathrm{q}_{\mathrm{ve}}}{\epsilon} \qquad (\mathbf{8})$$

Which is an uncoupled second order differential equation for $\boldsymbol{E}$.

Using the same procedure for (4) , we can get the second-order uncoupled equation for $\boldsymbol{H}$

$$\boldsymbol{\nabla} \times \boldsymbol{\nabla} \times \boldsymbol{H} = \boldsymbol{\nabla} \times \boldsymbol{J_i} + \sigma[\boldsymbol{\nabla} \times \boldsymbol{E}] + \epsilon \left[\boldsymbol{\nabla} \times \frac{\partial \boldsymbol{E}}{\partial \mathrm{t}}\right] = \boldsymbol{\nabla} \times \boldsymbol{J_i} + \sigma[\boldsymbol{\nabla} \times \boldsymbol{E}] + \epsilon \frac{\partial}{\partial \mathrm{t}}[\boldsymbol{\nabla} \times \boldsymbol{E}]$$

$$\boldsymbol{\nabla}(\boldsymbol{\nabla}.\boldsymbol{H}) - \boldsymbol{\nabla^2 H} = \boldsymbol{\nabla} \times \boldsymbol{J_i} + \sigma \left[-\boldsymbol{M_i} - \mu \frac{\partial \boldsymbol{H}}{\partial \mathrm{t}}\right] + \epsilon \frac{\partial}{\partial \mathrm{t}} \left[-\boldsymbol{M_i} - \mu \frac{\partial \boldsymbol{H}}{\partial \mathrm{t}}\right] \qquad (\mathbf{9})$$

Substituting Maxwell's fourth equation $\boldsymbol{\nabla}.\boldsymbol{B} = \mu(\boldsymbol{\nabla}.\boldsymbol{H}) = \mathrm{q}_{\mathrm{ve}}$ into equation $(\mathbf{9})$ and rearranging terms, we get

$$\boldsymbol{\nabla^2 H} = -\boldsymbol{\nabla} \times \boldsymbol{J_i} + \sigma \boldsymbol{M_i} + \frac{1}{\mu}[\nabla \mathrm{q}_{\mathrm{vm}}] + \mu\sigma \frac{\partial \boldsymbol{H}}{\partial \mathrm{t}} + \epsilon \frac{\partial \boldsymbol{M_i}}{\partial \mathrm{t}} + \mu\epsilon \frac{\partial^2 \boldsymbol{H}}{\partial \mathrm{t}^2} \qquad (\mathbf{10})$$

Which is an uncoupled second order differential equation for $\boldsymbol{H}$.

Equations (8) and (10) are called vector wave equations for $\boldsymbol{E}$ *and* $\boldsymbol{H}$. We will simply call them "Wave Equations". These two wave equations are complicated, but they can be simplified according to the media properties. A media may be sourceless, lossless or both. If the media is both sourceless ($\boldsymbol{J_i}$ =0, $\boldsymbol{M_i}$ =0, q_{ve} =0 , q_{vm} =0) and lossless ($\sigma = 0$), the wave equations simplify greatly and it is much more easier to derive an analytic solution for them.

For a source free medium ($\boldsymbol{J_i}$ =0, $\boldsymbol{M_i}$ =0, q_{ve} =0 , q_{vm} =0) , the wave equations simplify to

$$\boldsymbol{\nabla^2 E} = \mu\sigma \frac{\partial \boldsymbol{E}}{\partial \mathrm{t}} + \mu\epsilon \frac{\partial^2 \boldsymbol{E}}{\partial \mathrm{t}^2} \qquad (\mathbf{11})$$

$$\boldsymbol{\nabla^2 H} = \mu\sigma \frac{\partial \boldsymbol{H}}{\partial \mathrm{t}} + \mu\epsilon \frac{\partial^2 \boldsymbol{H}}{\partial \mathrm{t}^2} \qquad (\mathbf{12})$$

For a source free and lossless medium ($\boldsymbol{J_i}$ =0, $\boldsymbol{M_i}$ =0, q_{ve} =0 , q_{vm} =0 , $\sigma = 0$) , the wave equations simplify to

$$\boldsymbol{\nabla^2 E} = \mu\epsilon \frac{\partial^2 \boldsymbol{E}}{\partial \mathrm{t}^2} \qquad (\mathbf{13})$$

$$\boldsymbol{\nabla^2 H} = \mu\epsilon \frac{\partial^2 \boldsymbol{H}}{\partial \mathrm{t}^2} \qquad (\mathbf{14})$$

For time harmonic fields involving time variations of the form $e^{j\omega t}$, we can use phasor transform to replace the derivative term $\frac{\partial}{\partial t}$ with $j\omega$. The equations (8) and (10) can then be written as follows

$$\boldsymbol{\nabla^2 E} = \boldsymbol{\nabla} \times \boldsymbol{M_i} + \mathrm{j}\omega\mu \boldsymbol{J_i} + \mathrm{j}\omega\mu\sigma \boldsymbol{E} - \omega^2 \mu\epsilon \boldsymbol{E} + \frac{\boldsymbol{\nabla} \mathrm{q}_{\mathrm{ve}}}{\epsilon} \qquad (\mathbf{15})$$

$$\boldsymbol{\nabla^2 H} = -\boldsymbol{\nabla} \times \boldsymbol{J_i} + \sigma \boldsymbol{M_i} + \frac{1}{\mu}[\boldsymbol{\nabla} q_{vm}] + j\omega\mu\sigma \boldsymbol{H} + j\omega\epsilon \boldsymbol{M_i} - \omega^2\mu\epsilon \boldsymbol{H} \quad (\mathbf{16})$$

For a source free medium ($\boldsymbol{J_i}$ =0, $\boldsymbol{M_i}$ =0, q_{ve} =0 , q_{vm} =0) , ($\mathbf{15}$) and ($\mathbf{16}$) simplify to

$$\boldsymbol{\nabla^2 E} = j\omega\mu\sigma \boldsymbol{E} - \omega^2\mu\epsilon \boldsymbol{E} \; = \psi^2 \boldsymbol{E} \qquad (\mathbf{17})$$

$$\boldsymbol{\nabla^2 H} = \; j\omega\mu\sigma \boldsymbol{H} - \omega^2\mu\epsilon \, \boldsymbol{H} = \psi^2 \boldsymbol{H} \qquad (\mathbf{18})$$

$$\psi^2 = j\omega\mu\sigma - \omega^2\mu\epsilon = j\omega\mu[\sigma + j\omega\epsilon]$$

Where ψ is called as the lossy propagation constant.

Since ψ is complex valued, we can write it in terms of its real and imaginary parts

$$\psi = \alpha + j\beta$$

α : Attenuation constant (Nepers/meter)

β : Phase constant (Radians/meter)

ψ : Lossy propagation constant

For a source free and lossless medium ($\boldsymbol{J_i}$ =0, $\boldsymbol{M_i}$ =0, q_{ve} =0 , q_{vm} =0 , $\sigma = 0$) , ($\mathbf{15}$) and ($\mathbf{16}$) simplify to

$$\boldsymbol{\nabla^2 E} = \; -\omega^2\mu\epsilon \, \boldsymbol{E} = -k^2 \boldsymbol{E} \qquad (\mathbf{19})$$

$$\boldsymbol{\nabla^2 H} = \; -\omega^2\mu\epsilon \, \boldsymbol{H} = -k^2 \boldsymbol{H} \qquad (\mathbf{20})$$

$$k = \pm\omega\sqrt{\mu\epsilon}$$

k : Propagation constant (Radians/meter)

3.2 Wave equation in PML (Perfectly Matched Layer) media

PML is an anisotropic, lossy medium that is used to terminate the computational region for computer memory consideration. It is commonly used in scattering and radiation problems to limit the size of the computational medium and to simulate the computational solution as if the computational medium size is infinity. This is achieved by adjusting the parameters of the PML media such that the outer reflections are minimized so that the computational solution tends to the actual analytical one.

Since PML is a lossy medium, the wave that enters the PML is completely absorbed after a certain depth which is related with the wavelength of the incident wave. Remembering the vector wave equations in lossy media and considering cartesian coordinates for analysis, we can write the scalar {x,y,z} components of the vector wave equations in a lossy medium as

$$\nabla^2 E_x(x,y,z) = j\omega\mu\sigma E_x(x,y,z) - \omega^2\mu\epsilon \, E_x(x,y,z) = \psi^2 E_x(x,y,z)$$

$$\nabla^2 E_y(x,y,z) = j\omega\mu\sigma E_y(x,y,z) - \omega^2\mu\epsilon\, E_y(x,y,z) = \psi^2 E_y(x,y,z)$$

$$\nabla^2 E_z(x,y,z) = j\omega\mu\sigma E_z(x,y,z) - \omega^2\mu\epsilon\, E_z(x,y,z) = \psi^2 E_z(x,y,z)$$

$$\nabla^2 H_x(x,y,z) = j\omega\mu\sigma H_x(x,y,z) - \omega^2\mu\epsilon\, H_x(x,y,z) = \psi^2 H_x(x,y,z)$$

$$\nabla^2 H_y(x,y,z) = j\omega\mu\sigma H_y(x,y,z) - \omega^2\mu\epsilon\, H_y(x,y,z) = \psi^2 H_y(x,y,z)$$

$$\nabla^2 H_z(x,y,z) = j\omega\mu\sigma H_z(x,y,z) - \omega^2\mu\epsilon\, H_z(x,y,z) = \psi^2 H_z(x,y,z)$$

Which can be coupled into their vector forms that are previously described, as follows

$$\boldsymbol{\nabla^2 E} = j\omega\mu\sigma \boldsymbol{E} - \omega^2\mu\epsilon \boldsymbol{E} \;\; = \psi^2 \boldsymbol{E}$$

$$\boldsymbol{\nabla^2 H} = \; j\omega\mu\sigma \boldsymbol{H} - \omega^2\mu\epsilon\, \boldsymbol{H} = \psi^2 \boldsymbol{H}$$

$$\psi^2 = j\omega\mu\sigma - \omega^2\mu\epsilon = j\omega\mu[\sigma + j\omega\epsilon]$$

$$\psi = \alpha + j\beta \quad (\psi : \text{Lossy propagation constant})$$

α : Attenuation constant (Nepers/meter)

β : Phase constant (Radians/meter)

The lossy and anisotropic nature of the PML dictates that its conductivity tensor must not be a scalar one. The conductivity tensor of the PML is a diagonal matrix with parameters σ_x , σ_y and σ_z , but the permeability (μ) and the permittivity (ϵ) of the PML medium are treated as scalars and must have appropriate values related with the electric and magnetic conductivities of the PML to ensure reflectionless transmission of the incident wave into the PML medium.

In a 3D PML, we have the following electric and magnetic conductivity tensors

$$\boldsymbol{\sigma} = \begin{bmatrix} \sigma_x & 0 & 0 \\ 0 & \sigma_y & 0 \\ 0 & 0 & \sigma_z \end{bmatrix} \quad , \quad \boldsymbol{\sigma^*} = \begin{bmatrix} \sigma_x{}^* & 0 & 0 \\ 0 & \sigma_y{}^* & 0 \\ 0 & 0 & \sigma_z{}^* \end{bmatrix}$$

In a 2D PML, these tensors are expressed as

$$\boldsymbol{\sigma} = \begin{bmatrix} \sigma_x & 0 \\ 0 & \sigma_y \end{bmatrix} \quad , \quad \boldsymbol{\sigma^*} = \begin{bmatrix} \sigma_x{}^* & 0 \\ 0 & \sigma_y{}^* \end{bmatrix}$$

We will deal with a 2D PML medium, therefore the 2×2 conductivity tensors will be our concern, but we must choose σ_x , $\sigma_y, \sigma_x{}^*, \sigma_y{}^*$ such that there are no reflections from the PML boundaries. In Berenger's journal [2] it is suggested that we must choose the values of the conductivities such that they satisfy the below relationships

$$\frac{\sigma_x}{\epsilon_0} = \frac{\sigma_x{}^*}{\mu_0} \quad , \quad \frac{\sigma_y}{\epsilon_0} = \frac{\sigma_y{}^*}{\mu_0} \quad , \quad \frac{\sigma_z}{\epsilon_0} = \frac{\sigma_z{}^*}{\mu_0}$$

Where ϵ_0 and μ_0 are the permittivity and permeability of free space respectively, assuming that the computational medium which is surrounded by the PML, is simply free space.

Using Maxwell's equations, we can derive the vector wave equations that are valid inside the PML medium, since the perfectly matched layer is an artificial medium that is created for absorbing the outgoing waves, inside the PML medium we have

$$\boldsymbol{J_i} = 0,\ \boldsymbol{M_i} = 0,\ q_{ve} = 0,\ q_{vm} = 0$$

The first two equations of Maxwell can be written here as

$$\boldsymbol{\nabla \times E} = -\boldsymbol{\sigma^*.H} - \mu\frac{\partial \boldsymbol{H}}{\partial t} \qquad (\mathbf{1})$$

$$\boldsymbol{\nabla \times H} = \boldsymbol{\sigma.E} + \epsilon\frac{\partial \boldsymbol{E}}{\partial t} \qquad (\mathbf{2})$$

Taking the curl of both sides of the equations we have

$$\boldsymbol{\nabla \times \nabla \times E} = -\boldsymbol{\nabla \times [\sigma^*.H]} - \mu\left[\boldsymbol{\nabla \times}\frac{\partial \boldsymbol{H}}{\partial t}\right] = -\boldsymbol{\nabla \times [\sigma^*.H]} - \mu\frac{\partial}{\partial t}[\boldsymbol{\nabla \times H}] \qquad (\mathbf{3})$$

$$\boldsymbol{\nabla \times \nabla \times H} = \boldsymbol{\nabla \times [\sigma.E]} + \epsilon\left[\boldsymbol{\nabla \times}\frac{\partial \boldsymbol{E}}{\partial t}\right] = \boldsymbol{\nabla \times [\sigma.E]} + \epsilon\frac{\partial}{\partial t}[\boldsymbol{\nabla \times E}] \qquad (\mathbf{4})$$

First let us deal with (3) to determine the wave equation for $\boldsymbol{E}$

$$\boldsymbol{\nabla \times \nabla \times F} = \boldsymbol{\nabla(\nabla.F)} - \boldsymbol{\nabla^2 F} \qquad (\mathbf{5})$$

$$\boldsymbol{\nabla^2 E} - \boldsymbol{\nabla(\nabla.E)} = \boldsymbol{\nabla \times [\sigma^*.H]} + \mu\frac{\partial}{\partial \mathrm{t}}[\boldsymbol{\nabla \times H}] \qquad (\mathbf{6})$$

Taking the phasor transform of (6) we get (7) as

$$\boldsymbol{\nabla^2 E} - \boldsymbol{\nabla(\nabla.E)} = \boldsymbol{\nabla \times [\sigma^*.H]} + j\omega\mu[\boldsymbol{\nabla \times H}] \qquad (\mathbf{7})$$

$$\boldsymbol{\nabla.D} = q_{ve} \quad , \quad \boldsymbol{\nabla.E} = \frac{q_{ve}}{\epsilon} \quad , \quad since\ q_{ve} = 0\ , \qquad \boldsymbol{\nabla.E} = 0 \quad , \quad thus$$

$$\boldsymbol{\nabla^2 E} = \boldsymbol{\nabla \times [\sigma^*.H]} + j\omega\mu[\boldsymbol{\nabla \times H}] \qquad (\mathbf{8})$$

Substituting (2) into (8) and using the vector identity , $\boldsymbol{\nabla \times [\sigma^*.H]} = \boldsymbol{[\nabla \times \sigma^*].H}$, we get

$$\boldsymbol{\nabla^2 E} = \boldsymbol{[\nabla \times \sigma^*].H} + j\omega\mu[\boldsymbol{\sigma.E} + j\omega\epsilon\mathbf{E}] \qquad (\mathbf{9})$$

$$\boldsymbol{\nabla \times \sigma^*} = \boldsymbol{a_x}\left(\frac{\partial {\sigma_y}^*}{\partial \mathrm{z}} - \frac{\partial {\sigma_z}^*}{\partial \mathrm{y}}\right) + \boldsymbol{a_y}\left(\frac{\partial {\sigma_z}^*}{\partial \mathrm{x}} - \frac{\partial {\sigma_x}^*}{\partial \mathrm{z}}\right) + \boldsymbol{a_z}\left(\frac{\partial {\sigma_x}^*}{\partial \mathrm{y}} - \frac{\partial {\sigma_y}^*}{\partial \mathrm{x}}\right) = 0 \qquad (\mathbf{10})$$

$$\text{since} \quad \frac{\partial {\sigma_y}^*}{\partial \mathrm{z}} = \frac{\partial {\sigma_z}^*}{\partial \mathrm{y}} = \frac{\partial {\sigma_z}^*}{\partial \mathrm{x}} = \frac{\partial {\sigma_x}^*}{\partial \mathrm{z}} = \frac{\partial {\sigma_x}^*}{\partial \mathrm{y}} = \frac{\partial {\sigma_y}^*}{\partial \mathrm{x}} = 0$$

$$\boldsymbol{\nabla^2 E} = j\omega\mu[\boldsymbol{\sigma.E} + j\omega\epsilon\mathbf{E}] \qquad (\mathbf{11})$$

$$\boldsymbol{\nabla^2 E} = [j\omega\mu\boldsymbol{\sigma} - \omega^2\mu\epsilon]\boldsymbol{.E} \qquad (\mathbf{12})$$

Equation 12 can be written in terms of its components as

$$\nabla^2 E_x(x,y,z) = \mathrm{j}\omega\mu\sigma_x E_x(x,y,z) - \omega^2\mu\epsilon\, E_x(x,y,z) = {\psi_x}^2 E_x(x,y,z)$$

$$\nabla^2 E_y(x,y,z) = j\omega\mu\sigma_y E_y(x,y,z) - \omega^2\mu\epsilon\, E_y(x,y,z) = \psi_y{}^2 E_y(x,y,z)$$

$$\nabla^2 E_z(x,y,z) = j\omega\mu\sigma_z E_z(x,y,z) - \omega^2\mu\epsilon\, E_z(x,y,z) = \psi_z{}^2 E_z(x,y,z)$$

Where the coefficients $\psi_x{}^2$, $\psi_y{}^2$, $\psi_z{}^2$ are the propagation constants along x, y and z directions respectively.

$$\psi_x{}^2 = j\omega\mu\sigma_x - \omega^2\mu\epsilon = \alpha_x + j\beta_x$$

$$\psi_y{}^2 = j\omega\mu\sigma_y - \omega^2\mu\epsilon = \alpha_y + j\beta_y$$

$$\psi_z{}^2 = j\omega\mu\sigma_z - \omega^2\mu\epsilon = \alpha_z + j\beta_z$$

An identical procedure is used to derive the wave equation for $\boldsymbol{H}$, therefore the wave equation for $\boldsymbol{H}$ has exactly the same form as (12). But instead of going through the same procedure to derive the wave equation for $\boldsymbol{H}$, one can use the principle of duality. The dual of (12) yields

$$\boldsymbol{\nabla^2 H} = [j\omega\epsilon\boldsymbol{\sigma}^* - \omega^2\mu\epsilon].\boldsymbol{H} \qquad (\mathbf{13})$$

Equation 13 can be written in terms of its components as

$$\nabla^2 H_x(x,y,z) = j\omega\mu\sigma_x{}^* H_x(x,y,z) - \omega^2\mu\epsilon\, H_x(x,y,z) = \psi^2{}_x{}^* H_x(x,y,z)$$

$$\nabla^2 H_y(x,y,z) = j\omega\mu\sigma_y{}^* H_y(x,y,z) - \omega^2\mu\epsilon\, H_y(x,y,z) = \psi^2{}_y{}^* H_y(x,y,z)$$

$$\nabla^2 H_z(x,y,z) = j\omega\mu\sigma_z{}^* H_z(x,y,z) - \omega^2\mu\epsilon\, H_z(x,y,z) = \psi^2{}_z{}^* H_z(x,y,z)$$

Where the coefficients $\psi^2{}_x{}^*$, $\psi^2{}_y{}^*$, $\psi^2{}_z{}^*$ are the propagation constants along x,y and z directions respectively.

$$\psi^2{}_x{}^* = j\omega\mu\sigma_x{}^* - \omega^2\mu\epsilon \;=\; \alpha_x{}^* + j\beta_x{}^*$$

$$\psi^2{}_y{}^* = j\omega\mu\sigma_y{}^* - \omega^2\mu\epsilon \;=\; \alpha_y{}^* + j\beta_y{}^*$$

$$\psi^2{}_z{}^* = j\omega\mu\sigma_z{}^* - \omega^2\mu\epsilon \;=\; \alpha_z{}^* + j\beta_z{}^*$$

The PML must have a certain depth to prevent outer reflections by attenuating the outgoing waves. The depth of the PML is related with the wavelength of the incident wave. As the depth of the PML increases, the accuracy of preventing outer reflections also increases, however increasing the depth of the PML also increases the required computer memory. Therefore appropriate lower and upper limits must be determined to effectively minimize outer layer reflections by using minimum amount of computer memory.

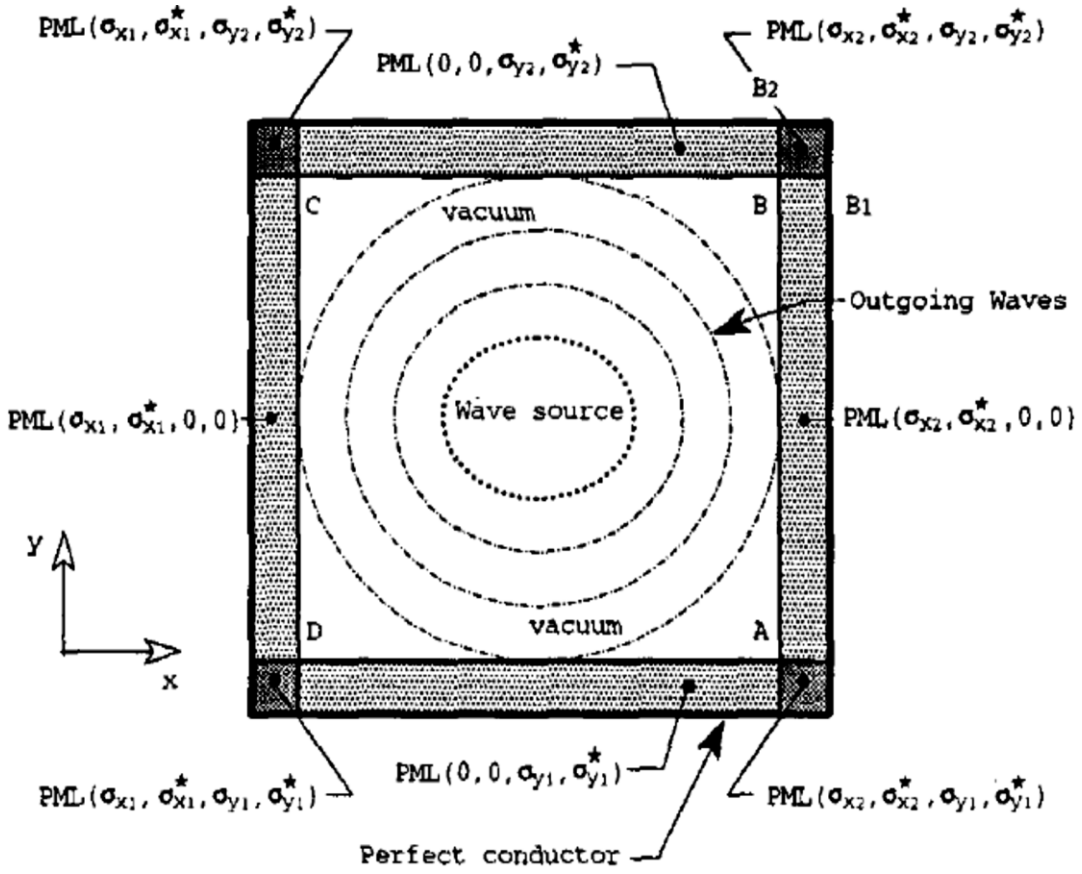

Figure3.1: Anisotropic structure of the PML [2]

Summary of the properties of PML

1) PML is a lossy medium with an associated conductance value in a given direction.

2) PML is an anisotropic medium, with a nonscalar conductivity tensor.

3) PML requires impedance matching with the computational media to prevent reflection.

4) PML requires a certain amount of depth to prevent outer reflections.

CHAPTER 4

MESH GENERATION

The finite element method requires the domain of interest to be discretized by a number of elements, the accuracy of the finite element method depends strongly on how accurately we have discretized the entire domain, i.e., the solution region. One of the biggest problems in the finite element method is to discretize the solution region accurately. The accuracy depends on the number of elements used and how accurately the discretized solution region resembles the actual solution region.

Since increasing the number of elements yields more accurate solutions, we generally require a large number of elements to discretize the region of interest. This requires a huge data preperation step for the geometry of the problem and for the elements in the solution region, since the coordinates of the boundary of the solution region and each of the elements must be given as inputs to the computer program. For problems requiring very accurate solutions we may have to use thousands of elements and for complex solution regions we may have to use even more. Thus manual data entry for domain discretization, which is usually called mesh generation, requires huge effort and too much time consumption and they are very likely to yield results with serious errors. That is why we come up with automatic mesh generation algorithms, which effectively, systematically and quickly discretize the region of interest to a specified number of elements. Using automatic mesh generation algorithms with different levels of automation we can greatly decrease the amount of necessary data entry to describe the problem at hand. Another big advantage is that since the process is now computer automized, calculation errors due to human imperfection become eliminated. Utilizing mesh generation algorithms with the modern tools of computer graphics, we can visualize the solutions of a given problem on a specified domain.

There are different mesh generation algorithms in literature. These mesh generation algorithms are created by considering the computational time efficiency and the complexity of the solution region. A difficulty arises when the solution region is not a rectangular, but an arbitrary solution region. Another problem in mesh generation is the computational time required to assemble each element in the solution region due to a large number of elements. Taking this fact into account, an optimization must be made between the number of elements used and the time spent for computation by checking the convergence of the computed solutions. Today's mesh generation programs use thousands of elements to discretize very complex domains involved in applications like structural analysis and electromagnetics in a very time efficient manner. Most basically computational time efficiency can be increased by efficient global node numbering and using an efficient element assembling algorithm as will be discussed later. We will consider here three basic mesh generation algorithms which involves

1) Mesh generation for rectangular regions.

2) Mesh generation for nonrectangular regions with curved boundaries.

3) Mesh refinement for computational accuracy.

The commonly used element for discretization is a triangle, since triangles easily fit to curved boundaries. Quadrilaterals can also be used for discretization, but since a quadrilateral can be split into two triangles and triangles fit better to curved boundaries, people prefer discretizing with triangles. Different types of elements (triangle, quadrilateral) can be used at the same solution region for discretization, but this will increase computational complexity. So, it is better to use only one type of element in a given solution region, which are usually triangles. Discretization requires that the elements must not overlap with each other.

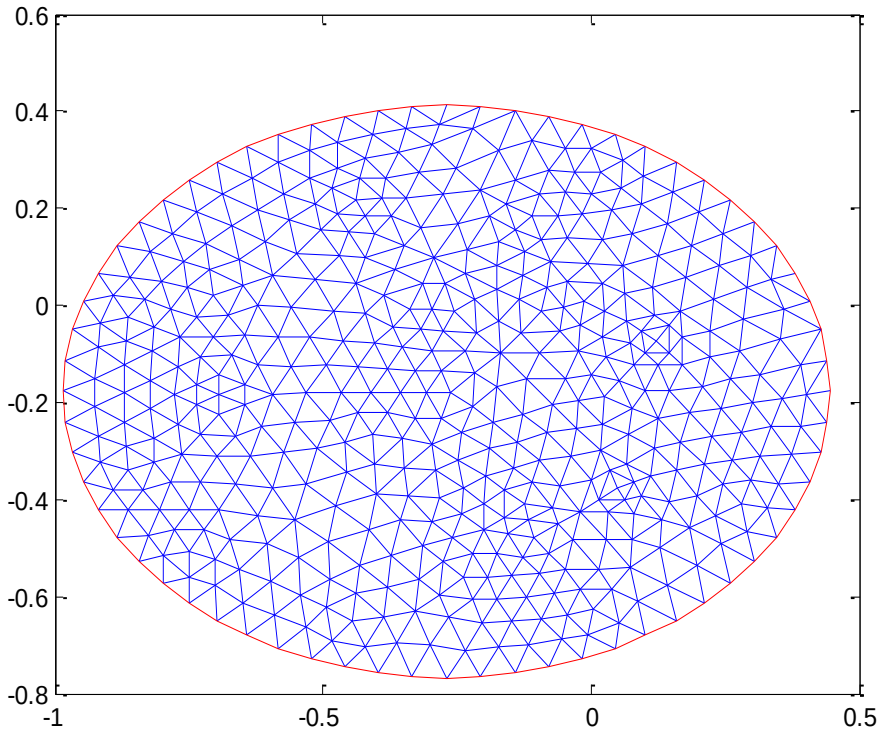

Figure 4.1 : Discretization of a region enclosed by a circle [3]

4.1 Mesh generation for rectangular domains

If we are dealing with a rectangular geometry of size a x b , the first thing to do is to divide the solution region into smaller rectangles, then these rectangles are divided into 2, each of which are triangular elements.The number of elements used in the solution region depends on how we divide the x and y directions. The more divisions we use in x and y directions, the more the number of elements becomes.

Assuming there are n_x divisions in the x axis and n_y divisions in the y axis,we find that there are 2 n_x n_y elements and $(n_x + 1)(n_y + 1)$ global nodes in the solution region.

Total number of elements = n_e= 2n_x n_y

Number of global nodes = n_d = (n_x + 1)($n_y + 1$)

Based on how we partition the rectangular geometry, we must determine an efficient algorithm for element and node numbering necessary for mesh generation, since the boundary is rectangular this is easy to do in a systematic way.

First we define two arrays containing the widths of each sub-rectangle along x and y directions as Δx_i and Δy_j where {i,j}={1,2,3,…,N}, here Δx_i indicates the distance between two global nodes that are adjacent to each other along the x direction, similarly Δy_j indicates the distance between two global nodes that are adjacent to each other along the y direction. After defining the arrays which contain the width information between global nodes along x and y directions, we start numbering the global nodes in a specified convention.The easiest convention is to number the nodes from left to right along the x axis, and from bottom to the top along the y axis. With this convention the global nodes and their x and y coordinates can be defined in a systematic way. An example 4x4 mesh with nonuniform spacing of the global nodes in both directions is shown in Figure 4.2 with the following specifications

Number of divisions along the x axis = n_x = 4

Number of divisions along the y axis = n_y = 4

Number of elements = 2 n_x n_y = 32

Number of global nodes = (n_x + 1)($n_y + 1$) = 25

Number of global nodes along the x axis = $n_x + 1 = 5$

Number of global nodes along the y axis = $n_y + 1 = 5$

Spacings between adjacent nodes along the x axis = Δx = {0.2 , 0.5 , 0.3 , 0.6}

Spacings between adjacent nodes along the y axis = Δy = {0.4 , 0.2 , 0.5 , 0.5}

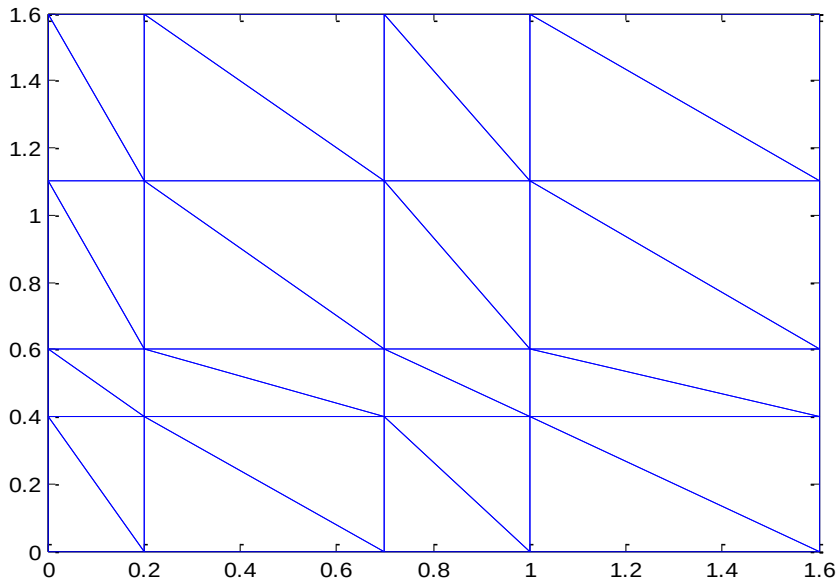

Figure 4.2 : Automatic mesh generation with nonuniform spacings

Using this convention, we can create rectangular meshes, both with uniform and nonuniform spacing of the global nodes. If the variable of interest varies very rapidly in some parts of the solution region, nonuniform spacing of the global nodes should be our preferance since we can narrowly space the global nodes in the specified part of the solution region such that there will be a larger number of elements in the specified region which will yield more accurate solutions. An example of such case is shown in Figure 4.3 assuming that there are rapid variations through the corners. If there are no rapid variations in the solution region , we can also use uniform spacing of the nodes such that $\Delta x_i = \Delta x$, $\Delta y_j = \Delta y$, {i , j}={1,2,3,…,N}.

An example 10x10 mesh with uniformly spaced nodes along the x and y axes is shown in Figure 4.4. In this example both Δx and Δy are equal to 1 and the node numbering convention is the same as before. Therefore the same formulas with the previous example apply. The spacings Δx and Δy can take different values other than 1 and Δx does not necessarily have to be equal to Δy for uniform spacing of the nodes.

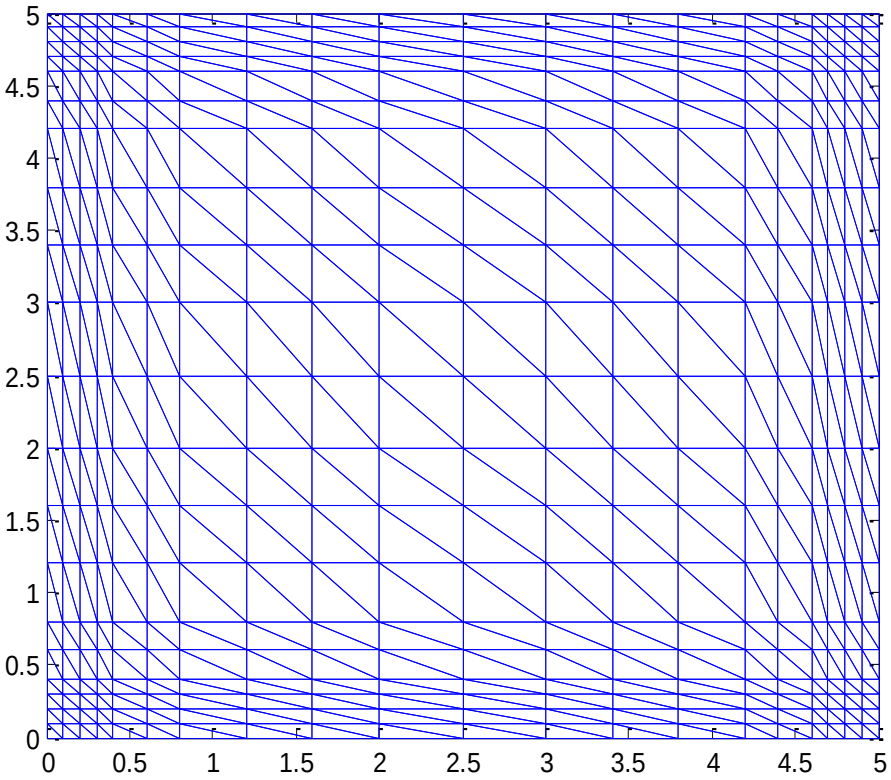

Figure4.3:Automatic mesh generation with nonuniform spacings

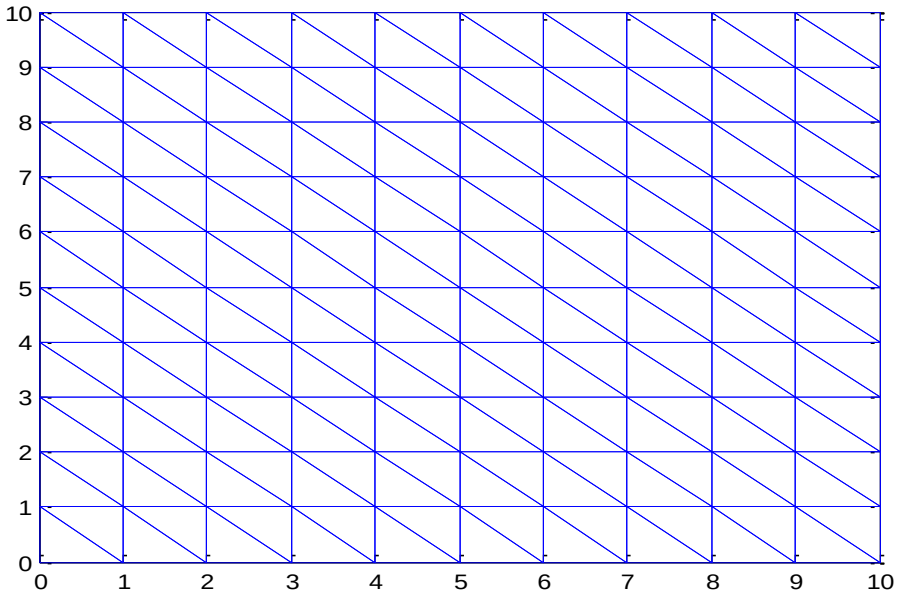

Figure4.4: Automatic mesh generation with uniform spacings

4.2 Mesh generation for regions with nonrectangular boundaries

When the boundary of the solution region is not rectangular, we need to determine a new systematic algorithm for discretizing the solution region. Since the boundary is now a curved boundary, we can discretize the solution region using quadrilaterals since quadrilaterals are efficient for approximating curved boundaries and they can be easily divided into triangles.

First we need to discretize the solution region very efficiently using quadrilaterals, we need to make sure that the approximate boundary formed by quadrilateral sides resembles the actual boundary of the solution region very well. When discretizing the solution region, another thing we must consider is to use minimum number of quadrilaterals in order to minimize the amount of input data. Note that here the only input data is the coordinates of the four corners of each quadrilateral. So the more quadrilaterals we use, the more input data we have to prepare manually. Instead we can use minimum amount of quadrilaterals for discretization, but we can develop an efficient mesh generation algorithm that discretizes each quadrilateral into a large number of triangles for accurate computation. So in this algorithm the solution region is discretized manually into a small number of quadrilaterals and each quadrilateral is automatically discretized into a large number of triangles.

So our task is to discretize a quadrilateral and to apply this idea to every quadrilateral in the solution region. We start with our simplest example of splitting a quadrilateral into four triangles as shown in Figure 4.5.

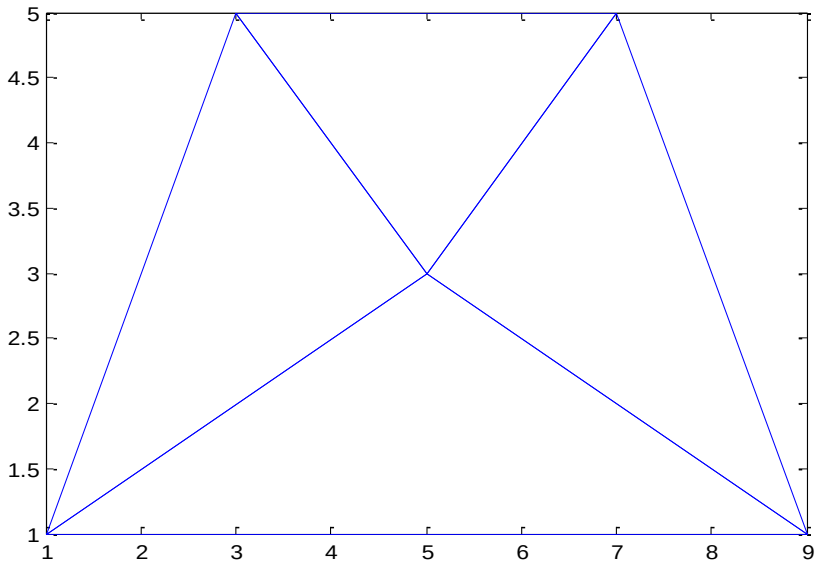

Figure4.5: Division of a quadrilateral into four triangles

To discretize a quadrilateral into a specified number of elements, there are a few ways. A good way is to define connection points or nodes on and inside the quadrilateral that are to be used to split the quadrilateral into sub-quadrilaterals.

Each sub-quadrilateral is then divided into four triangles as shown in figure, an example of a 2×2 division of a quadrilateral into four subquadrilaterals each with an inner connection point (node) is shown in Figure4.6.

Number of rows = $N_r = 2$

Number of columns = $N_c = 2$

Number of subquadrilaterals = $N_r\, N_c = 4$

Number of nodes = $(N_r + 1)(N_c + 1) + N_r\, N_c = 13$

Number of triangles in each subquadrilateral = $N = 4$

Total number of triangles = $N_r\, N_c\, N = 16$

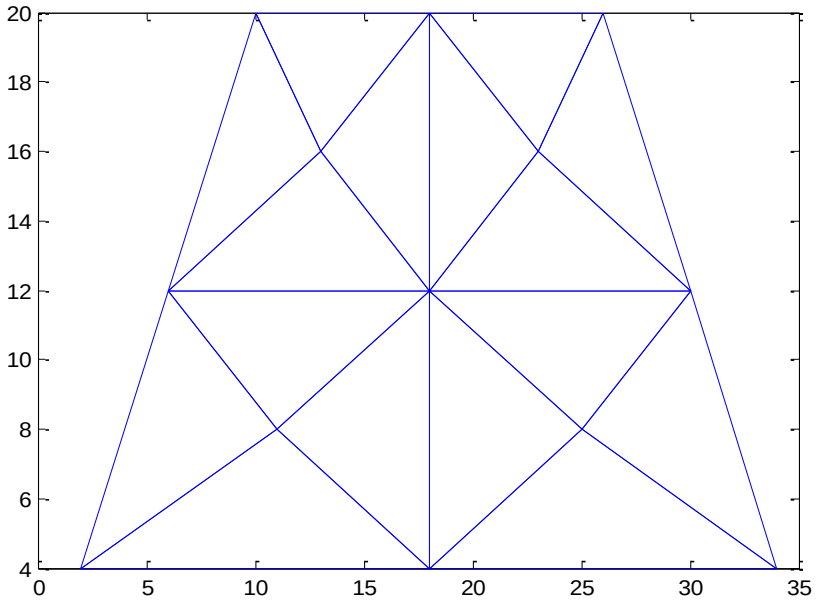

Figure4.6:Division of a quadrilateral into four subquadrilaterals

Similarly a 4× 4 division of a quadrilateral with a total number of 64 triangles (elements) and 41 nodes is shown in Figure4.7.

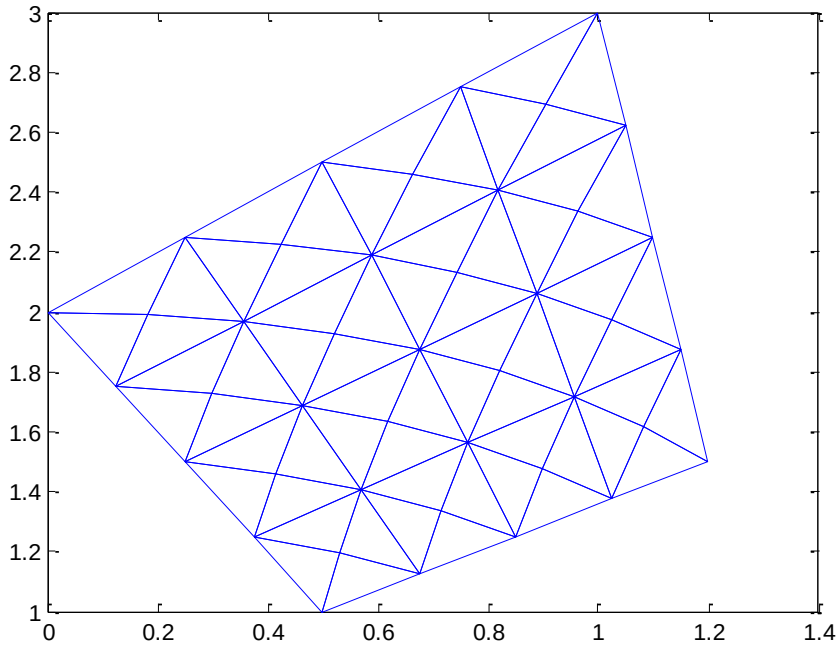

Figure4.7:Division of a quadrilateral into 16 subquadrilaterals

After determining a method for discretizing each quadrilateral in the solution region, it is up to a computer program that can systematically split each quadrilateral into triangles and manage connections between nodes after interconnecting each quadrilateral in the solution region. There are no limits for the maximum number of triangles that can be generated inside a quadrilateral. We can simply determine the total number of elements required to discretize a solution region that can yield the desired accuracy and split each quadrilateral accordingly. The computer program for a 4×4 division of a quadrilateral is given in the appendix part. Figures4.8 and 4.9 also show two regions with arbitrary boundaries which are discretized by quadrilaterals.

To increase the number of elements inside an $N \times N$ divided quadrilateral we can also use mesh refinement. A mesh refinement simply increases the overall number of triangles (elements) in a solution region. This can be accomplished in many different ways, here we achieve mesh refinement by splitting each triangle into a specified number of smaller triangles i.e the triangles inside each subquadrilateral is seperately splitted into smaller triangles to increase the number of total elements in the solution region for improved accuracy.

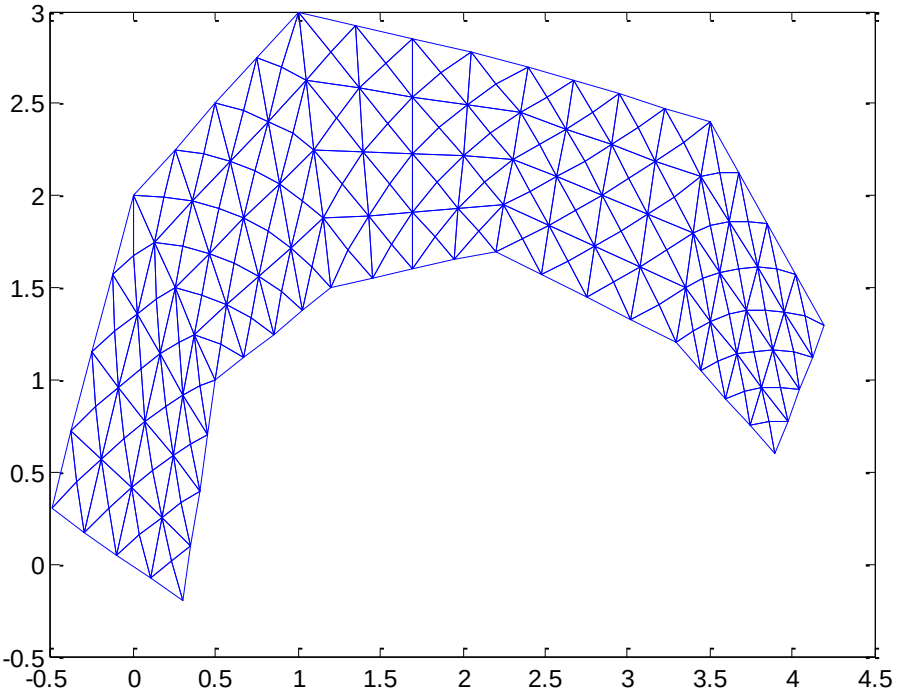

Figure4.8:Discretizing a region with an arbitrary boundary

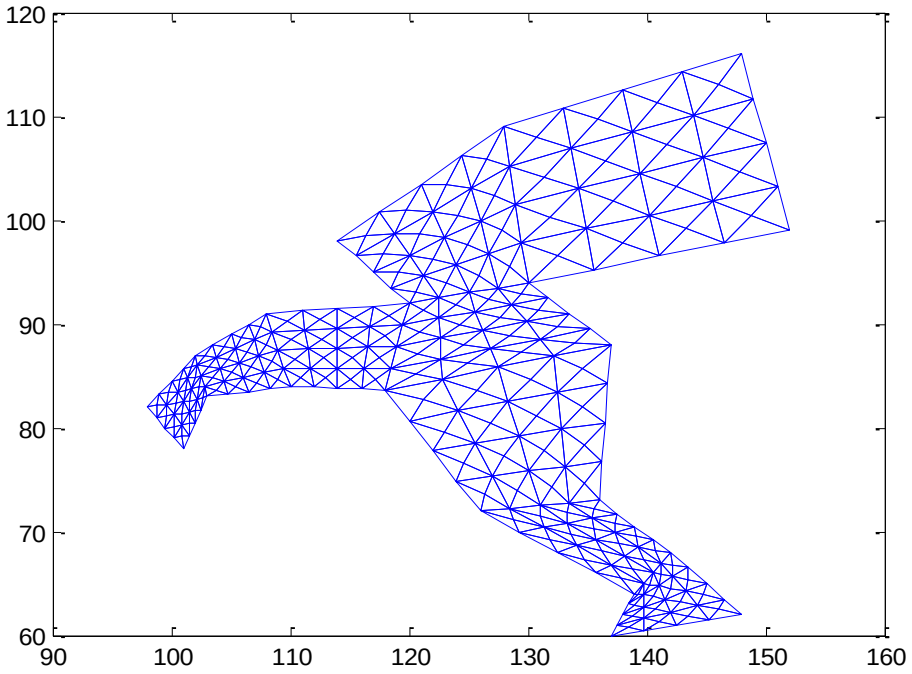

Figure4.9:Discretizing a region with an arbitrary boundary

4.3 Mesh refinement

Mesh refinement is generally used if the geometry of the solution region is complicated and irregular in size from one portion to another, or if the solution is expected to vary rapidly in some regions inside the overall solution region. In such regions where rapid changes occur we have to use more elements for accurate interpolation to the actual solution.

Mesh refinement can be achieved either by increasing the order of each element from 1 to a higher value, or, by simply dividing each element into smaller elements thereby increasing the total number of elements.

Increasing the order of each element means increasing the order of the interpolating polynomial by defining more nodes on each element, therefore interpolating the actual solution by a higher order interpolation function, which increases accuracy. But here we will simply divide each element into smaller elements by following a certain convention.

We can divide a triangular element into as much elements as we want to split a triangle into sub-triangles. We define a certain amount of nodes on each triangle according to the number of smaller triangles that we want to produce. The discretization of each triangle is shown in Figures 4.10, 4.11 and 4.12 each with a different discretization order N.

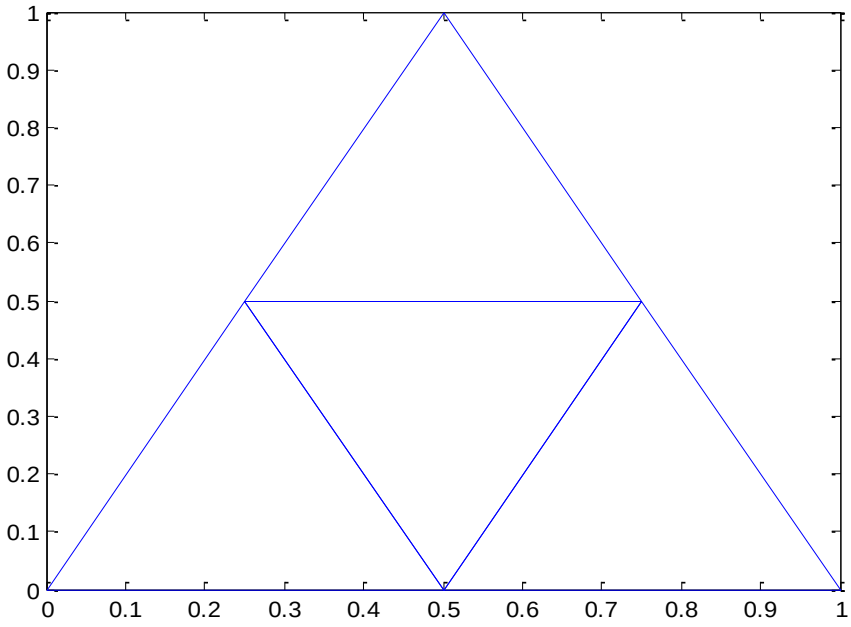

Figure 4.10: Discretization of a triangle into subtriangles, N=2

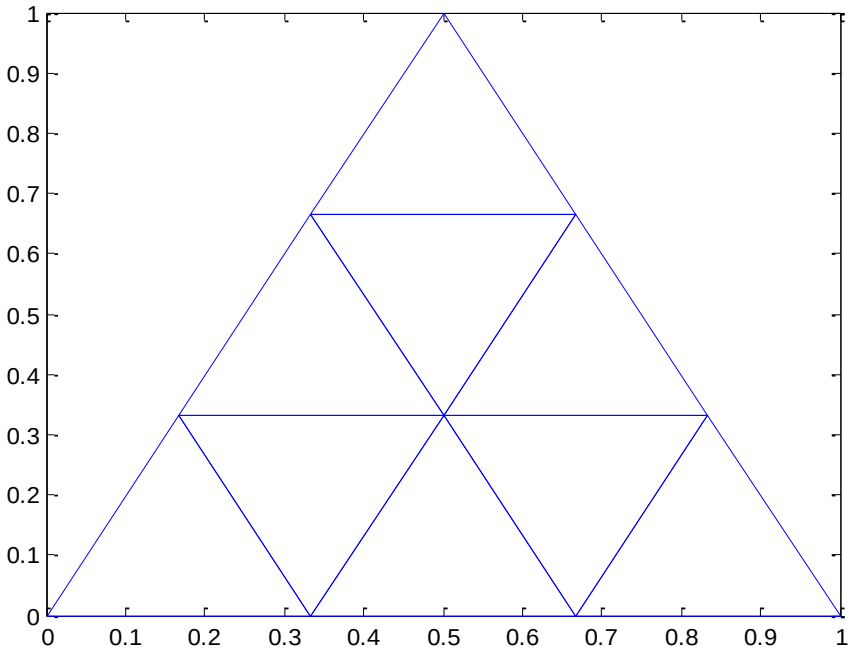

Figure 4.11:Discretization of a triangle into subtriangles, N=3

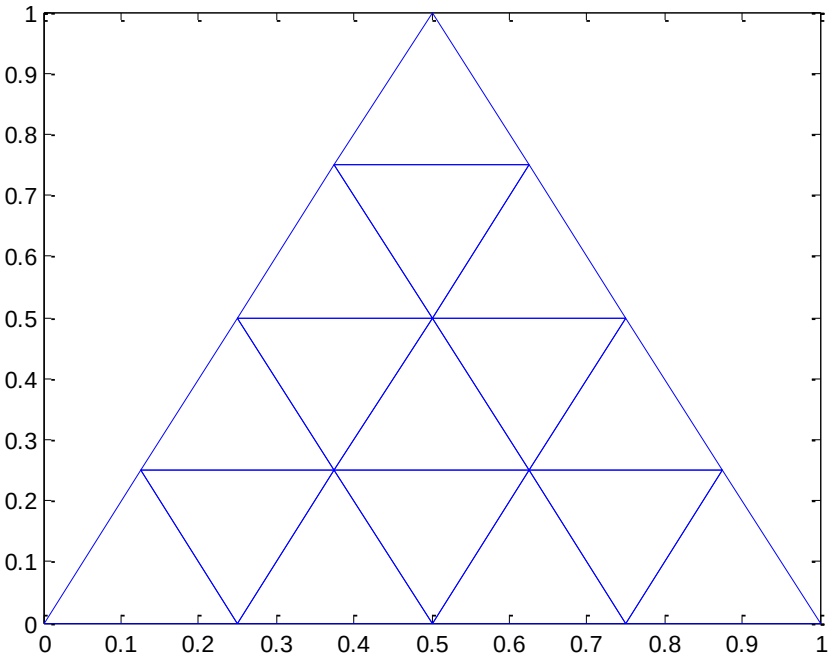

Figure4.12:Discretization of a triangle into subtriangles, N=4

Discretization Order	Number Of Nodes	Number Of Elements
1	3	1
2	6	4
3	10	9
4	15	16
5	21	25
6	28	36
.	.	.
.	.	.
.	.	.

To refine a generated mesh, we split each triangle in the original mesh to smaller triangles using a specified discretization order. As an example we can discretize each element of the geometry given in Figure 4.8 using a discretization order of N=4 as shown in Figure 4.13.

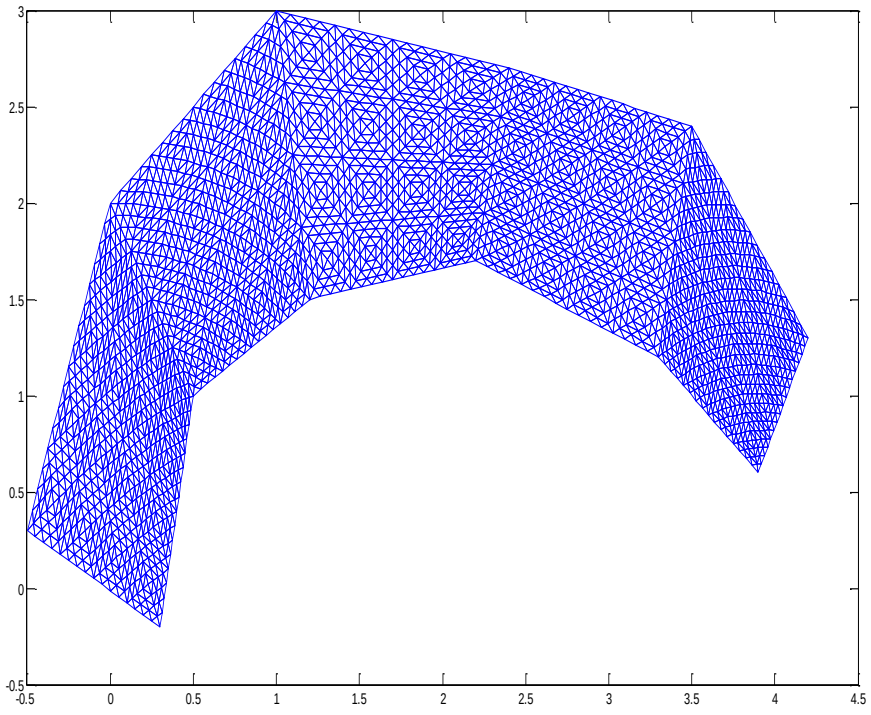

Figure4.13: Refined mesh for the geometry given in figure4.8

4.4 Generating Gaussian rough surfaces

A rough surface S, where S=h(x) , can be modeled by considering its height as a random variable with a certain mean and variance. In this sense generating rough surfaces can be thought as generating a random sequence with h representing the value of height at a certain location x, where x denotes the location of the surface height on an one-dimensional axis. Rough surfaces can be realistically modelled as Gaussian random sequences, i.e., with a Gaussian distributed h(x). Here h(x) is a Gaussian random sequence since for each discrete value of x=$\{x_1, x_2,\ldots, x_N\}$, we have a Gaussian distributed probability density function p(h(x_i)). Mathematically, " h " has the following probability density function

p(h) = $\frac{1}{\sqrt{2\pi}\sigma}$ exp($-\frac{(h-\mu)^2}{2\sigma^2}$) , where

h is the value of the surface height,

σ is the standard deviation of the distribution,

μ is the mean value of the distribution.

At each location of the surface corresponding to x_i , i=1,2, … ,N , we have a different value of height h_i . This is because the Gaussian probability density function for each random variable h_i , p(h_i) will generate different values of h_i at each computation. If we sample N locations x_i on an one-dimensional axis, the corresponding h_i on that axis for each x_i will be h(x_i) = h_i . So we can model rough surfaces as vectors of random variables

$$h=\begin{bmatrix} h_1 \\ h_2 \\ h_3 \\ . \\ . \\ . \\ h_N \end{bmatrix}$$

In order to generate an accurate Gaussian rough surface, we have to simulate an accurate Gaussian random number generator. There are various methods for generating random numbers from a specified distribution. Here we will use " The Rejection Sampling" method, since it is a simple and a powerful technique. In this method, we start with the two random variables R_1 and R_2 which are uniformly distributed on the interval (0,1).

$R_1 \sim U(0,1)$, $R_2 \sim U(0,1)$

where the sign ~ denotes distribution, and $U(0,1)$ denotes uniform distribution on the interval (0,1).

Our aim is to simulate a random variable with a desired probability distribution p(x) on a given interval a$\leq x \leq b$. In addition, we create another two uniformly distributed random variables C_1 and C_2 which depend on R_1 and R_2 as

$C_1 = a + (b - a)R_1$, $C_2 = \max\{p(x)\}R_2$

$C_1 \sim U(a, b)$, $C_2 \sim U(0, \max\{p(x)\})$

The algorithm accepts those values of C_1 as samples of the probability distribution p(x) , which satisfy the inequality

$C_2 \leq p(C_1)$

and those do not, are rejected. Basically in the rejection sampling technique, the values of C_2 that lie above the curve of the desired probability distribution are rejected, and the ones that are on or below the curve of the desired distribution are accepted as samples of the desired distribution.

Figures 4.14 to 4.16 show a Gaussian random process h(x) with x_i , $i = 1, \ldots, 100$, having a mean of μ= 0.5 and standard deviations of σ= {0.05, 0.1, 0.15} respectively that are generated using the rejection sampling method.

Here h(x_i)= h_i , and , p(h_i) = $\frac{1}{\sqrt{2\pi}\sigma}$ exp(−$\frac{(h_i-\mu)^2}{2\sigma^2}$) , i=1,2,…,100

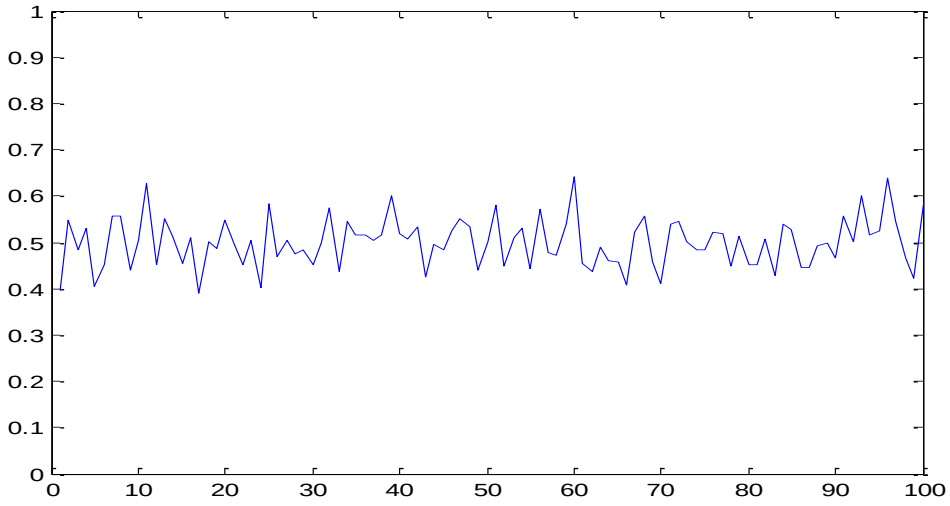

Figure 4.14:Gaussian random process with μ= 0.5 and σ= 0.05

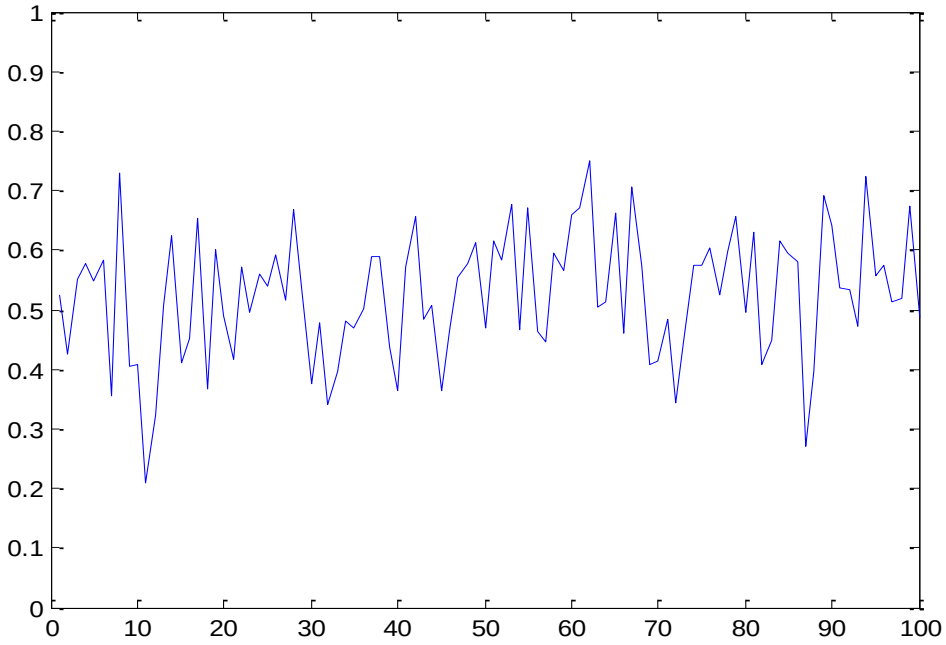

Figure4.15:Gaussian random process with μ= 0.5 and σ= 0.10

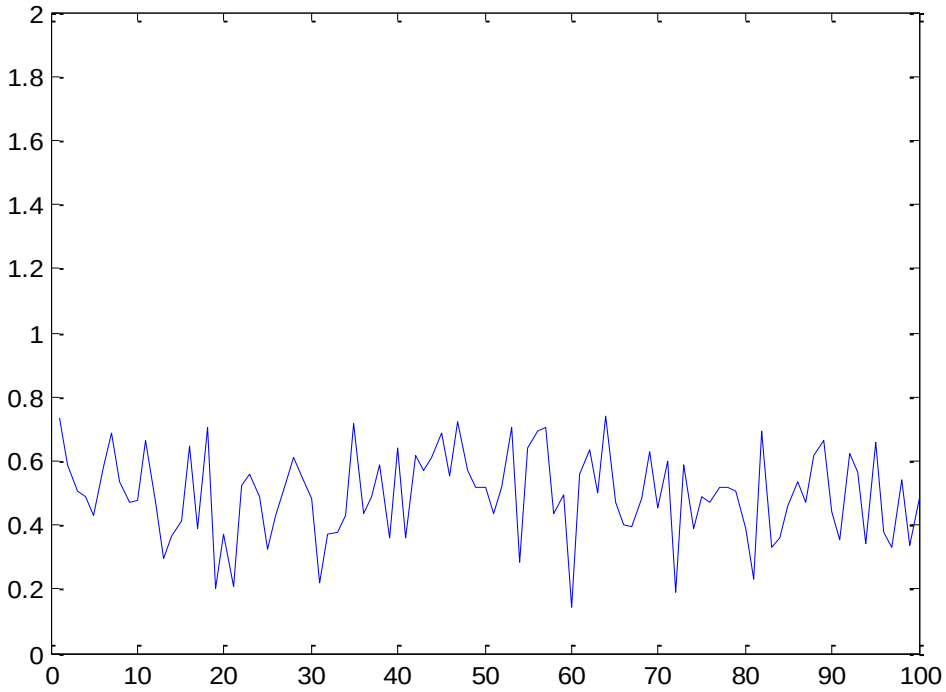

Figure4.16:Gaussian random process with μ= 0.5 and σ= 0.15

A question that arises is how exactly does the generated sequence behaves like Gaussian? We need to verify that the generated sequence has a Gaussian distribution. A basic and accurate method for classifying the resulting distribution of the generated sequence h is to group the samples according to their amplitudes. This is achieved by splitting the total amplitude range into a number of subranges of amplitudes. A couple of examples are shown below for different sequences with the following properties

N= Number of samples generated in the sequence

h = Amplitude of the samples in the sequence

$N_s =$ Number of amplitude subranges

Sequence 1 : μ=0.5, σ=0.1, N=1000 , N_s=10, h ~ [0.2,0.8]

Interval 1: $0.20 \leq h \leq 0.26$	Number of samples=0
Interval 2: $0.26 < h \leq 0.32$	Number of samples=0
Interval 3: $0.32 < h \leq 0.38$	Number of samples=8
Interval 4: $0.38 < h \leq 0.44$	Number of samples=66
Interval 5: $0.44 < h \leq 0.50$	Number of samples=253
Interval 6: $0.50 < h \leq 0.56$	Number of samples=335
Interval 7: $0.56 < h \leq 0.62$	Number of samples=257
Interval 8: $0.62 < h \leq 0.68$	Number of samples=74
Interval 9: $0.68 < h \leq 0.74$	Number of samples=7
Interval 10: $0.74 < h \leq 0.80$	Number of samples=0

Figure 4.17 shows the resulting distribution for sequence 1. The distribution somewhat resembles a Gaussian, but in order to improve the accuracy of approximation to a perfect Gaussian, the number of used sub-intervals must be increased.

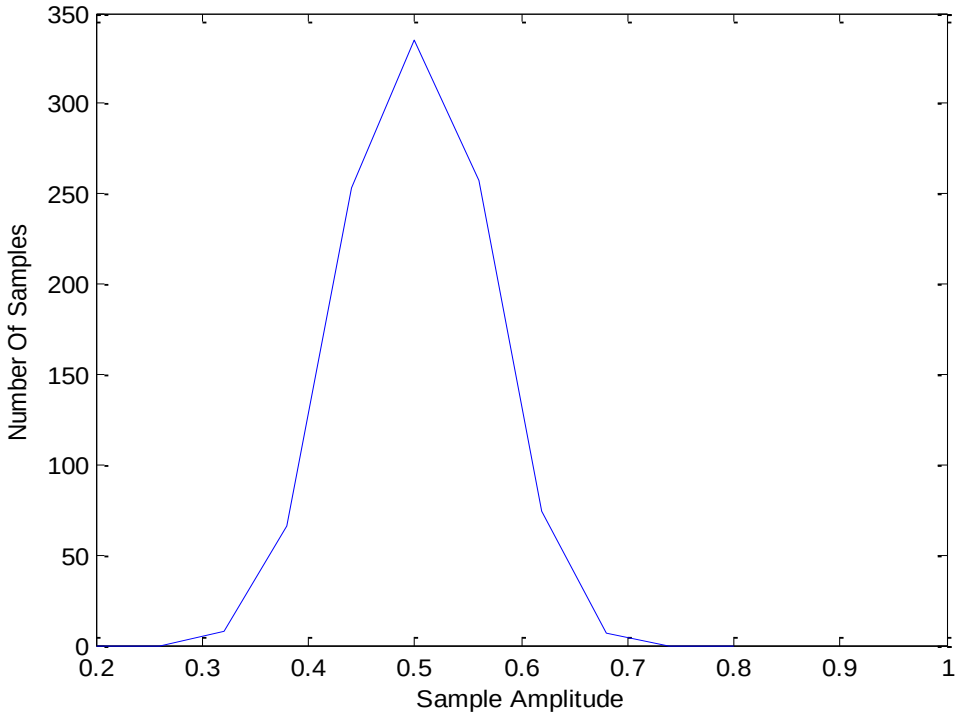

Figure4.17:The resulting distribution for sequence 1

Sequence 2 : μ=0.5, σ=0.1, N=10000 , N_s=20, h ~ [0.2,0.8]

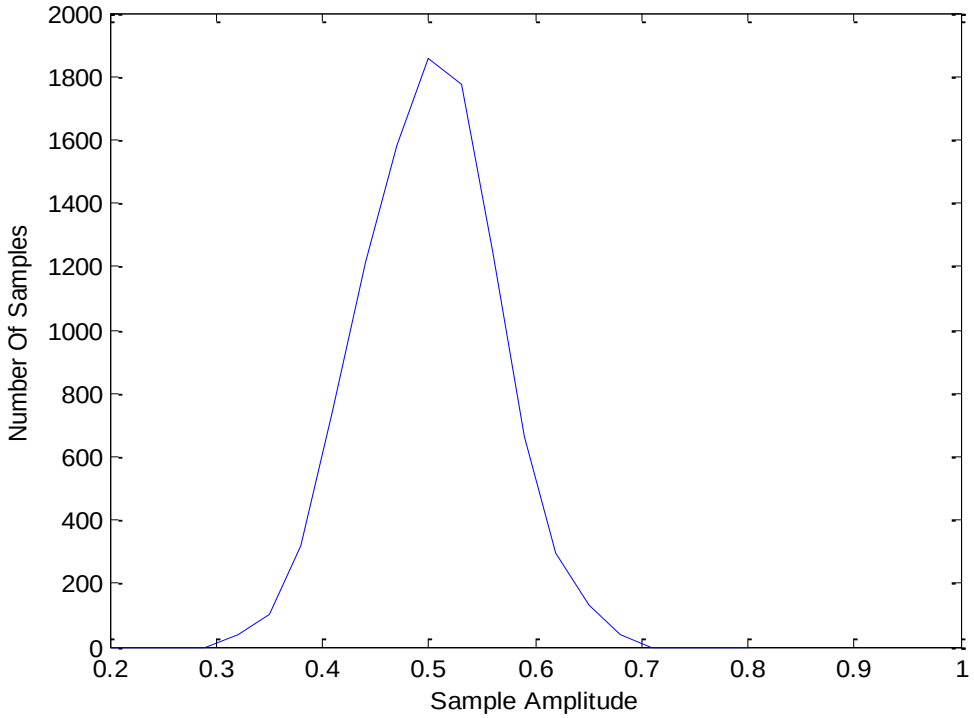

Figure4.18:The resulting distribution for sequence 2

Sequence 3 : μ=0.5, σ=0.1, N=10000 , N_s=100, h ~ [0.2,0.8]

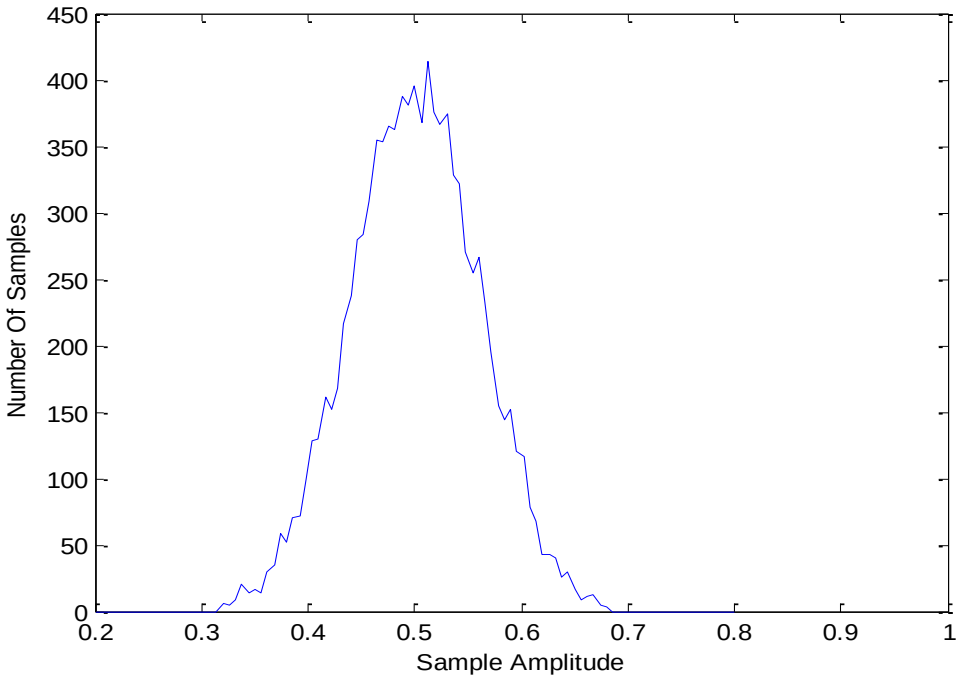

Figure4.19:The resulting distribution for sequence 3

Sequence 4 : μ=0.5 , σ=0.1, N=100000 , N_s=100, h ~ [0.2,0.8]

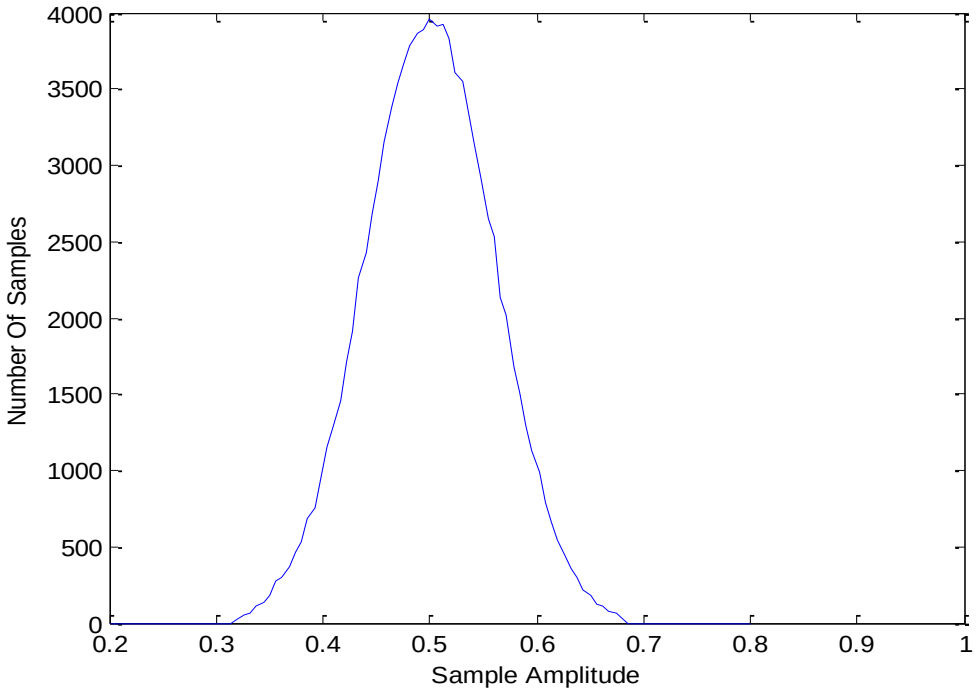

Figure4.20:The resulting distribution for sequence 4

4.5 Mesh generation for analyzing rough surface scattering problem

If we are analyzing a rough surface scattering problem, we should be careful when triangulating the region around the rough surface. Rough surface scattering problems can be analyzed in regions with a rectangular outer PML boundary. Therefore the previously described automatic mesh generation algorithm for rectangular domains can be used to triangulate the solution region, except the region near the rough surface since the rough surface has an irregular curvature due to its statistical property of having a Gaussian distribution with a certain mean and standard deviation. That is why we need a seperate triangulation around the rough surface and the rest of the solution region can be triangulated identically the same as the previous description of automatic mesh generation for rectangular regions. In order to seperate the two regions as the region around the rough surface and the rectangular solution region which is the complement of the region around the rough surface to the overall solution region, we call the region around the rough surface as the "near-surface" region and the remaining part as the "complement region" and we use an upper limit for the upper boundary of the near-surface region which is determined according to the mean and the standard deviation value of the rough surface height.

If we know the variance of the distribution of surface height, then we know that the range of the surface height (h) lies symmetrically within 3 standard deviations (σ) from the mean value (μ) as shown in Figure 4.21.

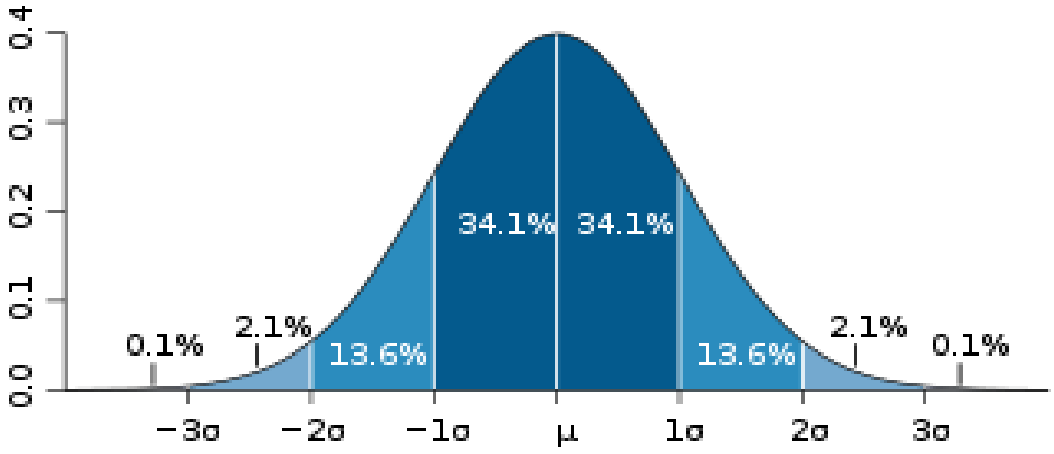

Figure4.21: $\mu - 3\sigma \leq h \leq \mu + 3\sigma$ [4]

Therefore, if we insert the upper limit at a little bit more than a 3σ distance from the mean value, then the near-surface region can fully contain the rough surface with the given mean and variance. Another important issue is the triangulation inside the near-surface region. Since the near-surface region contains the rough surface, we have to triangulate the region between the upper boundary and the rough surface. The problem here is that some triangles between the boundary and the rough surface may become very narrow or much smaller in size compared to other triangles due to abrupt changes in the height of the rough surface. To avoid this problem we have to set the limit of the near-surface region to a higher value than 3σ. Note that there is no certain deviation value from the mean value of the surface height to the upper limit, since the process is probabilistic, the surface height can take any

value. However the probability that the surface height may exceed a deviation of 3σ from the mean value is very small, therefore inserting the limit to a distance that is greater than 3σ will usually result in more accurate triangulation with a lower probability of turning out ill conditioned results. As we increase the limit from 3σ to higher values we get better results and the probability of getting ill conditioned results becomes smaller.

The overall solution region is terminated with an artificial absorbing medium that is called " PML" and is commonly used as an absorbing boundary condition in scattering or radiation problems to limit the use of computer memory to a specified amount and to effectively simulate the solution region to infinity by minimizing reflections from the outer boundary. PML was discussed in detail in its own section in the previous chapter, but here it is enough to know that PML surrounds the computational (solution) region and has a specified thickness required for termination of the solution region in order to be used as an artificial boundary. The thickness of the PML depends on the electrical characteristics of the impinging wave and the solution region of interest.

The PML is a lossy medium which attenuates the incident wave with a rate that depends on the conductivity value of the medium as described by Berenger [2]. Usually the attenuation of the incident wave is very rapid. Therefore we should use smaller triangles with narrower widths when discretizing the PML medium to handle rapid changes and to yield accurate results. The size of the total mesh depends on the size of the solution region that we have determined to analyze the scattering or radiation problem at hand and also the size of the PML region necessary for terminating the solution region in order to minimize reflections.

Figures 4.22 to 4.28 show some example meshes with rough surfaces having different mean and standard deviation values. The upper limits for rough surfaces is determined in conjunction with their statistical properties. Notice that the solution region in Figure 4.28 is discretized using more elements, and increasing the number of elements sharply increases the accuracy of computation.

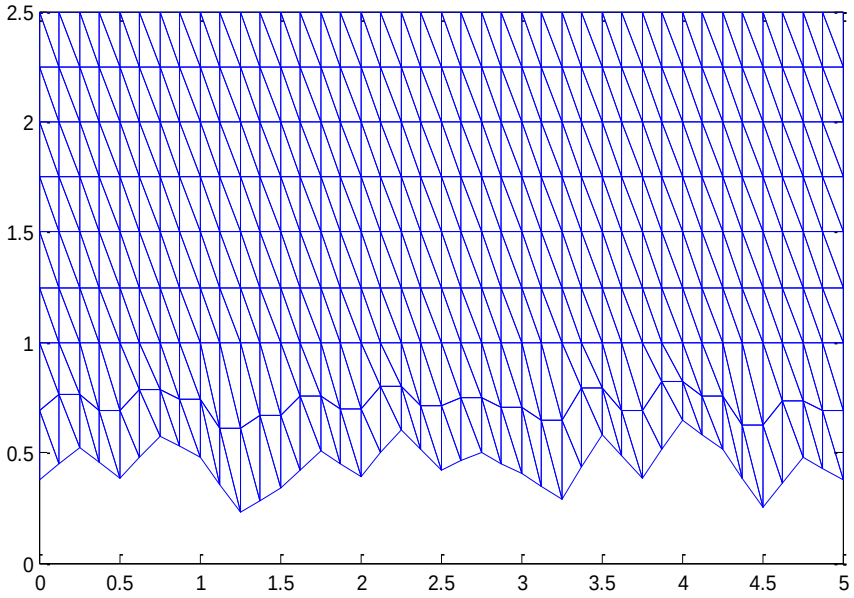

Figure4.22:Rough surface with std=0.15, mean=0.5, upper limit=1

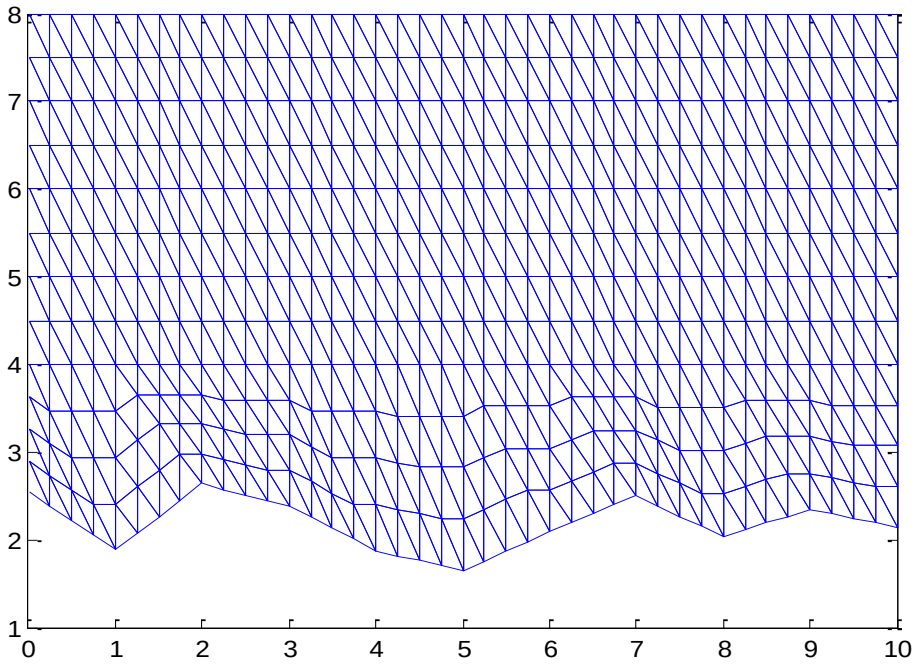

Figure4.23:Rough surface with std=0.5, mean=2, upper limit=4

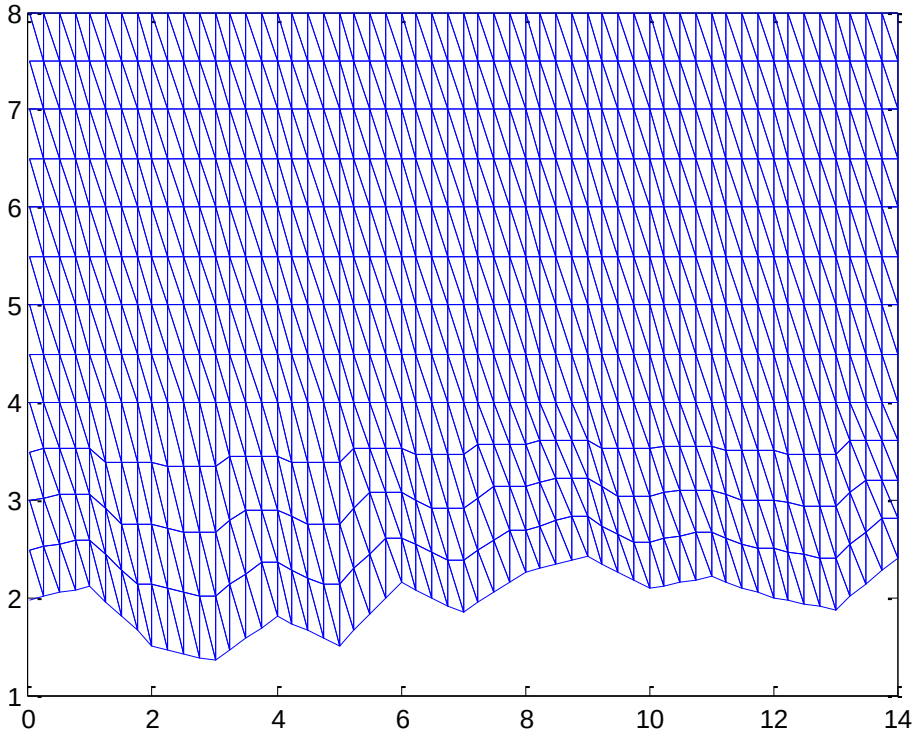

Figure4.24:Rough surface with std=0.3, mean=2, upper limit=4

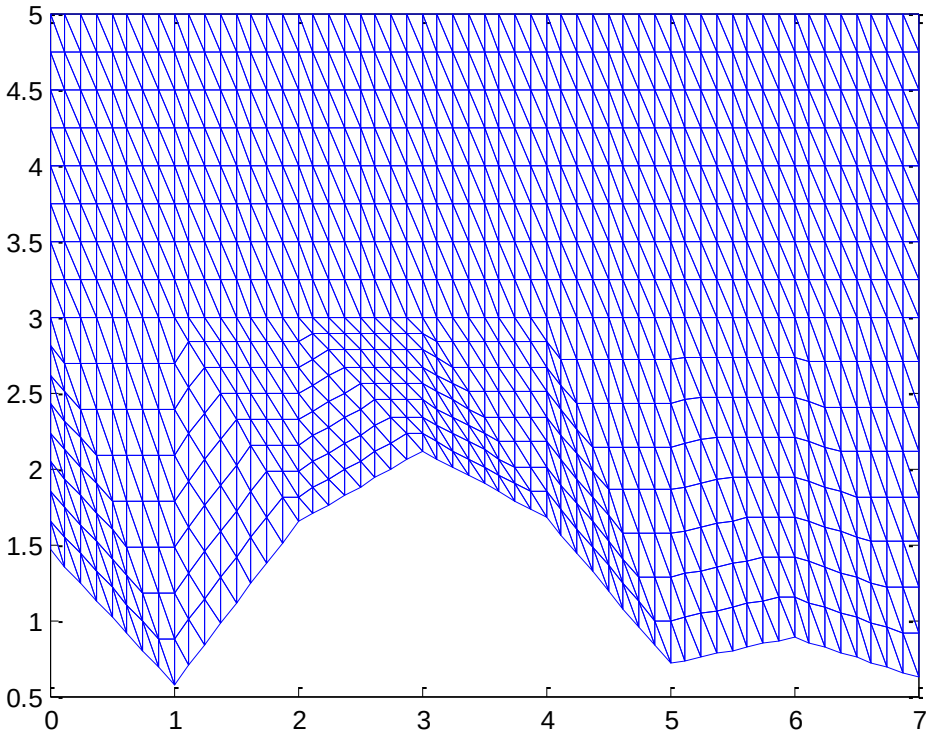

Figure4.25:Rough surface with std=0.4, mean=1.5, upper limit=3

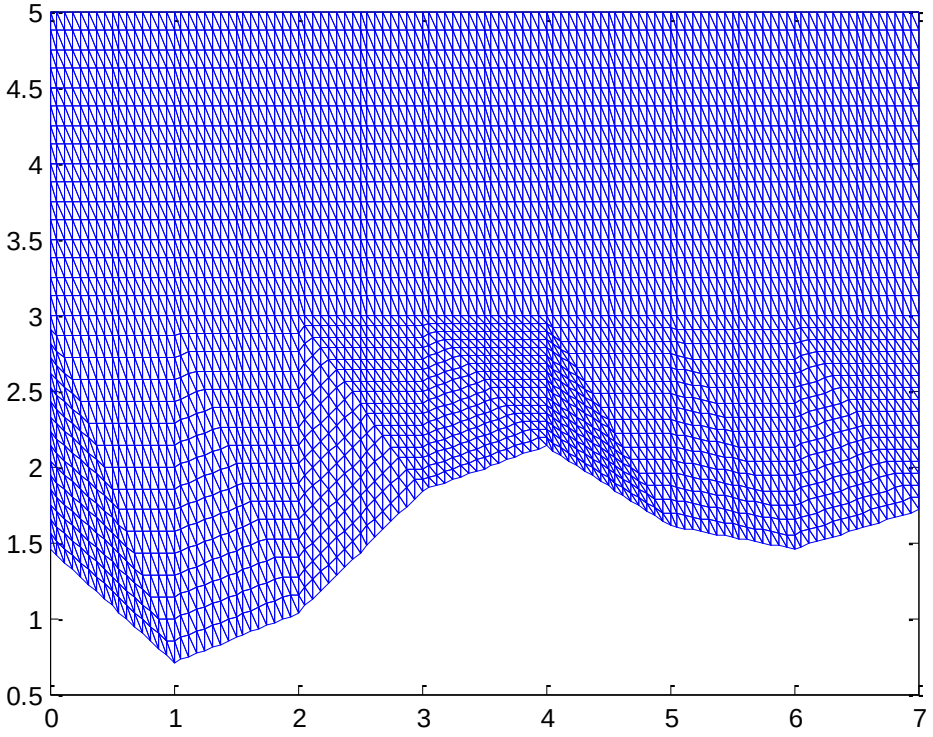

Figure4.26:Rough surface with std=0.4, mean=1.5, upper limit=3

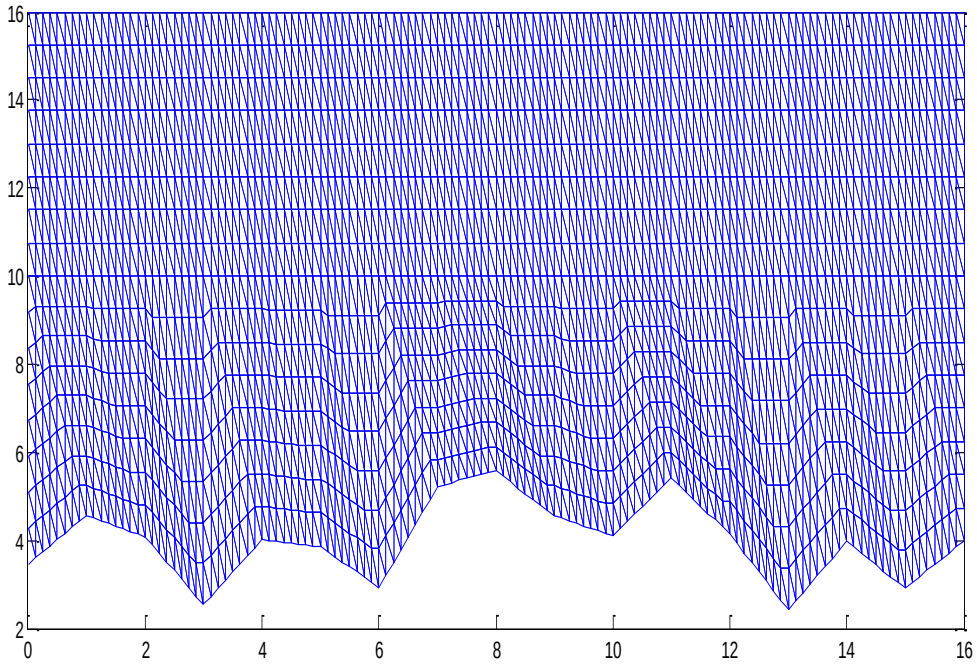

Figure4.27:Rough surface with std=1, mean=4, upper limit=10

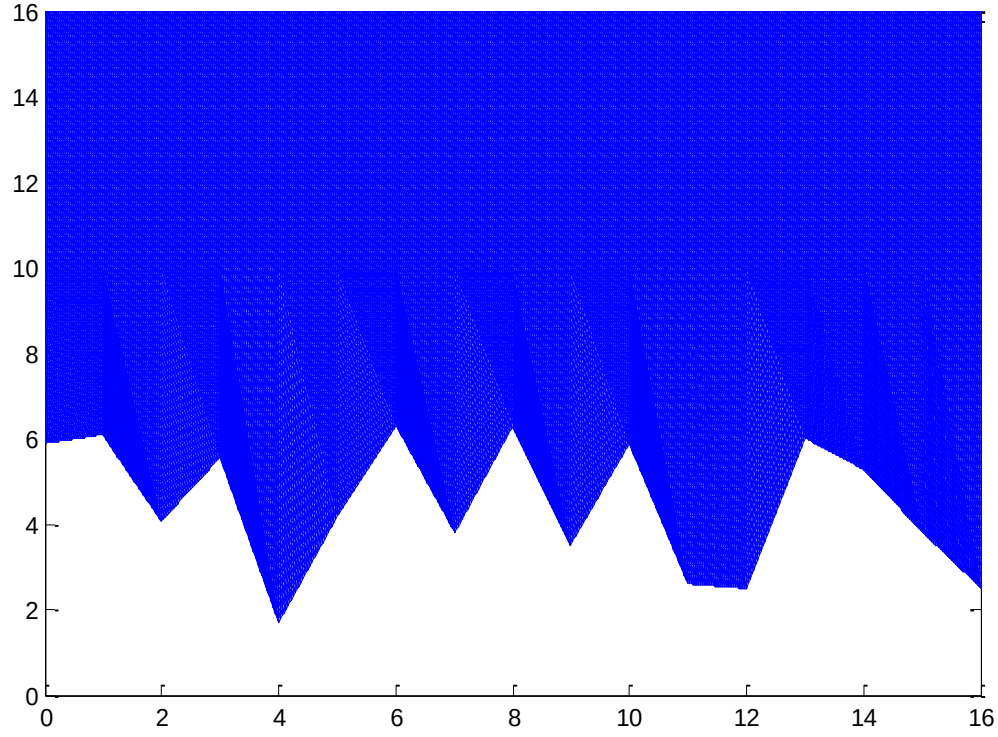

Figure4.28:Rough surface with std=1.5, mean=4, upper limit=10

CHAPTER 5

BASICS OF THE TWO DIMENSIONAL FINITE ELEMENT METHOD

In order to use the finite element method for solving a partial differential equation (PDE) , we first have to convert the PDE of interest into its functional or variational form. To convert a PDE into its functional form, we use the theory of calculus of variations which focuses on the theory of extreme values of functionals. A functional is obtained by an operator that operates on a function that is composed of one or more functions within certain limits. Given the values of the independent variables to determine the output of the function inside the operator, the output of a functional is a number which depends on the form of the function inside the operator, and the form of the operator as well. The output of a function depends only on the values of the independent variables.

Here we will deal with integral operators with certain limits that operate on a function. Our aim is to determine the extreme values of the functional and the function that yields these extreme values. The following discussion, up to section 5.3, is mostly referenced from [5].

Consider the functional $\psi(v)$ given below

$$\psi(v) = \int_{u_1}^{u_2} \xi(u, v, v')\ du$$

Here u is the independent variable and $v(u)$ is a function of u. Our goal is to find a function $v(u)$ that extremizes the functional $\psi(v)$ along with the boundary conditions

$$v(u_1) = U_1\ ,\ v(u_2) = U_2$$

The integrand $\xi(u, v, v')$ is a function with the independent variable u , the dependent variable v and its derivative v' . Here $\psi(v)$ is called a functional, or variational to be extremized.

The variational operator δ is used to calculate the variation of a given function. In our example, the variation δv of the function $v(u)$ is the infinitesimal change in v for a fixed value of u where δu=0. The variation δv of v vanishes at points where v is prescribed, since the prescribed value can not be varied, and it can take any value at points where it is not prescribed.

Since the integrand $\xi(u, v, v')$ is a function of v , a change in v as δv will result in a change in ξ which is $\delta\xi$. Recalling the total differential of ξ which is

$$d\xi = \frac{\partial \xi}{\partial u} du + \frac{\partial \xi}{\partial v} dv + \frac{\partial \xi}{\partial v'} dv'$$

We can write the first variation of ξ at v as

$$\delta\xi = \frac{\partial \xi}{\partial u}\delta u + \frac{\partial \xi}{\partial v}\delta v + \frac{\partial \xi}{\partial v'}\delta v'$$

We know that $\delta u = 0$ since u does not change as v changes to $v + \delta v$, $\delta\xi$ becomes

$$\delta\xi = \frac{\partial \xi}{\partial v}\delta v + \frac{\partial \xi}{\partial v'}\delta v'$$

If the functional depends on second or higher order derivatives as shown

$$\psi(v) = \int_{u_1}^{u_2} \xi(u, v, v', v'', \ldots., v^{(n)})\ du$$

Then the total differential and the first variational of ξ are respectively

$$d\xi = \frac{\partial \xi}{\partial u}du + \frac{\partial \xi}{\partial v}dv + \frac{\partial \xi}{\partial v'}dv' + \frac{\partial \xi}{\partial v''}dv'' + \cdots + \frac{\partial \xi}{\partial v^{(n)}}dv^{(n)}$$

$$\delta\xi = \frac{\partial \xi}{\partial v}\delta v + \frac{\partial \xi}{\partial v'}\delta v' + \frac{\partial \xi}{\partial v''}\delta v'' + \cdots + \frac{\partial \xi}{\partial v^{(n)}}\delta v^{(n)}$$

Thus the variational operator δ behaves like the differential operator.

If ξ_1=$\xi_1(v)$ and ξ_2=$\xi_2(v)$, then the properties of the variational operator are as follows

(i) $\quad \delta(\xi_1 \pm \xi_2) = \delta\xi_1 \pm \delta\xi_2$

(ii) $\quad \delta(\xi_1 \xi_2) = \xi_2\delta\xi_1 + \xi_1\delta\xi_2$

(iii) $\quad \delta\left(\frac{\xi_1}{\xi_2}\right) = \frac{\xi_2\delta\xi_1 - \xi_1\delta\xi_2}{{\xi_2}^2}$

(iv) $\quad \delta(\xi_1)^n = n(\xi_1)^{n-1}\delta(\xi_1)$

(v) $\quad \frac{d}{du}(\delta v) = \delta(\frac{dv}{du})$

(vi) $\quad \delta\int_a^b v(u)du = \int_a^b \delta v(u)du$

For the functional $\psi(v)$ to have an extremum, its variational must be zero , $\delta\psi$=0. This is the starting condition for converting PDE s into their functional forms since this necessary condition on the functional is usually in the form of a differential equation with boundary conditions on the required function.

5.1 Converting PDEs into their functional forms

Given a partial differential equation, we can obtain its functional form using the following procedure

1) Multiply the partial differential equation with the variational of the parameter of interest, and integrate over the solution region.

2) Use integration by parts to express the derivatives in terms of the variational term.

3) Apply the boundary conditions to the resulting equation and bring the variational operator outside the integral.

Let us start with a simple example of converting an ordinary differential equation into its functional form. Consider the differential equation

$$y'' - y + 2x = 0 \qquad , \quad 1 < x < 2$$

Let us determine the functional for this ordinary differential equation subject to the boundary conditions $y(1) = 1$, $y(2) = 1$

$$\frac{d^2y}{dx^2} - y + 2x = 0 \quad , \qquad 1 < x < 2$$

Then

$$\delta I = \int_1^2 \left(\frac{d^2y}{dx^2} - y + 2x\right)(\delta y)dx = 0$$

$$\delta I = \int_1^2 \frac{d^2y}{dx^2}\delta y dx - \int_1^2 y\delta y dx + 2\int_1^2 x\delta y dx = 0$$

Using integration by parts to express the derivatives inside the variational operator, the first term becomes

$$\int_1^2 \frac{d^2y}{dx^2}\delta y dx = \frac{dy}{dx}\delta y\,]_1^2 - \int_1^2 \frac{dy}{dx}\left(\frac{d}{dx}\delta y dx\right)$$

therefore δI becomes

$$\delta I = \frac{dy}{dx}\delta y\,]_1^2 - \int_1^2 \frac{dy}{dx}\frac{d}{dx}\delta y\, dx - \int_1^2 y\delta y dx + 2\int_1^2 x\delta y dx$$

Since a prescribed value can not be varied , $\delta y(1) = \delta y(2) = 0$. Therefore the first term vanishes , δI , using the properties of the variational operator δ , becomes

$$\delta I = -\delta\int_1^2 \frac{1}{2}\left(\frac{dy}{dx}\right)^2 dx - \delta\int_1^2 \frac{1}{2}y^2 dx + 2\delta\int_1^2 xy dx$$

$$\delta I = \frac{\delta}{2}\int_1^2 \left[-\left(\frac{dy}{dx}\right)^2 - y^2 + 4xy\right]\, dx$$

$$I(y) = \frac{1}{2}\int_1^2 [-y'^2 - y^2 + 4xy\,]dx$$

is the corresponding functional for the given differential equation.

Our interest here is to solve the inhomogenous wave equation using finite element method, so we must determine the functional form of the inhomogenous wave equation

$$\nabla^2\phi + k^2\phi = g$$

which will be solved by applying the finite element method to the functional form of the equation, assuming that we are solving the equation in a 2 dimensional region. Using the previously described procedure we will convert this PDE to its functional form as follows

$$\nabla^2\phi + k^2\phi - g = 0$$

$$\delta I = \iint [\, -\nabla^2\phi - k^2\phi + g\,]\, \delta\phi \, dx \, dy$$

$$\delta I = -\iint [\, \nabla^2\phi]\, \delta\phi \, dx \, dy - \iint [\, k^2\phi\,]\, \delta\phi \, dx \, dy + \iint [g]\, \delta\phi \, dx \, dy$$

The first term can be integrated using integration by parts, expanding the first term as

$$-\iint [\, \nabla^2\phi]\, \delta\phi \, dx \, dy = -\iint \left[\frac{\partial^2\phi}{\partial x^2}\right] \delta\phi \, dx \, dy - \iint \left[\frac{\partial^2\phi}{\partial y^2}\right] \delta\phi \, dx \, dy$$

and applying integration by parts by choosing $u = \delta\phi$, $dv = \frac{\partial}{\partial x}\left(\frac{\partial\phi}{\partial x}\right) dx$

$$-\int [\int \frac{\partial}{\partial x}\left(\frac{\partial\phi}{\partial x}\right) \delta\phi \; dx\,]\; dy = -\int [\, \frac{\partial\phi}{\partial x}\; \delta\phi - \int \frac{\partial\phi}{\partial x}\; \delta \frac{\partial\phi}{\partial x}\; dx\,]\; dy$$

$$\delta I = \iint [\, \frac{\partial\phi}{\partial x}\; \frac{\partial}{\partial x}\; \delta\phi + \frac{\partial\phi}{\partial y}\frac{\partial}{\partial y}\delta\phi - \delta\phi\; k^2\phi + \delta g\phi]\; dx\; dy \; - \int \delta\phi \frac{\partial\phi}{\partial x} dy - \int \delta\phi \frac{\partial\phi}{\partial y} dx$$

The single integrals become zero, if the boundary conditions are of the homogenous Dirichlet or Neumann type. As a result, for most of the radiation/scattering problems we have

$$\delta I = \iint [\, \frac{\partial\phi}{\partial x}\; \frac{\partial}{\partial x}\; \delta\phi + \frac{\partial\phi}{\partial y}\frac{\partial}{\partial y}\delta\phi - \delta\phi\; k^2\phi + \delta g\phi]\; dx\; dy$$

$$\delta I = \frac{\delta}{2}\iint [\, (\frac{\partial\phi}{\partial x})^2 \; + (\frac{\partial\phi}{\partial y})^2 - \; k^2\phi^2 + 2g\phi]\; dx\; dy$$

$$I(\phi) = \frac{1}{2}\iint [\, (\frac{\partial\phi}{\partial x})^2 \; + (\frac{\partial\phi}{\partial y})^2 - \; k^2\phi^2 + 2g\phi]\; dx\; dy$$

is the corresponding functional for the inhomogenous wave equation.

The functional forms of the PDEs that are used in electromagnetics are given below for a 2 dimensional solution region. Since we have determined the functional form of the inhomogenous wave equation, the functional forms of the other PDEs can be directly found by simplification.

Inhomogenous wave equation $\nabla^2\phi + k^2\phi = g$

$$I(\phi) = \frac{1}{2}\iint [\,(\frac{\partial\phi}{\partial x})^2 + (\frac{\partial\phi}{\partial y})^2 - k^2\phi^2 + 2g\phi]\,dx\,dy$$

Homogenous wave equation $\nabla^2\phi + k^2\phi = 0$

$$I(\phi) = \frac{1}{2}\iint [\,(\frac{\partial\phi}{\partial x})^2 + (\frac{\partial\phi}{\partial y})^2 - k^2\phi^2]\,dx\,dy$$

Poisson's equation $\nabla^2\phi = g$

$$I(\phi) = \frac{1}{2}\iint [\,\left(\frac{\partial\phi}{\partial x}\right)^2 + \left(\frac{\partial\phi}{\partial y}\right)^2 + 2g\phi]\,dx\,dy$$

Laplace's equation $\nabla^2\phi = 0$

$$I(\phi) = \frac{1}{2}\iint [\,\left(\frac{\partial\phi}{\partial x}\right)^2 + \left(\frac{\partial\phi}{\partial y}\right)^2]\,dx\,dy$$

$I(\phi)$ for inhomogenous wave equation can also be determined using Mikhlin's approach to solve the equation $L\phi = g$

$$I(\phi) = <L\phi\,,\phi> - 2<\phi, g>$$

where $L = \nabla^2[\,.\,] + k^2[\,.\,]$ is the operator of the equation.

Other methods for deriving variational principles to solve electromagnetic problems also exist in literature.

5.2 Solution of the Laplace equation using finite element method

We have already derived the functional for the inhomogenous wave equation

$$\nabla^2\phi + \mathrm{k}^2\phi = g$$

for a 2 dimensional solution region which is

$$I(\phi) = \frac{1}{2}\iint [\,(\frac{\partial\phi}{\partial x})^2 + (\frac{\partial\phi}{\partial y})^2 - k^2\phi^2 + 2\mathrm{g}\phi]\, dx\, dy$$

Choosing $k = 0$, $g = 0$, we get the functional for Laplace's equation $\nabla^2\phi = 0$ as

$$I(\phi) = \frac{1}{2}\iint [\,\left(\frac{\partial\phi}{\partial x}\right)^2 + \left(\frac{\partial\phi}{\partial y}\right)^2]\, dx\, dy$$

Laplace's equation describes electrostatic problems with $k = 0\ and\ g = 0$. To apply the finite element method to solve Laplace's equation in a 2 dimensional region, we need to follow the following procedure

1) Divide the solution region into finite elements, which are usually chosen as triangles.

2) Determine the interpolation functions (or shape functions) for each element in the solution region.

3)Assemble all elements inside the solution region to get the resulting system of equations, which is when solved, yields the approximate solution vector that we are looking for.

For a 2 dimensional solution region, we use either triangles or quadrilaterals to discretize the solution region, since triangles fit better to curved boundaries we prefer to discretize using triangles. After we decide which element type to use for discretization, we must derive the representing equations for each element in the solution region. In other words we need to determine the interpolation functions for each element. After determining the interpolation functions for each element in the solution region, we use the three node potential values (or field values) to determine a potential distribution function for each element. Combining the potential distributions of all elements in the solution region, we get the overall potential distribution of the solution region.

Figure 5.1 shows two solution regions, the one in the left being nonrectangular and other being rectangular. The nonrectangular solution region is discretized using both triangles and quadrilaterals, the rectangular one is discretized by using triangles only. Note that there is always an unavoidable discretization error for nonrectangular solution regions.

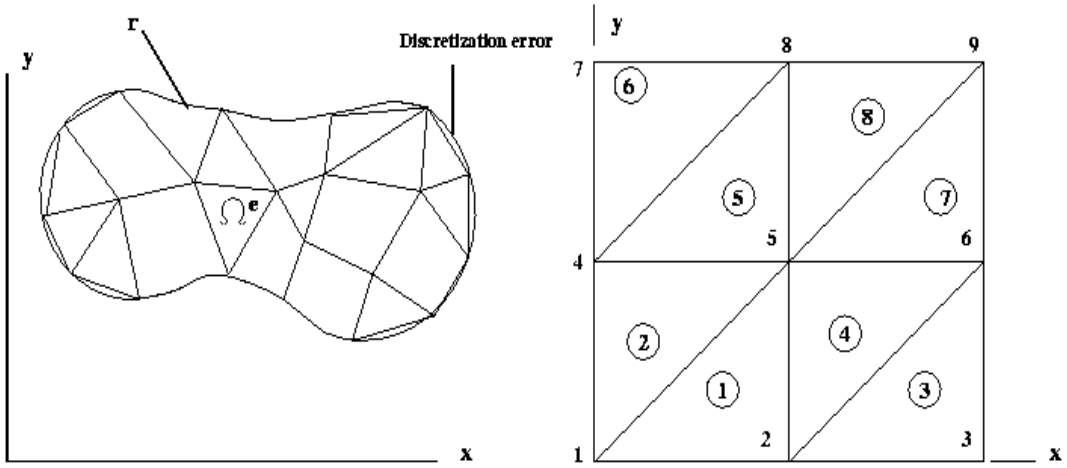

Figure5.1:Discretization of rectangular and nonrectangular geometries.

If we know the potential distribution inside each element, which is V_e(x,y), then the approximate solution for the total region becomes

$$V(x,y) = \sum_{e=1}^{N} V_e(\mathrm{x},\mathrm{y})$$

where N is the total number of elements used inside the solution region.

V_e(x,y) which is the potential distribution inside each element can be assumed to be in polynomial form as, $V_e(\mathrm{x},\mathrm{y}) = \mathrm{a} + \mathrm{bx} + \mathrm{cy}$, then for a given element with vertices $\{(x_1,y_1),(x_2,y_2),(x_3,y_3)\}$, we have

$$V_{e1} = a + bx_1 + cy_1$$

$$V_{e2} = a + bx_2 + cy_2$$

$$V_{e3} = a + bx_3 + cy_3$$

$$\begin{bmatrix} V_{e1} \\ V_{e2} \\ V_{e3} \end{bmatrix} = \begin{bmatrix} 1 & x_1 & y_1 \\ 1 & x_2 & y_2 \\ 1 & x_3 & y_3 \end{bmatrix} \begin{bmatrix} a \\ b \\ c \end{bmatrix}$$

$$\begin{bmatrix} a \\ b \\ c \end{bmatrix} = \begin{bmatrix} 1 & x_1 & y_1 \\ 1 & x_2 & y_2 \\ 1 & x_3 & y_3 \end{bmatrix}^{-1} \begin{bmatrix} V_{e1} \\ V_{e2} \\ V_{e3} \end{bmatrix}$$

Using this equation along with the polynomial approximation $V_e(\mathrm{x},\mathrm{y}) = \mathrm{a} + \mathrm{bx} + \mathrm{cy}$, if we express the potential inside an element in terms of the basis functions $\alpha_1, \alpha_2, \alpha_3$ as

$$V_e(x,y) = \sum_{i=1}^{3} \alpha_i(x,y)\, V_{ei}$$

Then we get $\alpha_1, \alpha_2, \alpha_3$ as

$$\alpha_1 = \frac{1}{2A}[(x_2y_3 - x_3y_2) + (y_2 - y_3)x + (\mathrm{x}_3 - \mathrm{x}_2)\mathrm{y}\,]$$

$$\alpha_2 = \frac{1}{2A}[(x_3y_1 - x_1y_3) + (y_3 - y_1)x + (\mathrm{x}_1 - \mathrm{x}_3)\mathrm{y}\,]$$

$$\alpha_3 = \frac{1}{2A}[(x_1y_2 - x_2y_1) + (y_1 - y_2)x + (\mathrm{x}_2 - \mathrm{x}_1)\mathrm{y}\,]$$

where A is the area of the element with coordinates $\{(x_1, y_1), (x_2, y_2), (x_3, y_3)\}$, and can be found from $A = \frac{1}{2}[\,(\mathrm{x}_2 - \mathrm{x}_1)(y_3 - y_1) - (\mathrm{x}_3 - \mathrm{x}_1)(y_2 - y_1)\,]$.

The value of the area is positive for counterclockwise numbering of the nodes, otherwise it is negative.

Using the equation

$$V_e(x, y) = \sum_{i=1}^{3} \alpha_i(x, y)\, V_{ei}$$

we can find the potential value anywhere inside an element, i.e., potential distribution is continuous unlike in the case of finite difference method where the potential values are known only at the grid points.

Element shape functions have the following two properties

$$\alpha_i = \begin{cases} 1 & , i = j \\ 0 & , i \neq j \end{cases}$$

$$\sum_{i=1}^{3} \alpha_i\,(x, y) = 1$$

For example, an element with vertices
$\{\,(1,1)\,, (0,0), (2,0)\,\} = \{\,(\mathrm{x}_1, \mathrm{y}_1), (\mathrm{x}_2, \mathrm{y}_2), (\mathrm{x}_3, \mathrm{y}_3)\,\}$, has

$$\alpha_1 = \frac{1}{2A}[(x_2y_3 - x_3y_2) + (y_2 - y_3)x + (\mathrm{x}_3 - \mathrm{x}_2)\mathrm{y}\,] = y$$

$$\alpha_2 = \frac{1}{2A}[(x_3y_1 - x_1y_3) + (y_3 - y_1)x + (\mathrm{x}_1 - \mathrm{x}_3)\mathrm{y}\,] = 1 - 0.5x - 0.5y$$

$$\alpha_3 = \frac{1}{2A}[(x_1y_2 - x_2y_1) + (y_1 - y_2)x + (\mathrm{x}_2 - \mathrm{x}_1)\mathrm{y}\,] = 0.5x - 0.5y$$

with potential values at the three vertices as , $V_{e1} = 10$, $V_{e2} = 5$, $V_{e3} = 2$, the potential distribution inside the triangle is determined by the function

$$V_e(x, y) = \sum_{i=1}^{3} \alpha_i(x, y)\, V_{ei} = 5 - \frac{3}{2}\,x + \frac{13}{2}\,y$$

In order to solve Laplace's equation, which has the functional

$$I(\phi) = \frac{1}{2}\iint [\ |\nabla\phi|^2\ ]\ \text{dxdy} = \frac{1}{2}\int [\ |\nabla\phi|^2\ ]\ \text{dS}$$

in a two dimensional solution region, we use the energy functional given by

$$W = \frac{1}{2}\int \in |E|^2\ dS = \frac{1}{2}\int \in |\nabla V|^2\ dS$$

where W is the energy per unit length. For a single element e , W becomes W_e , which is the energy per unit length inside an element e, given by

$$\text{W}_\text{e} = \tfrac{1}{2}\int \in |\text{E}_\text{e}|^2\ dS = \tfrac{1}{2}\int \in |\nabla V_\text{e}|^2\ dS$$

We have defined V_e , the potential distribution inside an element e as

$$V_e = \sum_{i=1}^{3} V_{ei}\,\alpha_i(x,y)$$

Therefore the gradient of the expression ∇V_e is

$$\nabla V_e = \sum_{i=1}^{3} V_{ei}\,\nabla\alpha_i(x,y)$$

Substituting this equation into the expression for $|\nabla V_e|^2$, we get

$$|\nabla V_e|^2 = \sum_{i=1}^{3}\sum_{j=1}^{3} V_{ei}V_{ej}\,\nabla\alpha_i.\nabla\alpha_j$$

Which is when substituted into the equation for W_e , yields

$$W = \frac{1}{2}\int \in [\ \sum_{i=1}^{3}\sum_{j=1}^{3} V_{ei}V_{ej}\,\nabla\alpha_i.\nabla\alpha_j\ ]\ dS$$

Moving the sums, along with V_{ei} and V_{ej} , out of the integral, we get

$$W_e = \frac{1}{2}\sum_{i=1}^{3}\sum_{j=1}^{3} \in V_{ei}\,[\int \nabla\alpha_i\,.\nabla\alpha_\text{j}\ \text{dS}\ ]\ V_{ej}$$

The term inside the brackets is defined as the {i,j} th entry of the element coefficient matrix [$C^{(e)}$] , that is defined as

$$C_{ij}{}^{(e)} = \int \nabla\alpha_i.\nabla\alpha_j\ dS$$

Therefore

$$W = \frac{1}{2} \sum_{i=1}^{3} \sum_{j=1}^{3} \in V_{ei}\, {C_{ij}}^{(e)}\, V_{ej}$$

which can be written in matrix form as (with t denoting transposition)

$$W_e = \frac{1}{2} \in [V_e]^t \left[C^{(e)}\right] [V_e] \quad , \qquad with \;\; [V_e] = \begin{bmatrix} V_{e1} \\ V_{e2} \\ V_{e3} \end{bmatrix}$$

$$\left[\, C^{(e)}\right] = \begin{bmatrix} {C_{11}}^{(e)} & {C_{12}}^{(e)} & {C_{13}}^{(e)} \\ {C_{21}}^{(e)} & {C_{22}}^{(e)} & {C_{23}}^{(e)} \\ {C_{31}}^{(e)} & {C_{32}}^{(e)} & {C_{33}}^{(e)} \end{bmatrix}$$

Since

$${C_{ij}}^{(e)} = \int \nabla\alpha_i . \nabla\alpha_j \, dS = \int \nabla\alpha_j . \nabla\alpha_i \, dS = {C_{ji}}^{(e)} \quad , \qquad \{i, j\} = \{\, 1,2,3 \,\}$$

The element coefficient matrix $[C^{(e)}]$ is symmetric.

With α_1, α_2 and α_3 already known, we can directly determine ${C_{ij}}^{(e)}$, $\{i, j\} = \{1,2,3\}$, as

$${C_{ij}}^{(e)} = \frac{1}{4A}[u_i u_j + v_i v_j]$$

$$u_1 = (y_2 - y_3)\,, \qquad u_2 = (y_3 - y_1)\,, \qquad u_3 = (y_1 - y_2)$$

$$v_1 = (x_3 - x_2)\,, \qquad v_2 = (x_1 - x_3)\,, \qquad v_3 = (x_2 - x_1)$$

$W_e = \frac{1}{2} \in [V_e]^t \left[C^{(e)}\right] [V_e]$, is defined for a single element. To get the total energy per unit length inside the overall solution region, we sum the energies of all elements in the region

$$W = \sum_{e=1}^{N} W_e = \frac{1}{2} \in [V]^t \, [C] \, [V] \quad , \quad V = \begin{bmatrix} V_1 \\ V_2 \\ V_3 \\ \vdots \\ V_n \end{bmatrix}$$

Where N is the number of elements and n is the number of nodes in the solution region.

$[C]$ is called the global coefficient matrix that is assembled using the individual element coefficient matrices, according to their connections.

W can be expanded from its matrix equation form to its general equation form as

$$W = \frac{1}{2} \in [V_1 \quad V_2 \quad V_3 \quad \cdot \quad \cdot \quad \cdot \quad V_n \;] \begin{bmatrix} C_{11} & \cdots & C_{1n} \\ \vdots & \ddots & \vdots \\ C_{n1} & \cdots & C_{nn} \end{bmatrix} \begin{bmatrix} V_1 \\ V_2 \\ \vdots \\ . \\ V_n \end{bmatrix}$$

$$W = \frac{1}{2} \in \begin{bmatrix} V_1C_{11} + V_2C_{21} + V_3C_{31} + \cdots + V_nC_{n1} \\ V_1C_{12} + V_2C_{22} + V_3C_{32} + \cdots + V_nC_{n2} \\ V_1C_{13} + V_2C_{23} + V_3C_{33} + \cdots + V_nC_{n3} \\ . \\ . \\ . \\ V_1C_{1n} + V_2C_{2n} + V_3C_{3n} + \cdots + V_nC_{nn} \end{bmatrix}^t \begin{bmatrix} V_1 \\ V_2 \\ V_3 \\ . \\ . \\ . \\ V_n \end{bmatrix}$$

$$W = [{V_1}^2C_{11} + V_1V_2C_{12} + V_1V_3C_{13} + V_1V_4C_{14} + \cdots + V_1V_nC_{1n} + V_2V_1C_{21} + {V_2}^2C_{22} +$$

$$V_2V_3C_{23} + V_2V_4C_{24} + \cdots + V_2V_nC_{2n} + V_3V_1C_{31} + V_3V_2C_{32} + \cdots + V_3V_nC_{3n}$$

$$+ V_4V_1C_{41} + V_4V_2C_{42} + \cdots + V_4V_nC_{4n} + \cdots + V_nV_{n-1}C_{n,n-1} + V_nV_nC_{nn}\ ]$$

It can be shown that Laplace's equation is satisfied, when W becomes minimum at all nodes inside the solution region, therefore we require

$$\frac{\partial W}{\partial V_1} = \frac{\partial W}{\partial V_2} = \frac{\partial W}{\partial V_3} = \cdots = \frac{\partial W}{\partial V_n} = 0$$

$$\frac{\partial W}{\partial V_k} = 0 \ , \ k = \{1,2,3, \dots, n\}$$

By satisfying the condition $\frac{\partial W}{\partial V_k} = 0 \ , \ k = \{1,2,3, \dots, n\}$, at every node in the solution region we get a system of linear equations

$$\frac{\partial W}{\partial V_1} = 0 = V_1C_{11} + V_2C_{12} + V_3C_{13} + \cdots + V_nC_{1n}$$

$$\frac{\partial W}{\partial V_2} = 0 = V_1C_{21} + V_2C_{22} + V_3C_{23} + \cdots + V_nC_{2n}$$

$$\frac{\partial W}{\partial V_3} = 0 = V_1C_{31} + V_2C_{32} + V_3C_{33} + \cdots + V_nC_{3n}$$

$$\frac{\partial W}{\partial V_4} = 0 = V_1C_{41} + V_2C_{42} + V_3C_{43} + \cdots + V_nC_{4n}$$

So in general $\frac{\partial W}{\partial V_k} = 0,$ yields

$$0 = \sum_{i=1}^{n} V_iC_{ki} = \sum_{\mathrm{i=1}}^{\mathrm{n}} \mathrm{V_i C_{ik}}$$

Which has a solution for an arbitrary free node k, given as

$$V_k = -\frac{1}{C_{kk}} \sum_{i=1,\ i \neq k}^{n} V_iC_{ki}$$

The global coefficient matrix is assembled using the individual element coefficient matrices according to the connections of the elements. The formation process is much easier to describe with an example. Consider the simplest example in Figure 5.2 of a square which is formed by the assemblage of two triangles, the resulting global coefficient matrix that describes the square geometry is the assemblage of the local coefficient matrices of the two triangles.

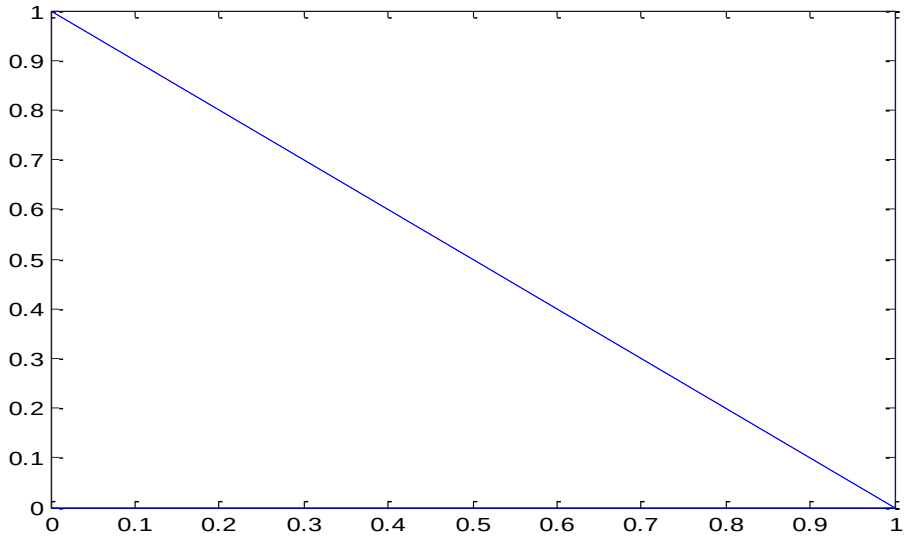

Figure 5.2: A mesh of two triangles.

Element	*Local node*	*Global node*	x	y
1	1	1	0	0
1	2	2	1	0
1	3	3	0	1
2	1	2	1	0
2	2	4	1	1
2	3	3	0	1

Using the definition of the entries of the element coefficient matrix, which is

$$C_{ij}{}^{(e)} = \int \nabla\alpha_i . \nabla\alpha_j \, dS = \int \nabla\alpha_j . \nabla\alpha_i \, dS = C_{ji}{}^{(e)} \quad , \qquad \{i,j\} = \{\, 1,2,3 \,\}$$

$$C_{ij}{}^{(e)} = \frac{1}{4A}[u_i u_j + v_i v_j]$$

$$u_1 = (y_2 - y_3)\,, \qquad u_2 = (y_3 - y_1)\,, \qquad u_3 = (y_1 - y_2)$$

$$v_1 = (x_3 - x_2)\,, \qquad v_2 = (x_1 - x_3)\,, \qquad v_3 = (x_2 - x_1)$$

we get the element coefficient matrices for the figure as

$$C^{(1)} = \begin{bmatrix} 1 & -0.5 & -0.5 \\ -0.5 & 0.5 & 0 \\ -0.5 & 0 & 0.5 \end{bmatrix} \quad , \quad C^{(2)} = \begin{bmatrix} 0.5 & -0.5 & -0.5 \\ -0.5 & 1 & -0.5 \\ 0 & -0.5 & 0.5 \end{bmatrix}$$

According to the coordinate list of the local nodes of the two elements and the global coordinates, the assembly is done as follows

$C_{11} = {C_{11}}^{(1)}$, *global node* 1 *exists only at the local node of the first element.*

$C_{12} = {C_{12}}^{(1)}$, *global nodes* 1 *and* 2 *exist simultaneously at local nodes* 1 *and* 2 *in the first element.*

$C_{13} = {C_{13}}^{(1)}$, *global nodes* 1 *and* 3 *exist simultaneously at local nodes* 1 *and* 3 *in element* 1.

$C_{12} = C_{21}$, *due to the symmetric property of the global coefficient matrix.*

$C_{22} = {C_{11}}^{(2)} + {C_{22}}^{(1)}$, *global node* 2 *exists at local node* 2 *in element* 1 *and at local node* 1 *in element* 2 .

$C_{23} = {C_{23}}^{(1)} + {C_{13}}^{(2)}$, *global nodes* 2 *and* 3 *exist simultaneously at local nodes* 2 *and* 3 *in element* 1 *and at local nodes* 1 *and* 3 *in element* 2.

$C_{31} = C_{13}$, *due to the symmetric property of the global coefficient matrix.*

$C_{32} = C_{23}$, *due to the symmetric property of the global coefficient matrix.*

$C_{33} = {C_{33}}^{(2)} + {C_{33}}^{(1)}$, *global node* 3 *exists at local node* 3 *in element* 1 *and at local node* 3 *in element* 2 .

$C_{14} = C_{41} = 0$, *since the global nodes* 1 *and* 4 *are not directly connected.*

The resulting global coefficient matrix is found as

$$C = \begin{bmatrix} 1 & -0.5 & -0.5 & 0 \\ -0.5 & 1 & 0 & -0.5 \\ -0.5 & 0 & 1 & -0.5 \\ 0 & -0.5 & -0.5 & 1 \end{bmatrix}$$

Consider a hexagonal geometry as a more complicated example with 6 elements and 7 global nodes with the given coordinate list

Element	*Local node*	*Global node*	x	y
1	1	1	0	0
1	2	2	1	1
1	3	3	-1	1
2	1	1	0	0
2	2	3	-1	1
2	3	4	-2	0
3	1	1	0	0
3	2	4	-2	0
3	3	5	-1	-1
4	1	1	0	0
4	2	5	-1	-1
4	3	6	1	-1
5	1	1	0	0
5	2	6	1	-1
5	3	7	2	0
6	1	1	0	0
6	2	7	2	0
6	3	2	1	1

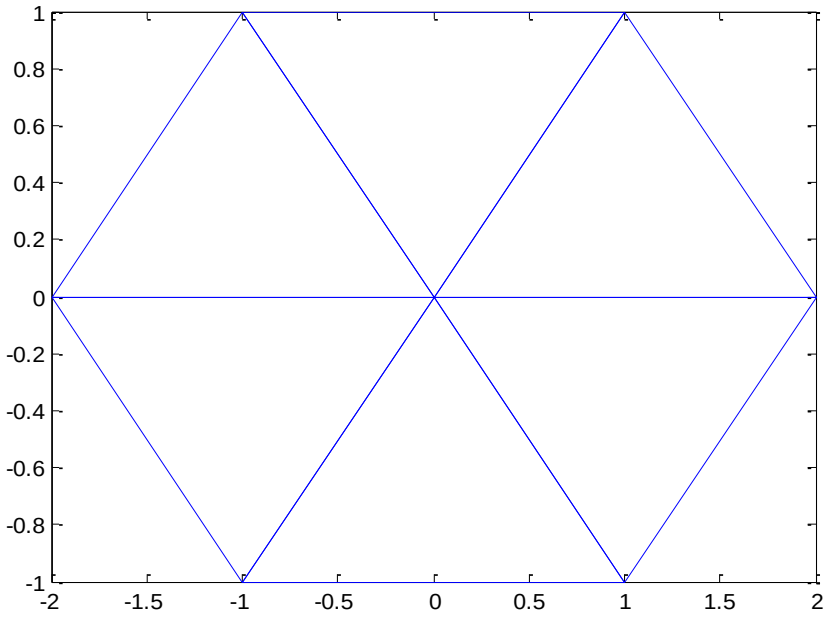

Figure 5.3: A hexagonal mesh of six triangles.

$$C^{(1)} = \begin{bmatrix} 1 & -0.5 & -0.5 \\ -0.5 & 0.5 & 0 \\ -0.5 & 0 & 0.5 \end{bmatrix}, \quad C^{(2)} = \begin{bmatrix} 0.5 & -0.5 & 0 \\ -0.5 & 1 & -0.5 \\ 0 & -0.5 & 0.5 \end{bmatrix}$$

$$C^{(3)} = \begin{bmatrix} 0.5 & 0 & -0.5 \\ 0 & 0.5 & -0.5 \\ -0.5 & -0.5 & 1 \end{bmatrix}, \quad C^{(4)} = \begin{bmatrix} 1 & -0.5 & -0.5 \\ -0.5 & 0.5 & 0 \\ -0.5 & 0 & 0.5 \end{bmatrix}$$

$$C^{(5)} = \begin{bmatrix} 0.5 & -0.5 & 0 \\ -0.5 & 1 & -0.5 \\ 0 & -0.5 & 0.5 \end{bmatrix}, \quad C^{(6)} = \begin{bmatrix} 0.5 & 0 & -0.5 \\ 0 & 0.5 & -0.5 \\ -0.5 & -0.5 & 1 \end{bmatrix}$$

$$C = \begin{bmatrix} 4 & -1 & -1 & 0 & -1 & -1 & 0 \\ -1 & 1.5 & 0 & 0 & 0 & 0 & -0.5 \\ -1 & 0 & 1.5 & -0.5 & 0 & 0 & 0 \\ 0 & 0 & -0.5 & 1 & -0.5 & 0 & 0 \\ -1 & 0 & 0 & -0.5 & 1.5 & 0 & 0 \\ -1 & 0 & 0 & 0 & 0 & 1.5 & -0.5 \\ 0 & -0.5 & 0 & 0 & 0 & -0.5 & 1 \end{bmatrix}$$

Where $C^{(i)}$, $i = 1, \dots, 6$ are the element coefficient matrices and C is the global coefficient matrix. Since most of the global nodes are not directly connected to each other, C is a sparse matrix as expected.

5.3 Solution of the wave equation using finite element method

We have already derived the functional $I(\phi)$ for the inhomogenous wave equation. To solve the inhomogenous wave equation by using finite element method, we have to satisfy

the given boundary conditions and we have to minimize the functional $I(\phi)$ at each free node inside the solution region. Again, first we need to express $I(\phi)$ in terms of the global coefficient matrix to obtain a matrix equation form of $I(\phi)$**.** We will follow an identical procedure as we did for Laplace's equation. Recall that the inhomogenous wave equation

$$\nabla^2\phi + \mathrm{k}^2\phi = g$$

is expressed in its functional form as

$$I(\phi) = \frac{1}{2}\iint [\,(\frac{\partial\phi}{\partial x})^2 + (\frac{\partial\phi}{\partial y})^2 - k^2\phi^2 + 2\mathrm{g}\phi]\,dx\,dy$$

$$= \frac{1}{2}\iint [\,|\nabla\phi|^2 - k^2\phi^2 + 2\mathrm{g}\phi]\,dS$$

Our aim is to determine the unknown ϕ at every free node inside the solution region. The wave equation is inhomogenous, thus a prescribed source function g also exists in the solution region. We start by expressing $\phi\ and\ g$ in terms of the element shape functions

$$\phi_e(x,y) = \sum_{i=1}^{3} \alpha_i(x,y)\ \phi_{ei}$$

$$\mathrm{g}_e(x,y) = \sum_{i=1}^{3} \alpha_i(x,y)\ \mathrm{g}_{ei}$$

Where ϕ_{ei} and g_{ei} are the values of ϕ and g at node i in element e .

Substituting the expressions for ϕ_e and g_e into $I(\phi)$, we get $I(\phi_e)$ as

$$I(\phi_e) = \frac{1}{2}\sum_{\mathrm{i}=1}^{3}\sum_{\mathrm{j}=1}^{3} \phi_{ei}\,\phi_{ej}\int\int(\nabla\alpha_i\,.\,\nabla\alpha_\mathrm{j})\,\mathrm{dS} \quad - \frac{\mathrm{k}^2}{2}\sum_{\mathrm{i}=1}^{3}\sum_{\mathrm{j}=1}^{3} \phi_{ei}\,\phi_{ej}\int\int(\alpha_i\,\alpha_\mathrm{j})\,\mathrm{dS}$$

$$+ \sum_{\mathrm{i}=1}^{3}\sum_{\mathrm{j}=1}^{3} \phi_{ei}\,\mathrm{g}_{ej}\int\int(\alpha_i\,\alpha_\mathrm{j})\,\mathrm{dS}$$

Where the element coefficient matrices are defined as

$$C_{ij}{}^{(e)} = \int\int \nabla\alpha_i.\nabla\alpha_j\,dS \quad , \quad T_{ij}{}^{(e)} = \int\int \alpha_i\,\alpha_j\,dS$$

$$with \quad T_{ij}{}^{(e)} = \int\int \alpha_i\,\alpha_j\,dS \;=\; \begin{cases} \mathrm{A}/12 & \mathrm{i} \neq \mathrm{j} \\ \mathrm{A}/6 & \mathrm{i} = \mathrm{j} \end{cases}$$

In matrix form, we can write $I(\phi_e)$ as

$$I(\phi_e) = \frac{1}{2}\,[\phi_e]^\mathrm{t}\left[\mathrm{C}^{(\mathrm{e})}\right][\phi_e] - \frac{\mathrm{k}^2}{2}[\phi_e]^\mathrm{t}\left[\mathrm{T}^{(\mathrm{e})}\right][\phi_e] + [\phi_e]^\mathrm{t}\left[\mathrm{T}^{(\mathrm{e})}\right][\mathrm{g}_e]$$

where $[\phi_e] = [\phi_{e1}, \phi_{e2}, \phi_{e3}]^\mathrm{t}$, $[\mathrm{g}_e] = [\mathrm{g}_{e1}, \mathrm{g}_{e2}, \mathrm{g}_{e3}]^\mathrm{t}$

$I(\phi_e)$ is defined for a single element. To determine $I(\phi)$ which is defined for the assemblage of all elements, we sum the functionals $I(\phi_e)$, $e = 1,2, \dots, n,$ of each element in the solution region , so that $I(\phi)$ becomes

$$I(\phi) = \sum_{e=1}^{N} I(\phi_e)$$

$$= \frac{1}{2} [\phi]^t [C] [\phi] - \frac{k^2}{2} [\phi]^t [T] [\phi] + [\phi]^t [T] [g]$$

$[\phi] = [\phi_1, \phi_2, \phi_3, \dots, \phi_N]^t$, $[g] = [g_1, g_2, g_3, \dots, g_N]^t$

Where [C] and [T] are global coefficient matrices.

We can expand the matrix equation for $I(\phi)$ into its algebraic form and then minimize $I(\phi)$ at every free node in the solution region. To do this we split $I(\phi)$ into three parts as described below

$$I(\phi) = I_1(\phi) + I_2(\phi) + I_3(\phi) = \frac{1}{2} [\phi]^t [C] [\phi] - \frac{k^2}{2} [\phi]^t [T] [\phi] + [\phi]^t [T] [g]$$

$$I_1(\phi) = \frac{1}{2} [\phi]^t [C] [\phi] \quad , \quad I_2(\phi) = -\frac{k^2}{2} [\phi]^t [T] [\phi] \quad , \quad I_3(\phi) = [\phi]^t [T] [g]$$

$$I_1(\phi) = \frac{1}{2} [\left(\phi_1{}^2 C_{11} + \phi_1\phi_2 C_{12} + \phi_1\phi_3 C_{13} + \cdots + \phi_1\phi_n C_{1n} \right) + \left(\phi_2\phi_1 C_{21} + \phi_2{}^2 C_{22} + \phi_2\phi_3 C_{23} + \cdots + \phi_2\phi_n C_{2n} \right) + \left(\phi_3\phi_1 C_{31} + \phi_3\phi_2 C_{32} + \phi_3{}^2 C_{33} + \cdots + \phi_3\phi_n C_{3n} \right) + \dots + \left(\phi_n\phi_1 C_{n1} + \phi_n\phi_2 C_{n2} + \phi_n\phi_3 C_{n3} + \cdots + \phi_n\phi_n C_{nn} \right)]$$

$$I_2(\phi) = \frac{-k^2}{2} [\left(\phi_1{}^2 T_{11} + \phi_1\phi_2 T_{12} + \phi_1\phi_3 T_{13} + \cdots + \phi_1\phi_n T_{1n} \right) + \left(\phi_2\phi_1 T_{21} + \phi_2{}^2 T_{22} + \phi_2\phi_3 T_{23} + \cdots + \phi_2\phi_n T_{2n} \right) + \left(\phi_3\phi_1 T_{31} + \phi_3\phi_2 T_{32} + \phi_3{}^2 T_{33} + \cdots + \phi_3\phi_n T_{3n} \right) + \dots + \left(\phi_n\phi_1 T_{n1} + \phi_n\phi_2 T_{n2} + \phi_n\phi_3 T_{n3} + \cdots + \phi_n\phi_n T_{nn} \right)]$$

$$I_3(\phi) = [\left(\phi_1 g_1 T_{11} + \phi_2 g_1 T_{12} + \cdots + \phi_n g_1 T_{1n} \right) + \left(\phi_1 g_2 T_{21} + \phi_2 g_2 T_{22} + \cdots + \phi_2 g_n T_{2n} \right) + \left(\phi_1 g_3 T_{31} + \phi_2 g_3 T_{32} + \cdots + \phi_n g_3 T_{3n} \right) + \dots + \left(\phi_1 g_n T_{n1} + \phi_2 g_n T_{n2} + \phi_3 g_n T_{n3} + \cdots + \phi_n g_n T_{nn} \right)]$$

We are trying to determine the vector $[\phi] = [\phi_1, \phi_2, \phi_3, \ \dots \ , \phi_N]^t$, which satisfies $\frac{\partial I(\phi)}{\partial \phi_k} = 0$ at all free nodes ϕ_k , $k = 1,2, \dots, n$. So we need to determine the expression for $\frac{\partial I(\phi)}{\partial \phi_k}$, $k = 1,2, \dots, n$. The process is as described below

$$\frac{\partial I(\phi)}{\partial \phi_k} = \frac{\partial I_1(\phi)}{\partial \phi_k} + \frac{\partial I_2(\phi)}{\partial \phi_k} + \frac{\partial I_3(\phi)}{\partial \phi_k}$$

$$\frac{\partial I_1(\phi)}{\partial \phi_1} = \phi_1 C_{11} + \phi_2 C_{12} + \phi_3 C_{13} + \cdots + \phi_n C_{1n}$$

$$\frac{\partial I_1(\phi)}{\partial \phi_2} = \phi_1 C_{21} + \phi_2 C_{22} + \phi_3 C_{23} + \cdots + \phi_n C_{2n}$$

$$\frac{\partial I_1(\phi)}{\partial \phi_3} = \phi_1 C_{31} + \phi_2 C_{32} + \phi_3 C_{33} + \cdots + \phi_n C_{3n}$$

$$\frac{\partial I_1(\phi)}{\partial \phi_n} = \phi_1 C_{n1} + \phi_2 C_{n2} + \phi_3 C_{n3} + \cdots + \phi_n C_{nn}$$

Therefore, in general, we have

$$\frac{\partial I_1(\phi)}{\partial \phi_k} = \sum_{i=1}^{n} \phi_i C_{ki} = \phi_1 C_{k1} + \phi_2 C_{k2} + \phi_3 C_{k3} + \cdots + \phi_n C_{kn}$$

Similarly

$$\frac{\partial I_2(\phi)}{\partial \phi_1} = -\mathrm{k}^2 \left[\phi_1 T_{11} + \phi_2 T_{12} + \phi_3 T_{13} + \cdots + \phi_n T_{1n}\right]$$

$$\frac{\partial I_2(\phi)}{\partial \phi_2} = -\mathrm{k}^2 \left[\phi_1 T_{21} + \phi_2 T_{22} + \phi_3 T_{23} + \cdots + \phi_n T_{2n}\right]$$

$$\frac{\partial I_2(\phi)}{\partial \phi_3} = -\mathrm{k}^2 \left[\phi_1 T_{31} + \phi_2 T_{32} + \phi_3 T_{33} + \cdots + \phi_n T_{3n}\right]$$

.

.

$$\frac{\partial I_2(\phi)}{\partial \phi_n} = -\mathrm{k}^2 \left[\phi_1 T_{n1} + \phi_2 T_{n2} + \phi_3 T_{n3} + \cdots + \phi_n T_{nn}\right]$$

$$\frac{\partial I_2(\phi)}{\partial \phi_k} = -\mathrm{k}^2 \left[\phi_1 T_{k1} + \phi_2 T_{k2} + \phi_3 T_{k3} + \cdots + \phi_n T_{kn}\right] = -\mathrm{k}^2 \sum_{i=1}^{n} \phi_i T_{ki}$$

$I_3(\phi)$ contains the source term g therefore

$$\frac{\partial I_3(\phi)}{\partial \phi_1} = \left[\mathrm{g}_1 T_{11} + \mathrm{g}_2 T_{12} + \mathrm{g}_3 T_{13} + \cdots + \mathrm{g}_n T_{1n}\right]$$

$$\frac{\partial I_3(\phi)}{\partial \phi_2} = [g_1 T_{21} + g_2 T_{22} + g_3 T_{23} + \cdots + g_n T_{2n}]$$

$$\frac{\partial I_3(\phi)}{\partial \phi_3} = [g_1 T_{31} + g_2 T_{32} + g_3 T_{33} + \cdots + g_n T_{3n}]$$

In general

$$\frac{\partial I_3(\phi)}{\partial \phi_k} = \sum_{i=1}^{n} g_i T_{ki} = [g_1 T_{k1} + g_2 T_{k2} + g_3 T_{k3} + \cdots + g_n T_{kn}]$$

Therefore , $\frac{\partial I(\phi)}{\partial \phi_k} = \frac{\partial I_1(\phi)}{\partial \phi_k} + \frac{\partial I_2(\phi)}{\partial \phi_k} + \frac{\partial I_3(\phi)}{\partial \phi_k} = 0$, is expressed as

$$\frac{\partial I(\phi)}{\partial \phi_k} = \sum_{i=1}^{n} \phi_i C_{ki} - k^2 \sum_{i=1}^{n} \phi_i T_{ki} + \sum_{i=1}^{n} g_i T_{ki} = 0$$

$$\frac{\partial I(\phi)}{\partial \phi_k} = \sum_{i=1}^{n} \phi_i C_{ki} - k^2 \phi_i T_{ki} + g_i T_{ki} = 0$$

$$\frac{\partial I(\phi)}{\partial \phi_k} = \sum_{i=1}^{n} \phi_i [C_{ki} - k^2 T_{ki}] + g_i T_{ki} = 0$$

If there are no sources in the solution region , $g = 0$, then the equation simplifies to

$$\frac{\partial I(\phi)}{\partial \phi_k} = \sum_{i=1}^{n} \phi_i [C_{ki} - k^2 T_{ki}] = 0$$

Equations are given for a homogenous medium with a constant value of the wavenumber k which is determined from the constitutive parameters of the medium. If the medium is a homogenous, isotropic, and lossless , k , is given as

$$k = \omega\sqrt{\mu\epsilon}$$

As we increase the mesh size and the number of elements used, the resolution also increases and we get better simulation results. However this greatly increases the required computation time of the problem. In order to find the solution of the wave equation in a given solution region with the specified boundary conditions, first, the computer assigns global node numbers to the coordinates of each node inside the mesh, then it determines the element coefficient matrices of each element in the solution region and finally it assembles all element coefficient matrices. Especially the assembling process requires a great amount of computation time. Therefore when simulating the solution of a partial differential equation in a given solution region, a huge trade-off exists between resolution and computation time.

When the medium is not homogenous, or when the wavenumber, k, is not a constant but an element varying quantity, we have to introduce a different element coefficient matrix that takes the variation of 'k' from one element to another, into account. For an element varying wavenumber 'k' the functional $I(\phi_e)$ becomes

$$I(\phi_e) = \frac{1}{2}\sum_{i=1}^{3}\sum_{j=1}^{3}\phi_{ei}\,\phi_{ej}\int\int(\nabla\alpha_i\,.\,\nabla\alpha_j)\,dS \;-\frac{1}{2}\sum_{i=1}^{3}\sum_{j=1}^{3}\phi_{ei}\,\phi_{ej}\,{k_e}^2\int\int(\alpha_i\,\alpha_j)\,dS$$

$$+\sum_{i=1}^{3}\sum_{j=1}^{3}\phi_{ei}\,g_{ej}\int\int(\alpha_i\,\alpha_j)\,dS$$

$$C_{ij}^{(e)} = \int\int\nabla\alpha_i.\nabla\alpha_j\,dS \quad , \quad T_{ij}^{(e)} = \int\int\alpha_i\,\alpha_j\,dS$$

$$I(\phi_e) = \frac{1}{2}\sum_{i=1}^{3}\sum_{j=1}^{3}\phi_{ei}\,\phi_{ej}\left[\int\int(\nabla\alpha_i\,.\nabla\alpha_j)\,dS \;-\; {k_e}^2\int\int(\alpha_i\alpha_j)\,dS\right]$$

$$+\sum_{i=1}^{3}\sum_{j=1}^{3}\phi_{ei}\,g_{ej}\int\int(\alpha_i\,\alpha_j)\,dS$$

Here, we can introduce the coefficient matrix $M_{ij}^{(e)}$, which is defined as

$$M_{ij}^{(e)} = C_{ij}^{(e)} - {k_e}^2\,T_{ij}^{(e)}$$

$$M_{ij}^{(e)} = \left[\int\int(\nabla\alpha_i\,.\nabla\alpha_j)\,dS \;-\; {k_e}^2\int\int(\alpha_i\alpha_j)\,dS\right]$$

Therefore $I(\phi_e)$ can be written as

$$I(\phi_e) = \frac{1}{2}\sum_{i=1}^{3}\sum_{j=1}^{3}\phi_{ei}\,\phi_{ej}\,M_{ij}^{(e)} + \sum_{i=1}^{3}\sum_{j=1}^{3}\phi_{ei}\,g_{ej}\,T_{ij}^{(e)}$$

$$I(\phi_e) = \frac{1}{2}\sum_{i=1}^{3}\sum_{j=1}^{3}\phi_{ei}\left[\phi_{ej}\,M_{ij}^{(e)} + 2\,g_{ej}\,T_{ij}^{(e)}\right]$$

$I(\phi_e)$, for element varying ‘k’ , can be written in matrix form as

$$I(\phi_e) = \frac{1}{2}\,[\phi_e]^t\left[M^{(e)}\right][\phi_e] + [\phi_e]^t\left[T^{(e)}\right][g_e]$$

Summing $I(\phi_e)$ for all elements in the solution region, we get

$$I(\phi) = \sum_{e=1}^{N} I(\phi_e)$$

$$I(\phi) = \frac{1}{2}\,[\phi]^t\,[M]\,[\phi] + [\phi]^t\,[T]\,[g]$$

$[\phi] = [\phi_1, \phi_2, \phi_3, \ldots, \phi_N]^t$, $[g] = [g_1, g_2, g_3, \ldots, g_N]^t$

Where [M] and [T] are global coefficient matrices. [M] and [T] are assembled using the previously described procedure in which we have assembled [C].

$$I(\phi) = I_M(\phi) + I_g(\phi)$$

$$I_M(\phi) = \frac{1}{2}\,[\phi]^t\,[M]\,[\phi] \quad , \quad I_g(\phi) = [\phi]^t\,[T]\,[g]$$

Following the same procedure as before, we have

$$\frac{\partial I(\phi)}{\partial \phi_k} = \frac{\partial I_M(\phi)}{\partial \phi_k} + \frac{\partial I_g(\phi)}{\partial \phi_k} = 0 \quad , \quad for\ all\ free\ nodes$$

$$\frac{\partial I_M(\phi)}{\partial \phi_k} = \sum_{i=1}^{n} \phi_i M_{ki} = \phi_1 M_{k1} + \phi_2 M_{k2} + \phi_3 M_{k3} + \cdots + \phi_n M_{kn}$$

$$\frac{\partial I_g(\phi)}{\partial \phi_k} = \sum_{i=1}^{n} g_i T_{ki} = \left[g_1 T_{k1} + g_2 T_{k2} + g_3 T_{k3} + \cdots + g_n T_{kn}\right]$$

Therefore, we have

$$\frac{\partial I(\phi)}{\partial \phi_k} = \sum_{i=1}^{n} \phi_i M_{ki} + g_i T_{ki} = 0$$

$$\sum_{i=1}^{n} \phi_i M_{ki} = -\sum_{i=1}^{n} g_i T_{ki}$$

If there are no sources in the solution region

$$\sum_{i=1}^{n} \phi_i M_{ki} = 0$$

Using the last two identities , ϕ_i , i=1,2,…,n , can be easily solved. In this procedure we have treated the wavenumber ‘k’ as an element variable instead of a global node variable, but at the same time we have treated the source ‘g’ as a node variable. We can also assume that ‘g’ is an element variable along with ‘k’ , but then we would have to define another element coefficient matrix regarding the source ‘g’, this is the easiest approach for computation.

As the final case, consider that both k_e and g_e are element variables, in that case $I(\phi_e)$ becomes

$$I(\phi_e) = \frac{1}{2}\sum_{i=1}^{3}\sum_{j=1}^{3} \phi_{ei}\,\phi_{ej}\left[\int\int (\nabla\alpha_i \,.\, \nabla\alpha_j)\,dS \;-\; {k_e}^2 \int\int (\alpha_i \alpha_j)\,dS\right] + g_e \sum_{i=1}^{3}\sum_{j=1}^{3} \phi_{ei} \int\int (\alpha_i\,\alpha_j)\,dS$$

Therefore $I(\phi_e)$ can be written as

$$I(\phi_e) = \frac{1}{2}\sum_{i=1}^{3}\sum_{j=1}^{3}\phi_{ei}\,\phi_{ej}\,M_{ij}^{(e)} + g_e\sum_{\mathrm{i=1}}^{3}\sum_{\mathrm{j=1}}^{3}\phi_{ei}T_{ij}^{(e)}$$

Since $T_{ij}^{(e)}$ is symmetric, i.e , $T_{ij}^{(e)} = T_{ji}^{(e)}$, we can also write

$$I(\phi_e) = \frac{1}{2}\sum_{i=1}^{3}\sum_{j=1}^{3}\phi_{ei}\,\phi_{ej}\,M_{ij}^{(e)} + g_e\sum_{\mathrm{i=1}}^{3}\sum_{\mathrm{j=1}}^{3}\phi_{ei}\,T_{ji}^{(e)}$$

This equation can be written in matrix form as

$$I(\phi_e) = \frac{1}{2}\,[\phi_e]^{\mathrm{t}}\left[\mathrm{M}^{(\mathrm{e})}\right][\phi_e] + [\phi_e]^{\mathrm{t}}\left[\mathrm{N}^{(\mathrm{e})}\right]\mathrm{g}_e$$

In order for $I(\phi_e)$ to be a scalar quantity , $[\phi_e]^{\mathrm{t}}\left[\mathrm{N}^{(\mathrm{e})}\right]\mathrm{g}_e$, must also be scalar, which dictates that the element coefficient matrix $\left[\mathrm{N}^{(\mathrm{e})}\right]\mathrm{g}_e$ must actually be a [3x1] vector. Therefore, concerning g_e , we have an element coefficient vector , $\mathrm{F}^{(\mathrm{e})} = \left[\mathrm{N}^{(\mathrm{e})}\right]\mathrm{g}_e$,

which is

$$\mathrm{F}^{(\mathrm{e})} = \mathrm{g}_e\begin{bmatrix} T_{11}^{(e)} + T_{12}^{(e)} + T_{13}^{(e)} \\ T_{21}^{(e)} + T_{22}^{(e)} + T_{23}^{(e)} \\ T_{31}^{(e)} + T_{32}^{(e)} + T_{33}^{(e)} \end{bmatrix}, \qquad where\ \ \mathrm{N}^{(\mathrm{e})} = \begin{bmatrix} T_{11}^{(e)} + T_{12}^{(e)} + T_{13}^{(e)} \\ T_{21}^{(e)} + T_{22}^{(e)} + T_{23}^{(e)} \\ T_{31}^{(e)} + T_{32}^{(e)} + T_{33}^{(e)} \end{bmatrix}$$

Therefore

$$I(\phi_e) = \frac{1}{2}\,[\phi_e]^{\mathrm{t}}\left[\mathrm{M}^{(\mathrm{e})}\right][\phi_e] + [\phi_e]^{\mathrm{t}}\left[\mathrm{F}^{(\mathrm{e})}\right]$$

Summing $I(\phi_e)$ for all elements in the solution region

$$I(\phi) = \sum_{e=1}^{N} I(\phi_e)$$

$$I(\phi) = \frac{1}{2}\,[\phi]^{\mathrm{t}}\,[\mathrm{M}]\,[\phi] + [\phi]^{\mathrm{t}}\,[\mathrm{F}]$$

$$\frac{\partial I(\phi)}{\partial \phi_k} = 0 \quad , \quad for\ all\ free\ nodes$$

Which yields to

$$\frac{\partial I(\phi)}{\partial \phi_k} = \sum_{i=1}^{n}[\,\phi_i M_{ki} + F_k\,] = 0$$

$$\sum_{i=1}^{n}\phi_i M_{ki} = -\,F_k$$

Using this identity , ϕ_i , i=1,2,…,n , can be easily solved.

The question here is, how do we assemble the element coefficient vector [F] ? Since we know how to assemble [M] , [T] or [C] from the previous discussion, as they are assembled identically the same, after assembling [M] , we can easily assemble [F] . The assemblage of [F] can be best described by an example.

Consider the element coefficient matrix [M] given below, first we look at the main diagonal of [M] and then we observe how the indices of the main diagonal of [M] are assembled from the element coefficient matrices $M^{(e)}$. The assemblage of [F] using $F^{(e)}$ is identical to that of M_{ii} from $M^{(e)}$.

$$[M] = \begin{bmatrix} M_{11}{}^{(1)} + M_{33}{}^{(2)} & M_{12}{}^{(1)} & M_{13}{}^{(1)} + M_{31}{}^{(2)} & M_{32}{}^{(2)} & 0 \\ M_{21}{}^{(1)} & M_{22}{}^{(1)} & M_{23}{}^{(1)} & 0 & 0 \\ M_{31}{}^{(1)} + M_{13}{}^{(1)} & M_{32}{}^{(1)} & M_{33}{}^{(1)} + M_{11}{}^{(2)} & M_{12}{}^{(2)} + M_{21}{}^{(3)} & M_{23}{}^{(3)} \\ M_{23}{}^{(2)} & 0 & M_{21}{}^{(2)} + M_{12}{}^{(3)} & M_{22}{}^{(2)} + M_{11}{}^{(3)} & M_{13}{}^{(3)} \\ 0 & 0 & M_{32}{}^{(3)} & M_{31}{}^{(3)} & M_{33}{}^{(3)} \end{bmatrix}$$

When we look at the main diagonal, we see that

$M_{11} = M_{11}{}^{(1)} + M_{33}{}^{(2)}$, therefore , $F_1 = F_1{}^{(1)} + F_3{}^{(2)}$.

$M_{22} = M_{22}{}^{(1)}$, therefore , $F_2 = F_2{}^{(1)}$.

$M_{33} = M_{33}{}^{(1)} + M_{11}{}^{(2)}$, therefore , $F_3 = F_3{}^{(1)} + F_1{}^{(2)}$.

$M_{44} = M_{22}{}^{(2)} + M_{11}{}^{(3)}$, therefore , $F_4 = F_2{}^{(2)} + F_1{}^{(3)}$.

$M_{55} = M_{33}{}^{(3)}$, therefore , $F_5 = F_3{}^{(3)}$.

Therefore the global [F] vector is

$$[F] = \begin{bmatrix} F_1{}^{(1)} + F_3{}^{(2)} \\ F_2{}^{(1)} \\ F_3{}^{(1)} + F_1{}^{(2)} \\ F_2{}^{(2)} + F_1{}^{(3)} \\ F_3{}^{(3)} \end{bmatrix}$$

The coefficient matrices [M] and [F] indicate that we are assembling elements in a solution region that consists of 3 elements and 5 nodes.

Note that the symmetry property of the element coefficient matrices and the global coefficient matrices provides speed for computation, since we only have to calculate the upper triangular part of the matrices.

5.4 Prescribed and free nodes of a solution region

In order to evaluate the solution at all nodes inside a given region, we need to know the solution at the boundary of the given region. The nodes at the boundary are known as the prescribed nodes of the solution region where the solution is already known or prescribed.

For the solution of Helmholtz equation or phasor domain wave equation, the values of prescribed nodes at the boundary of the solution region can be determined using the incident or incoming wave that impinges on the boundary of the solution region. Using the general boundary conditions described in chapter 2, the prescribed node values can be determined directly from the incident field if the wave equation contains no source term, i.e g=0. But if the source term is not zero, the prescribed node values can be determined using the boundary conditions that occur when there are sources at the boundary between two different media (see chapter 2).

Consider the FEM (Finite Element Method) solution of a 2D homogenous wave equation. The FEM solution to this problem can be obtained by solving the system linear of equations generated by the previously found formula

$$\frac{\partial I(\phi)}{\partial \phi_k} = \sum_{i=1}^{n} \phi_i \left[C_{ki} - k^2 T_{ki}\right] = 0 \quad , \quad k = \omega\sqrt{\mu\epsilon}$$

$$\phi_1[C_{11} - k^2T_{11}] + \phi_2[C_{12} - k^2T_{12}] + \cdots + \phi_n[C_{1n} - k^2T_{1n}] = 0$$

$$\phi_1[C_{21} - k^2T_{21}] + \phi_2[C_{22} - k^2T_{22}] + \cdots + \phi_n[C_{2n} - k^2T_{2n}] = 0$$

$$\phi_1[C_{31} - k^2T_{31}] + \phi_2[C_{32} - k^2T_{32}] + \cdots + \phi_n[C_{3n} - k^2T_{3n}] = 0$$

$$\phi_1[C_{41} - k^2T_{41}] + \phi_2[C_{42} - k^2T_{42}] + \cdots + \phi_n[C_{4n} - k^2T_{4n}] = 0$$

$$\vdots$$

$$\phi_1[C_{n1} - k^2T_{n1}] + \phi_2[C_{n2} - k^2T_{n2}] + \cdots + \phi_n[C_{nn} - k^2T_{nn}] = 0$$

$$\frac{\partial I(\phi)}{\partial \phi_k} = \sum_{i=1}^{n} \phi_i \left[C_{ki} - k^2 T_{ki}\right] = 0 \quad , \quad k = \omega\sqrt{\mu\epsilon}$$

$$\phi_i = \left\{ \begin{array}{ll} \phi_{free} = \phi_f & , \quad if\ the\ node\ is\ not\ on\ the\ boundary \\ \phi_{prescribed} = \phi_p & , \quad if\ the\ node\ is\ on\ the\ boundary \end{array} \right\}$$

Since the prescribed node values are known, we can rewrite the system of linear equations as

$$\phi_{f1}\left[C_{1,f1} - k^2 T_{1,f1}\right] + .. + \phi_{fn}\left[C_{1,fn} - k^2 T_{1,fn}\right] = \phi_{p1}\left[C_{1,p1} - k^2 T_{1,p1}\right] + .. + \phi_{pn}\left[C_{1,pn} - k^2 T_{1,pn}\right]$$

$$\phi_{f1}\left[C_{2,f1} - k^2 T_{2,f1}\right] + .. + \phi_{fn}\left[C_{2,fn} - k^2 T_{2,fn}\right] = \phi_{p1}\left[C_{2,p1} - k^2 T_{2,p1}\right] + .. + \phi_{pn}\left[C_{2,pn} - k^2 T_{2,pn}\right]$$

$$\phi_{f1}\left[C_{3,f1} - k^2 T_{3,f1}\right] + .. + \phi_{fn}\left[C_{3,fn} - k^2 T_{2,fn}\right] = \phi_{p1}\left[C_{3,p1} - k^2 T_{3,p1}\right] + .. + \phi_{pn}\left[C_{3,pn} - k^2 T_{3,pn}\right]$$

$$\bullet$$

$$\bullet$$

$$\phi_{f1}\left[C_{n,f1} - k^2 T_{n,f1}\right] + .. + \phi_{fn}\left[C_{n,fn} - k^2 T_{n,fn}\right] = \phi_{p1}\left[C_{n,p1} - k^2 T_{n,p1}\right] + .. + \phi_{pn}\left[C_{n,pn} - k^2 T_{n,pn}\right]$$

Which can be solved for $\{\phi_{f1}\ ,\ \phi_{f2}\ ,\ \phi_{f3}\ , \ldots\ , \phi_{fn}\}$.

As an example, the hexagon shown below has six nodes on the boundary, so it has six prescribed nodes. The node at the center of the hexagon is the only node that is not on the boundary, so there is only one free node. Assume that we want to solve the homogenous Helmholtz equation for the geometry given below. Since we have only one free node, only a single equation will be enough to get the value of ϕ at the center of the hexagon, which is the only unknown. The equation is

$$\phi_{f1}\left[C_{1,f1} - k^2 T_{1,f1}\right] = \phi_{p1}\left[C_{1,p1} - k^2 T_{1,p1}\right] + \ldots + \phi_{p6}\left[C_{1,p6} - k^2 T_{1,p6}\right]$$

Where $\{f_1\ ,\ p_1\ , \ldots\ , p_6\}$ are the assigned node numbers.

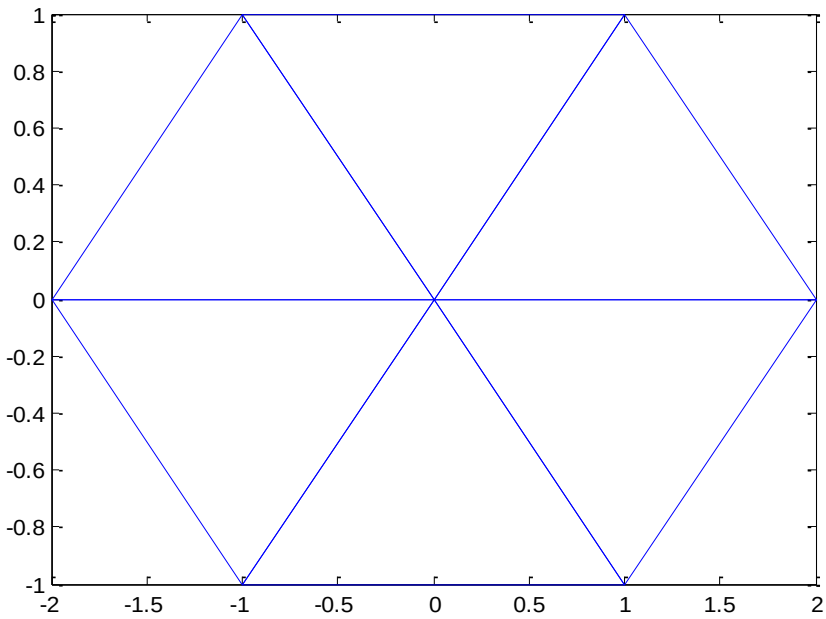

Figure 5.4: A hexagonal mesh of six triangles.

5.5 Examples of 2D FEM solutions of the Helmholtz equation in a closed region

Consider the hexagon example given in the previous section. If the prescribed nodes at the boundary are numbered as $\{\phi_1, \phi_2, \phi_3, \phi_4, \phi_5, \phi_6\}$ and the free node at the center is numbered as ϕ_7, we can solve for ϕ_7 by using the linear system

$$\frac{\partial I(\phi)}{\partial \phi_k} = \sum_{i=1}^{n} \phi_i \, [C_{ki} - k^2 T_{ki}] \; = 0 \qquad , \qquad k = \omega\sqrt{\mu\epsilon}$$

Since in that case there is only one free node, we need only one equation to solve

$$\phi_1[C_{11} - k^2 T_{11}] + \phi_2[C_{12} - k^2 T_{12}] + \cdots + \phi_7[C_{17} - k^2 T_{17}] = 0$$

$$\phi_7 = -\frac{[C_{11} - k^2 T_{11}]}{[C_{17} - k^2 T_{17}]}\phi_1 - \frac{[C_{12} - k^2 T_{12}]}{[C_{17} - k^2 T_{17}]}\phi_2 - \cdots - \frac{[C_{16} - k^2 T_{16}]}{[C_{17} - k^2 T_{17}]}\phi_6$$

$$C_{ij}{}^{(e)} = \frac{1}{4A}[u_i u_j + v_i v_j]$$

$$u_1 = (y_2 - y_3)\,, \qquad u_2 = (y_3 - y_1)\,, \qquad u_3 = (y_1 - y_2)$$

$$v_1 = (x_3 - x_2)\,, \qquad v_2 = (x_1 - x_3)\,, \qquad v_3 = (x_2 - x_1)$$

$$T_{ij}{}^{(e)} = \int\int \alpha_i \, \alpha_j \, dS \; = \begin{cases} \mathrm{A}/12 & \mathrm{i} \neq \mathrm{j} \\ \mathrm{A}/6 & \mathrm{i} = \mathrm{j} \end{cases}$$

The global matrices C and T are assembled from $C_{ij}{}^{(e)}$ *and* $T_{ij}{}^{(e)}$ *as before*.

As another example, consider a triangular mesh with 15 nodes where 3 of the nodes are in the interior region of the triangle and the others are at the boundary.

$$\phi_i = \left\{ \begin{array}{ll} \phi_{free} = \phi_{13,14,15} & , \quad \textit{the nodes are not on the boundary} \\ \phi_{prescribed} \quad = \phi_{1,\ldots,12} & , \quad \textit{the nodes are on the boundary} \end{array} \right\}$$

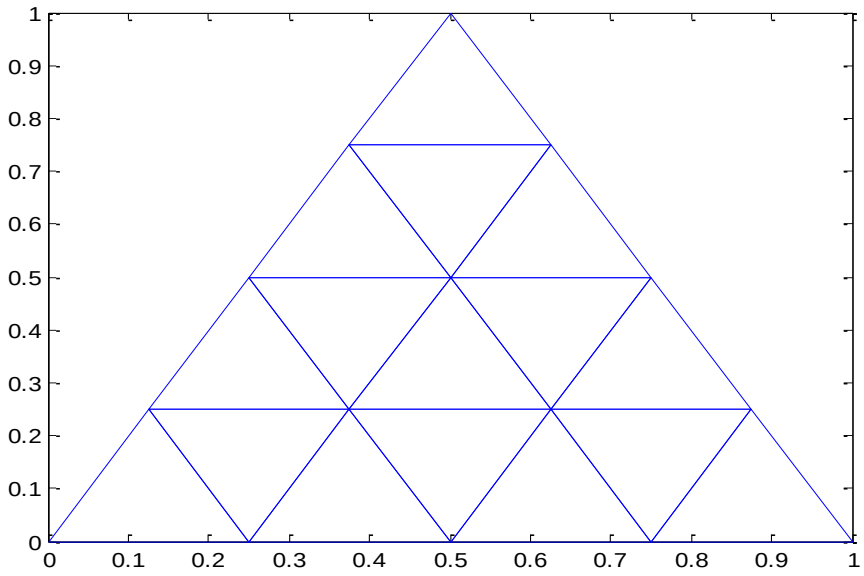

Figure 5.5: A triangular mesh of sixteen triangles.

Since there are only three free nodes, we need to solve only three equations, for n=15

$$\phi_{f1}[C_{1,f1}-k^2T_{1,f1}]+..+\phi_{fn}[C_{1,fn}-k^2T_{1,fn}]=\phi_{p1}[C_{1,p1}-k^2T_{1,p1}]+..+\phi_{pn}[C_{1,pn}-k^2T_{1,pn}]$$

$$\phi_{f1}[C_{2,f1}-k^2T_{2,f1}]+..+\phi_{fn}[C_{2,fn}-k^2T_{2,fn}]=\phi_{p1}[C_{2,p1}-k^2T_{2,p1}]+..+\phi_{pn}[C_{2,pn}-k^2T_{2,pn}]$$

$$\phi_{f1}[C_{3,f1}-k^2T_{3,f1}]+..+\phi_{fn}[C_{3,fn}-k^2T_{2,fn}]=\phi_{p1}[C_{3,p1}-k^2T_{3,p1}]+..+\phi_{pn}[C_{3,pn}-k^2T_{3,pn}]$$

$$\bullet$$

$$\bullet$$

$$\phi_{f1}[C_{n,f1}-k^2T_{n,f1}]+..+\phi_{fn}[C_{n,fn}-k^2T_{n,fn}]=\phi_{p1}[C_{n,p1}-k^2T_{n,p1}]+..+\phi_{pn}[C_{n,pn}-k^2T_{n,pn}]$$

The free node values $\phi_{free}=\phi_{13,14,15}$ can be found by reordering the terms and using any of the three equations from the system. The general formula for the solution of a given free node which is in a solution region that has n nodes can be achieved by reordering the terms of the linear system as

$$\phi_i = -\sum_{j=1,\ j\neq i,\ 1\leq k\leq n}^{j=n}\frac{[C_{kj}-k^2T_{kj}]}{[C_{ki}-k^2T_{ki}]}\phi_j \quad , \qquad where$$

$$i\ is\ a\ free\ node\ , n\ is\ the\ total\ number\ of\ nodes,\ \ k\ is\ any\ node\ between\ 1\ and\ N.$$

For this triangular solution region with n=15 and i={13,14,15} , we have

$$\phi_i = -\sum_{j=1,\ j\neq i,\ 1\leq k\leq 15}^{j=15}\frac{[C_{kj}-k^2T_{kj}]}{[C_{ki}-k^2T_{ki}]}\phi_j \quad , \quad i\ is\ a\ free\ node\ .$$

$$\phi_{13} = -\sum_{j=1,\ j\neq 13,\ 1\leq k\leq 15}^{j=15} \frac{[C_{kj} - k^2 T_{kj}]}{[C_{k,13} - k^2 T_{k,13}]}\phi_j$$

$$\phi_{14} = -\sum_{j=1,\ j\neq 14,\ 1\leq k\leq 15}^{j=15} \frac{[C_{kj} - k^2 T_{kj}]}{[C_{k,14} - k^2 T_{k,14}]}\phi_j$$

$$\phi_{15} = -\sum_{j=1,\ j\neq 15,\ 1\leq k\leq 15}^{j=15} \frac{[C_{kj} - k^2 T_{kj}]}{[C_{k,15} - k^2 T_{k,15}]}\phi_j$$

Solving this 3×3 system, we can get the values of ϕ at the free nodes.

Using FEM we convert the Helmholtz equation into an $N \times N$ system of linear equations, especially problems that involve closed solution regions are very easy to solve using FEM. The following example is given here using MATLAB/ PDE Toolbox. This toolbox is very useful for closed boundary problems and it offers a high order of mesh refinement feature to produce more accurate results. This example involves a rectangular boundary with a Dirichlet boundary condition.

Ex : $\nabla^2\phi + 100\pi^2\phi = 0$, $\phi = \begin{cases} \phi_p = 1 \ , \ On\ the\ boundary\ of\ the\ square \\ \phi_f \ , \ Inside\ the\ square\ region\ R: -0.4 \leq \{x, y\} \leq 0.4 \end{cases}$

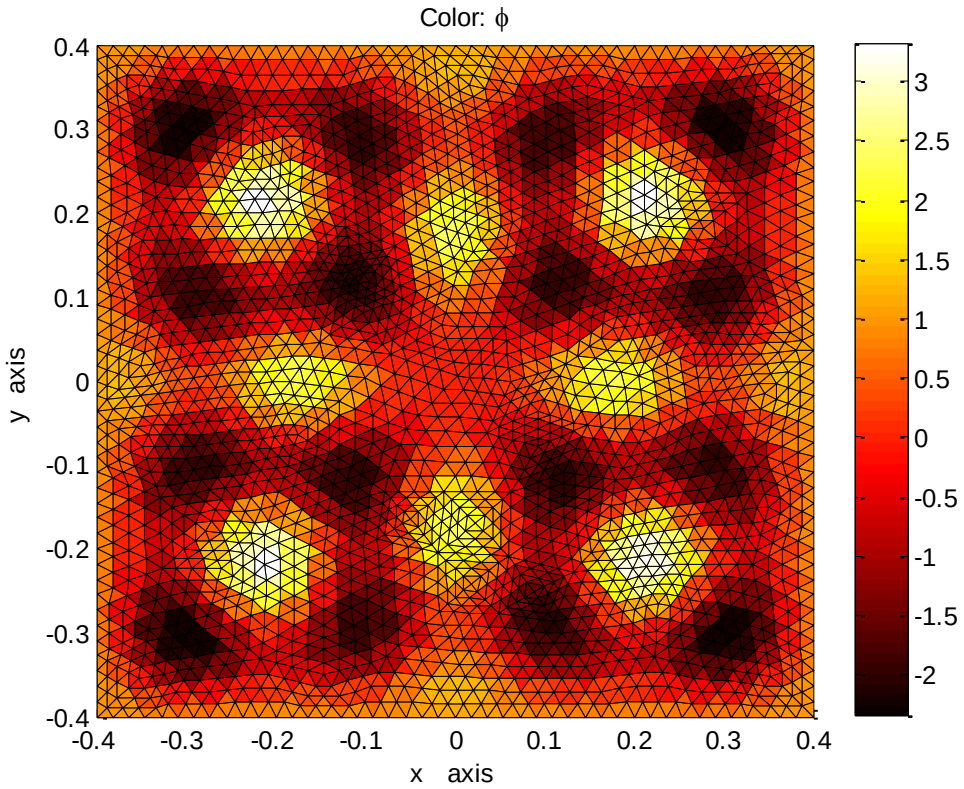

Figure5.6:Discretization of the rectangular region R, and the distribution of ϕ.

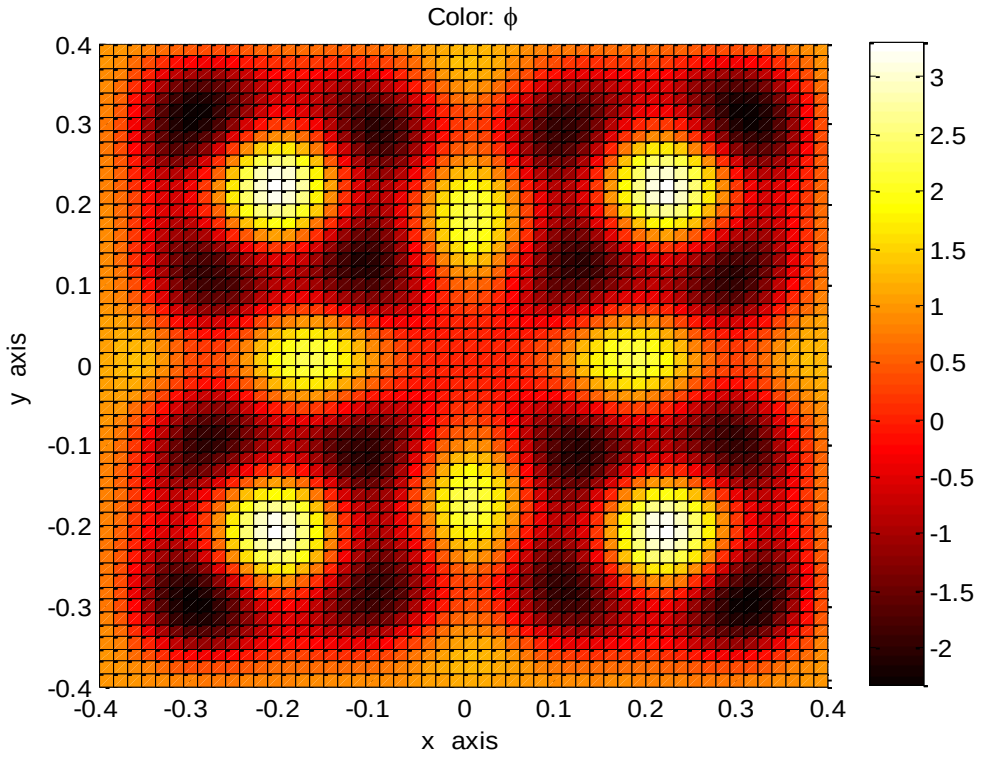

Figure5.7:The actual distribution of ϕ inside R.

CHAPTER 6

APPLICATION OF FEM ON ROUGH SURFACE SCATTERING PROBLEMS

We have previously described the conversion of the scalar wave equation in phasor form, into a linear system of equations. After this conversion we discretize the solution region using triangles and assemble the global coefficient matrix using the individual coefficient matrices of each element in the region to solve the linear system. In order to solve the linear system, we need prescribed values, which can be obtained by imposing the boundary conditions at the surface boundary. Having the global coefficient matrix values and the prescribed node values at hand, we can solve the linear system of equations to get the node values everywhere inside the solution region.

Since we know the coordinates of each element in the solution region, assembling the global coefficient matrix can be thought as the easy part. What is important is to impose the surface boundary condition on the rough surface.

In electromagnetics, surfaces, whether flat or arbitrary in shape, indicate the sudden change of constitutive parameters in an unbounded domain or space. Therefore a surface can be dielectric, good conductor, weak conductor, or a perfect conductor. Depending on the constitutive parameters of the surface an incident field produces a scattered field and a transmitted field on the surface. Here, we want to obtain the scattered field as we are interested in the domain where the incident field exists.

For perfect electric conductor (PEC) surfaces, the tangential component of the scattered field is equal to the incident field in magnitude and there is a 180° phase difference between the two. Basically for a TM_z incident wave, we have

$$E_z^{\,s} = -E_z^{\,inc} \quad on\ perfect\ electric\ conductors$$

However, if the surface boundary is not a PEC, then we must use an impedance boundary condition on the surface, one approach is to use *Kirchoff's approximation* which approximates each point on the surface with a tangent plane at that point and evaluates the scattered field on that point as if the point is on a flat surface (tangential planar surface). Another approach is to apply the impedance boundary condition embedded in the finite element method itself by modifying the coefficient matrices of elements that are on the surface. In this approach, element coefficient matrices of surface elements are modified to include the loss effect of the surface, but the coefficient matrices of elements that are not on the surface remain unchanged. In the end, all of the element coefficient matrices are assembled to form the global coefficient matrix as before and using the incident field and the surface loss factor we form the output result vector and solve the linear system. We will use this latter approach and explain it in detail.

Electromagnetic scattering problems involve open boundaries, and open boundary problems are more complicated compared to problems involving closed boundaries. When we are dealing with open boundary problems, we have to limit our computational domain of interest to a manageable size, otherwise the size of the computational region is infinite. This can be achieved by applying grid truncation techniques known as *Absorbing Boundary Conditions(ABC)*. There are lots of ABC formulations in literature, the most commonly used one is Berenger's *Perfectly Matched Layer (PML)* [2], which suggests the use of an artificial absorbing layer of material to realize the absorbing boundary condition. After the introduction of an initial PML model by Berenger in 1994, the concept has been further developed by many others. Modifications made on the initial concept of PML have led to much more applicable and accurate PML realizations regarding the realization of absorbing boundary conditions. One of them is the *Locally Conformal Perfectly Matched Layer*, which uses a non-Maxwellian approach to impose an absorbing boundary condition and achieves non-Maxwellian PML realization by using complex coordinate transformation. We will use the locally conformal PML approach and explain it in some detail, more detailed information about locally conformal PML can be found in the journal by Ozgun and Kuzuoglu[6].

Recall that the finite element method solution of a scalar 2D homogenous wave equation in phasor domain can be determined for each node ϕ_i , from the linear system

$$\frac{\partial I(\phi)}{\partial \phi_k} = \sum_{i=1}^{n} \phi_i \left[C_{ki} - k^2 T_{ki}\right] = 0 \quad , \quad k = \omega\sqrt{\mu\epsilon}$$

$$\phi_1[C_{11} - k^2T_{11}] + \phi_2[C_{12} - k^2T_{12}] + \cdots + \phi_n[C_{1n} - k^2T_{1n}] = 0$$
$$\phi_1[C_{21} - k^2T_{21}] + \phi_2[C_{22} - k^2T_{22}] + \cdots + \phi_n[C_{2n} - k^2T_{2n}] = 0$$
$$\phi_1[C_{31} - k^2T_{31}] + \phi_2[C_{32} - k^2T_{32}] + \cdots + \phi_n[C_{3n} - k^2T_{3n}] = 0$$
$$\phi_1[C_{41} - k^2T_{41}] + \phi_2[C_{42} - k^2T_{42}] + \cdots + \phi_n[C_{4n} - k^2T_{4n}] = 0$$
$$\bullet$$
$$\bullet$$
$$\bullet$$
$$\phi_1[C_{n1} - k^2T_{n1}] + \phi_2[C_{n2} - k^2T_{n2}] + \cdots + \phi_n[C_{nn} - k^2T_{nn}] = 0$$

$$\phi_i = \begin{cases} \phi_{free} = \phi_f \quad , & if\ the\ node\ is\ not\ on\ the\ boundary \\ \phi_{prescribed} = \phi_p \quad , & if\ the\ node\ is\ on\ the\ boundary \end{cases}$$

Using the incident field and the appropriate boundary condition on a given rough surface, we can get the field values of the rough surface nodes, which are called *prescribed nodes* therefore we can rewrite the system in terms of free and prescribed nodes as

$$\phi_{f1}\left[C_{1,f1}-k^2T_{1,f1}\right]+..+\phi_{fn}\left[C_{1,fn}-k^2T_{1,fn}\right]=\phi_{p1}\left[C_{1,p1}-k^2T_{1,p1}\right]+..+\phi_{pn}\left[C_{1,pn}-k^2T_{1,pn}\right]$$

$$\phi_{f1}\left[C_{2,f1}-k^2T_{2,f1}\right]+..+\phi_{fn}\left[C_{2,fn}-k^2T_{2,fn}\right]=\phi_{p1}\left[C_{2,p1}-k^2T_{2,p1}\right]+..+\phi_{pn}\left[C_{2,pn}-k^2T_{2,pn}\right]$$

$$\phi_{f1}\left[C_{3,f1}-k^2T_{3,f1}\right]+..+\phi_{fn}\left[C_{3,fn}-k^2T_{2,fn}\right]=\phi_{p1}\left[C_{3,p1}-k^2T_{3,p1}\right]+..+\phi_{pn}\left[C_{3,pn}-k^2T_{3,pn}\right]$$

$$\bullet$$

$$\bullet$$

$$\phi_{f1}\left[C_{n,f1}-k^2T_{n,f1}\right]+..+\phi_{fn}\left[C_{n,fn}-k^2T_{n,fn}\right]=\phi_{p1}\left[C_{n,p1}-k^2T_{n,p1}\right]+..+\phi_{pn}\left[C_{n,pn}-k^2T_{n,pn}\right]$$

Which can be solved for $\{\phi_{f1}\,,\ \phi_{f2}\,,\ \phi_{f3}\,,\ldots\,,\phi_{fn}\}$.

However, since we are interested in an open boundary problem which is rough surface scattering, we must first limit the size of the computational domain such that it will be enough for us to observe the scattered field behaviour. Because, in order to solve a linear system, we need to know the size of the linear system and the size of the linear system is determined by the total number of nodes in the solution region. Using PML, we can limit our solution region to a manageable size and only after we limit our solution region, we can get the total number of nodes in our solution region. Therefore the first thing to do when dealing with a scattering problem, is to limit the size of the domain in accordance with our solution region of interest and the required computer memory. This is achieved by using PML as an absorbing boundary condition. Due to its accuracy and ease of implementation, we will use the *Locally Conformal Perfectly Matched Layer* as described in[6].

After the implementation of a locally conformal PML, we must determine the values of the prescribed nodes using a surface impedance boundary condition over the rough surface. Having determined the size of the computational domain and the values of the prescribed nodes, we can solve the resulting linear system to get the node (field) values everywhere.

So, first we will limit the size of the computational domain using a locally conformal PML and then we will impose an impedance boundary condition over a given rough surface. Therefore we will now discuss these two topics respectively, before proceeding into the solution of a rough surface scattering problem.

6.1 Locally-conformal perfectly matched layer

The perfectly matched layer (PML) is an artificial layer that is used to bound the computational domain when we are dealing with an unbounded domain. A PML must completely absorb the outgoing waves without yielding any reflections for any given frequency and incidence angle. In other words a PML must be reflectionless to provide accurate results.

In problems involving scattering, radiation or propagation of waves the physical domain extends to infinity, but since we have a limited computer memory, we should restrict the actual solution region to a region with limited size which is determined by the PML boundary. The restricted solution region effectively simulates the solution as if the solution goes to infinity provided that the PML is reflectionless and it completely attenuates the outgoing waves.

Many of the current PML formulations in FEM literature use artificial absorbing materials which have certain constitutive parameters. These constitutive parameters are defined such that the resulting PML is an anisotropic, lossy medium associated with the necesary conditions to enable reflectionless transmission and attenuation of the outgoing waves. In locally-conformal PML technique, we do not need to use an artificial material with certain constitutive parameters, we only transform the actual coordinates of the PML medium with their complex counterparts using an effective mathematical transformation given in [6]. This is a very simple and an effective PML formulation that accurately provides reflectionless transmission of the outgoing waves.

In the locally-conformal PML method, we define the complex coordinate transformation which maps the coordinates of a point P in the PML region Ω into its complex counterpart $\tilde{P}$ in the complex PML region Γ , where $\Omega \in R^2$, $\Gamma \in C^2$, by using the following transformation (see [6])

$$\overrightarrow{r_c} = \vec{r} + \frac{1}{jk} f(\xi)\hat{n}(\xi) \qquad , \quad \vec{r} \in R^2, \qquad \overrightarrow{r_c} \in C^2, \qquad k = w\sqrt{\mu\epsilon}$$

$$f(\xi) = \frac{\alpha \xi^m}{m\|\overrightarrow{r_{out}} - \overrightarrow{r_{in}}\|^{m-1}}$$

$$\xi = \|\vec{r} - \overrightarrow{r_{in}}\| \ , \qquad \overrightarrow{r_{in}} \in \partial\Omega_{\text{in}} \ , \qquad \hat{n}(\xi) = \frac{\vec{r} - \overrightarrow{r_{in}}}{\|\vec{r} - \overrightarrow{r_{in}}\|}$$

$$\overrightarrow{r_c} = \vec{r} + \frac{1}{jk} \frac{\alpha \xi^m}{m\|\overrightarrow{r_{out}} - \overrightarrow{r_{in}}\|^{m-1}} \hat{n}(\xi)$$

$$\overrightarrow{r_c} = \vec{r} + \frac{1}{jk} \frac{\alpha \xi^m}{m\|\overrightarrow{r_{out}} - \overrightarrow{r_{in}}\|^{m-1}} \frac{\vec{r} - \overrightarrow{r_{in}}}{\|\vec{r} - \overrightarrow{r_{in}}\|}$$

Where $\vec{r} \in R^2$, $\overrightarrow{r_c} \in C^2$ are the position vectors of the points P in free space and $\tilde{P}$ in complex space respectively ; $\overrightarrow{r_{out}}$ is the position vector of P_{out}, $\hat{n}(\xi)$ is the unit vector along the direction of propagation and $k = w\sqrt{\mu\epsilon}$ is the wavenumber. Usually α is chosen as 10^4 due to increased accuracy and m can be chosen as 2 or 3 depending on the accuracy of computation, and it is related to the decay of the wave inside Ω .

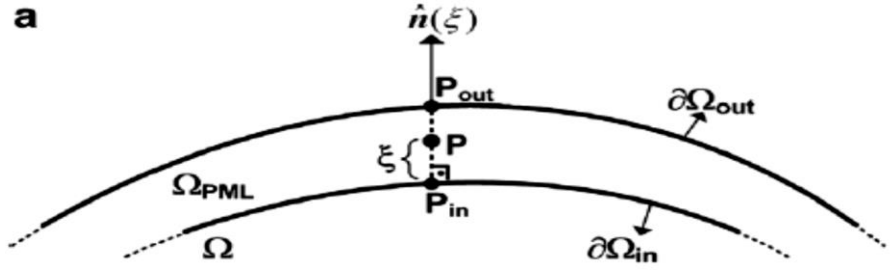

Figure6.1:Locally conformal PML implementation, a PML with smooth curvature[6].

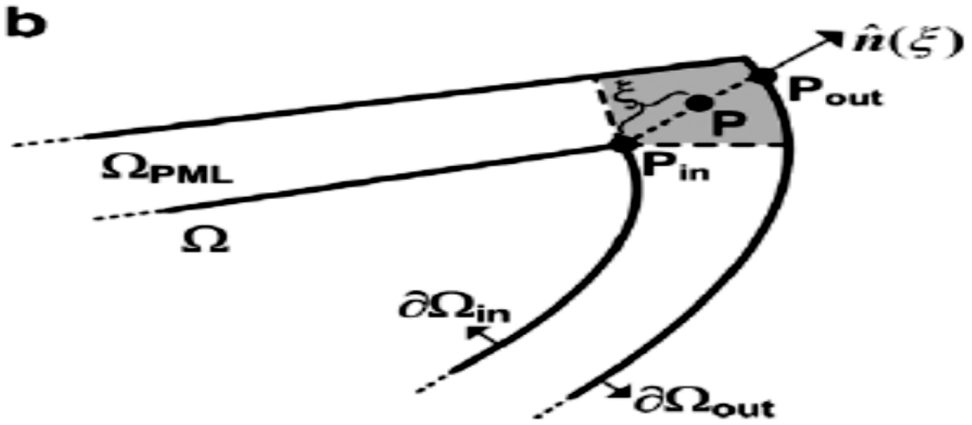

Figure6.2:Locally conformal PML implementation, a PML with curvature discontinuity[6].

$$\overrightarrow{r_c} = \vec{r} + \frac{1}{jk}\ \frac{\alpha\xi^m}{m\|\overrightarrow{r_{out}} - \overrightarrow{r_{in}}\|^{m-1}}\ \frac{\vec{r} - \overrightarrow{r_{in}}}{\|\vec{r} - \overrightarrow{r_{in}}\|}\quad ,\quad \xi = \|\vec{r} - \overrightarrow{r_{in}}\|\ ,\qquad \overrightarrow{r_{in}} \in \partial\Omega_{\text{in}}$$

$$\overrightarrow{r_c} = \vec{r} + \frac{1}{jk}\ \frac{\alpha\|\vec{r} - \overrightarrow{r_{in}}\|^m}{m\|\overrightarrow{r_{out}} - \overrightarrow{r_{in}}\|^{m-1}}\ \frac{\vec{r} - \overrightarrow{r_{in}}}{\|\vec{r} - \overrightarrow{r_{in}}\|}\quad ,\qquad \overrightarrow{r_{in}} \in \partial\Omega_{\text{in}}$$

This equation for $\overrightarrow{r_c}$ transforms the actual coordinates represented by the position vector $\vec{r}$ into complex coordinates represented by the complex position vector $\overrightarrow{r_c}$ and enables the PML to effectively absorb the outgoing waves and to minimize reflections. This transformation also meets with the following three conditions which should be satisfied for a successful PML realization[6]:

(i) the outgoing wave in the neighborhood of the point P_{in} must be transmitted into Ω_{PML} without any reflection.

(ii) the transmitted wave must be subjected to a monotonic decay within Ω_{PML} .

(iii) the magnitude of the transmitted wave must be negligible on $\partial\Omega_{\text{PML}}$.

In this thesis, we are analyzing rough surface scattering problem, therefore a rectangular PML can be used to absorb the outgoing waves. The equation for $\overrightarrow{r_c}$ greatly simplifies over PMLs with rectangular boundaries. It can be proven that for a rectangular PML, the transformation

$$\overrightarrow{r_c} = \vec{r} + \frac{1}{jk} \frac{\alpha \|\vec{r} - \overrightarrow{r_{in}}\|^m}{m\|\overrightarrow{r_{out}} - \overrightarrow{r_{in}}\|^{m-1}} \frac{\vec{r} - \overrightarrow{r_{in}}}{\|\vec{r} - \overrightarrow{r_{in}}\|} \quad , \quad \overrightarrow{r_{in}} \in \partial\Omega_{\text{in}}$$

In conjunction with figure6.3, simplifies into [6]

$$\tilde{x} = x + \frac{\alpha}{jk}(x - x_{in}) \ , \ \tilde{y} = y \quad (in\ region\ 1)$$

$$\tilde{y} = y + \frac{\alpha}{jk}(y - y_{in}) \ , \ \tilde{x} = x \quad (in\ region\ 2)$$

$$\tilde{x} = x + \frac{\alpha}{jk}(x - x_{in}) \quad , \ \tilde{y} = y + \frac{\alpha}{jk}(y - y_{in}) \quad (in\ region\ 3)$$

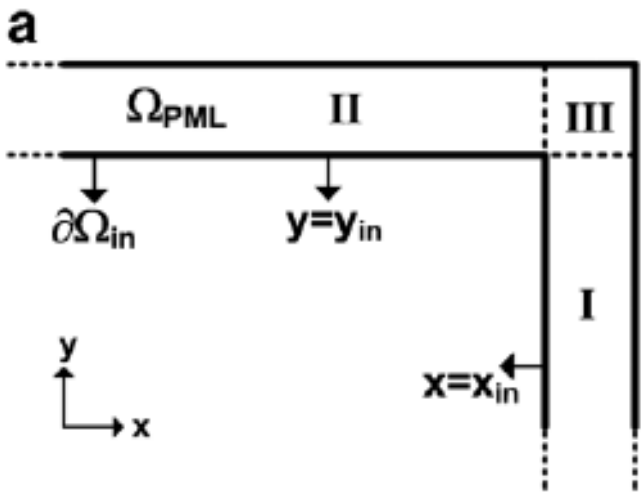

Figure6.3:Locally conformal PML implementation, a rectangular PML [6].

Locally-conformal PML formulation, mathematically imitates an anisotropic, lossy PML by transforming real coordinates inside the PML region into complex coordinates and therefore absorbs the outgoing waves without reflection. Here the approach is geometrical rather than electrical, yet its simplicity makes it more favorable than PMLs that are implemented using artificial material formulations.

In FEM formulations, we approximate the actual solution within each element in the solution region using interpolating polynomials, i.e. basis functions. These functions are based on real coordinates of the elements. Since we have complex coordinates inside the PML region after applying the transformation, the basis functions of the elements inside the PML region are complex as well. For triangular elements we have

$$\Phi_e(x,y) = \sum_{i=1}^{3} \alpha_i(x,y)\, \Phi_{ei}$$

$$\alpha_1 = \frac{1}{2A}[(x_2y_3 - x_3y_2) + (y_2 - y_3)x + (\mathrm{x}_3 - \mathrm{x}_2)\mathrm{y}\,]$$

$$\alpha_2 = \frac{1}{2A}[(x_3y_1 - x_1y_3) + (y_3 - y_1)x + (\mathrm{x}_1 - \mathrm{x}_3)\mathrm{y}\,]$$

$$\alpha_3 = \frac{1}{2A}[(x_1y_2 - x_2y_1) + (y_1 - y_2)x + (\mathrm{x}_2 - \mathrm{x}_1)\mathrm{y}\,]$$

If we consider region 3 in Figure6.3 as an example, after complex coordinate transformation, the coordinates and the formulation become

$$\tilde{x}_i = x_i + \frac{\alpha}{jk}(x_i - x_{in}) \quad , \quad \tilde{y}_i = y_i + \frac{\alpha}{jk}(y_i - y_{in})$$

$$\tilde{\alpha}_1 = \frac{1}{2A}[(\tilde{x}_2\tilde{y}_3 - \tilde{x}_3\tilde{y}_2) + (\tilde{y}_2 - \tilde{y}_3)x + (\tilde{x}_3 - \tilde{x}_2)\mathrm{y}\,]$$

$$\tilde{\alpha}_2 = \frac{1}{2A}[(\tilde{x}_3\tilde{y}_1 - \tilde{x}_1\tilde{y}_3) + (\tilde{y}_3 - \tilde{y}_1)x + (\tilde{x}_1 - \tilde{x}_3)\mathrm{y}\,]$$

$$\tilde{\alpha}_3 = \frac{1}{2A}[(\tilde{x}_1\tilde{y}_2 - \tilde{x}_2\tilde{y}_1) + (\tilde{y}_1 - \tilde{y}_2)x + (\tilde{x}_2 - \tilde{x}_1)\mathrm{y}\,]$$

$$\tilde{\Phi}_e(x,y) = \sum_{i=1}^{3} \tilde{\alpha}_i(x,y)\tilde{\Phi}_{ei}$$

After the transformation, we follow the previously described FEM procedure, here the coordinates of the elements inside the PML region are complex, this will cause the outgoing waves to decay gradually and efficiently and enables us to analyze scattering problems accurately.

6.2.1 Imposing boundary conditions on the rough surface – Kirchoff's approximation

The incident TM_z wave hits on the rough surface boundary and based on the constitutive rough surface parameters, there will be a scattered field on the rough surface boundary. In the case of an infinite and a perfectly flat boundary, the incident and reflected fields are related with the $Fresnel\ reflection\ coefficients\ \Gamma_{TE}\ and\ \Gamma_{TM}$ which are given for TM_z and TE_z polarizations as

$$\Gamma_{TM} = \frac{Z_2\cos(\theta_i) - Z_1\cos(\theta_t)}{Z_2\cos(\theta_i) + Z_1\cos(\theta_t)} \quad , \quad \Gamma_{TE} = \frac{Z_2\cos(\theta_t) - Z_1\cos(\theta_i)}{Z_2\cos(\theta_t) + Z_1\cos(\theta_i)}$$

$$k_1 sin(\theta_i) = k_2 sin(\theta_t) \quad , \quad Snell's\ law\ of\ refraction$$

$$k_1 = j\beta_1 \quad , \quad k_2 = \alpha_2 + j\beta_2$$

$$\alpha_2 = \omega\sqrt{\mu\epsilon}\left\{\frac{1}{2}\left[\sqrt{1 + (\frac{\sigma}{\omega\epsilon})^2} - 1\right]\right\}^{1/2} \quad , \quad \beta_2 = \omega\sqrt{\mu\epsilon}\left\{\frac{1}{2}\left[\sqrt{1 + (\frac{\sigma}{\omega\epsilon})^2} + 1\right]\right\}^{1/2}$$

$$\alpha_2 : Attenuation\ constant\ of\ the\ lossy\ rough\ surface$$

$$\beta_2 : Phase\ constant\ of\ the\ lossy\ rough\ surface$$

$$\theta_t = sin^{-1}\left(\frac{j\beta_1}{\alpha_2 + j\beta_2} sin(\theta_i)\right)$$

$$Z_i = \begin{cases} Z_2 = \sqrt{\dfrac{j\omega\mu_2}{\sigma + j\omega\epsilon_2}} \ , & for\ the\ lossy\ flat\ surface\ boundary \\ Z_1 = \sqrt{\dfrac{\mu_1}{\epsilon_1}} \ , & for\ the\ computational\ domain \end{cases}$$

$$E_{z,\ sca,\ flat\ surface} = (\Gamma_{TM})\left(E_{z,\ inc,\ flat\ surface}\right)$$

$$H_{z,\ sca,\ flat\ surface} = (\Gamma_{TE})\left(H_{z,\ inc,\ flat\ surface}\right)$$

As for rough surfaces, since the surface is not flat, Fresnel reflection coefficients Γ_{TE} , Γ_{TM} are not applicable because on a rough surface the surface normal is not constant but keeps changing from one surface point to another, therefore the incidence angle θ_i and the refraction angle θ_t differs at each point on the rough surface.

Since at every point on the rough surface, the surface normal may change instantaneously, the incidence and refraction angles may also change instantaneously. Based on this assumption we may modify the Fresnel reflection coefficients to include this instantaneous effect such that for an instantaneous incidence angle θ_i' and an instantaneous refraction angle θ_t' we have instantaneous fresnel reflection coefficients Γ_{TM}' and Γ_{TE}', this is known as *Kirchoff's approximation*, which assumes that the surface is locally smooth and thus the field at a point on the surface is equal to the field that would be present on a tangent plane at that point. However Kirchoff's approximation fails to evaluate field values at sharp edges on a rough surface since at sharp edges derivative does not exist and thus no tangent plane approximation is available. The coefficients Γ_{TM}' and Γ_{TE}' are given as follows[7]

$$\Gamma_{TM}' = \frac{Z_2\cos(\theta_i') - Z_1\cos(\theta_t')}{Z_2\cos(\theta_i') + Z_1\cos(\theta_t')} \quad , \quad \Gamma_{TE}' = \frac{Z_2\cos(\theta_t') - Z_1\cos(\theta_i')}{Z_2\cos(\theta_t') + Z_1\cos(\theta_i')}$$

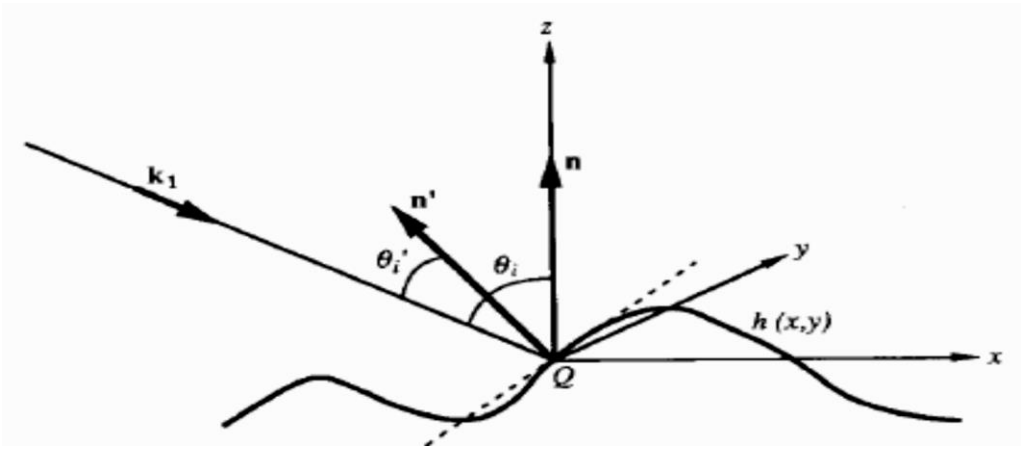

Figure6.4: Variation of the incidence angle and the surface normal on a rough surface [7]

So, if there are N rough surface points at which the scattered field is evaluated using the incident field and the instantaneous Fresnel coefficients, and if we define a normal vector $\boldsymbol{n}$ that describes the surface normal at each point on the surface, using Kirchoff's approximation, at an arbitrary point on the surface where $n = n_k$, the incident and scattered fields are related as

$$E_{z,\ sca,\ rough\,surface}(k) = \left(\frac{Z_2\cos(\theta_{i,k}') - Z_1\cos(\theta_{t,k}')}{Z_2\cos(\theta_{i,k}') + Z_1\cos(\theta_{t,k}')}\right)\left(E_{z,\ inc,\ rough\,surface}(k)\right)$$

$$H_{z,\ sca,\ rough\,surface}(k) = \left(\frac{Z_2\cos(\theta_{t,k}') - Z_1\cos(\theta_{i,k}')}{Z_2\cos(\theta_{t,k}') + Z_1\cos(\theta_{i,k}')}\right)\left(H_{z,\ inc,\ rough\,surface}(k)\right)$$

$$\theta_{t,k} = sin^{-1}\left(\frac{j\beta_1}{\alpha_2 + j\beta_2}sin(\theta_{i,k})\right)$$

$$E_{z,\ sca,\ rough\,surface}(k) = \Gamma_{TM}'(k)\,E_{z,\ inc,\ rough\,surface}(k)$$

$$H_{z,\ sca,\ rough\,surface}(k) = \Gamma_{TE}'(k)\,H_{z,\ inc,\ rough\,surface}(k)$$

$$\Gamma_{TM}'(n = n_k) = \Gamma_{TM}'(k) \quad , \quad \Gamma_{TE}'(n = n_k) = \Gamma_{TE}'(k)$$

$$\boldsymbol{n} = [n_1, n_2, n_3, \dots, n_{k-1}, n_k, \dots, n_N] \quad , \quad normal\ vector$$

$$E_{z,\ sca,\ rough\,surface} = (\Gamma_{TM}')\left(E_{z,\ inc,\ rough\,surface}\right) \quad for\ TM_z\ polarization$$

$$H_{z,\ sca,\ rough\,surface} = (\Gamma_{TE}')\left(H_{z,\ inc,\ rough\,surface}\right) \quad for\ TE_z\ polarization$$

For a good conductor, we must have $\left(\frac{\sigma}{\omega\epsilon}\right)^2 \gg 1$, if we consider sea surface as our rough surface, at radar frequencies sea surface behaves almost like a perfect electric conductor (PEC), therefore along the rough surface we should approximately have

$$E_{z,\ sca,\ rough\,surface} = -\left(E_{z,\ inc,\ rough\,surface}\right) \quad for\ TM_z\ polarization$$

As an example, for sea surface with σ=5S/m and f=3GHz, we have

$$\left(\frac{\sigma}{\omega\epsilon}\right)^2 = 897.55 \gg 1$$

Which behaves almost like a PEC, so when we are dealing with a sea surface at a radar frequency we can simply take $\Gamma_{TM}' = -1$ along the sea surface.

The following is the list of values of $\left(\frac{\sigma}{\omega\epsilon}\right)^2$ that gives an idea about, up to which range the sea surface behaves like a perfect electric conductor.

$$\left(\frac{\sigma}{\omega\epsilon}\right)^2 = \begin{cases} 8078 \gg 1 & f = 1GHz & approximately\ PEC \\ 2020 \gg 1 & f = 2GHz & approximately\ PEC \\ 897.55 \gg 1 & f = 3GHz & approximately\ PEC \\ 323.11 \gg 1 & f = 5GHz & approximately\ PEC \\ 126.22 \gg 1 & f = 8GHz & approximately\ PEC \\ 80.78 \gg 1 & f = 10GHz & approximately\ PEC \\ 20.19 \gg 1 & f = 20GHz & approximately\ PEC \end{cases}$$

Kirchoff's approximation is one of the most employed numerical methods. It is valid for locally smooth surfaces and is also known as *tangent plane approximation*. In high frequencies it is the same as the *physical optics (PO)* approximation. In this model the field on the surface is assimilated to the field that would be produced by a tangent plane at the same point. Thus it depends only on the Fresnel reflection coefficient at the local incidence angle. Kirchoff's approximation is a local approximation in the sense that the supposed field at a surface point does not depend on other surface points[7].

Kirchoff's approximation is especially very accurate for imposing boundary conditions numerically with a computer program. Though the approximation is accurate in general, small errors may occur depending on the incidence angle of the incoming wave for very rough surfaces. The amount of error further reduces if the rough surface medium is a good conductor, because as the conductivity of the medium increases the angle of incidence becomes mathematically less critical. Recall that for a PEC rough surface, the local reflection coefficients are all the same along the rough surface no matter what the incidence angle is. As a result, for sea surfaces at radar frequencies, the accuracy of the Kirchoff's approximation further improves. The accuracy of the approximation also improves if the conductivity is very small and the rough surface medium can be considered as a perfect dielectric, similarly because the angle of incidence becomes mathematically less critical.

In summary, if

$$\left(\frac{\sigma}{\omega\epsilon}\right)^2 \gg 1 \quad or \quad \left(\frac{\sigma}{\omega\epsilon}\right)^2 \ll 1$$

The accuracy of the Kirchoff's approximation further increases.

6.2.2 Imposing boundary conditions on the rough surface using FEM

We know that the tangential component of the electric field is continuous at the boundary between two different media, as stated by the boundary condition

$$\boldsymbol{n} \times (\boldsymbol{E_2} - \boldsymbol{E_1}) = \boldsymbol{0} \quad , \ along\ the\ boundary\ or\ interface$$

Where

$$\boldsymbol{E_1} = \boldsymbol{E_{inc}} + \boldsymbol{E_{sca}} \quad , \quad \boldsymbol{E_2} = \boldsymbol{E_{tra}}$$

$$\boldsymbol{E_{inc}} : \boldsymbol{Incident\ electric\ field}\ (\boldsymbol{medium\ 1})$$

$$\boldsymbol{E_{sca}} : \boldsymbol{Scattered\ electric\ field}\ (\boldsymbol{medium\ 1})$$

$$\boldsymbol{E_{tra}} : \boldsymbol{Transmitted\ electric\ field}\ (\boldsymbol{medium\ 2})$$

In medium1, the wave equation for the total field $\boldsymbol{E_1}$ is given as

$$\nabla^2 \boldsymbol{E_1} + \mathrm{k}^2 \boldsymbol{E_1} = 0 \quad , \quad k = \omega\sqrt{\mu\epsilon} \quad (wavenumber)$$

Which can be written as

$$\nabla^2(\boldsymbol{E_{inc}} + \boldsymbol{E_{sca}}) + \omega^2\mu\epsilon(\boldsymbol{E_{inc}} + \boldsymbol{E_{sca}}) = 0$$

Also, the wave equations for the incident field and the scattered field are given as

$$\nabla^2 \boldsymbol{E_{inc}} + \omega^2\mu\epsilon \boldsymbol{E_{inc}} = 0$$

$$\nabla^2 \boldsymbol{E_{sca}} + \omega^2\mu\epsilon \boldsymbol{E_{sca}} = 0$$

Assuming that we have a 2D rough surface problem defined on the x-y plane, for a TM_z incident wave, we have

$$\nabla^2(\boldsymbol{E_{z,inc}} + \boldsymbol{E_{z,sca}}) + \omega^2\mu\epsilon(\boldsymbol{E_{z,inc}} + \boldsymbol{E_{z,sca}}) = 0$$

$$\nabla^2 \boldsymbol{E_{z,inc}} + \omega^2\mu\epsilon \boldsymbol{E_{z,inc}} = 0 \quad , \quad \nabla^2 \boldsymbol{E_{z,sca}} + \omega^2\mu\epsilon \boldsymbol{E_{z,sca}} = 0$$

If medium 2 is an imperfectly conducting lossy media, along the boundary between the two media, the wave equation must be modified to include the loss factor as stated

$$\nabla^2(\boldsymbol{E_{z,inc}} + \boldsymbol{E_{z,sca}}) + (\omega^2\mu\epsilon - \mathrm{j}\omega\mu\sigma)(\boldsymbol{E_{z,inc}} + \boldsymbol{E_{z,sca}}) = 0 \quad , \quad at\ the\ interface$$

Since the tangential component of the electric field is continuous at the interface, we have

$$\boldsymbol{E_{z,inc}} + \boldsymbol{E_{z,sca}} = \boldsymbol{E_{z,tra}} \quad , \quad along\ the\ boundary\ or\ interface$$

Therefore, the following formulations are equal

$$\nabla^2 \boldsymbol{E_{z,tra}} + (\omega^2\mu\epsilon - \mathrm{j}\omega\mu\sigma)\, \boldsymbol{E_{z,tra}} = 0 \quad , \quad at\ the\ interface$$

$$\nabla^2(\boldsymbol{E_{z,inc}} + \boldsymbol{E_{z,sca}}) + (\omega^2\mu\epsilon - \mathrm{j}\omega\mu\sigma)(\boldsymbol{E_{z,inc}} + \boldsymbol{E_{z,sca}}) = 0 \quad , \quad at\ the\ interface$$

As a result, at the interface the following identity is satisfied

$$\nabla^2 \boldsymbol{E_{z,sca}} + (\omega^2\mu\epsilon - \mathrm{j}\omega\mu\sigma)\boldsymbol{E_{z,sca}} = -\nabla^2 \boldsymbol{E_{z,inc}} - \omega^2\mu\epsilon \boldsymbol{E_{z,inc}} + \mathrm{j}\omega\mu\sigma \boldsymbol{E_{z,inc}}$$

Along the boundary between the two media.

Since

$$\nabla^2 \boldsymbol{E_{z,inc}} + \omega^2\mu\epsilon \boldsymbol{E_{z,inc}} = 0$$

is satisfied everywhere in space, at the boundary we have

$$\nabla^2 \boldsymbol{E_{z,sca}} + (\omega^2\mu\epsilon - \mathrm{j}\omega\mu\sigma)\boldsymbol{E_{z,sca}} = \mathrm{j}\omega\mu\sigma \boldsymbol{E_{z,inc}}$$

Which may also be expressed as

$$\nabla^2 \boldsymbol{E_{z,sca}} + \omega^2 \mu\epsilon \boldsymbol{E_{z,sca}} = \mathrm{j}\omega\mu\sigma(\boldsymbol{E_{z,inc}} + \boldsymbol{E_{z,sca}})$$

$$\boldsymbol{J_{conduction}} = \boldsymbol{J_c} = \boldsymbol{J_z} = \sigma(\boldsymbol{E_{z,inc}} + \boldsymbol{E_{z,sca}})$$

$$\nabla^2 \boldsymbol{E_{z,sca}} + \omega^2 \mu\epsilon \boldsymbol{E_{z,sca}} = \mathrm{j}\omega\mu \boldsymbol{J_z}$$

For FEM analysis, we will use the following set of formulations to determine the scattered field everywhere in medium1

$$\nabla^2 \boldsymbol{E_{z,sca}} + (\omega^2 \mu\epsilon - \mathrm{j}\omega\mu\sigma)\boldsymbol{E_{z,sca}} = \mathrm{j}\omega\mu\sigma \boldsymbol{E_{z,inc}} \quad , \quad at\ the\ boundary \quad (1)$$

$$\nabla^2 \boldsymbol{E_{z,sca}} + \omega^2 \mu\epsilon \boldsymbol{E_{z,sca}} = 0 \quad , \quad elsewhere \qquad (2)$$

Recall that in 5.3, for the "element to element" varying case, the functional inside an element was defined as

$$I(\phi_e) = \frac{1}{2} \sum_{\mathrm{i}=1}^{3} \sum_{\mathrm{j}=1}^{3} \phi_{ei}\, \phi_{ej} \left[\int\int (\nabla\alpha_i \,.\, \nabla\alpha_\mathrm{j})\, \mathrm{dS} \;-\; {k_e}^2 \int\int (\alpha_i \alpha_\mathrm{j})\, \mathrm{dS} \right] + \; g_e \sum_{\mathrm{i}=1}^{3} \sum_{\mathrm{j}=1}^{3} \phi_{ei} \int\int (\alpha_i\, \alpha_\mathrm{j})\, \mathrm{dS}$$

$$I(\phi_e) = \; \frac{1}{2} \sum_{i=1}^{3} \sum_{j=1}^{3} \phi_{ei}\, \phi_{ej}\; {M_{ij}}^{(e)} \; + \; g_e \sum_{\mathrm{i}=1}^{3} \sum_{\mathrm{j}=1}^{3} \phi_{ei} {T_{ij}}^{(e)} \qquad (3)$$

$$I(\phi_e) = \frac{1}{2}\, [\phi_e]^{\mathrm{t}} \left[\mathrm{M}^{(\mathrm{e})}\right] [\phi_e] + \; [\phi_e]^{\mathrm{t}} \left[\mathrm{N}^{(\mathrm{e})}\right] \mathrm{g}_e$$

$${C_{ij}}^{(e)} = \int\int \nabla\alpha_i . \nabla\alpha_j \, dS \quad , \quad {T_{ij}}^{(e)} = \int\int \alpha_i\, \alpha_j \, dS$$

$${M_{ij}}^{(e)} = \; {C_{ij}}^{(e)} - {k_e}^2 \, {T_{ij}}^{(e)} \quad (4)$$

$${M_{ij}}^{(e)} = \left[\; \int\int (\nabla\alpha_i \,.\, \nabla\alpha_\mathrm{j})\, \mathrm{dS} \;-\; {k_e}^2 \int\int (\alpha_i \alpha_\mathrm{j})\, \mathrm{dS} \; \right]$$

$$\mathrm{F}^{(\mathrm{e})} = \mathrm{g}_e \begin{bmatrix} {T_{11}}^{(e)} + {T_{12}}^{(e)} + {T_{13}}^{(e)} \\ {T_{21}}^{(e)} + {T_{22}}^{(e)} + {T_{23}}^{(e)} \\ {T_{31}}^{(e)} + {T_{32}}^{(e)} + {T_{33}}^{(e)} \end{bmatrix}, \qquad where \;\; \mathrm{N}^{(\mathrm{e})} = \begin{bmatrix} {T_{11}}^{(e)} + {T_{12}}^{(e)} + {T_{13}}^{(e)} \\ {T_{21}}^{(e)} + {T_{22}}^{(e)} + {T_{23}}^{(e)} \\ {T_{31}}^{(e)} + {T_{32}}^{(e)} + {T_{33}}^{(e)} \end{bmatrix}$$

$$I(\phi_e) = \frac{1}{2}\, [\phi_e]^{\mathrm{t}} \left[\mathrm{M}^{(\mathrm{e})}\right] [\phi_e] + \; [\phi_e]^{\mathrm{t}} \left[\mathrm{F}^{(\mathrm{e})}\right]$$

Summing for all elements, we have

$$I(\phi) = \sum_{e=1}^{N} I(\phi_e)$$

$$I(\phi) = \frac{1}{2} [\phi]^t [M] [\phi] + [\phi]^t [F]$$

Therefore, the FEM solution is given by (5)

$$\frac{\partial I(\phi)}{\partial \phi_k} = 0 \quad , \quad for\ all\ free\ nodes$$

$$\frac{\partial I(\phi)}{\partial \phi_k} = \sum_{i=1}^{n} [\ \phi_i M_{ki} + F_k\ ] = 0$$

$$\sum_{i=1}^{n} \phi_i M_{ki} = - F_k \quad (5)$$

For elements, which have one of its three sides at the boundary, we should introduce the source and loss factor, since

$$\nabla^2 \boldsymbol{E_{z,sca}} + (\omega^2 \mu\epsilon - j\omega\mu\sigma)\boldsymbol{E_{z,sca}} = j\omega\mu\sigma \boldsymbol{E_{z,inc}} \quad , \quad at\ the\ boundary \quad (1)$$

$$\nabla^2 \boldsymbol{E_{z,sca}} + \omega^2 \mu\epsilon \boldsymbol{E_{z,sca}} = 0 \quad , \ elsewhere \qquad (2)$$

$$g_e = \begin{cases} g_{e1} = j\omega\mu\sigma \boldsymbol{E_{z,inc}} & , \quad at\ the\ boundary \\ g_{e2} = 0 & , \quad elsewhere\ in\ medium1 \end{cases}$$

$$k_e{}^2 = \begin{cases} k_{e1}{}^2 = \omega^2\mu\epsilon - j\omega\mu\sigma & , \quad at\ the\ boundary \\ k_{e2}{}^2 = \omega^2\mu\epsilon & , \quad elsewhere\ in\ medium1 \end{cases}$$

$\boldsymbol{E_{z,inc}}$ should be evaluated at the center of each surface element.

Therefore, for surface elements having one complete side (two nodes) at the boundary

$$I(\phi_{e1}) = \frac{1}{2} \sum_{i=1}^{3} \sum_{j=1}^{3} \phi_{ei}\, \phi_{ej} \left[\int\int (\nabla\alpha_i \,.\, \nabla\alpha_j)\, dS \ - \ k_{e1}{}^2 \int\int (\alpha_i \alpha_j)\, dS \right] + \ g_{e1} \sum_{i=1}^{3} \sum_{j=1}^{3} \phi_{ei} \int\int (\alpha_i\, \alpha_j)\, dS$$

For all of the other elements

$$I(\phi_{e2}) = \frac{1}{2} \sum_{i=1}^{3} \sum_{j=1}^{3} \phi_{ei}\, \phi_{ej} \left[\int\int (\nabla\alpha_i \,.\, \nabla\alpha_j)\, dS \ - \ k_{e2}{}^2 \int\int (\alpha_i \alpha_j)\, dS \right] \ , \ since \ \ g_{e2} = 0$$

The rest of the procedure is to assemble all elements as described previously, after forming the global coefficient matrix and the source vector, we can solve (5) to get the field values everywhere in medium1. After solving the linear system (5) , we can see that the field values at the boundary automatically satisfy the impedance boundary condition along the whole boundary. The resulting linear system can be written in its expanded form as

$$\phi_1 M_{11} + \phi_2 M_{12} + \cdots + \phi_n M_{1n} = \mathrm{F}_1$$

$$\phi_1 M_{21} + \phi_2 M_{22} + \cdots + \phi_n M_{2n} = \mathrm{F}_2$$

$$\phi_1 M_{31} + \phi_2 M_{32} + \cdots + \phi_n M_{3n} = \mathrm{F}_3$$

$$\bullet$$

$$\bullet$$

$$\phi_1 M_{n1} + \phi_2 M_{n2} + \cdots + \phi_n M_{nn} = \mathrm{F}_n$$

Section 5.3 can be revisited to recall the assembling procedure of the elements.

6.3 Examples of rough surface scattering using FEM

Until now we have described the fundamental concepts that are necessary for solving the problem of rough surface scattering using FEM, basically we have discussed the followings

1)Mesh generation for nonrectangular regions.

2)Basics of the finite element method and its formulation.

3)Locally conformal perfectly matched layer.

4)Imposing boundary condition on a given rough surface.

Once these concepts are fully understood and implemented, FEM can be applied on scattering and radiation problems.

We will now see some examples of rough surface scattering using FEM, here we will concentrate on four parameters to specify a rough surface scattering problem

1)PML width along x and y directions.

2)Frequency of the incident wave

3)Conductivity of the rough surface boundary.

4)Mesh size of the computational region(excluding PML).

Angle measure: *Angle is measured from the positive x axis, that is,*

$\Phi=0^{\circ}$ *for positive x axis,* $\Phi=90^{\circ}$ *for positive y axis and* $\Phi=180^{\circ}$ *for negative x axis.*

Incident wave: *The incident wave is a uniform plane wave and has an amplitude of 100V/m, its incidence angle will be specified in each example.*

$$\boldsymbol{E}_{z,inc} = \boldsymbol{a}_z 100 e^{jk(\cos\phi_i\ x + \sin\phi_i\ y)} \quad , \quad in\ phasor\ domain\ with\ e^{j\omega t}\ convention.$$

λ : Wavelength , ξ : Standard deviation value of the surface roughness

Ex1: *Cond=5 S/m, Angle of incidence*=90°, *Computational mesh size*=$10\lambda \times 10\lambda$

Frequency=3GHz, Wavelength= λ=*0.1m, PML Width*= λ , $\xi = 0.25\lambda$

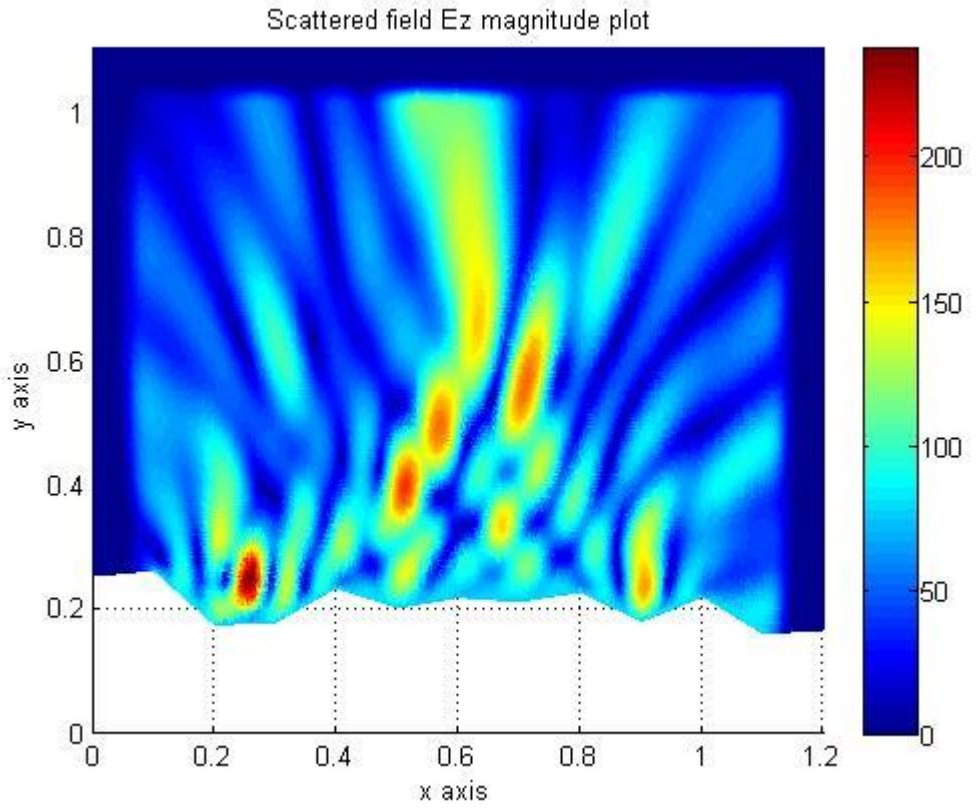

Figure6.5: Scattering from a rough surface with the given parameters, magnitude plot

Note: In this chapter, all magnitude plots are in terms of (Volts/meter) and all phase plots are in terms of radians.

Ex1: *Cond=5 S/m, Angle of incidence*=90°, *Computational mesh size*=$10\lambda \times 10\lambda$

Frequency=3GHz, Wavelength= λ*=0.1m, PML Width*= λ , $\xi = 0.25\lambda$

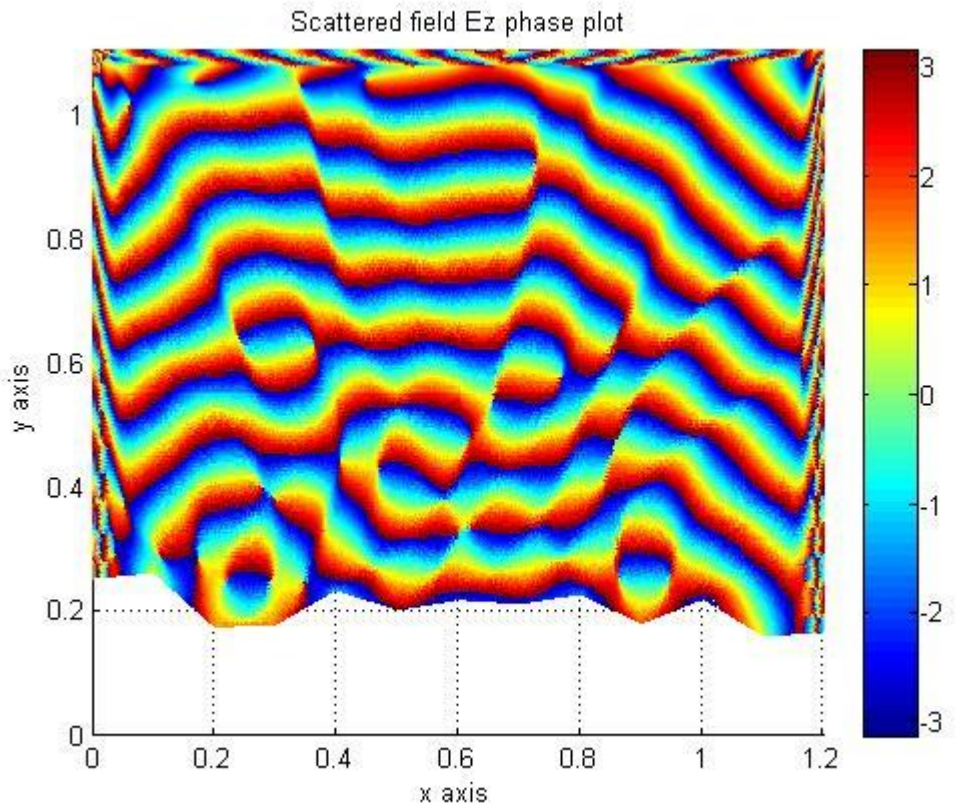

Figure6.6: Scattering from a rough surface with the given parameters, phase plot

Ex2: *Cond=5 S/m, Angle of incidence*=90°, *Computational mesh size*=$10\lambda \times 10\lambda$

Frequency=3GHz, Wavelength= λ*=0.1m, PML Width*= $\lambda/2$, $\xi = 0.30\lambda$

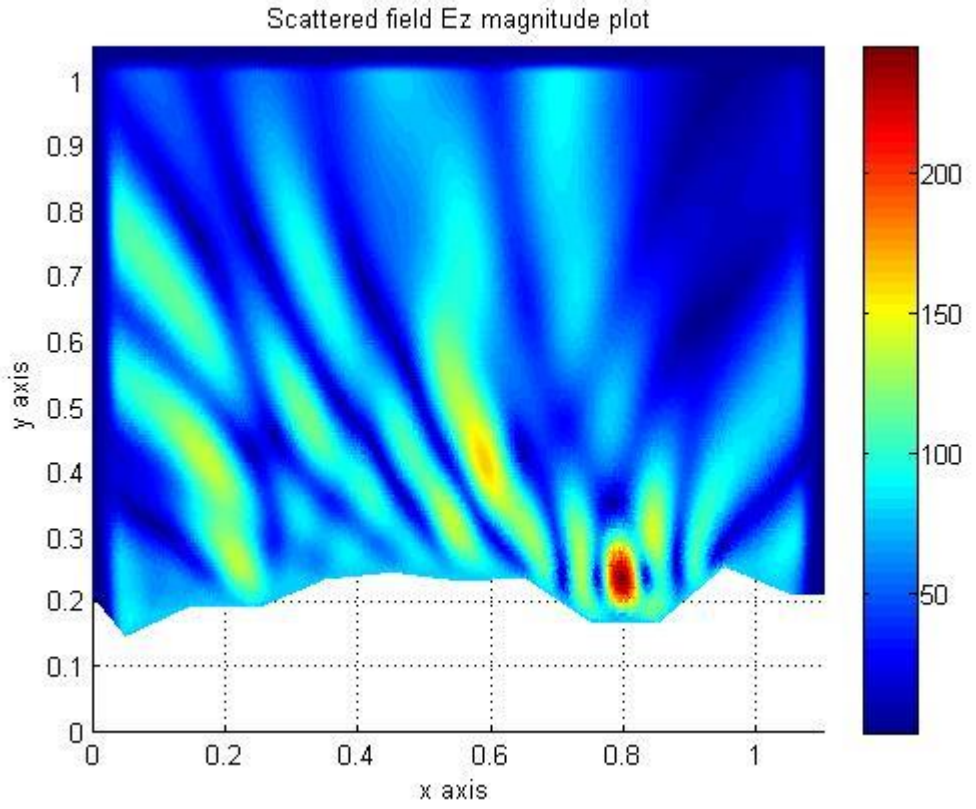

Figure6.7: Scattering from a rough surface with the given parameters, magnitude plot

Ex2: *Cond=5 S/m, Angle of incidence*=90°, *Computational mesh size*=$10\lambda \times 10\lambda$

Frequency=3GHz, Wavelength= λ*=0.1m, PML Width*= $\lambda/2$, $\xi = 0.30\lambda$

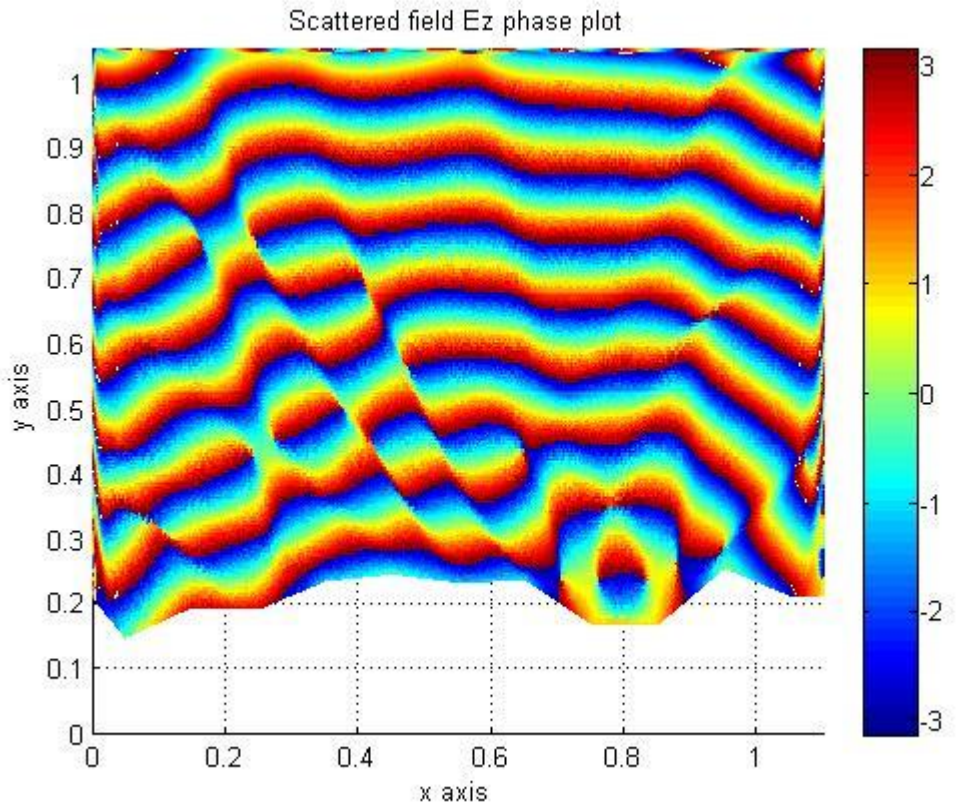

Figure6.8: Scattering from a rough surface with the given parameters, phase plot

Ex3: *Cond=5 S/m, Angle of incidence*=135°, *Computational mesh size*=$10\lambda \times 10\lambda$

Frequency=3GHz, Wavelength= λ*=0.1m, PML Width*= λ , $\xi = 0.40\lambda$

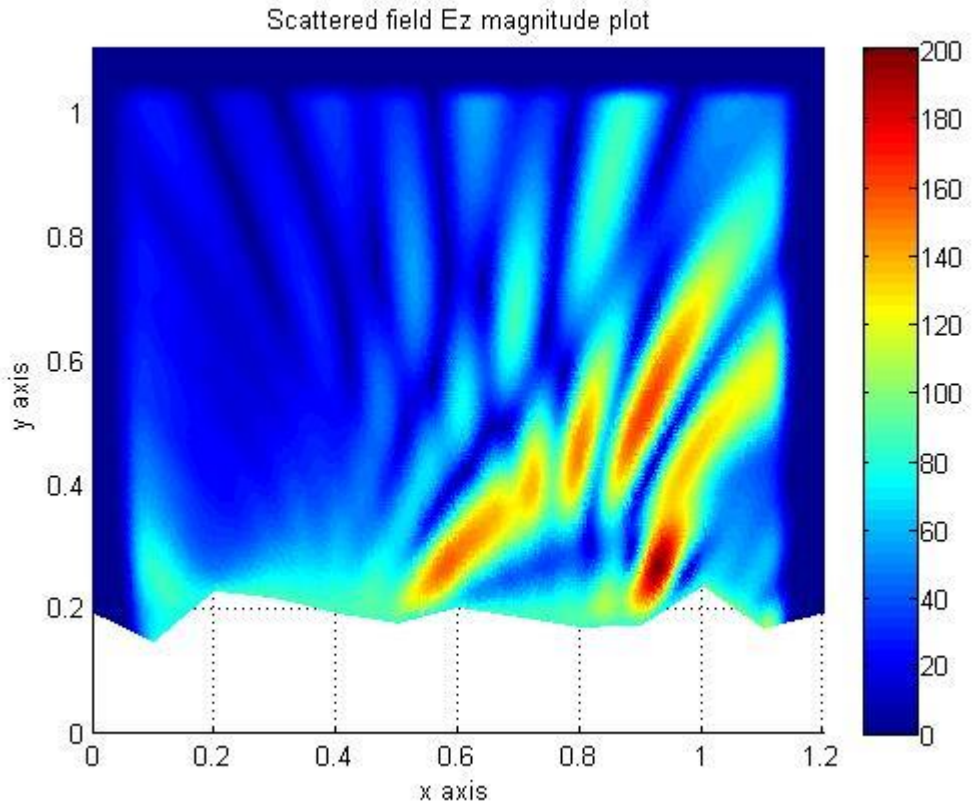

Figure6.9: Scattering from a rough surface with the given parameters, magnitude plot

Ex3: *Cond=5 S/m, Angle of incidence*=135°, *Computational mesh size*=$10\lambda \times 10\lambda$

Frequency=3GHz, Wavelength= λ*=0.1m, PML Width*= λ , $\xi = 0.40\lambda$

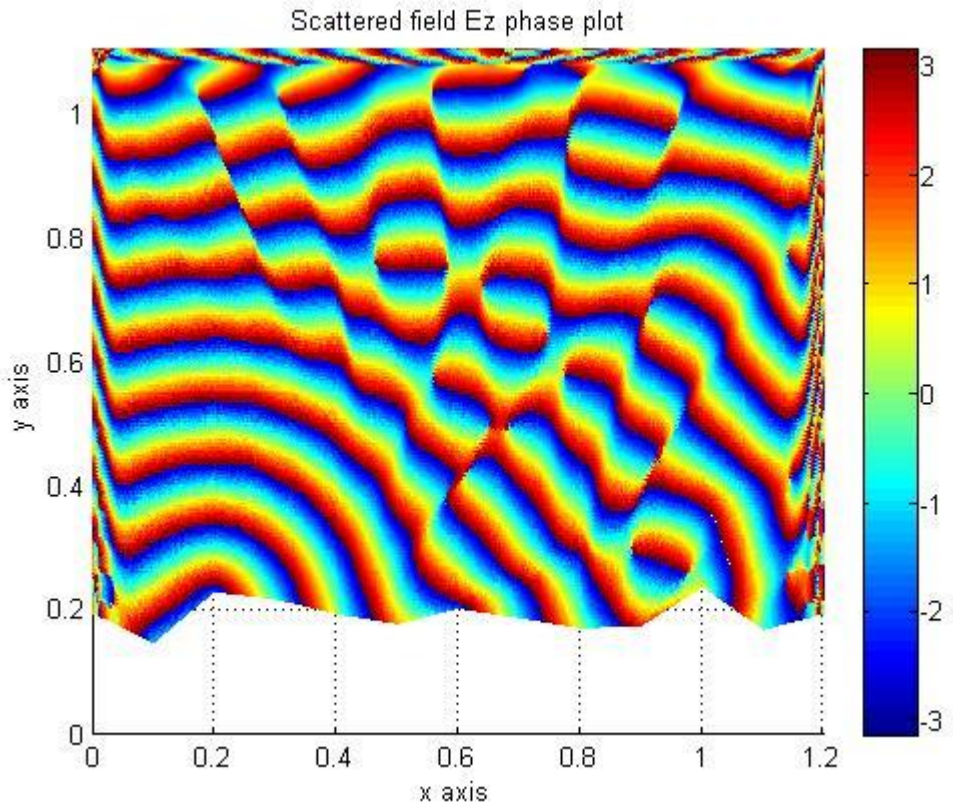

Figure6.10: Scattering from a rough surface with the given parameters, phase plot

Ex4: *Cond=5 S/m, Angle of incidence*=135°, *Computational mesh size*=$10\lambda \times 10\lambda$

Frequency=3GHz, Wavelength= λ*=0.1m, PML Width*= $\lambda/2$, $\xi = 0.40\lambda$

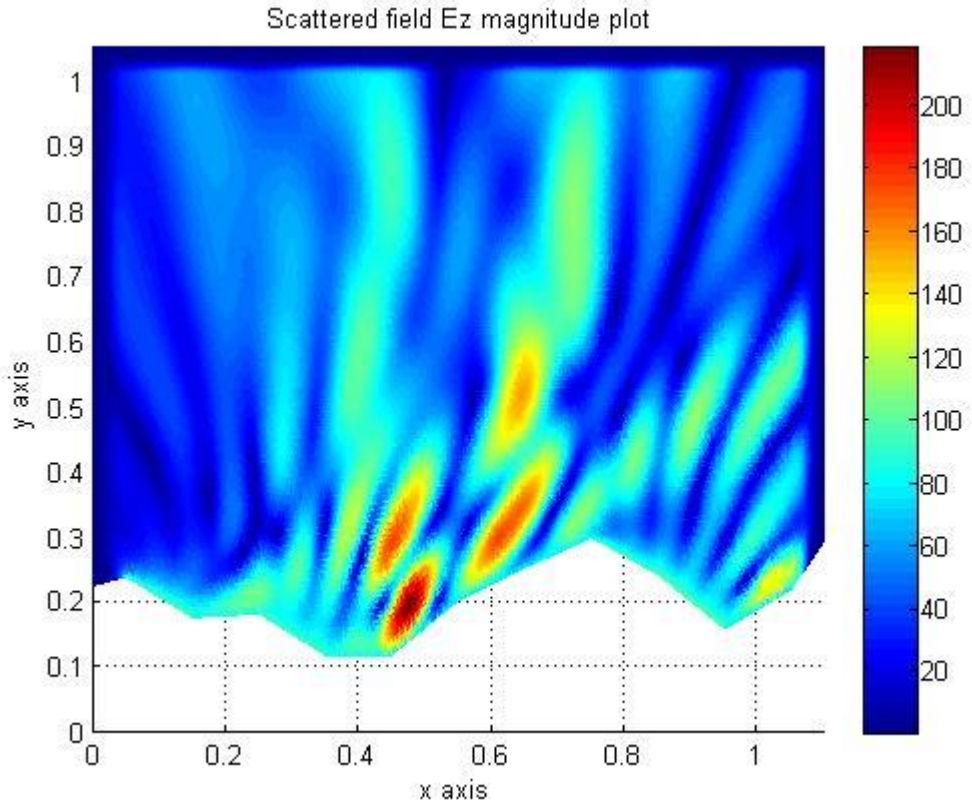

Figure6.11: Scattering from a rough surface with the given parameters, magnitude plot

Ex4: *Cond=5 S/m, Angle of incidence*=135°, *Computational mesh size*=$10\lambda \times 10\lambda$

Frequency=3GHz, Wavelength= λ*=0.1m, PML Width*= $\lambda/2$, $\xi = 0.40\lambda$

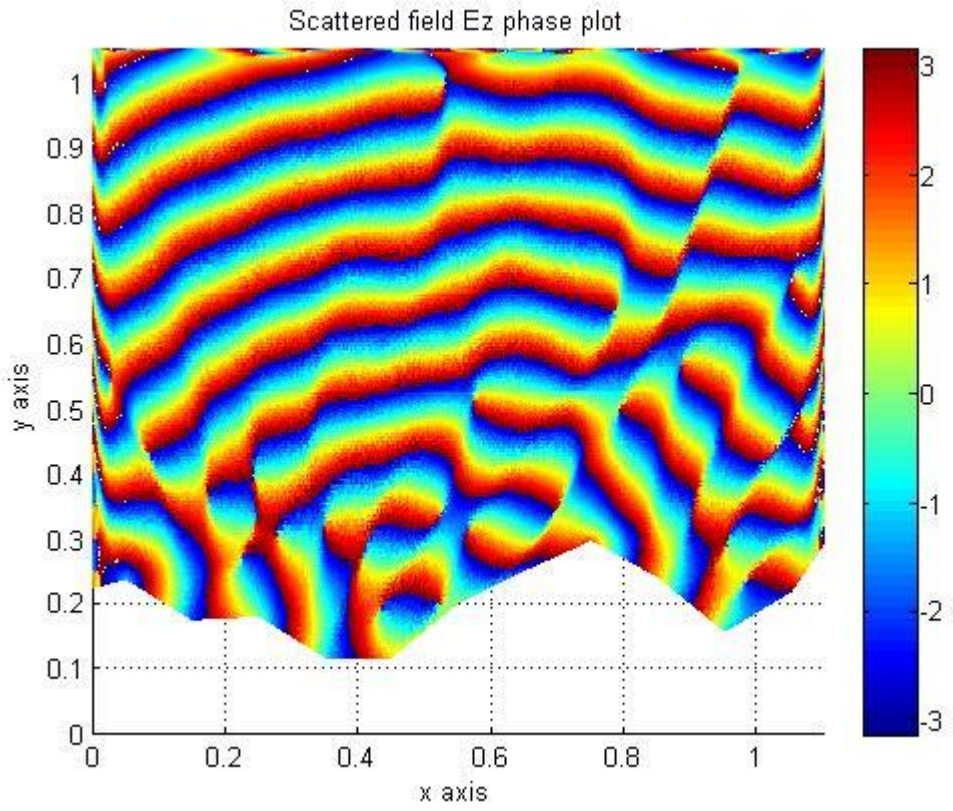

Figure6.12: Scattering from a rough surface with the given parameters, phase plot

Ex5: *Cond=100S/m, Angle of incidence*=135°, *Computational mesh size*=$10\lambda \times 10\lambda$

Frequency=3GHz, Wavelength= λ*=0.1m, PML Width*= λ , $\xi = 0.50\lambda$

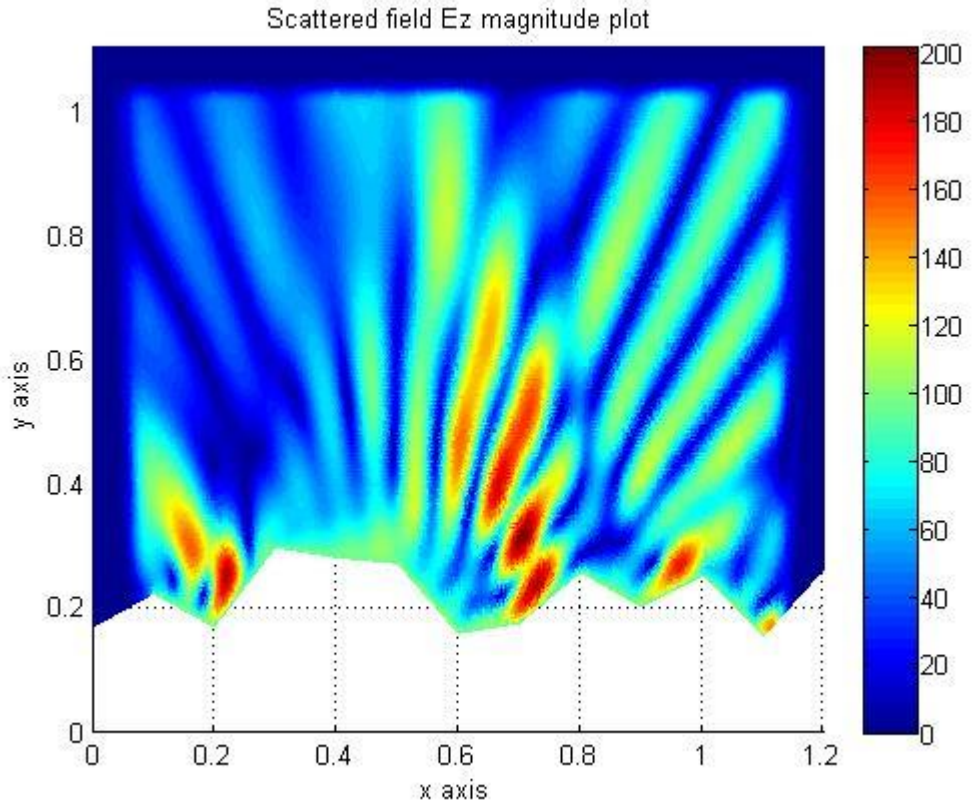

Figure6.13: Scattering from a rough surface with the given parameters, magnitude plot

Ex5: *Cond=100S/m, Angle of incidence*=135°, *Computational mesh size*=$10\lambda \times 10\lambda$

Frequency=3GHz, Wavelength= λ*=0.1m, PML Width*= λ , $\xi = 0.50\lambda$

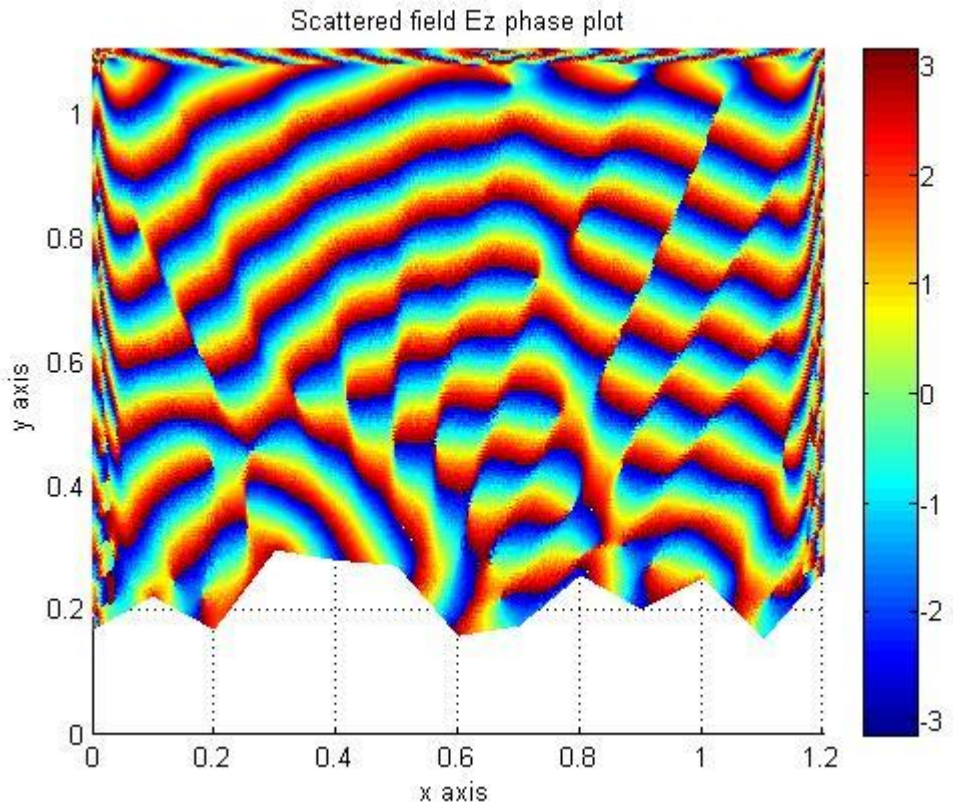

Figure6.14: Scattering from a rough surface with the given parameters, phase plot

Ex6: *Cond=100S/m, Angle of incidence*=135°, *Computational mesh size*=$10\lambda \times 10\lambda$

Frequency=3GHz, Wavelength= λ*=0.1m, PML Width*= $\lambda/2$, $\xi = 0.50\lambda$

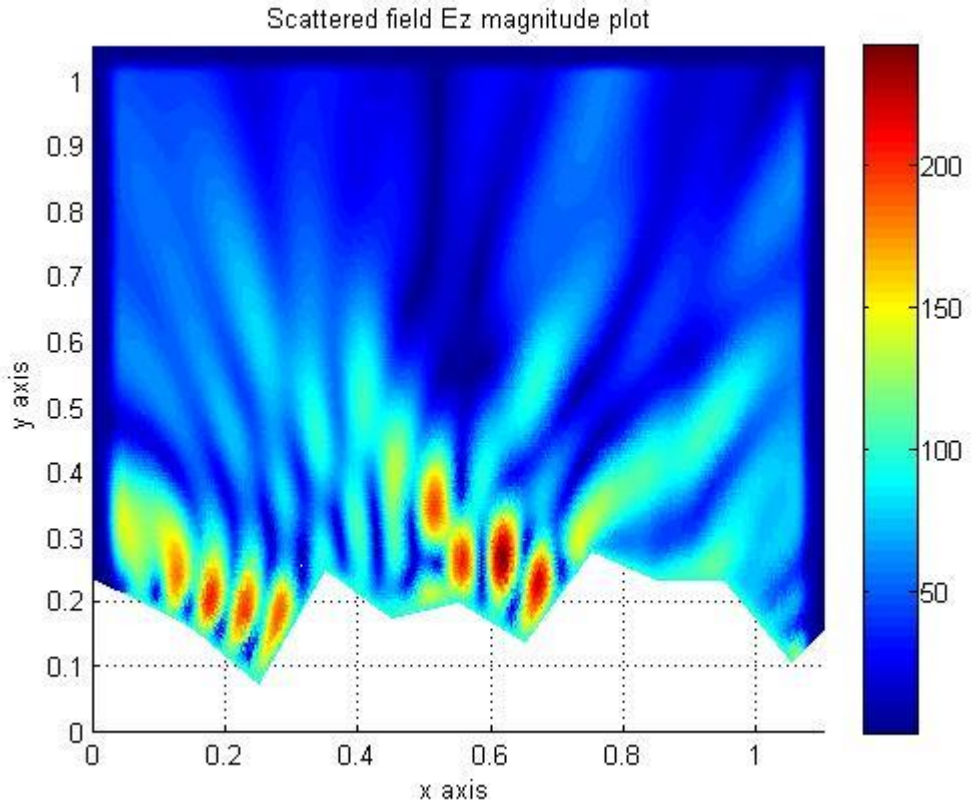

Figure6.15: Scattering from a rough surface with the given parameters, magnitude plot

Ex6: *Cond=100S/m, Angle of incidence*=135°, *Computational mesh size*=$10\lambda \times 10\lambda$

Frequency=3GHz, Wavelength= λ*=0.1m, PML Width*= $\lambda/2$, $\xi = 0.50\lambda$

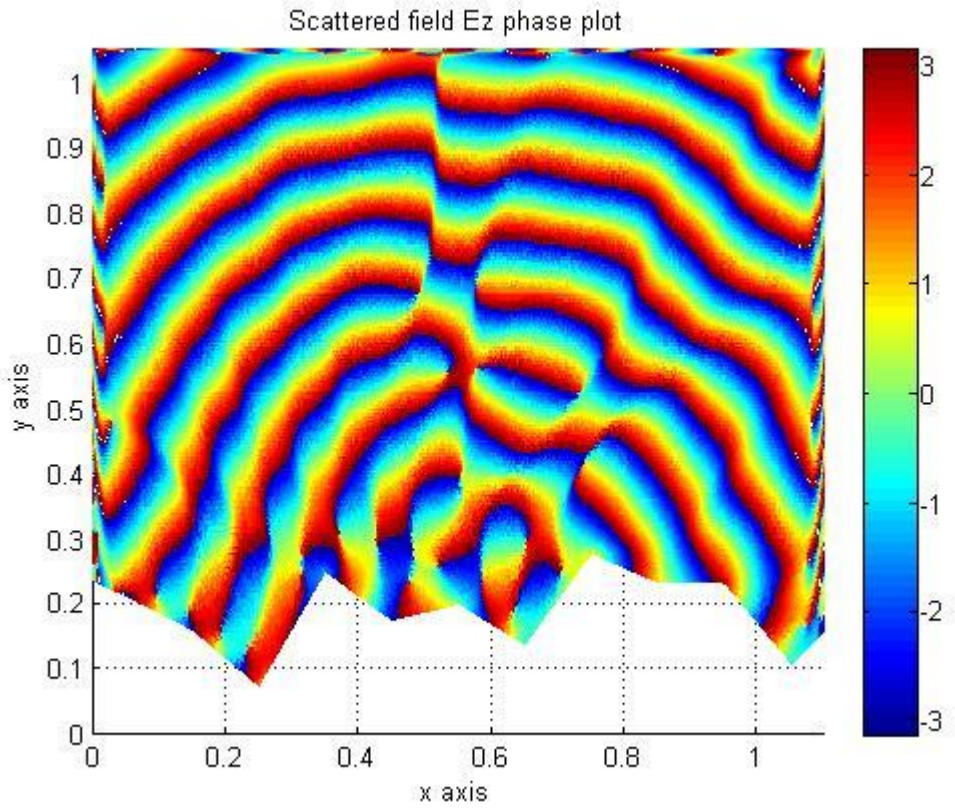

Figure6.16: Scattering from a rough surface with the given parameters, phase plot

Ex7: *Cond=100S/m, Angle of incidence*=135°, *Computational mesh size*=$10\lambda \times 10\lambda$

Frequency=3GHz, Wavelength= λ*=0.1m, PML Width*= λ , $\xi = \lambda$

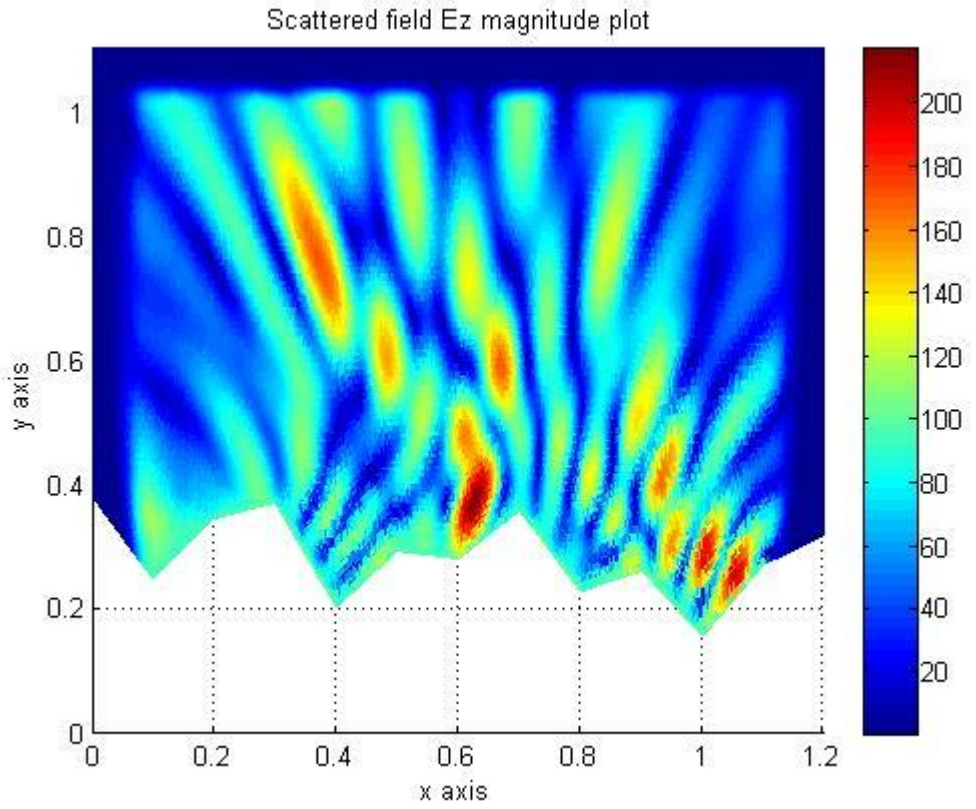

Figure6.17: Scattering from a rough surface with the given parameters, magnitude plot

Ex7: *Cond=100S/m, Angle of incidence*=135°, *Computational mesh size*=$10\lambda \times 10\lambda$

Frequency=3GHz, Wavelength= λ*=0.1m, PML Width*= λ , $\xi = \lambda$

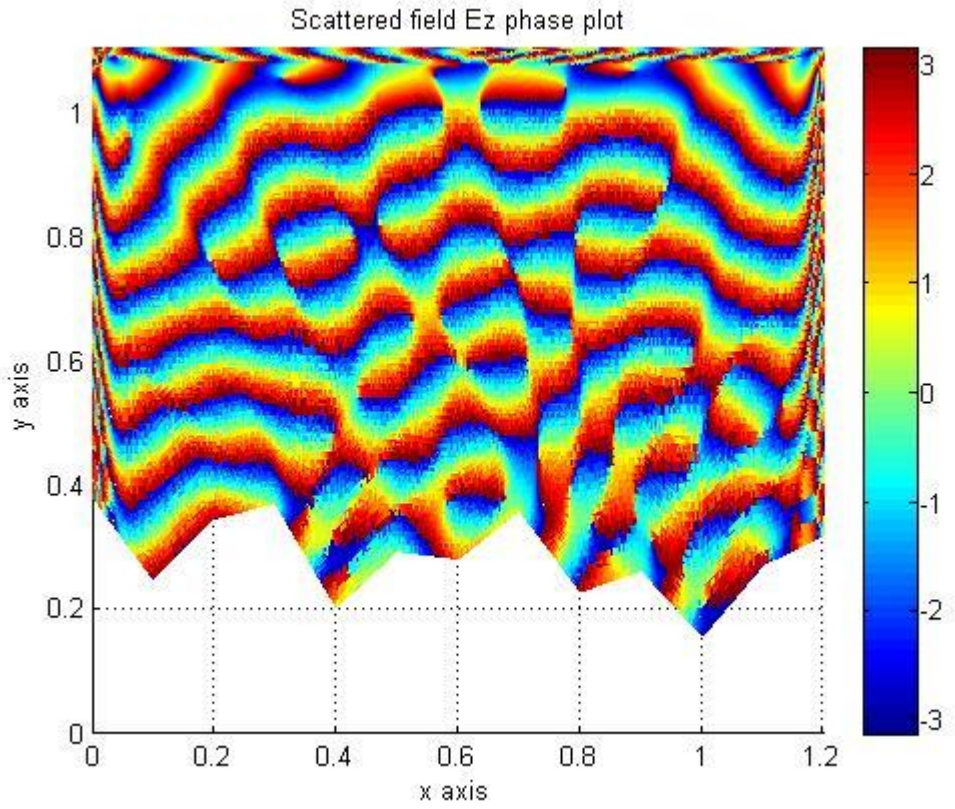

Figure6.18: Scattering from a rough surface with the given parameters, phase plot

Ex8: *Cond=5S/m, Angle of incidence*=90°, *Computational mesh size*=$10\lambda \times 10\lambda$

Frequency=3GHz, Wavelength= λ=*0.1m, PML Width*= λ , $\xi = \lambda$

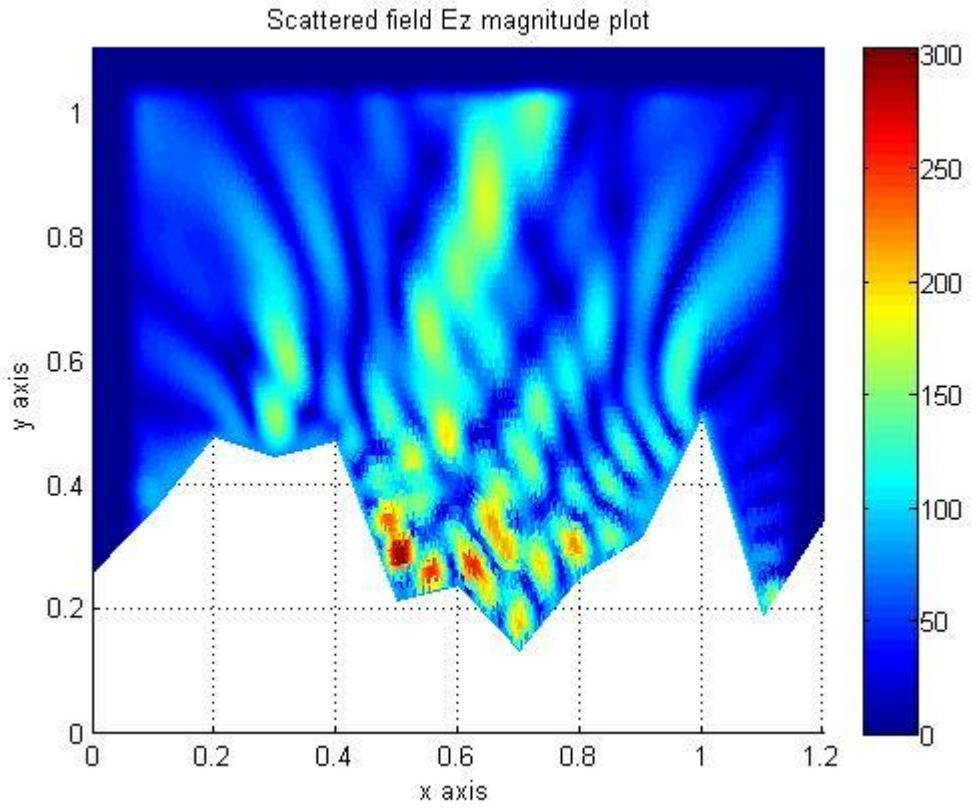

Figure6.19: Scattering from a rough surface with the given parameters, magnitude plot

Ex8: *Cond=5S/m, Angle of incidence*=90°, *Computational mesh size*=$10\lambda \times 10\lambda$

Frequency=3GHz, Wavelength= λ=*0.1m, PML Width*= λ , $\xi = \lambda$

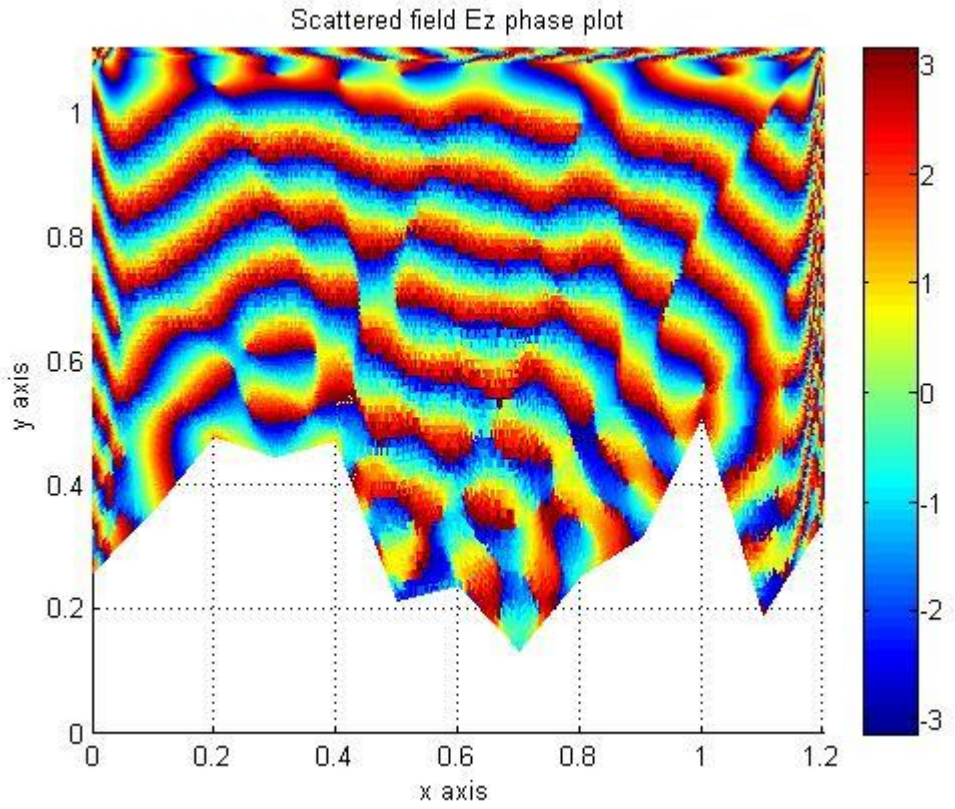

Figure6.20: Scattering from a rough surface with the given parameters, phase plot

Ex9: *Cond=5S/m, Angle of incidence*=180°, *Computational mesh size*=$10\lambda \times 10\lambda$

Frequency=3GHz, Wavelength= λ=*0.1m, PML Width*= λ , $\xi = \lambda/4$

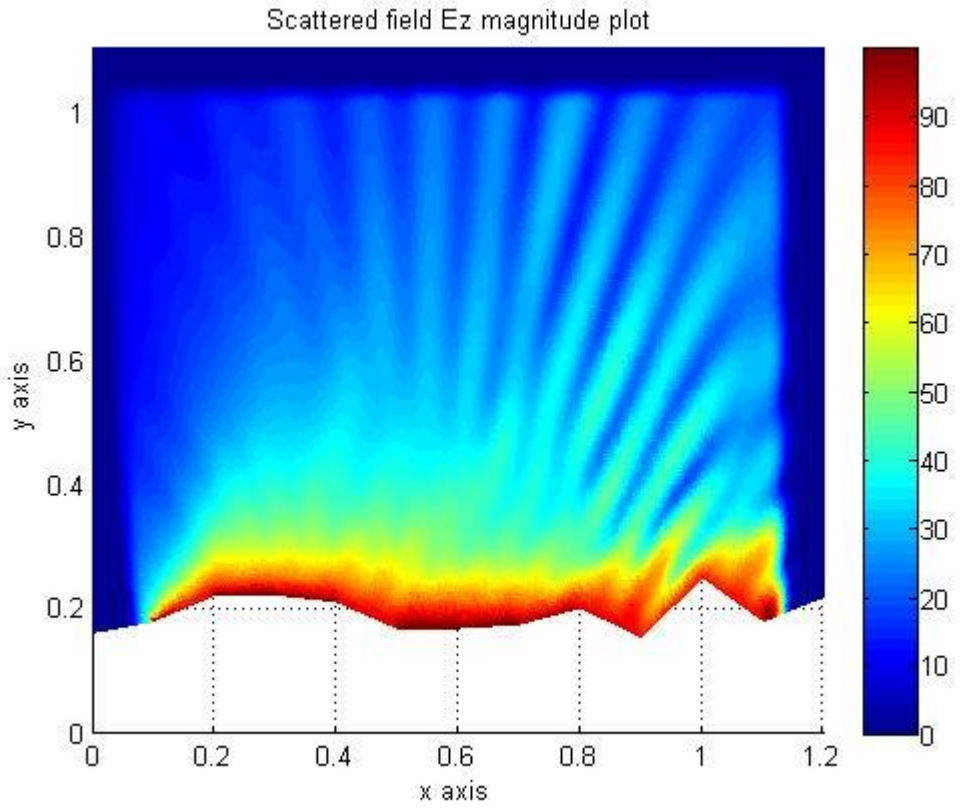

Figure6.21: Scattering from a rough surface with the given parameters, magnitude plot

Ex9: *Cond=5S/m, Angle of incidence*=180°, *Computational mesh size*=$10\lambda \times 10\lambda$

Frequency=3GHz, Wavelength= λ*=0.1m, PML Width*= λ , $\xi = \lambda/4$

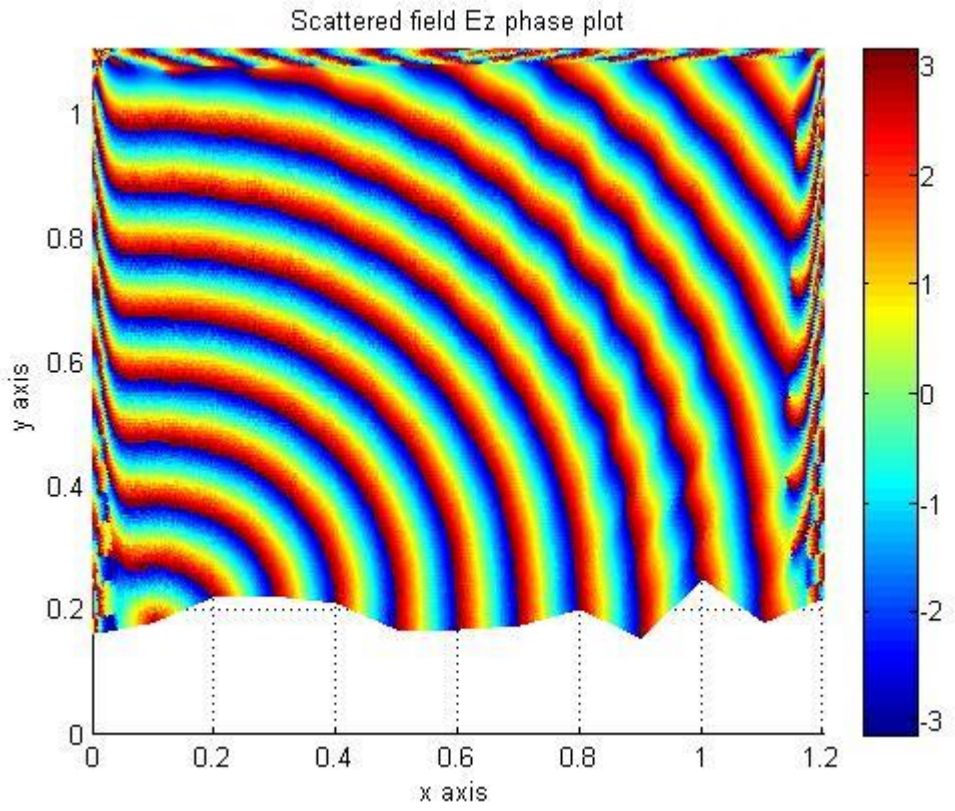

Figure6.22: Scattering from a rough surface with the given parameters, phase plot

Ex10: *Cond=5S/m, Angle of incidence*=180°, *Computational mesh size*=$10\lambda \times 10\lambda$

Frequency=3GHz, Wavelength= λ=*0.1m, PML Width*= λ , $\xi = \lambda/2$

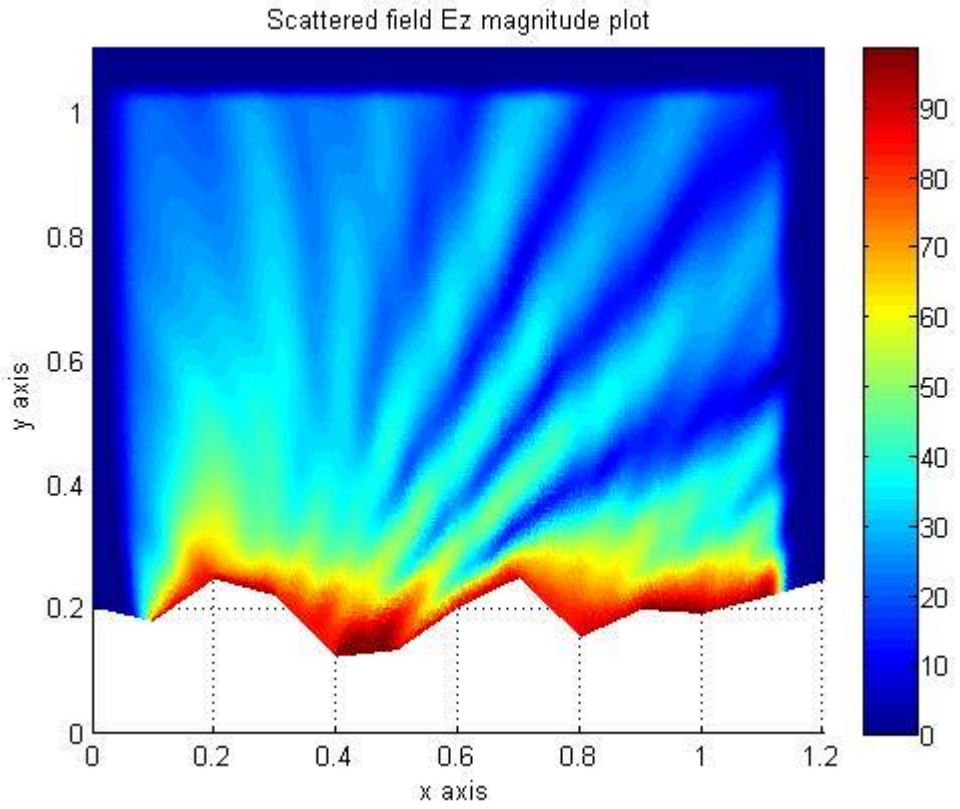

Figure6.23: Scattering from a rough surface with the given parameters, magnitude plot

Ex10: *Cond=5S/m, Angle of incidence*=180°, *Computational mesh size*=$10\lambda \times 10\lambda$

Frequency=3GHz, Wavelength= λ*=0.1m, PML Width=* λ , $\xi = \lambda/2$

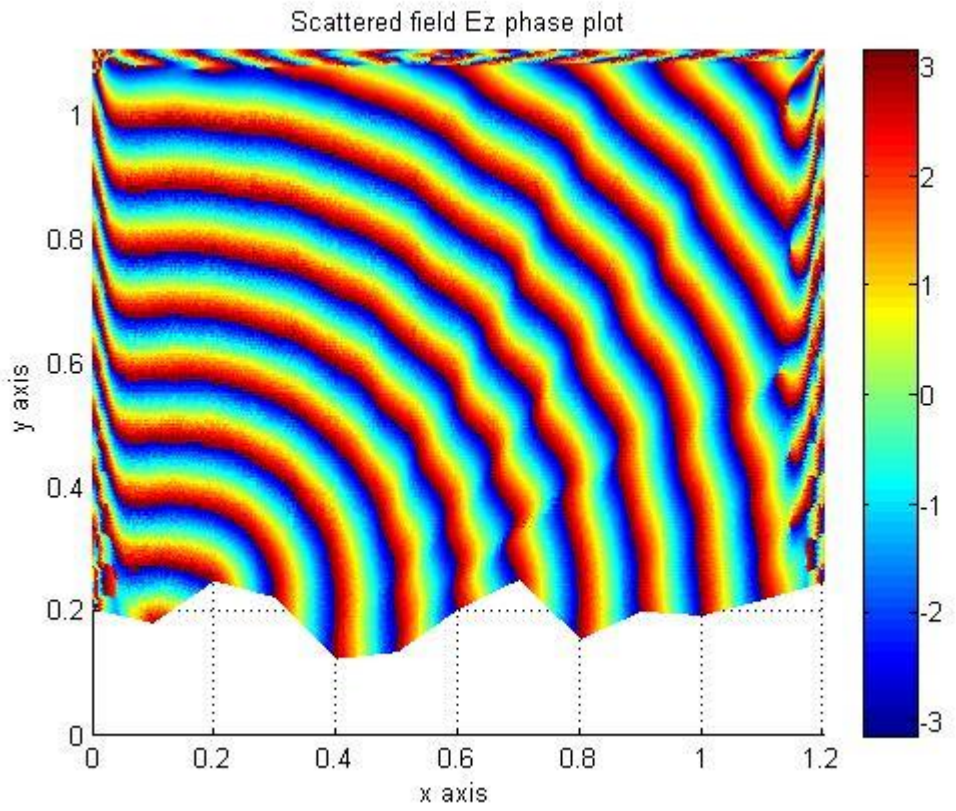

Figure6.24: Scattering from a rough surface with the given parameters, phase plot

Notes:

- Especially for very rough surfaces, the number of elements used may fall short, this causes a lower resolution and to increase the resolution of the scattered field plot, the number of elements used must be increased by using mesh refinement.

- Rough surfaces cause abrupt changes in phase pattern.

- PML thickness should be $\lambda/2$ *or* λ *for high accuracy.*

6.4 Comparison of FEM solutions with analytical solutions

FEM is based on the functionals of partial differential equations whose solutions are desired, we have previously derived the functional for the Helmholtz equation as

$$\nabla^2\phi + \mathrm{k}^2\phi = g \quad , \quad k = \omega\sqrt{\mu\epsilon}$$

$$I(\phi) = \frac{1}{2}\iint [\,(\frac{\partial\phi}{\partial x})^2 + (\frac{\partial\phi}{\partial y})^2 - k^2\phi^2 + 2\mathrm{g}\phi]\, dx\, dy$$

$$I(\phi) = \frac{1}{2}\iint [\,|\nabla\phi|^2 - k^2\phi^2 + 2\mathrm{g}\phi]\, dS$$

The FEM solution of the Helmholtz equation is obtained by minimizing its functional at every point in the solution region as

$$\frac{\partial I(\phi)}{\partial \phi_k} = \sum_{i=1}^{n} \phi_i\,[C_{ki} - k^2 T_{ki}] + \mathrm{g}_i T_{ki} = 0$$

If there are no sources in the solution region the solution becomes

$$\frac{\partial I(\phi)}{\partial \phi_k} = \sum_{i=1}^{n} \phi_i\,[C_{ki} - k^2 T_{ki}] = 0$$

Recall that in chapter2, the most general form of wave equation was given as

$$\nabla^2 \boldsymbol{E} = \boldsymbol{\nabla} \times \boldsymbol{M_i} + \mathrm{j}\omega\mu \boldsymbol{J_i} + \mathrm{j}\omega\mu\sigma \boldsymbol{E} - \omega^2\mu\epsilon \boldsymbol{E} + \frac{\boldsymbol{\nabla} \mathrm{q_{ve}}}{\epsilon}$$

Since our domain of interest in analyzing the rough surface problem is lossless and contains no impressed sources, we have ($\boldsymbol{J_i} = 0, \boldsymbol{M_i} = 0, \mathrm{q_{ve}} = 0, \mathrm{q_{vm}} = 0$) , therefore the general form of the wave equation simplifies into the homogenous Helmholtz equation

$$\nabla^2 \boldsymbol{E} + \omega^2\mu\epsilon \boldsymbol{E} = 0$$

However, when an incident plane wave hits the rough surface, it induces an electrical current distribution on the rough surface, therefore our rough surface scattering problem is not sourceless along the rough surface boundary. The incident plane wave can be thought as a conduction current source along the rough surface boundary and the wave equation can be modified as

$$\nabla^2 \boldsymbol{E} + \omega^2\mu\epsilon \boldsymbol{E} = \mathrm{j}\omega\mu \boldsymbol{J_c}$$

$\mathbf{J_i}$ = Impressed electric current density (amperes/square meter)

$\mathbf{J_c}$ = Conduction electric current density (amperes/square meter)

If the incident wave is a TM_z plane wave, this equation becomes a scalar equation and can be written as

$$\nabla^2 E_z + \omega^2\mu\epsilon E_z = \mathrm{j}\omega\mu J_z$$

Where $\mathbf{J} = \boldsymbol{a_z} \mathrm{J_z}$ is the source current density along the rough surface.

The integral solution for the inhomogenous wave equation

$$\nabla^2 E_z + \omega^2 \mu \epsilon E_z = j\omega\mu J_z$$

In the case of a free space, is known to be

$$E_z(x,y) = E_z(\rho) = -\frac{k\eta_0}{4}\int_S J_z(\boldsymbol{\rho}')\ {H_0}^2(k|\boldsymbol{\rho}-\boldsymbol{\rho}'|)dS'$$

Therefore if we know the conduction current density J_z on the rough surface boundary, we can solve for the scattered field ${E_z}^s(x,y)$ by solving the above integral. Therefore

$${E_z}^s(x,y) = {E_z}^s(\rho) = -\frac{k\eta_0}{4}\int_S J_z(\boldsymbol{\rho}')\ {H_0}^2(k|\boldsymbol{\rho}-\boldsymbol{\rho}'|)dS'$$

But the problem is, neither the current density on the rough surface boundary nor the scattered field on the rough surface boundary is known. However the scattered field on the rough surface boundary can be determined from the incident field using the Impedance boundary condition formulation as discussed in the previous section. Since our aim is to evaluate the integral expression (analytical formulation) numerically, and to compare the analytical results with the FEM results, we can directly use the FEM solution of the scattered electric field on the rough surface so that the only unknown remaining in the integral expression is the induced current density. In 2D rough surface scattering problem, the rough surface is described as a contour, so the integral is taken on a contour *C*.

$${E_z}^s(x,y) = {E_z}^s(\rho) = -\frac{k\eta_0}{4}\int_C J_z(\boldsymbol{\rho}')\ {H_0}^2(k|\boldsymbol{\rho}-\boldsymbol{\rho}'|)dC'$$

Since the induced current density J_z is the only unknown in this expression, we can determine it using the method of moments.

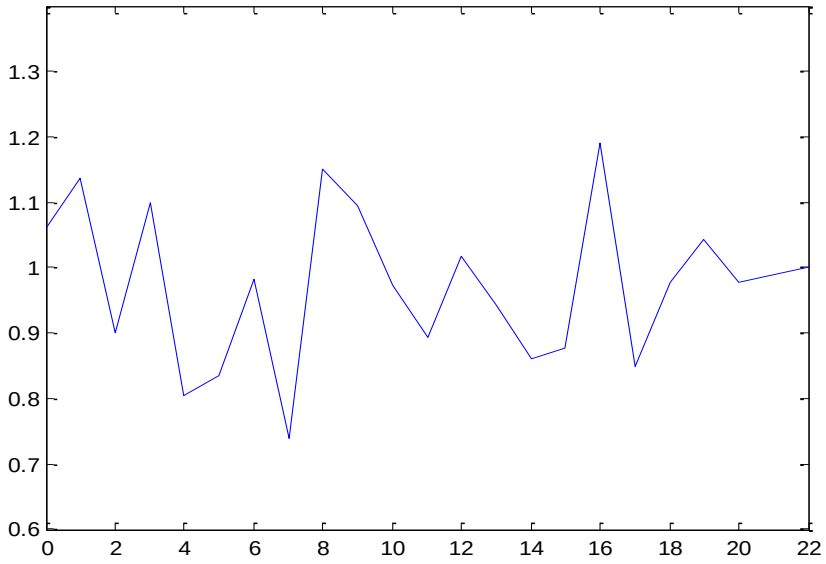

Figure6.25:An example rough surface contour.

We divide the boundary *C* into N segments and apply the point matching technique. On each segment ΔC_n , the equation becomes

$$E_z{}^s(\rho_n) = -\frac{k\eta_0}{4}\sum_{m=1}^{N} J_z(\rho_m)\, H_0{}^2(k|\rho_n - \rho_m|)\Delta C_m$$

Notice that the integration is replaced by summation, applying this formula for all segments on the rough surface contour, we get the system of linear equations as

$$\begin{bmatrix} E_z{}^s(\rho_1) \\ E_z{}^s(\rho_2) \\ \vdots \\ E_z{}^s(\rho_N) \end{bmatrix} = \begin{bmatrix} A_{11} & A_{12} & \dots & A_{1N} \\ A_{21} & A_{22} & \dots & A_{2N} \\ \vdots & \vdots & \vdots & \vdots \\ A_{N1} & A_{N2} & \dots & A_{NN} \end{bmatrix} \begin{bmatrix} J_z(\rho_1) \\ J_z(\rho_2) \\ \vdots \\ J_z(\rho_N) \end{bmatrix}$$

Solving for J_z , we have

$$\begin{bmatrix} J_z(\rho_1) \\ J_z(\rho_2) \\ \vdots \\ J_z(\rho_N) \end{bmatrix} = \begin{bmatrix} A_{11} & A_{12} & \dots & A_{1N} \\ A_{21} & A_{22} & \dots & A_{2N} \\ \vdots & \vdots & \vdots & \vdots \\ A_{N1} & A_{N2} & \dots & A_{NN} \end{bmatrix}^{-1} \begin{bmatrix} E_z{}^s(\rho_1) \\ E_z{}^s(\rho_2) \\ \vdots \\ E_z{}^s(\rho_N) \end{bmatrix}$$

Where

$$A_{mn} \cong \begin{cases} -\frac{k\eta_0}{4}\Delta C_n H_0{}^2\left(k\sqrt{(x_n - x_m)^2 + (y_n - y_m)^2}\right) & , \quad m \neq n \\ -\frac{k\eta_0}{4}\left[1 - j\frac{2}{\pi}\log_{10}\left(\frac{\gamma k \Delta C_n}{4e}\right)\right. & , \quad m = n \end{cases}$$

Where$\{x_n\, , y_n\}$ is the midpoint of ΔC_n , e=2.718, and γ=1.781.

After finding J_z on each point on the rough surface contour, we can directly use

$$E_z{}^s(x,y) = \; E_z{}^s(\rho) = -\frac{k\eta_0}{4}\int_C J_z(\boldsymbol{\rho}')\; H_0{}^2\,(k|\boldsymbol{\rho} - \boldsymbol{\rho}'|)dC'$$

to get the scattered field at each point $\{x, y\}$ in the 2D solution region. In discrete form this integral is expressed as

$$E_z{}^s(x,y) = -\frac{k\eta_0}{4}\sum_{m=1}^{N} J_z(x_m\, , y_m)\, H_0{}^2\left(k\sqrt{(x - x_m)^2 + (y - y_m)^2}\right)\Delta C_m \qquad (i)$$

In FEM formulation $\phi = E_z{}^s(x,y)$ is expressed as

$$\frac{\partial I(\phi)}{\partial \phi_k} = \sum_{i=1}^{n} \phi_i\,[C_{ki} - k^2 T_{ki}] \;=\; \sum_{i=1}^{n} E_{zi}{}^s\,[C_{ki} - k^2 T_{ki}] \;=\; 0 \qquad (ii)$$

$$\sum_{i=1}^{n} E_{z,fem}{}^s(i)\,[C_{ki} - k^2 T_{ki}] \;=\; 0 \qquad (ii)$$

$$E_{z,an}{}^{s}(x_i, y_i) = -\frac{k\eta_0}{4}\sum_{m=1}^{N} J_z(x_m, y_m)\, H_0{}^{2}\left(k\sqrt{(x_i - x_m)^2 + (y_i - y_m)^2}\right)\Delta C_m$$

$$E_{z,an}{}^{s}(x_i, y_i) = E_{z,an}{}^{s}(i) \qquad (i)$$

If there are M nodes in the solution region, the total error is given by

$$Error = \sum_{i=1}^{M} \frac{\left| E_{z,fem}{}^{s}(i) - E_{z,an}{}^{s}(i)\right|^2}{\left| E_{z,an}{}^{s}(i)\right|^2}$$

We will now compare (i) and (ii) to see the error between the two approximations.

Ex1: $\mathbf{E}^{inc} = \mathbf{a_z}\, 100 e^{\mathrm{jk}(-0.707\mathrm{x}+0.707\mathrm{y})}$, *with supressed* $e^{j\omega t}$ *time dependence.*

f=3Ghz, k=20π, λ=0.1m, pmlwidth=λ, surface conductance=5S/m

Meshsize=$12\lambda \times 12\lambda$, $\sigma_{roughness} = 0$ $(Flat\ surface)$

Number of elements =147456, Number of nodes=74305

$\sigma_{roughness}$: $Standard\ deviation\ of\ surface\ roughness$

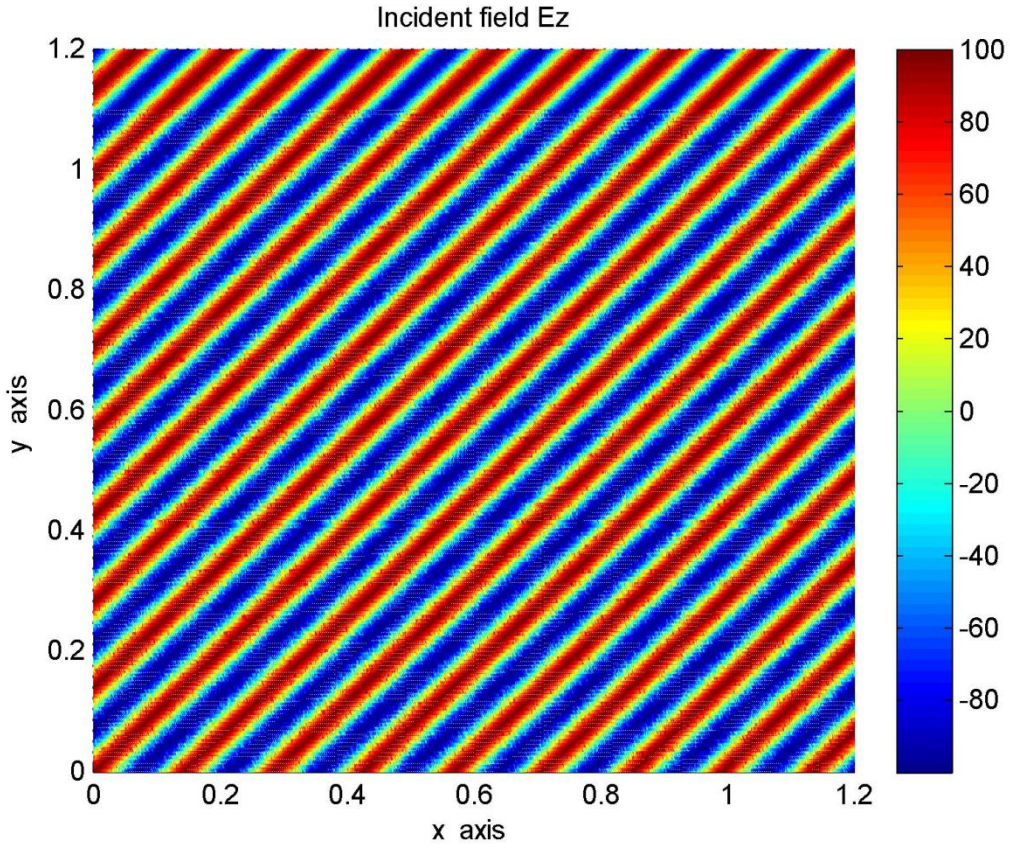

Figure6.26: Incident field of example1

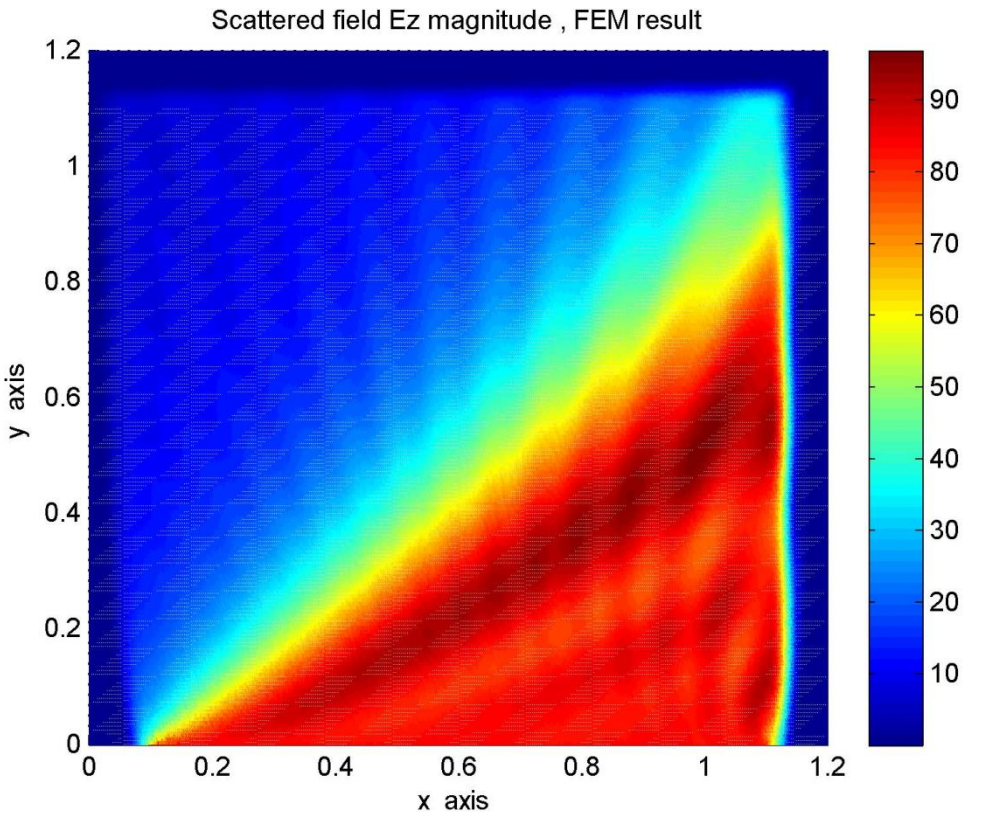

Figure6.27: Scattered field magnitude plot of example1, FEM result.

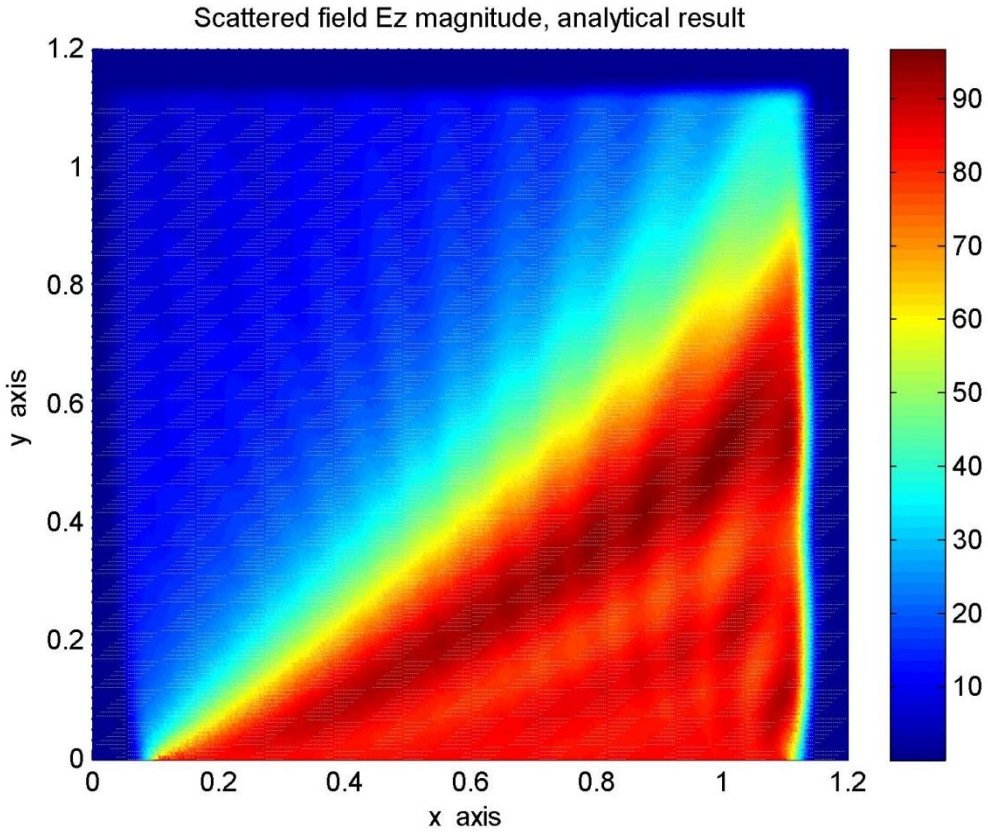

Figure6.28: Scattered field magnitude plot of example1, analytical result.

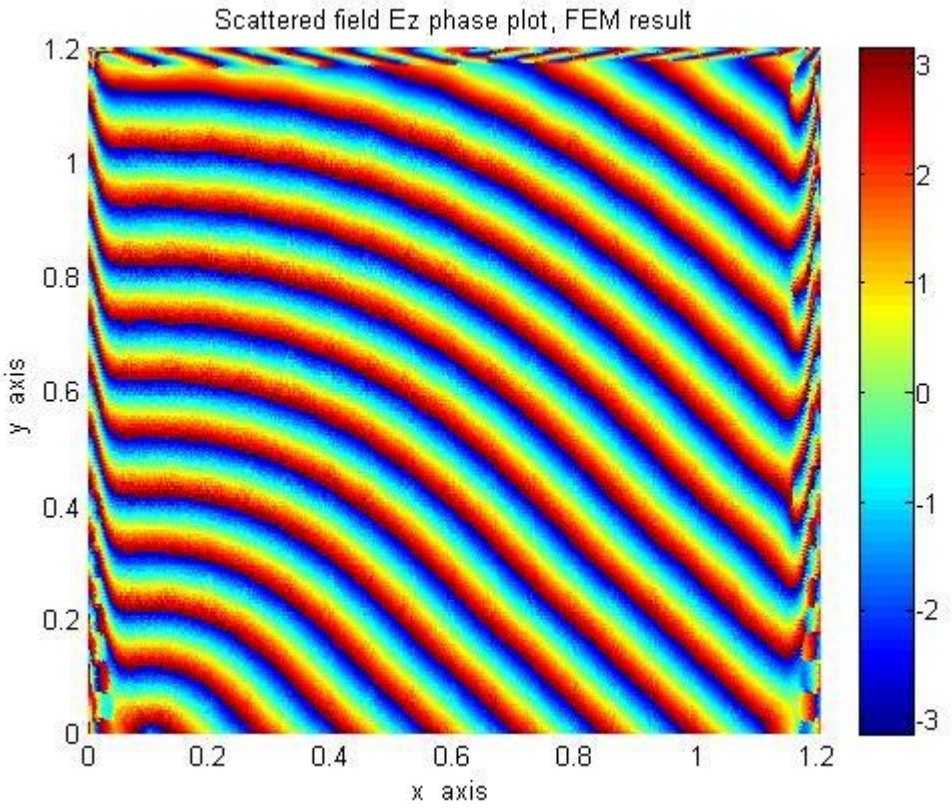

Figure6.29: Scattered field phase plot of example1, FEM result.

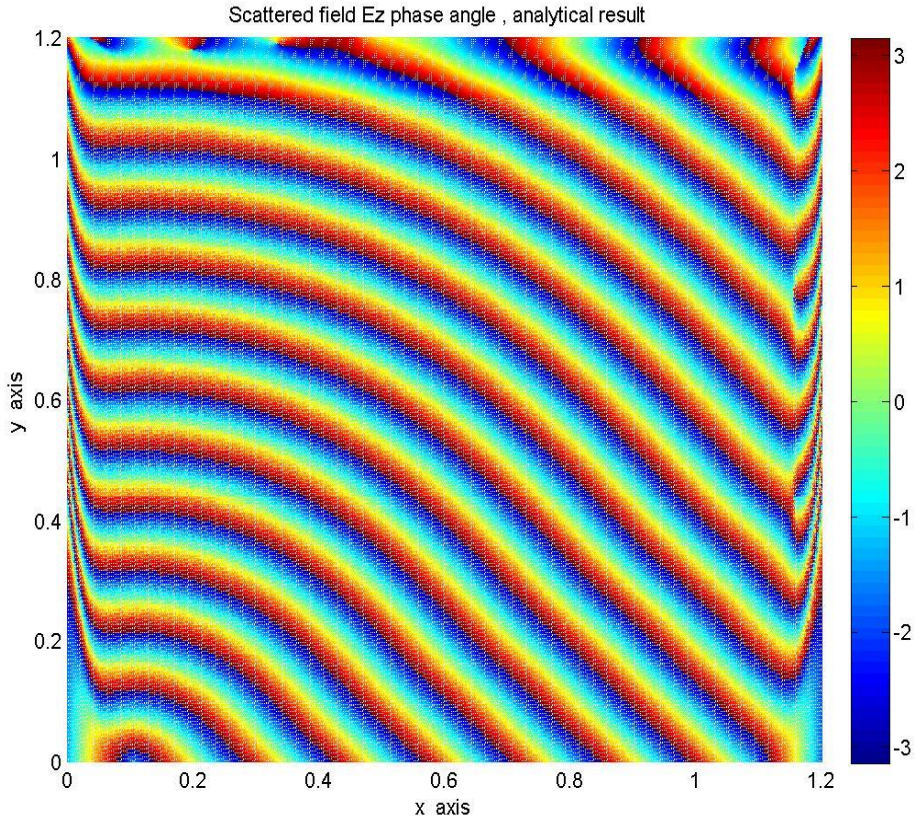

Figure6.30: Scattered field phase plot of example1, analytical result.

With the parameters specified in this example, the error between the FEM solution and the analytical solution is found to be

$$Error = \sum_{i=1}^{M=74305} \frac{\left| {E_{z,fem}}^{s}(i) - {E_{z,an}}^{s}(i) \right|^2}{\left| {E_{z,an}}^{s}(i) \right|^2} \approx 0.266\%$$

Ex2: $\mathbf{E}^{inc} = \mathbf{a_z}\, 100 e^{jky}$, *with supressed* $e^{j\omega t}$ *time dependence.*

f=3Ghz, k=20π, λ=0.1m, pmlwidth=λ, surface conductance=5S/m

Meshsize=$12\lambda \times 12\lambda$, $\sigma_{roughness} = 0$ $(Flat\ surface)$

Number of elements =147456, Number of nodes=74305

$\sigma_{roughness}$: $Standard\ deviation\ of\ surface\ roughness$

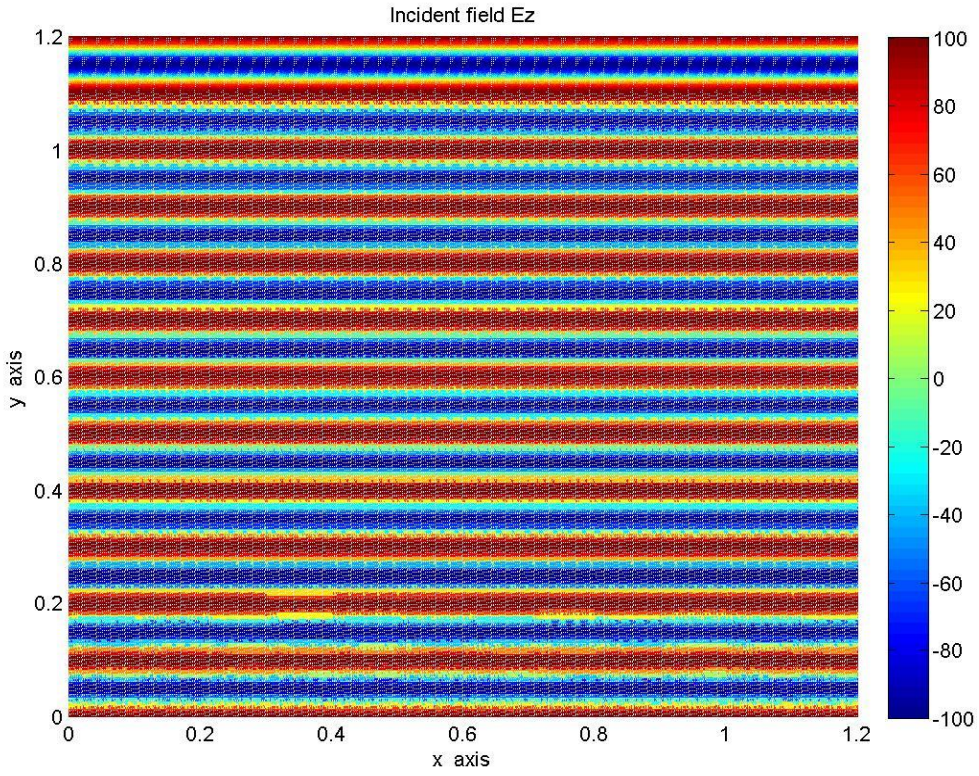

Figure6.31: Incident field of example2

$${E_{z,an}}^{s}(x_i, y_i) = -\frac{k\eta_0}{4} \sum_{m=1}^{N} J_z(x_m, y_m)\, {H_0}^2 \left(k\sqrt{(x_i - x_m)^2 + (y_i - y_m)^2} \right) \Delta C_m \quad (i)$$

$$\sum_{i=1}^{n} {E_{z,fem}}^{s}(i)\, [C_{ki} - k^2 T_{ki}] = 0 \quad (ii)$$

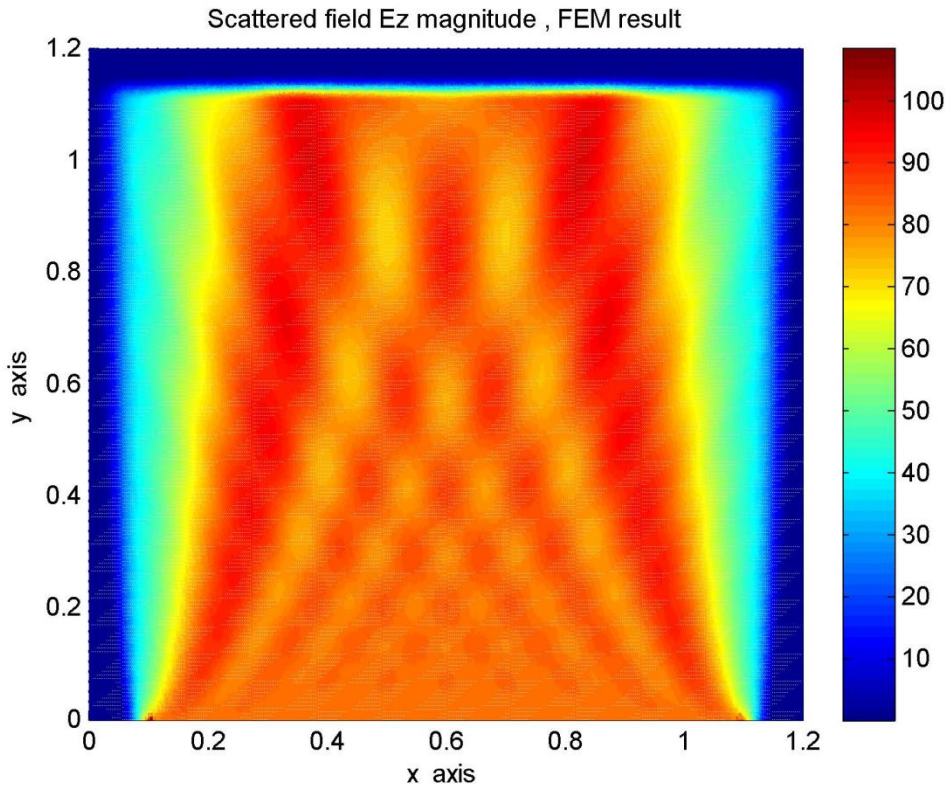

Figure6.32: Scattered field magnitude plot of example2, FEM result.

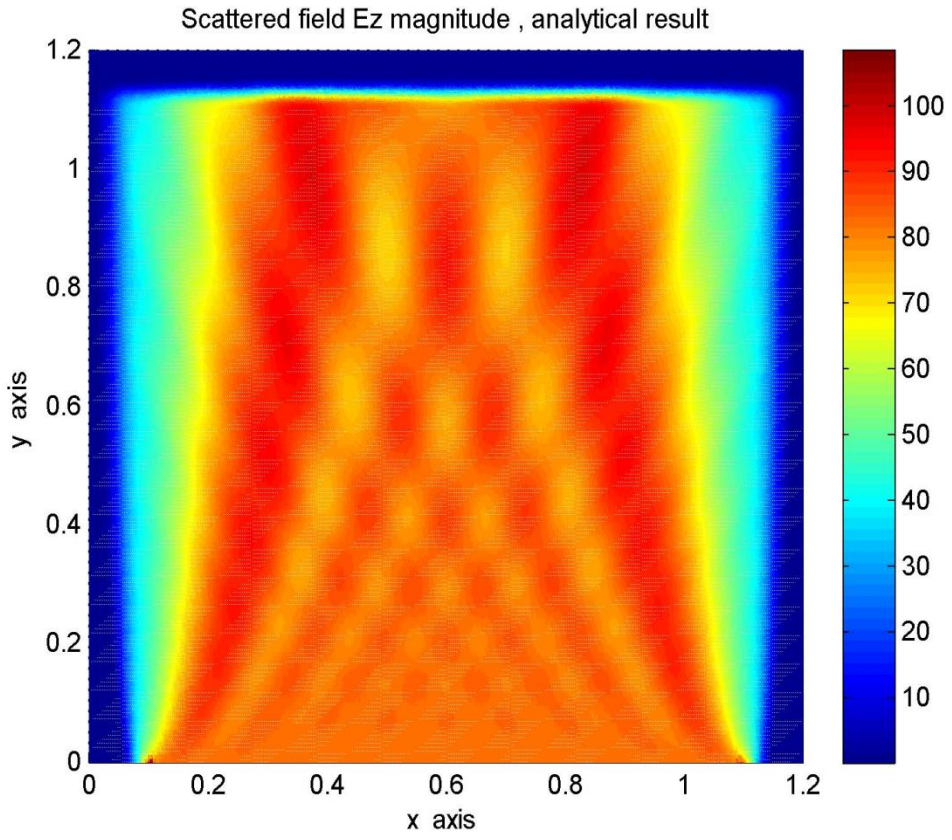

Figure6.33: Scattered field magnitude plot of example2, analytical result.

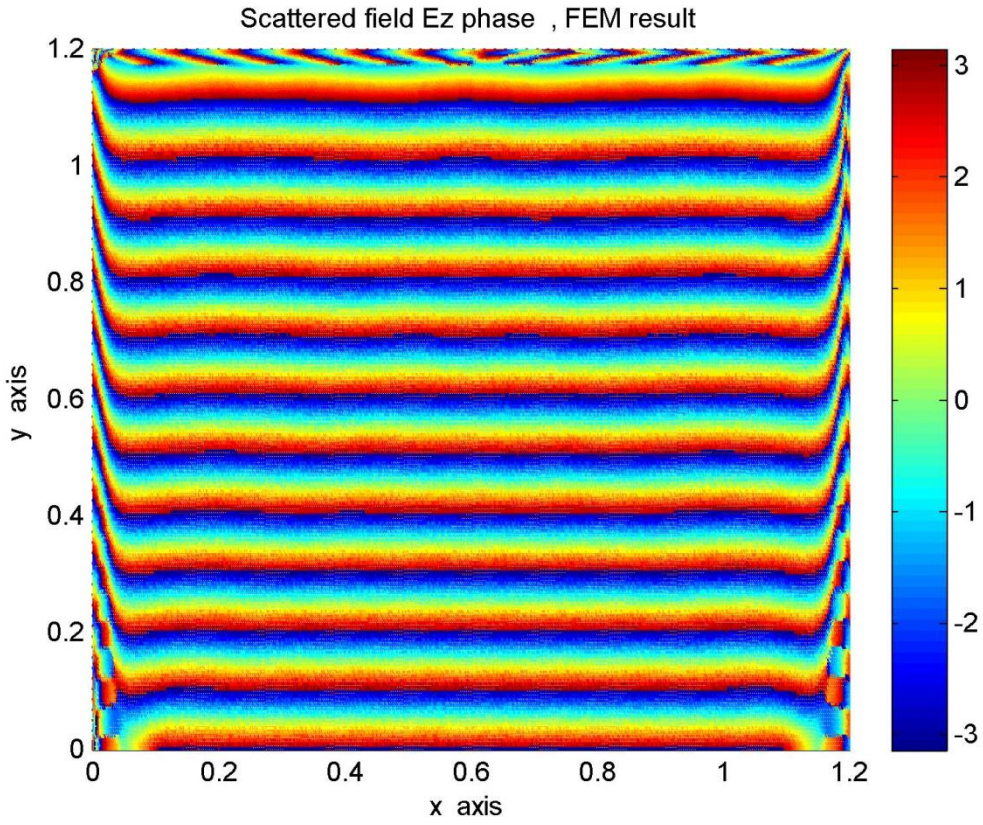

Figure6.34: Scattered field phase plot of example2, FEM result.

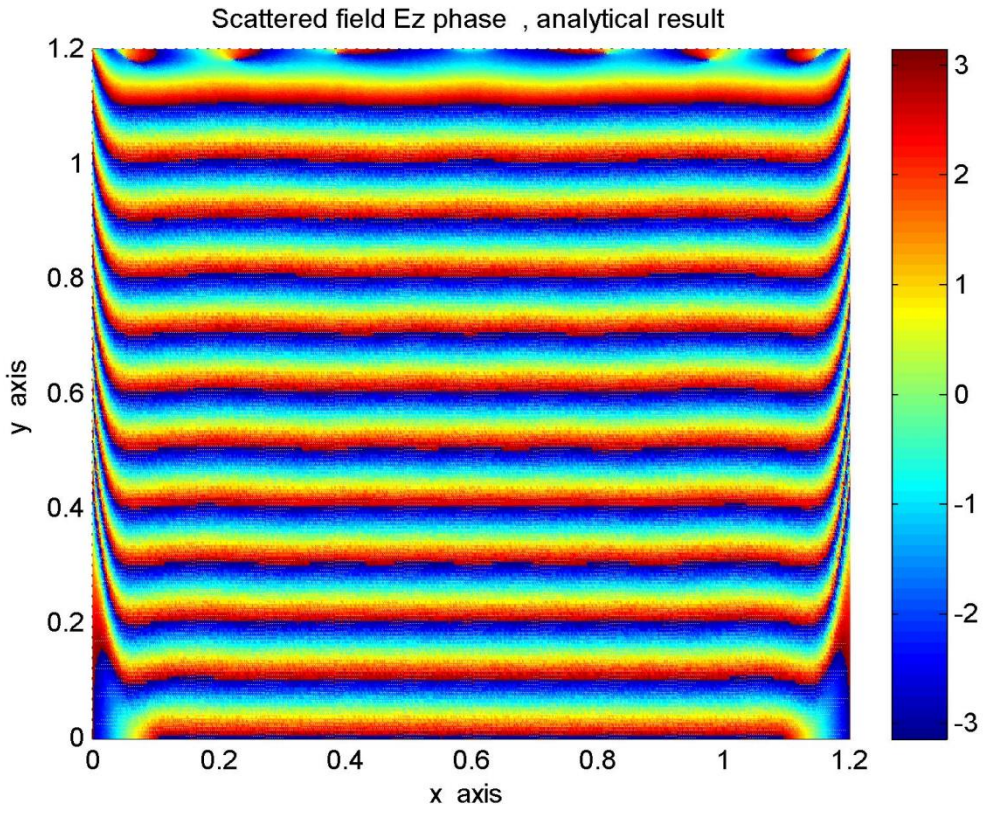

Figure6.35: Scattered field phase plot of example2, analytical result.

$$Error = \sum_{i=1}^{M=74305} \frac{\left| {E_{z,fem}}^{s}(i) - {E_{z,an}}^{s}(i) \right|^2}{\left| {E_{z,an}}^{s}(i) \right|^2} \approx 0.439\%$$

Ex3: $\mathbf{E}^{inc} = \mathbf{a_z}\, 100 e^{jky}$, *with supressed* $e^{j\omega t}$ *time dependence.*

f=3Ghz, k=20π, λ=0.1m, pmlwidth=λ, surface conductance=5S/m

Meshsize=$12\lambda \times 12\lambda$, $\sigma_{roughness} = \frac{\lambda}{2}$ $(Rough\ surface)$

Number of elements =122880, Number of nodes=61985

$\sigma_{roughness}$: $Standard\ deviation\ of\ surface\ roughness$

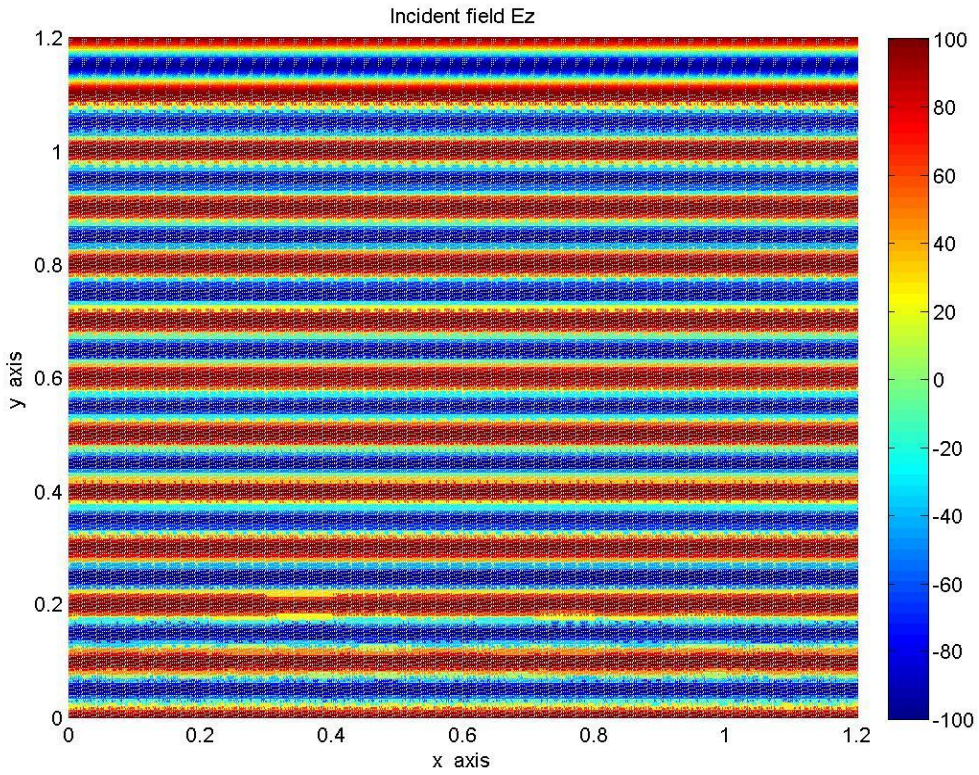

Figure6.36: Incident field of example3

$$E_{z,an}{}^{s}(x_i, y_i) = -\frac{k\eta_0}{4} \sum_{m=1}^{N} J_z(x_m, y_m)\, {H_0}^2 \left(k\sqrt{(x_i - x_m)^2 + (y_i - y_m)^2} \right) \Delta C_m \quad (i)$$

$$\sum_{i=1}^{n} {E_{z,fem}}^{s}(i)\, [C_{ki} - k^2 T_{ki}] = 0 \quad (ii)$$

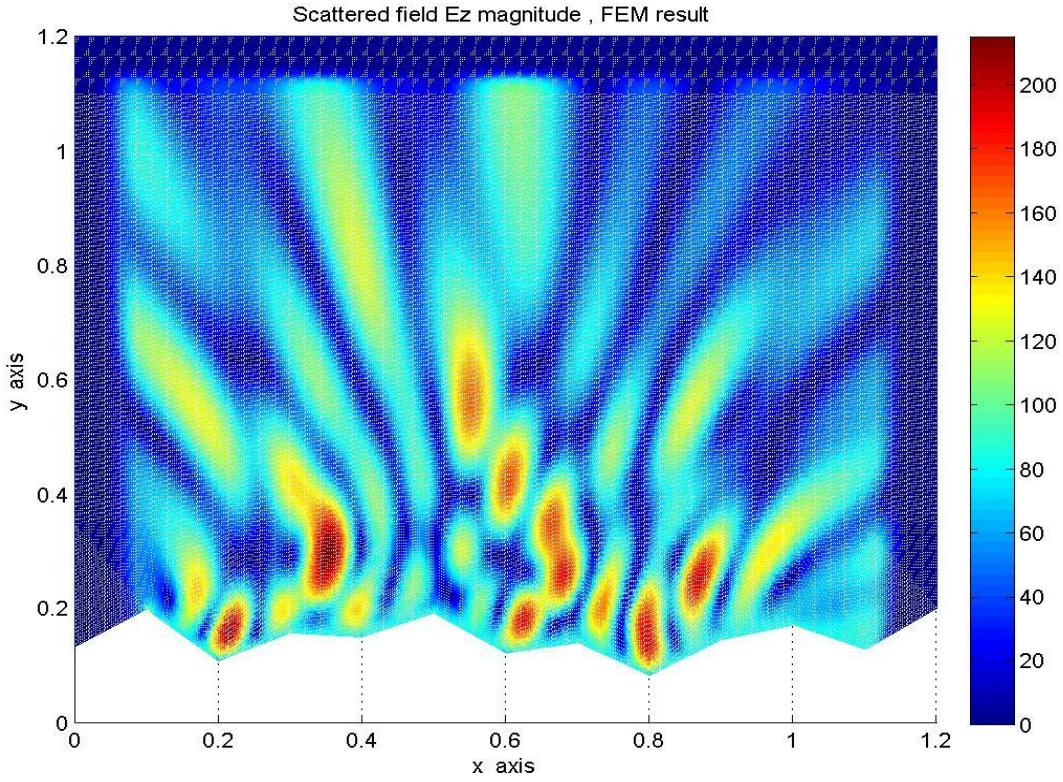

Figure6.37: Scattered field magnitude plot of example3, FEM result.

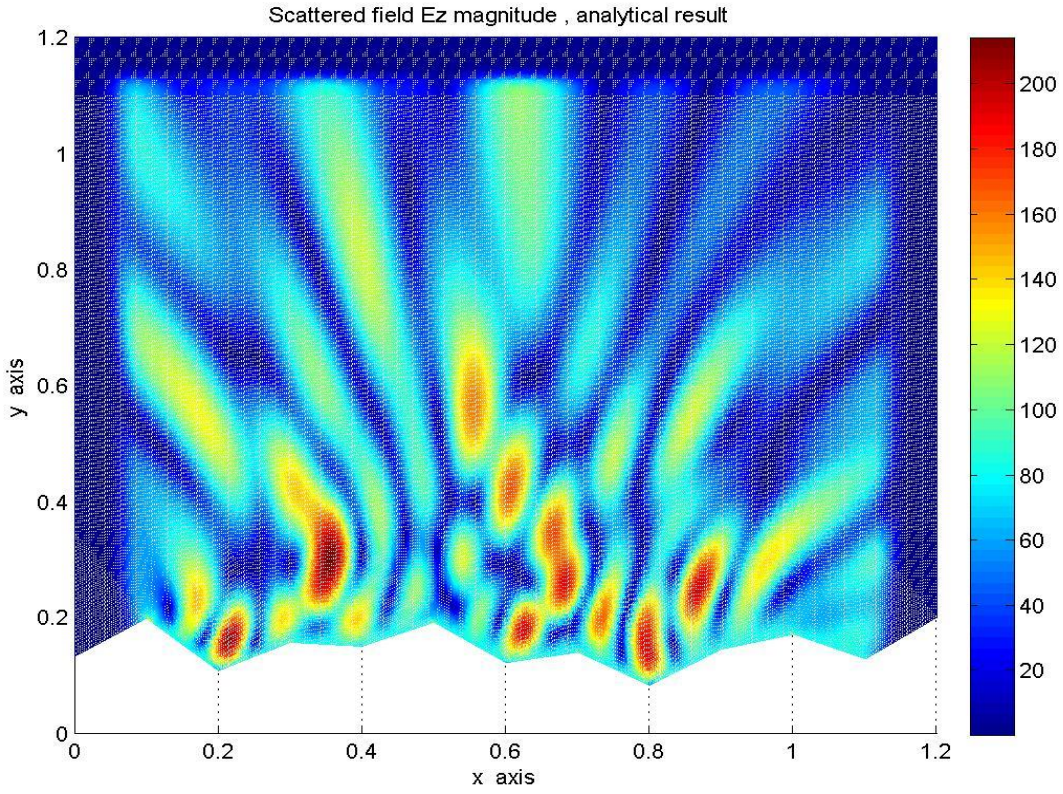

Figure6.38: Scattered field magnitude plot of example3, analytical result.

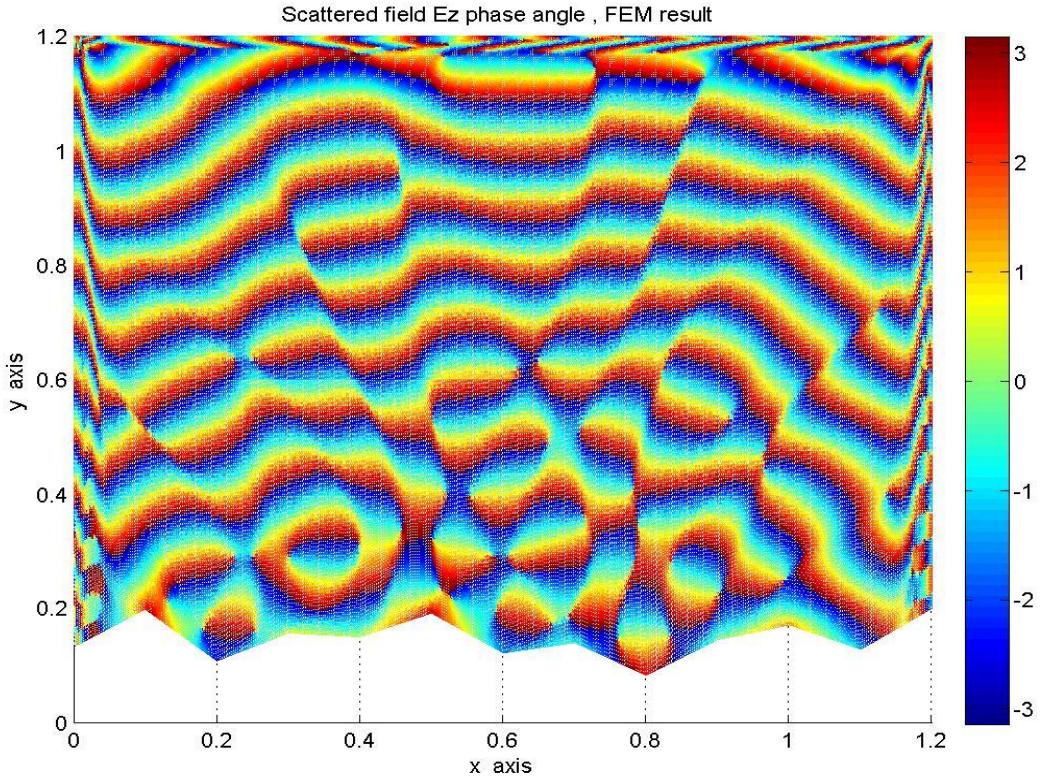

Figure6.39: Scattered field phase plot of example3, FEM result.

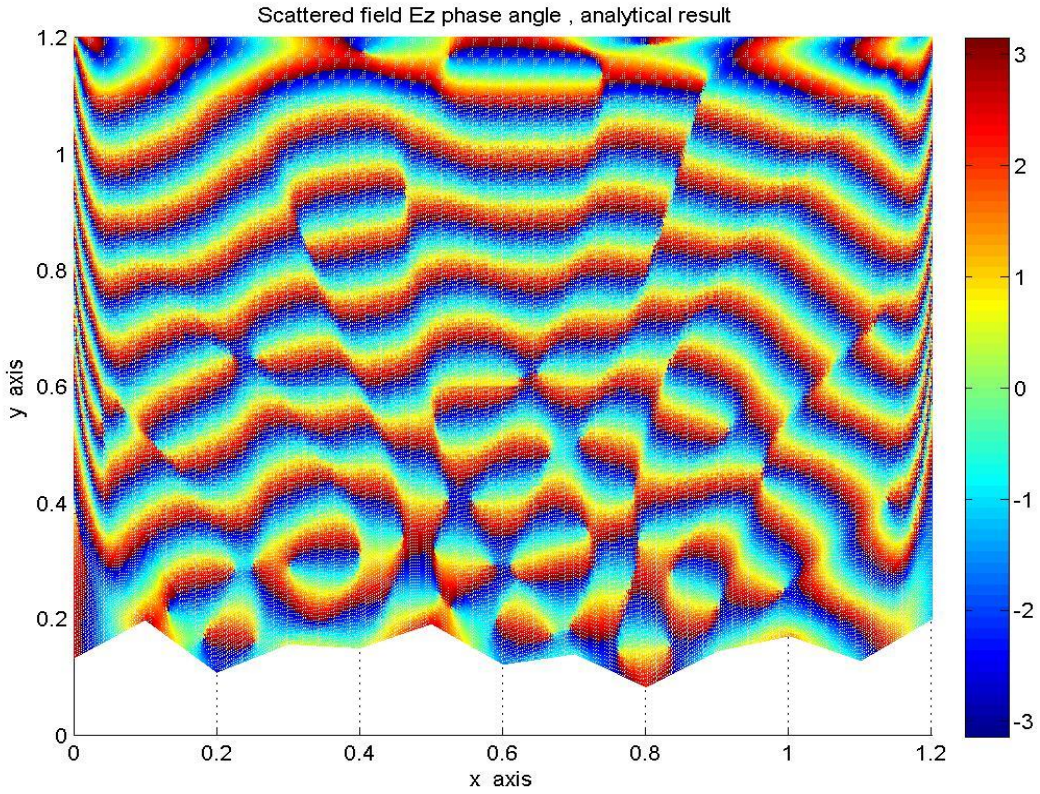

Figure6.40: Scattered field phase plot of example3, analytical result.

$$Error = \sum_{i=1}^{M=61985} \frac{\left| E_{z,fem}{}^{s}(i) - E_{z,an}{}^{s}(i) \right|^2}{\left| E_{z,an}{}^{s}(i) \right|^2} \approx 0.319\%$$

Ex4: $\mathbf{E}^{inc} = \mathbf{a_z}\, 100 e^{\mathrm{jk}(-0.707x+0.707y)}$, *with supressed* $e^{j\omega t}$ *time dependence.*

f=3Ghz, k=20π, λ=0.1m, pmlwidth=λ, surface conductance=5S/m

Meshsize=$12\lambda \times 12\lambda$, $\sigma_{roughness} = \frac{2\lambda}{5}$ $(Rough\ surface)$

Number of elements =122880, Number of nodes=61985

$\sigma_{roughness}$: $Standard\ deviation\ of\ surface\ roughness$

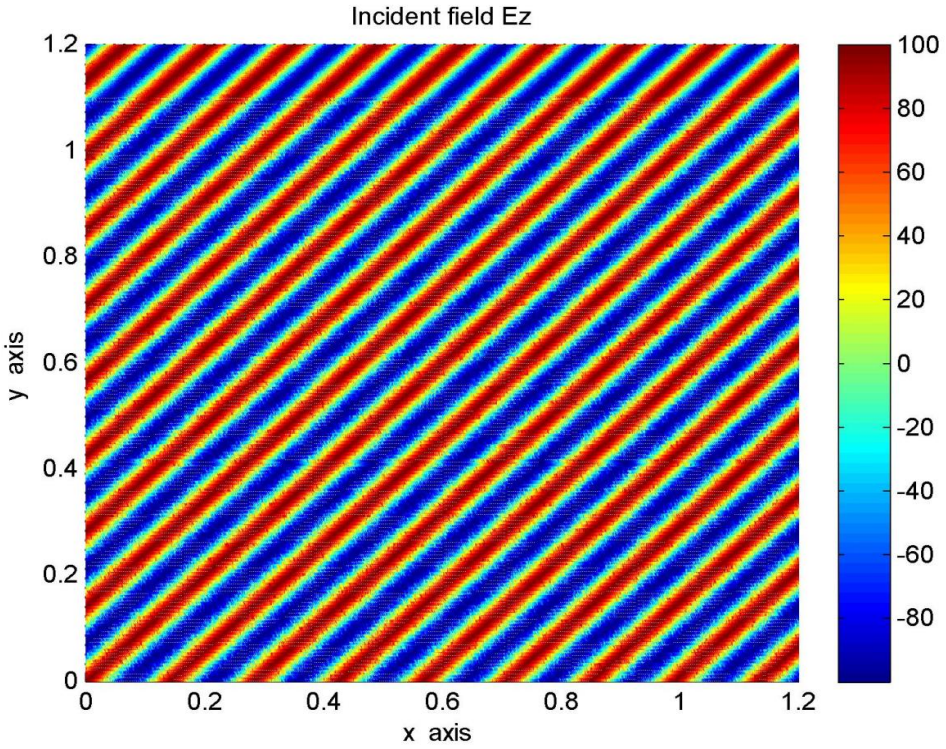

Figure6.41: Incident field of example4

$$E_{z,an}{}^{s}(x_i, y_i) = -\frac{k\eta_0}{4} \sum_{m=1}^{N} J_z(x_m, y_m)\, {H_0}^2 \left(k\sqrt{(x_i - x_m)^2 + (y_i - y_m)^2} \right) \Delta C_m \quad (i)$$

$$\sum_{i=1}^{n} E_{z,fem}{}^{s}(i)\, [C_{ki} - k^2 T_{ki}] = 0 \quad (ii)$$

$$Error = \sum_{i=1}^{M=74305} \frac{\left| E_{z,fem}{}^{s}(i) - E_{z,an}{}^{s}(i) \right|^2}{\left| E_{z,an}{}^{s}(i) \right|^2} \approx 0.204\%$$

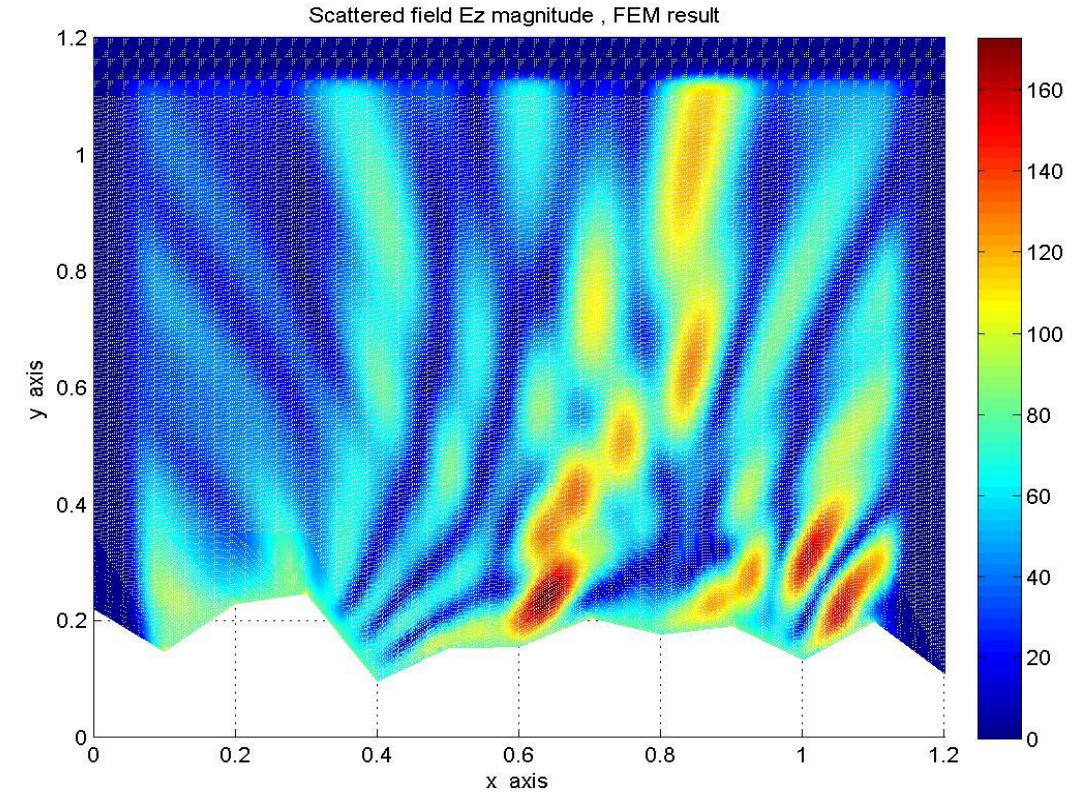

Figure6.42: Scattered field magnitude plot of example4, FEM result.

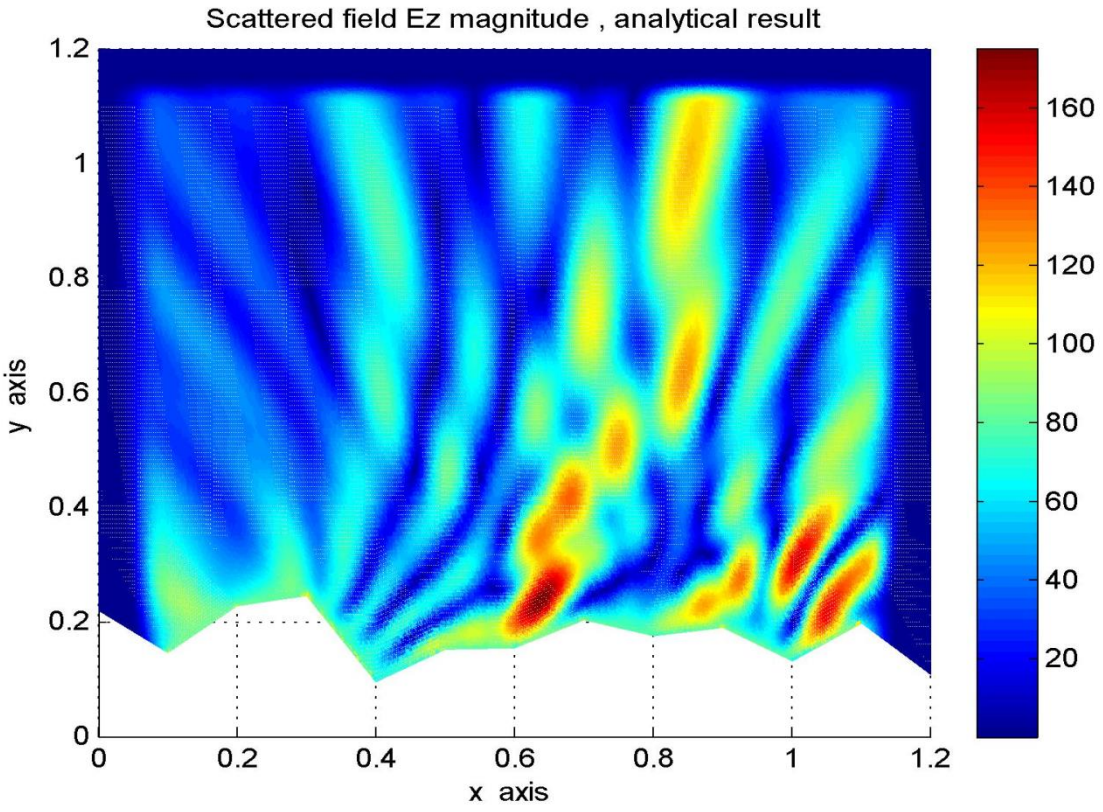

Figure6.43: Scattered field magnitude plot of example4, analytical result.

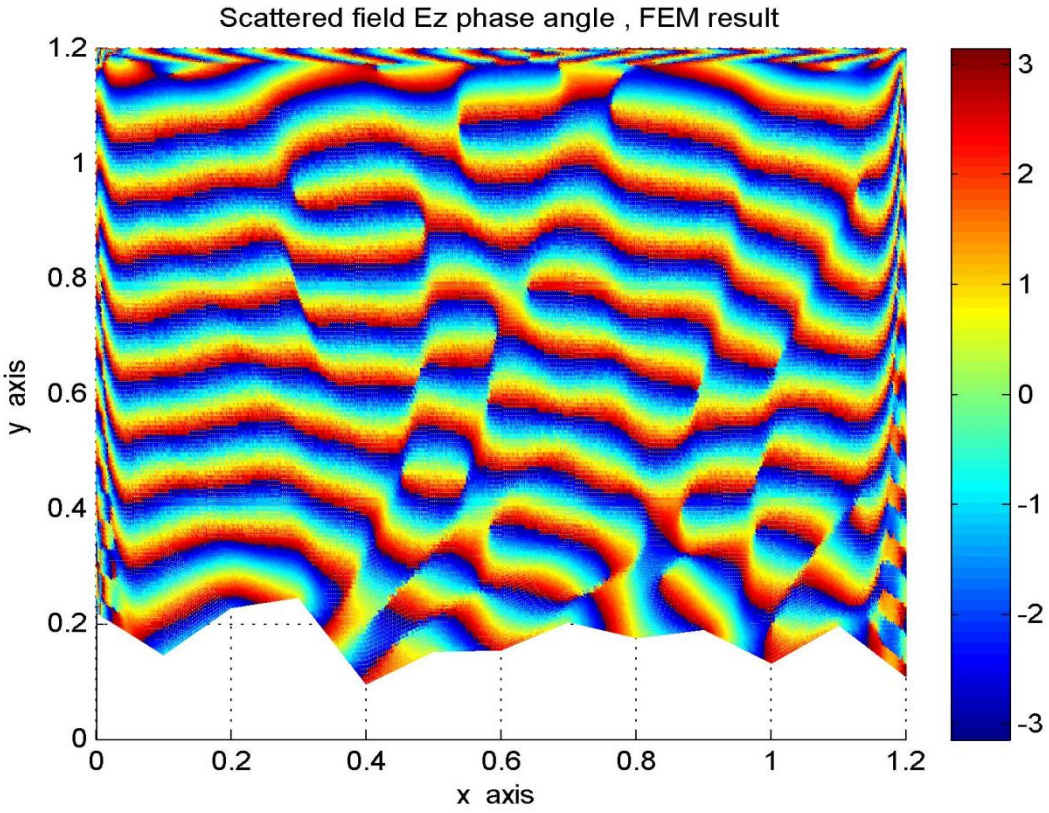

Figure6.44: Scattered field phase plot of example4, FEM result.

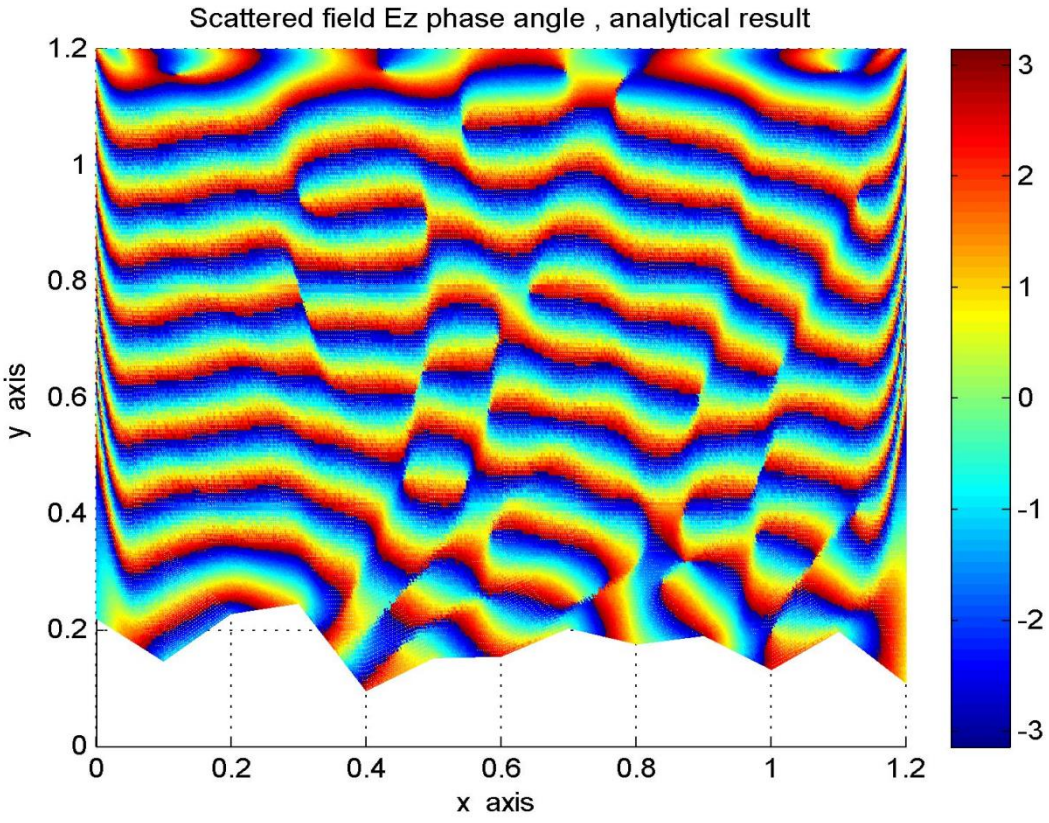

Figure6.45: Scattered field phase plot of example4, analytical result.

CHAPTER 7

FAR FIELD ANALYSIS OF THE ROUGH SURFACE SCATTERING PROBLEM

In analyzing the rough surface scattering problem, what we are really interested in is the far field scattered field pattern. In this chapter we will analyze the far field rough surface scattered field patterns and investigate how the roughness of the surface affects the pattern.

It is known that as the roughness of the scattering surface increases, the far field scattered field pattern becomes more distorted, and after some roughness level the major lobe of the far field pattern will be completely lost.

For a given incidence angle, our aim is to determine the level of roughness, up to which the far field pattern still contains the major beam (lobe) in the direction of specular reflection.

We will also calculate the correlation coefficients of rough surface scattered field patterns with that of a flat surface scattered field pattern for a given incidence angle to determine the similarity of the two patterns and to detect the level of roughness that causes a significant decrease in the correlation coefficient.

For our analysis we will use a rough surface with a width of 20λ that is symmetrically placed around the origin, along the horizontal axis, which will be sufficient for an accurate analysis of the far field scattered field pattern as surface widths of more than 10λ does not affect the far field pattern significantly.

For each of the examples and cases given below, the patterns obtained are mean patterns of 100 measurements and the problem parameters are chosen to be some common values for analyzing scattering from sea surfaces at a radar frequency, they are chosen to be as follows

Frequency: *The frequency in all of the examples is set to 3GHz.*

Wavelength: *λ=0.1m, since f=3GHz.*

Rough surface conductivity: *Sea surface conductivity=σ=5S/m.*

Rough surface width: $-10\lambda \leq x \leq 10\lambda$, x *is the horizontal axis.*

Angle measure: *Angle is measured from the positive x axis, that is,*

Φ=0° *for positive x axis,* Φ=90° *for positive y axis and* Φ=180° *for negative x axis.*

Incident wave: *The incident wave is a uniform plane wave and has an amplitude of 100V/m, it's incidence angle will be specified in each example.*

$$\boldsymbol{E}_{z,inc} = \boldsymbol{a}_z 100 e^{jk(cos\phi_i\ x + sin\phi_i\ y)} \quad , \quad in\ phasor\ domain\ with\ e^{j\omega t}\ convention.$$

Note : Φ is in degrees and phase values are in radians for all plots in this chapter.

Far field measurement distance from the origin: *Since we want to determine the far field pattern, the distance from the origin where the center of the rough surface alignment is, must be greater than the Rayleigh distance.*

$$\rho > \frac{2D^2}{\lambda} \quad , \quad where\ \rho = \frac{2D^2}{\lambda}\ is\ the\ Rayleigh\ distance$$

$D=20\lambda$ *, therefore* $\rho = \frac{2D^2}{\lambda} = 800\lambda = 80$, $since\ \lambda = 0.1m\ \ at\ f = 3GHz.$

In all of the following examples, the radius of measurement is chosen to be $\rho = 1000m$ *from the origin so that our far field assumption is very well satisfied.*

$$x=\rho\cos(\Phi) \quad , \quad y=\rho\sin(\Phi) \quad , \quad \rho=\sqrt{x^2+y^2}$$

where, $0 \leq \Phi \leq 180^{\circ}$, and the increment of the measurement is $\Delta\Phi = 0.18^{\circ}$, therefore we measure the scattered field values at 1000 different points around the upper semicircle.

Statistics of the rough surface: *The rough surfaces are all gaussian distributed with zero mean, their standard deviation values which are given in terms of wavelength, will determine their roughness level and will be specified in each of the examples. The probability density function of the surface height is given as*

$$p(h) = \frac{1}{\sqrt{2\pi}\sigma}\ exp\left(-\frac{(h-\mu)^2}{2\sigma^2}\right) \quad , where$$

h, is the value of the surface height

σ, is the standard deviation of the surface height

μ , is the mean value of the surface height

Note that in our case $\mu=0$, *so that* $p(h) = \frac{1}{\sqrt{2\pi}\sigma}\ exp\left(-\frac{h^2}{2\sigma^2}\right)$. *An example rough surface is given in the below figure with* $\mu=0$ *and* $\sigma=0.01m$.

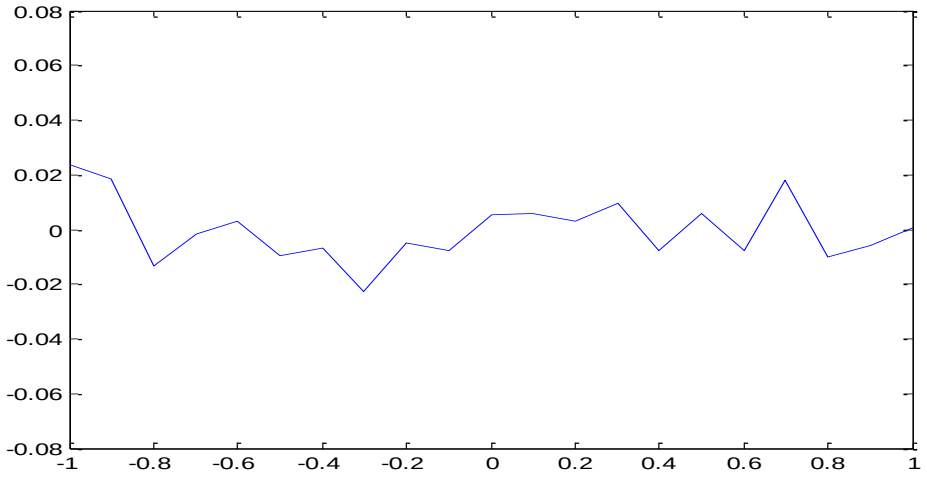

Figure7.1: An example rough surface contour

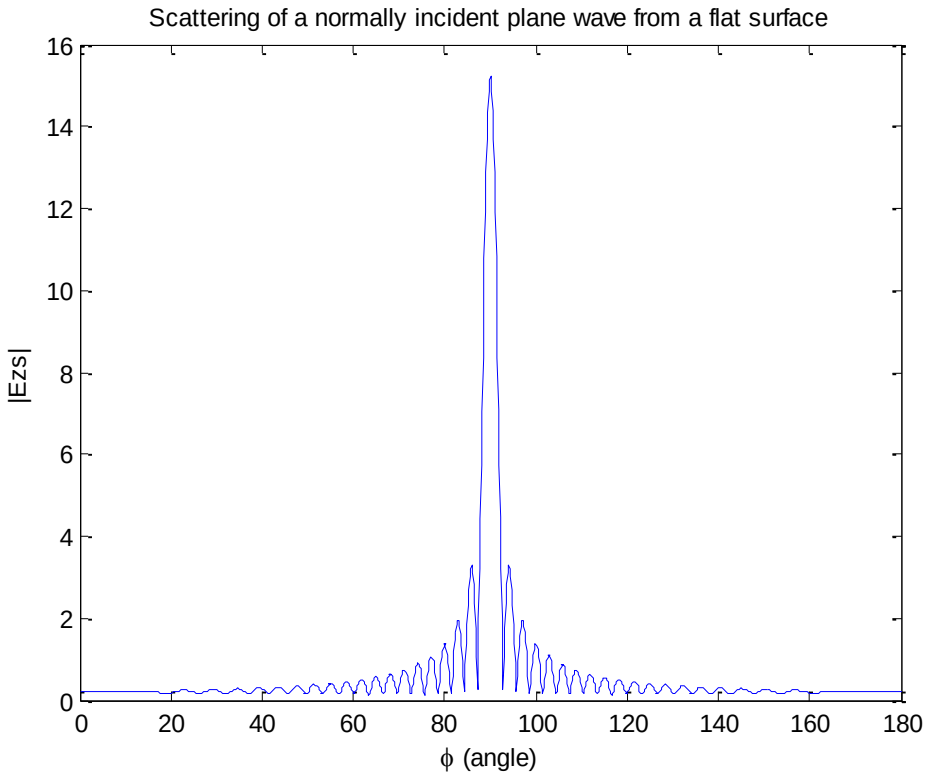

Figure7.2: Scattering of a normally incident plane wave from a flat surface, magnitude plot.

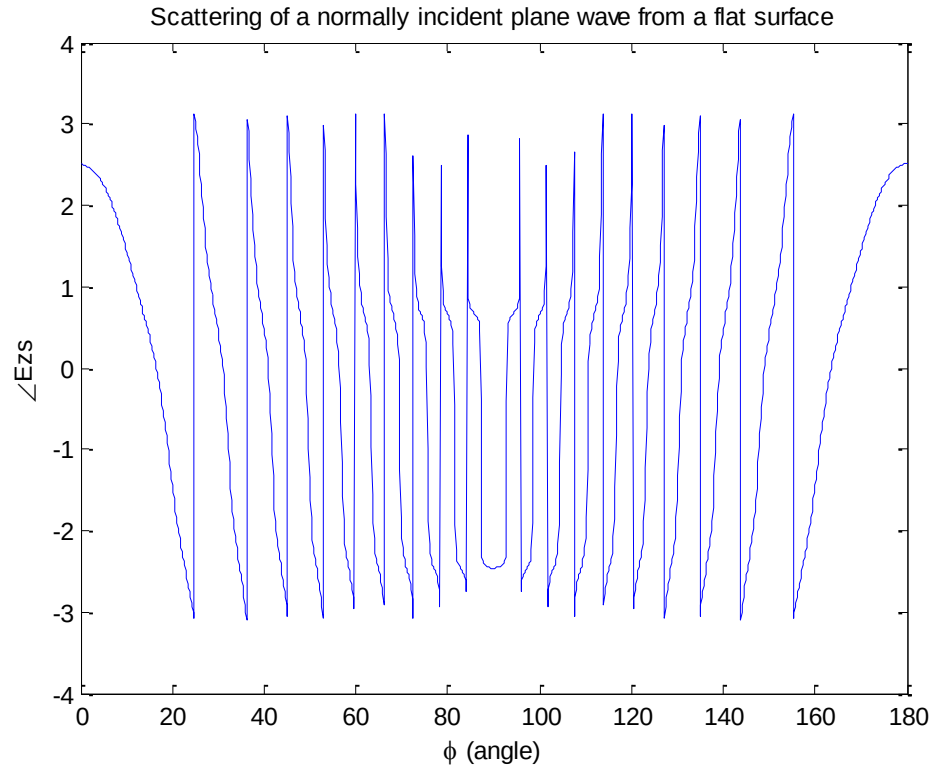

Figure7.3: Scattering of a normally incident plane wave from a flat surface, phase plot.

Ex1: Angle of Incidence= 90° , Surface roughness= $\frac{\lambda}{40}$, Mean pattern of 100 simulations

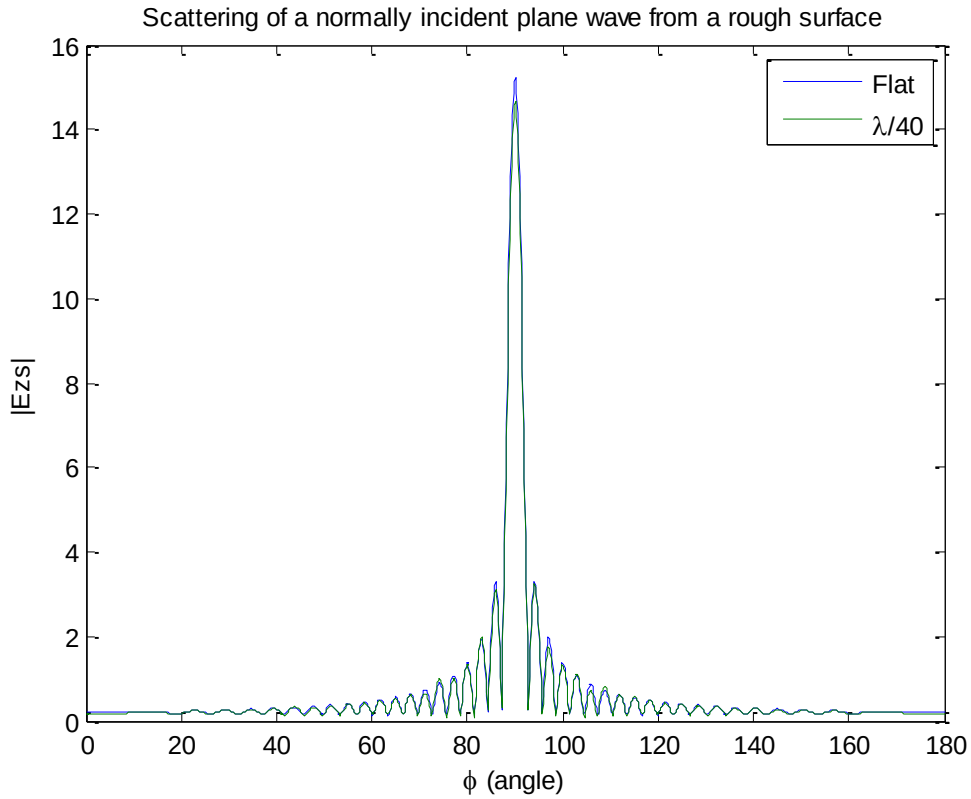

Figure7.4: Scattering of a normally incident plane wave by a rough surface, magnitude plot.

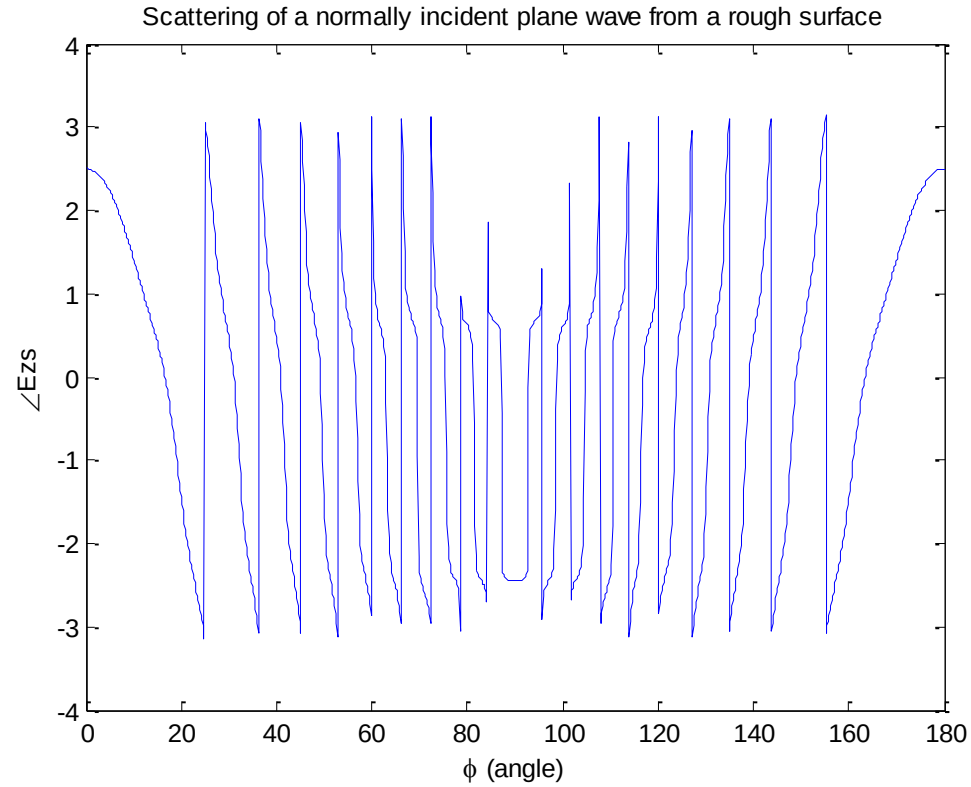

Figure7.5: Scattering of a normally incident plane wave by a rough surface, phase plot.

Ex2: Angle of Incidence= 90° , Surface roughness= $\frac{\lambda}{20}$, Mean pattern of 100 simulations

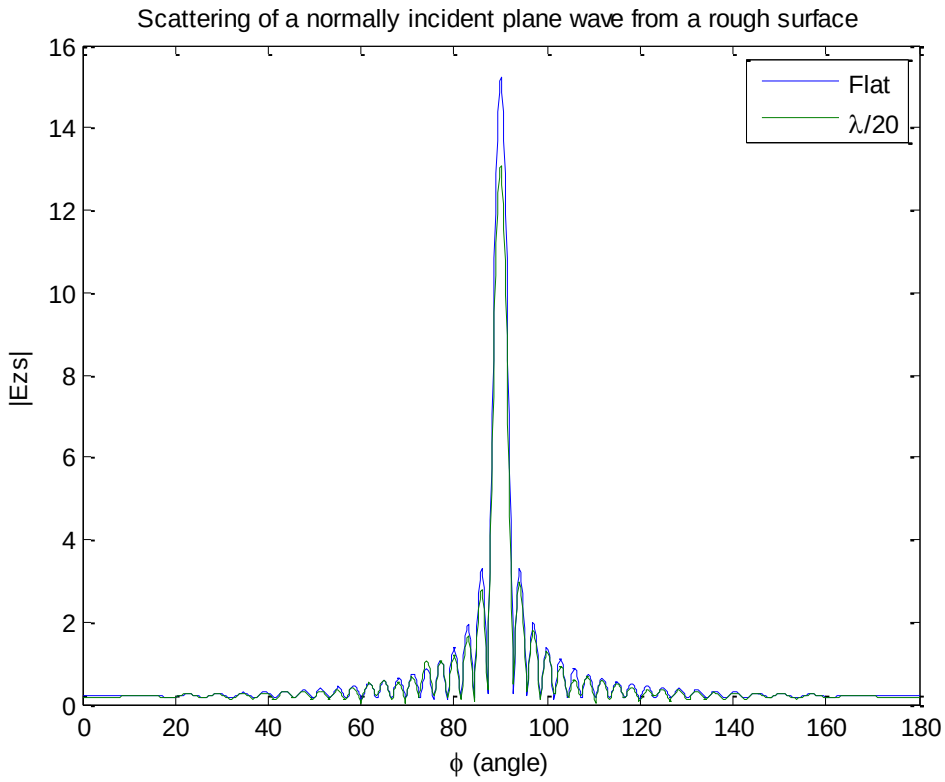

Figure7.6: Scattering of a normally incident plane wave by a rough surface, magnitude plot.

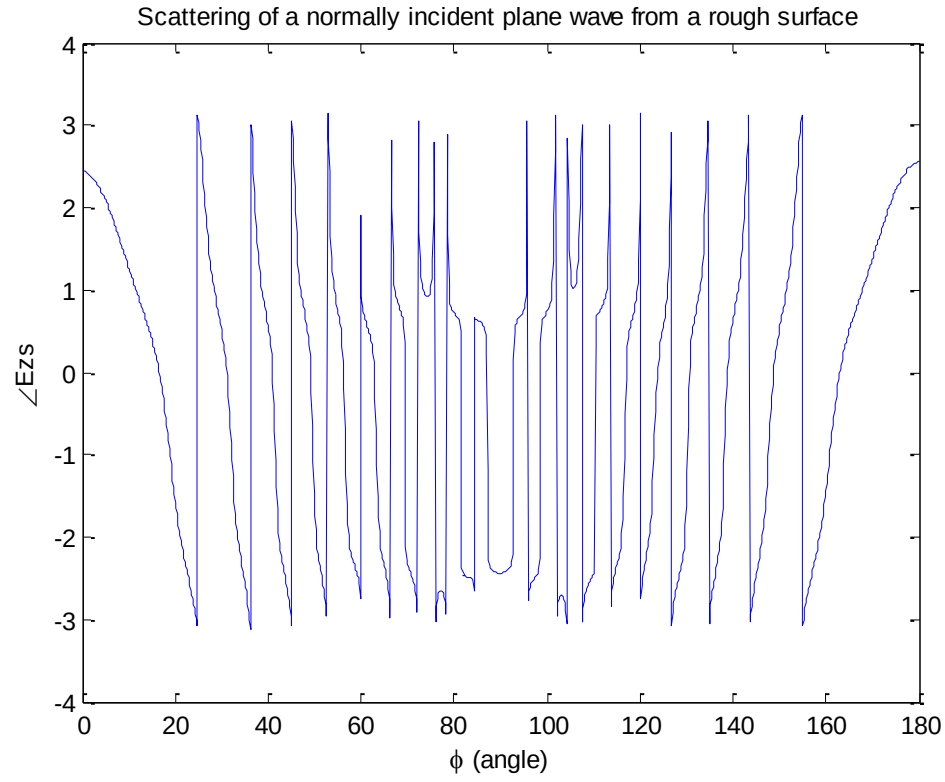

Figure7.7: Scattering of a normally incident plane wave by a rough surface, phase plot.

Ex3: Angle of Incidence= 90° , Surface roughness= $\frac{\lambda}{10}$, Mean pattern of 100 simulations

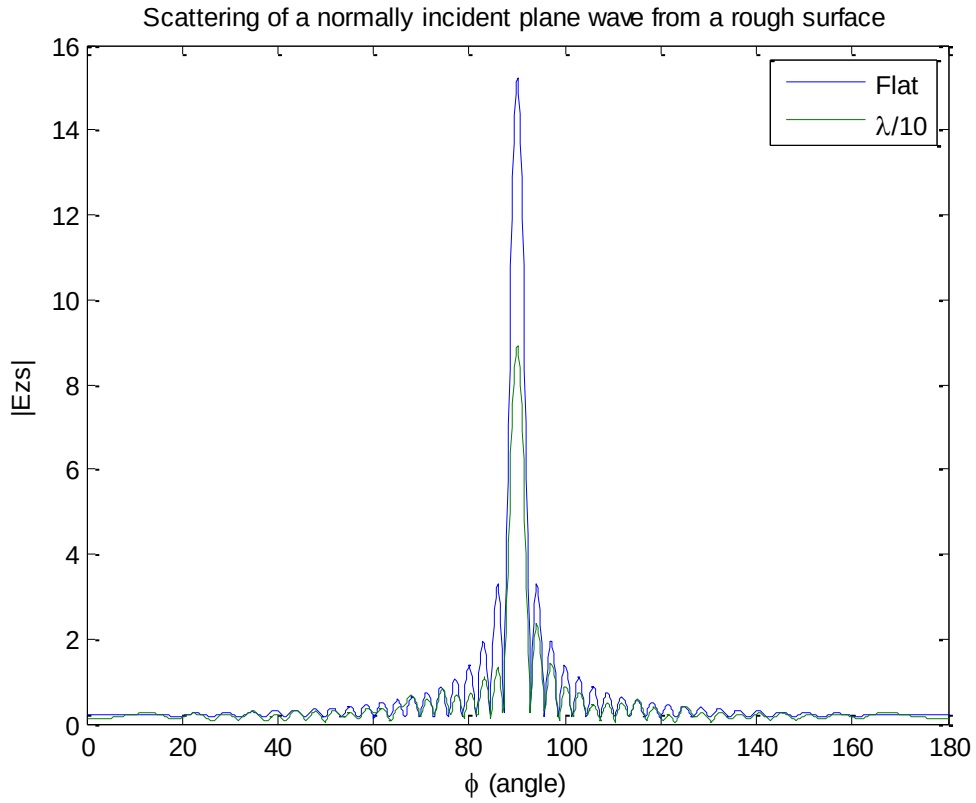

Figure7.8: Scattering of a normally incident plane wave by a rough surface, magnitude plot.

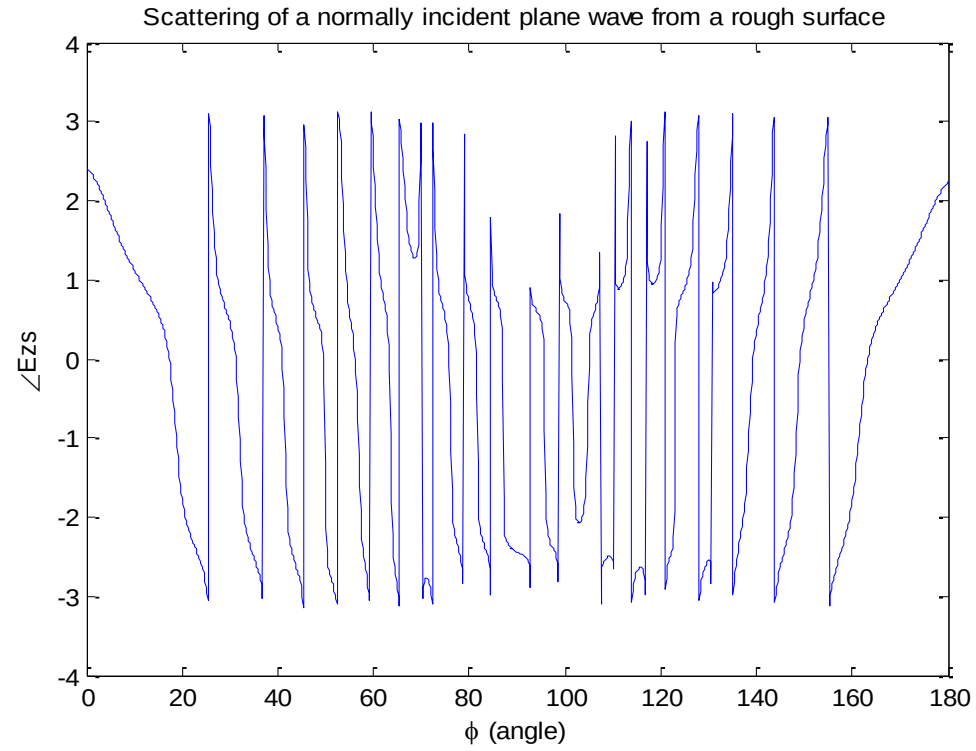

Figure7.9: Scattering of a normally incident plane wave by a rough surface, phase plot.

Ex4: Angle of Incidence= 90° , Surface roughness= $\frac{\lambda}{5}$, Mean pattern of 100 simulations

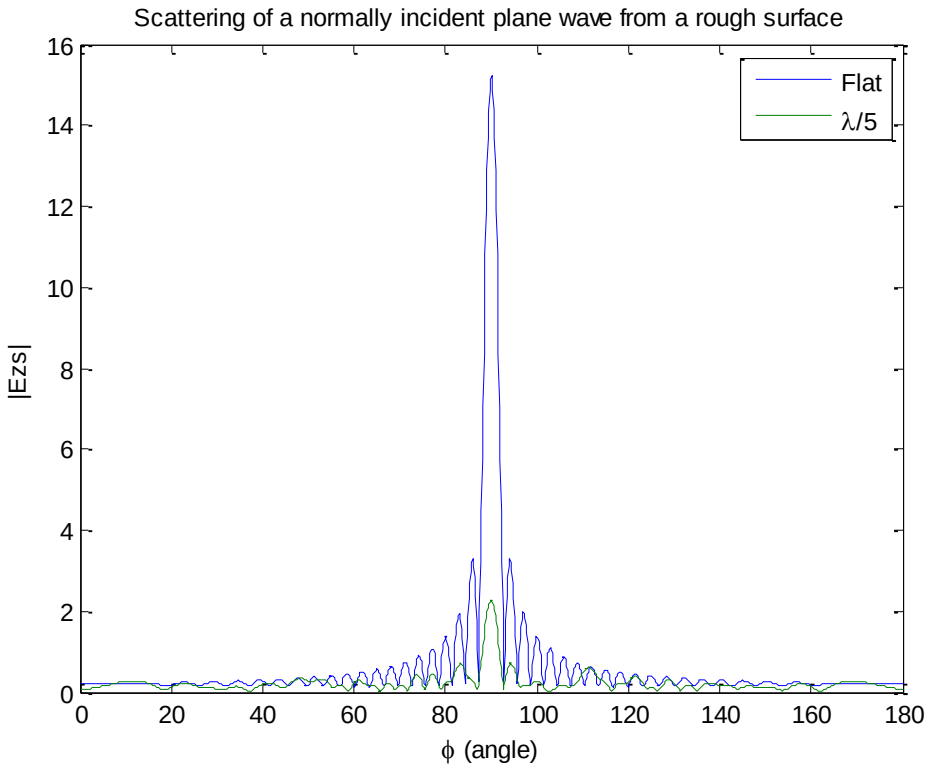

Figure7.10: Scattering of a normally incident plane wave by a rough surface, magnitude plot.

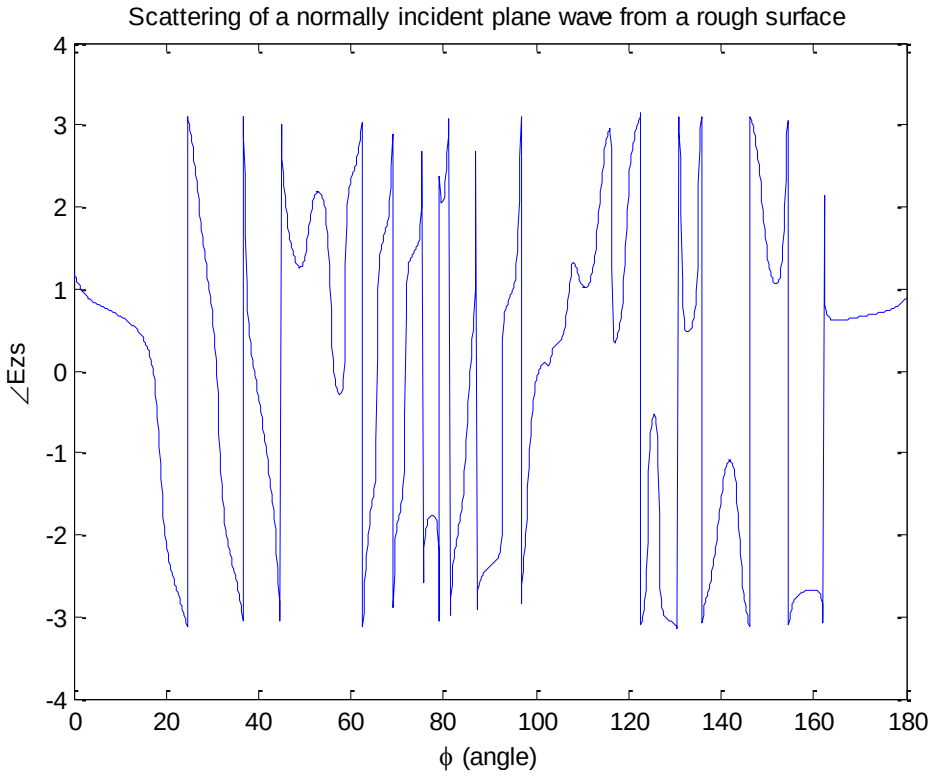

Figure7.11: Scattering of a normally incident plane wave by a rough surface, phase plot.

Ex5: Angle of Incidence= 90° , Surface roughness= $\frac{\lambda}{4}$, Mean pattern of 100 simulations

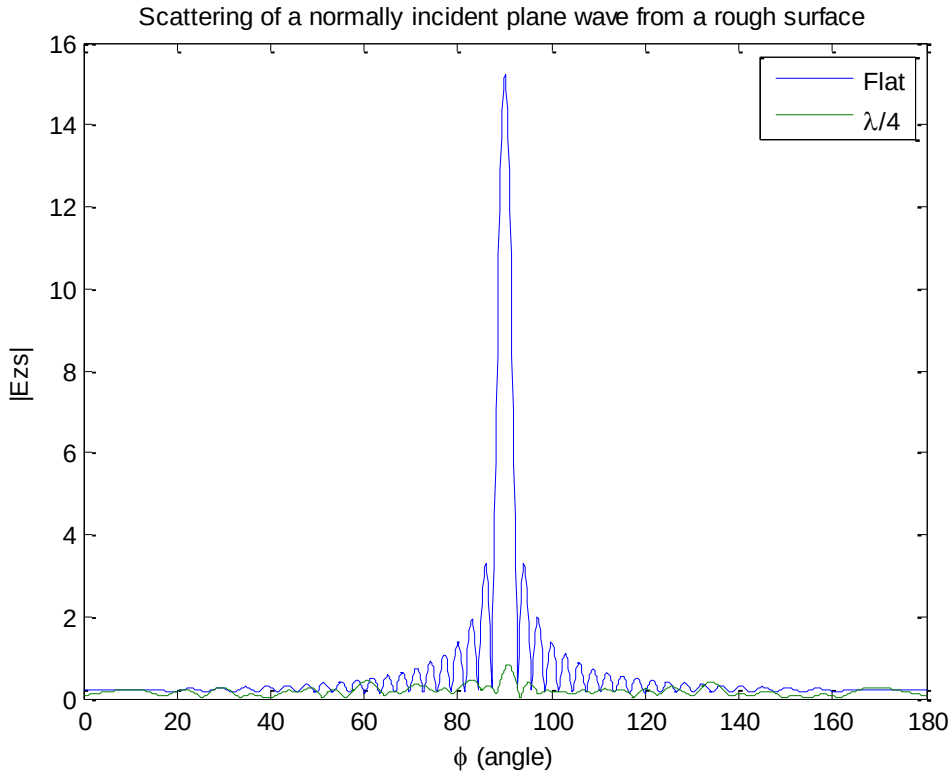

Figure7.12: Scattering of a normally incident plane wave by a rough surface, magnitude plot.

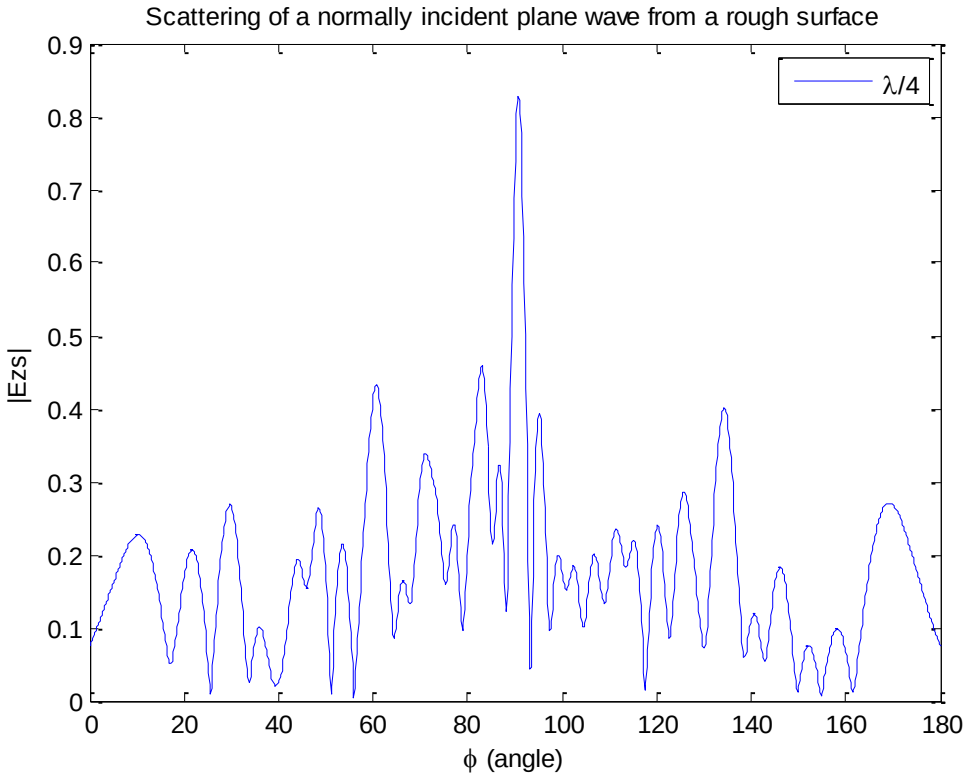

Figure7.13: Scattering of a normally incident plane wave by a rough surface, magnitude plot.

Ex6: Angle of Incidence= 90° , Surface roughness= $\frac{\lambda}{3}$, Mean pattern of 100 simulations

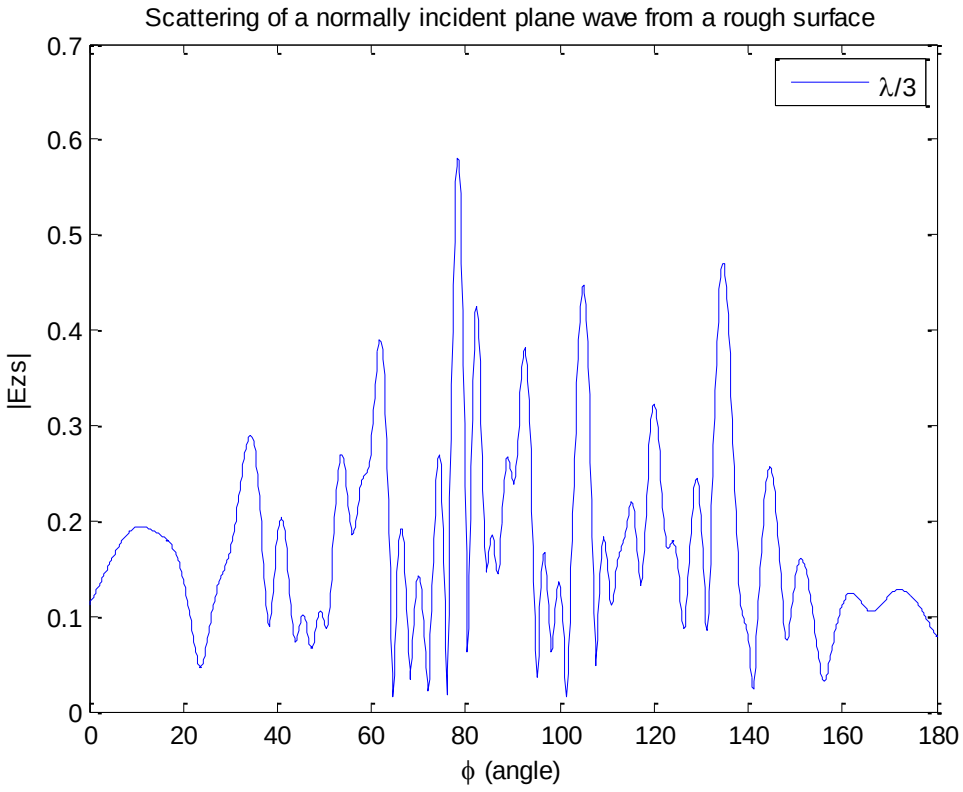

Figure7.14: Scattering of a normally incident plane wave by a rough surface, magnitude plot.

If the main lobe of the pattern is uncertain, i.e, if there are many grating lobes, it means that the pattern does not contain much useful information. For the pattern to contain information there should be only one major lobe with a much higher amplitude value than the minor lobes. But as the surface roughness increases, we should expect more grating lobes and less information. So our purpose is to find the critical surface roughness standard deviation value that is the threshold value for the pattern to be detectable.

As we can see in figure 7.13, the main lobe in the specular direction is lost, so if the surface roughness is more than $\frac{\lambda}{4}$, the incident field direction is not much detectable regardless of the roughness level of the surface this observation is almost the same for all incidence angles. In addition, various measurements of the correlation coefficient of the pattern that occurs when the scattering surface is flat, and the pattern that occurs when the scattering surface has a roughness standard deviation of more than $\frac{\lambda}{4}$, yields out almost zero. So as the surface roughness increases, the flat surface pattern and the rough surface patterns become more uncorrelated. However, this is not the case for grazing angles as we will see in the upcoming examples.

Ex7: Angle of Incidence= 135° , Surface roughness= $\frac{\lambda}{20}$, Mean pattern of 100 simulations

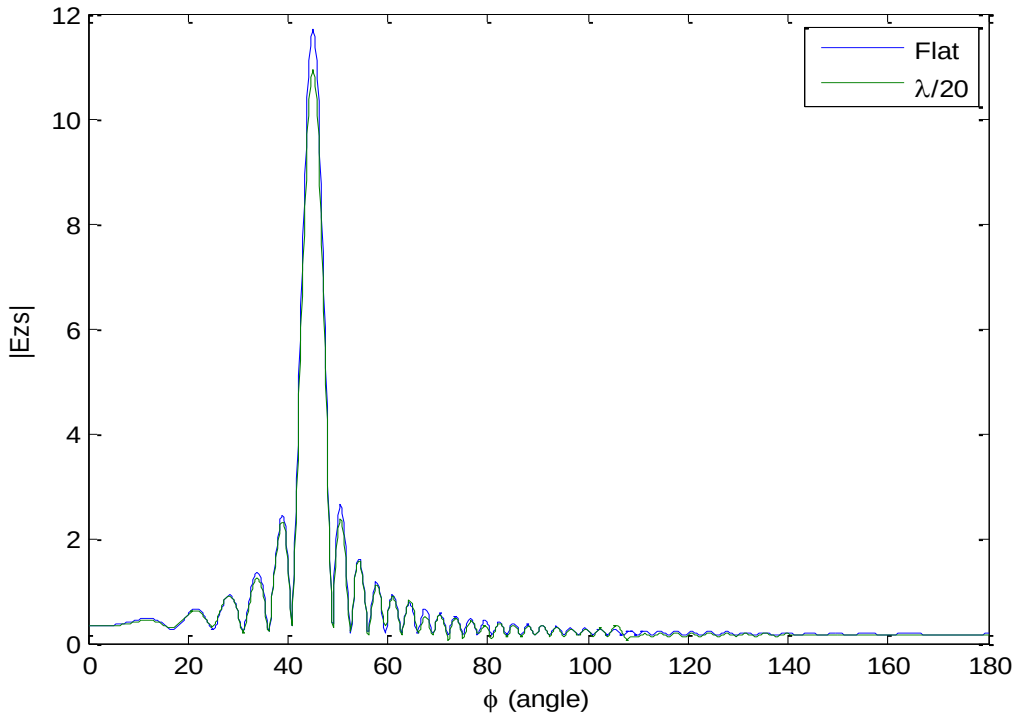

Figure7.15: Scattering of an obliquely incident plane wave by a rough surface

Ex8: Angle of Incidence= 135° , Surface roughness= $\frac{\lambda}{10}$, Mean pattern of 100 simulations

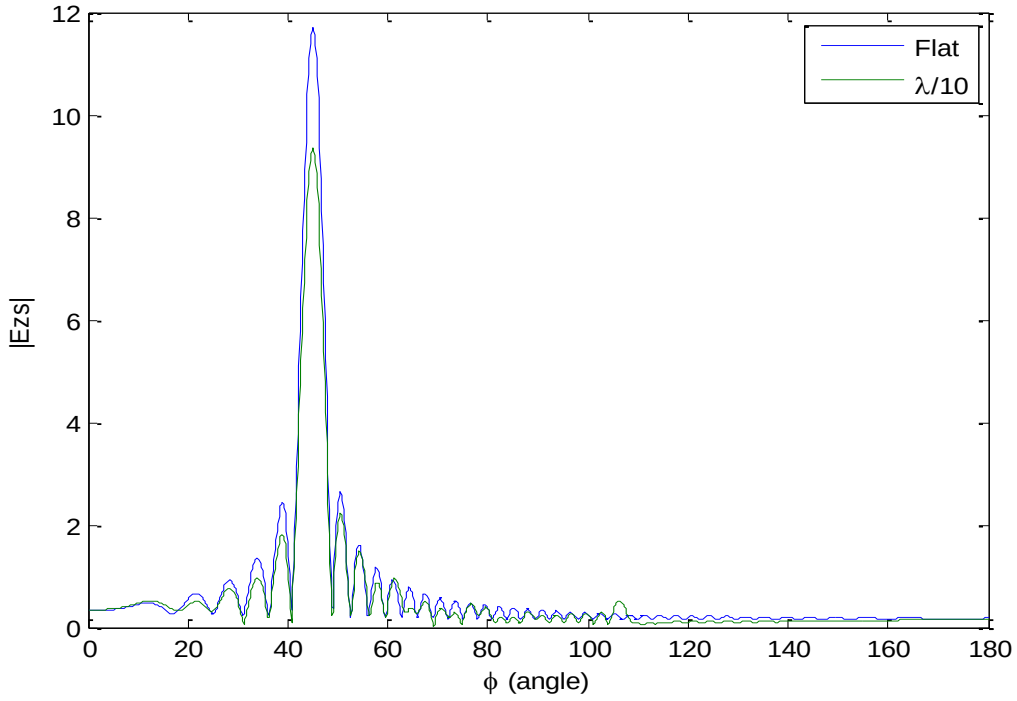

Figure7.16: Scattering of an obliquely incident plane wave by a rough surface

Ex9: Angle of Incidence= 135° , Surface roughness= $\frac{\lambda}{5}$, Mean pattern of 100 simulations

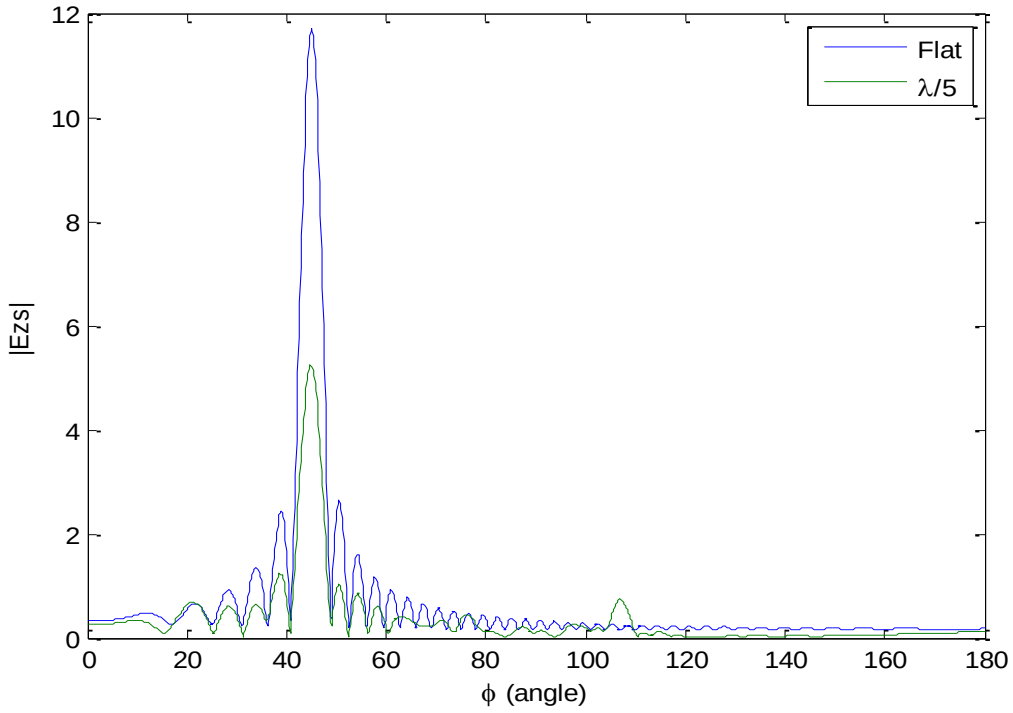

Figure7.17: Scattering of an obliquely incident plane wave by a rough surface

Ex10: Angle of Incidence= 135° , Surface roughness= $\frac{\lambda}{4}$, Mean pattern of 100 simulations

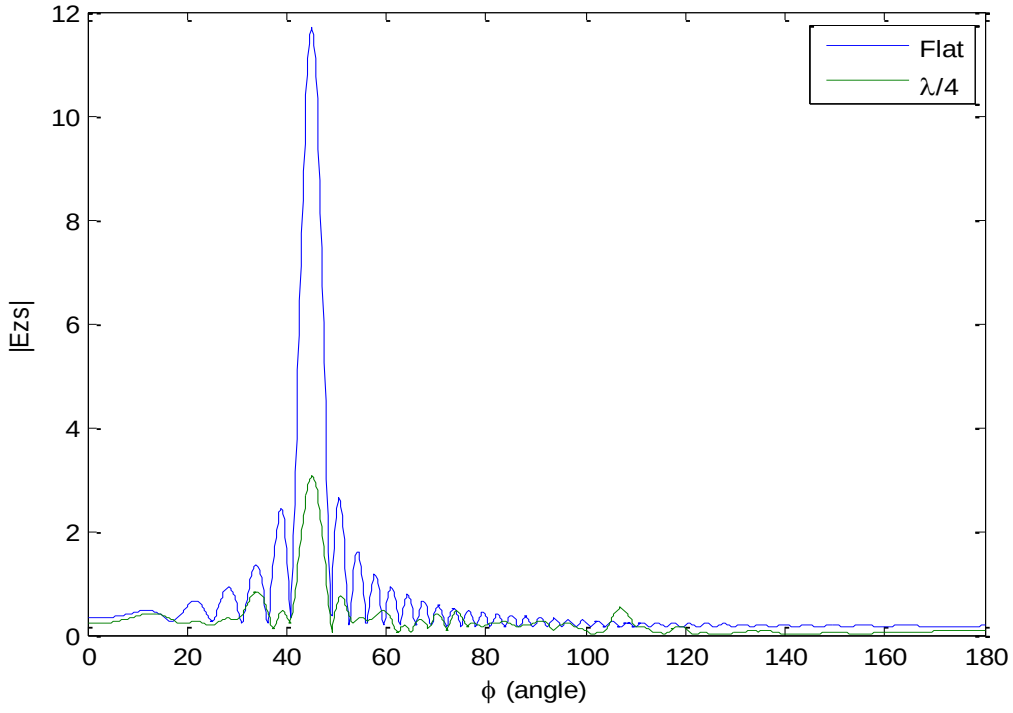

Figure7.18: Scattering of an obliquely incident plane wave by a rough surface

Ex11: Angle of Incidence= 135° , Surface roughness= $\frac{\lambda}{3}$, Mean pattern of 100 simulations

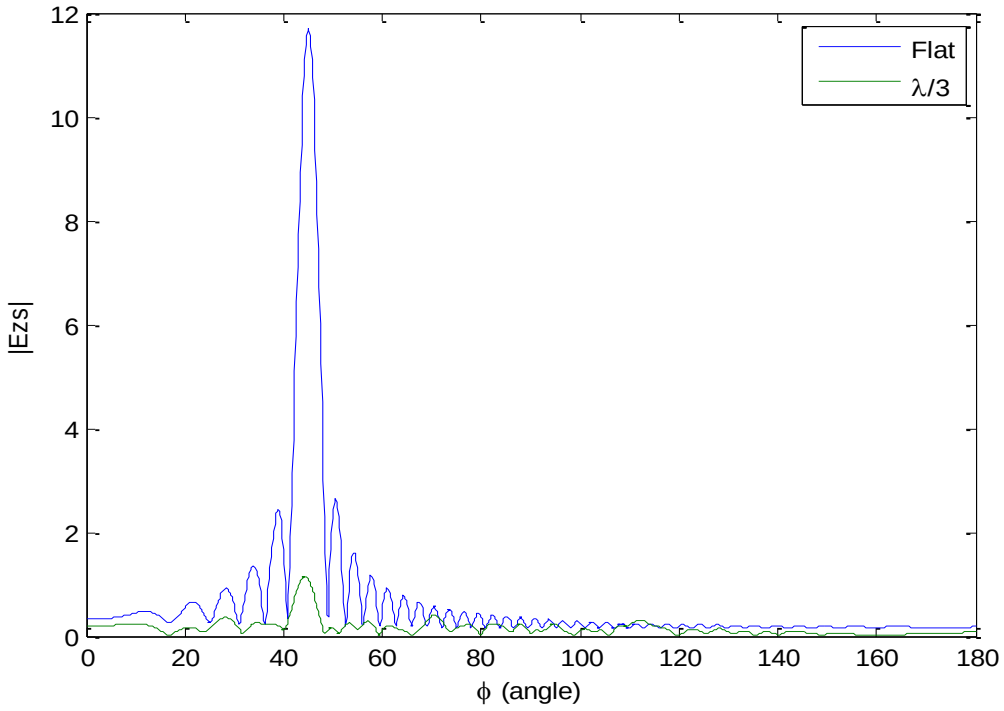

Figure7.19: Scattering of an obliquely incident plane wave by a rough surface.

Ex12: Angle of Incidence= 135° , Surface roughness= $\frac{\lambda}{2}$, Mean pattern of 100 simulations

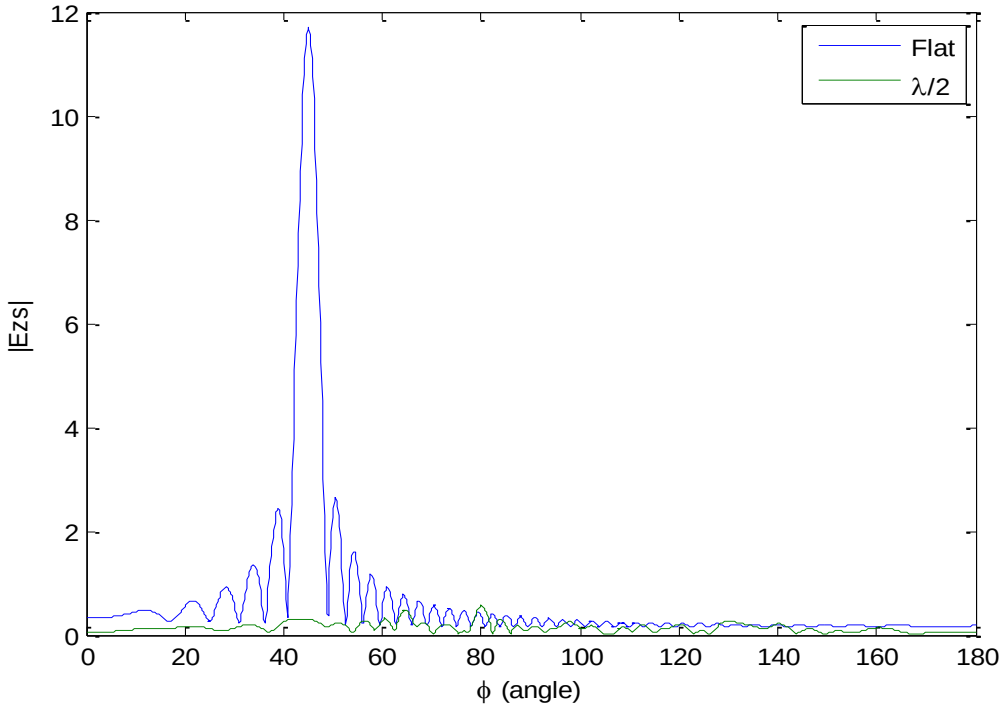

Figure7.20: Scattering of an obliquely incident plane wave by a rough surface.

Ex13: Angle of Incidence ≅ 175°, Surface roughness= $\frac{\lambda}{20}$, Mean pattern of 100 simulations

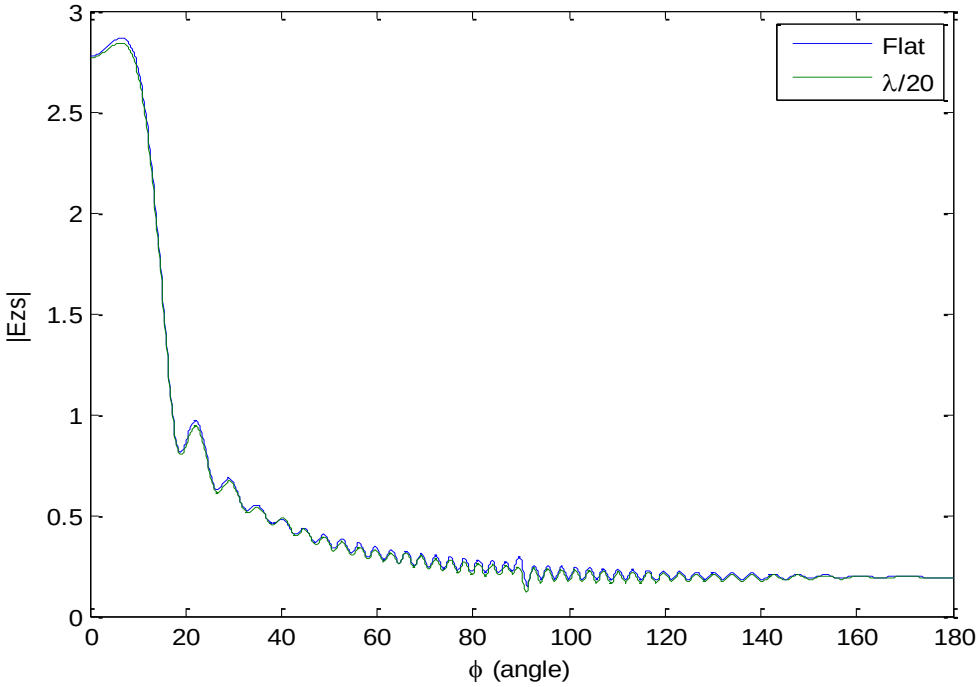

Figure7.21: Scattering of a plane wave at a grazing angle by a rough surface.

Ex14: Angle of Incidence ≅ 175°, Surface roughness= $\frac{\lambda}{10}$, Mean pattern of 100 simulations

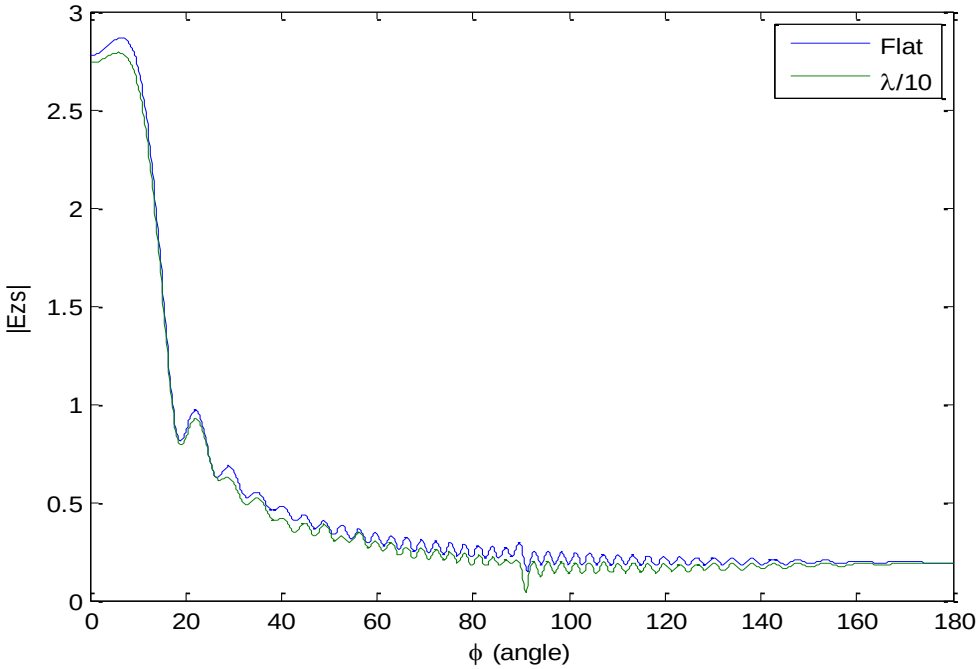

Figure7.22: Scattering of a plane wave at a grazing angle by a rough surface.

Ex15: Angle of Incidence ≅ 175°, Surface roughness= $\frac{\lambda}{5}$, Mean pattern of 100 simulations

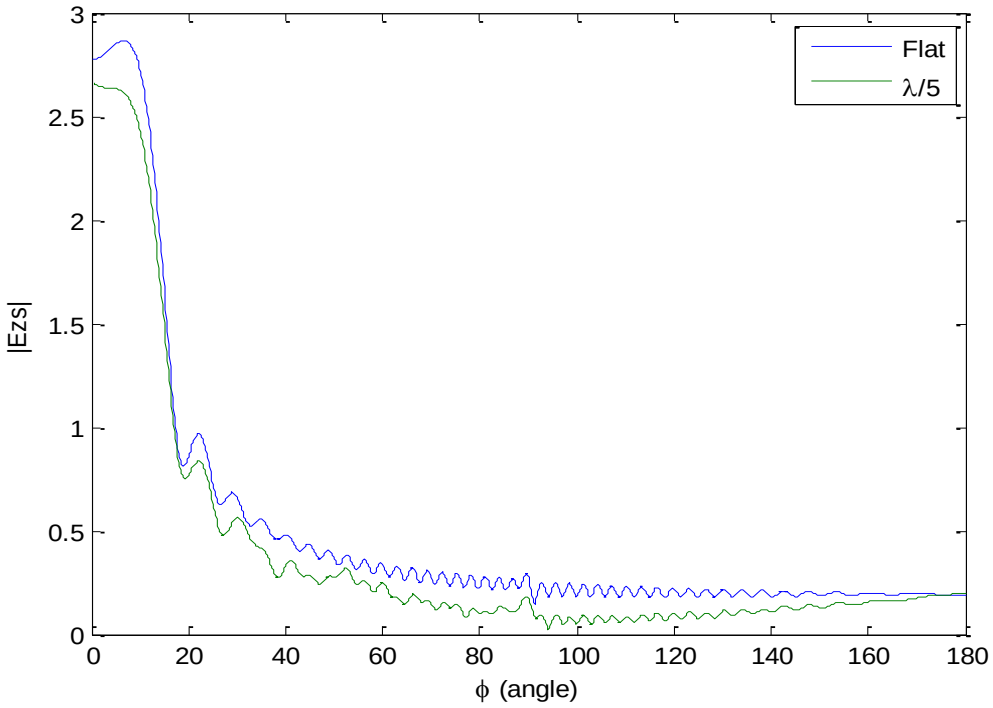

Figure7.23: Scattering of a plane wave at a grazing angle by a rough surface.

Ex16: Angle of Incidence ≅ 175°, Surface roughness= $\frac{\lambda}{4}$, Mean pattern of 100 simulations

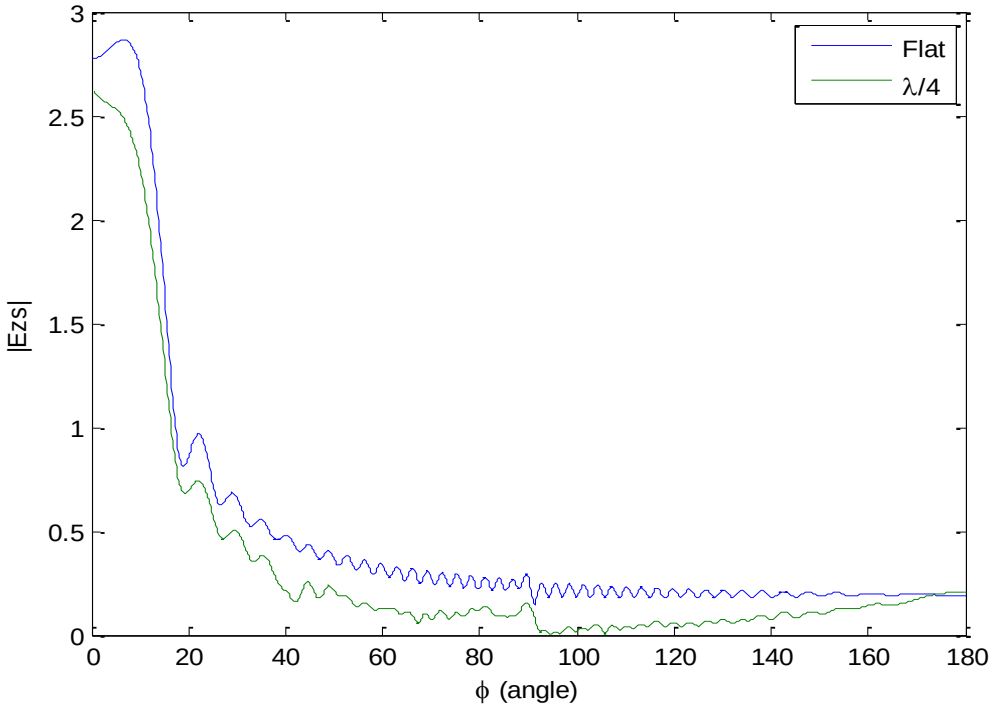

Figure7.24: Scattering of a plane wave at a grazing angle by a rough surface.

Ex17: Angle of Incidence ≅ 175°, Surface roughness= $\frac{\lambda}{3}$, Mean pattern of 100 simulations

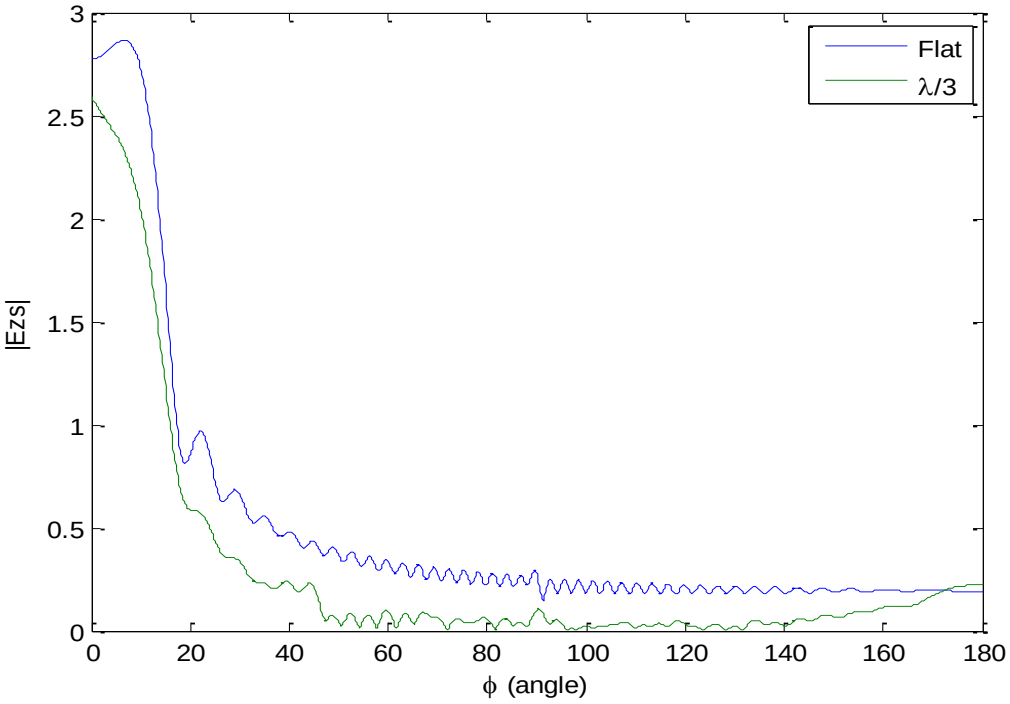

Figure7.25: Scattering of a plane wave at a grazing angle by a rough surface.

Ex18: Angle of Incidence ≅ 175°, Surface roughness= $\frac{\lambda}{2}$, Mean pattern of 100 simulations

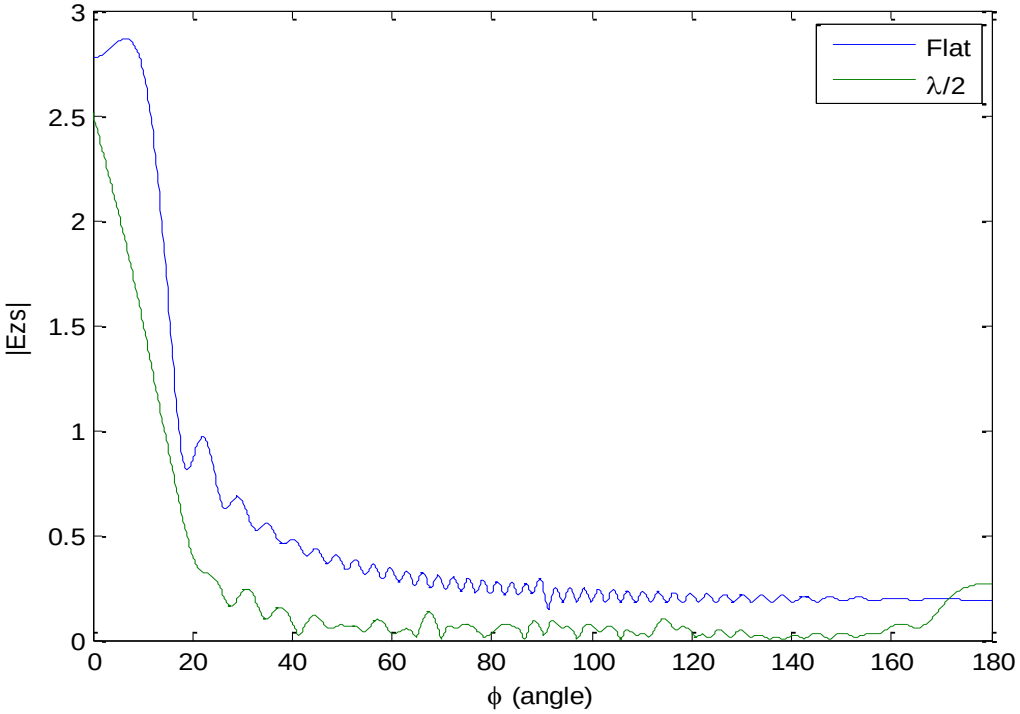

Figure7.26: Scattering of a plane wave at a grazing angle by a rough surface.

7.1 Relation of the peak power of the scattered field patterns with surface roughness

The peak amplitude of the scattered field decreases along the direction of reflection as the surface roughness increases. Our purpose is to determine the relation between the peak scattered field amplitude decay and the surface roughness. In the literature, there are many different formulas relating the amount of decay to the surface roughness, however none of them is perfectly accurate and some of them proved to be accurate only for some certain roughness levels and incidence angles. The most famous relation of power decay with surface roughness is derived by Ament, as,

$$\rho_s = \exp\left[-8\left(\frac{\pi\sigma_h\, cos(\phi_i)}{\lambda}\right)^2\right] \quad , \quad Ament's\ formula$$

However, Boithias later claimed that the relation is also depending on the modified bessel function of order zero, and modified the formula as

$$\rho_s = \exp\left[-8\left(\frac{\pi\sigma_h\, cos(\phi_i)}{\lambda}\right)^2\right] I_0\left[8\left(\frac{\pi\sigma_h\, cos(\phi_i)}{\lambda}\right)^2\right] \quad , \quad Boithias'\ formula$$

It should be noted that when the bessel function argument is small, Boithias' Formula is equal to Ament's Formula. The factor σ_h is the roughness standard deviation of a surface.

We will now calculate and see which of the formulas is more accurate by measuring the peak scattered field amplitudes with respect to different surface roughness levels. In addition, we will also calculate the correlation coefficient (cor.coef) between the scattered field pattern of a flat surface and the scattered field patterns of rough surfaces with different roughness levels to check the similarity of the patterns.

$$\sigma_X = Standard\ deviation\ of\ the\ random\ variable\ X$$

$$\sigma_Y = Standard\ deviation\ of\ the\ random\ variable\ Y$$

$$\mu_X = Mean\ of\ the\ random\ variable\ X$$

$$\mu_Y = Mean\ of\ the\ random\ variable\ Y$$

$$E\,[.] = \ Expectation\ operator$$

$$cov(X,Y) = Covariance\ \ operator$$

$$\rho_{x,y} = \frac{E[(X-\mu_X)(Y-\mu_Y)]}{(\sigma_X\sigma_Y)} = \frac{cov(X,Y)}{(\sigma_X\sigma_Y)} \quad , \quad Correlation\ coefficient\ of\ X\ and\ Y.$$

$$\rho_{(\frac{\lambda}{N},flat)} = \ Cor.coef\ of\ the\ scattered\ field\ patterns\ of\ rough\ and\ flat\ surfaces$$

Table 7.1:List of scattered field peak values and magnitude of the cor.coef w.r.t angle.

Incidence Angle	Surface Roughness	Scattered field Peak Amplitude	$\rho_{(\frac{\lambda}{N},flat)}$
$\approx 180^{\circ}$	$\lambda/40$	2.8563	1
$\approx 180^{\circ}$	$\lambda/20$	2.8321	0.9998
$\approx 180^{\circ}$	$\lambda/10$	2.7956	0.9993
$\approx 180^{\circ}$	$\lambda/8$	2.7760	0.9986
$\approx 180^{\circ}$	$\lambda/5$	2.7308	0.9932
$\approx 180^{\circ}$	$\lambda/4$	2.7069	0.9874
$\approx 180^{\circ}$	$\lambda/3$	2.6944	0.9751
$\approx 180^{\circ}$	$\lambda/2$	2.7161	0.9477
$\approx 180^{\circ}$	λ	3.2480	0.8148
165°	$\lambda/40$	4.8616	1
165°	$\lambda/20$	4.8073	0.9999
165°	$\lambda/10$	4.6435	0.9984
165°	$\lambda/8$	4.5258	0.9970
165°	$\lambda/5$	4.1064	0.9931
165°	$\lambda/4$	3.6886	0.9895
165°	$\lambda/3$	2.9747	0.9734
165°	$\lambda/2$	2.0006	0.9286
165°	λ	0.4717	0.4647
150°	$\lambda/40$	8.6796	0.9999
150°	$\lambda/20$	8.4580	0.9996
150°	$\lambda/10$	7.8537	0.9982
150°	$\lambda/8$	7.3928	0.9974
150°	$\lambda/5$	5.6561	0.9873
150°	$\lambda/4$	4.3337	0.9714
150°	$\lambda/3$	2.9879	0.9429
150°	$\lambda/2$	0.8482	0.6853
150°	λ	0.5210	0.2399
135°	$\lambda/40$	11.5215	0.9998
135°	$\lambda/20$	10.9627	0.9993
135°	$\lambda/10$	9.4086	0.9953
135°	$\lambda/8$	8.5308	0.9948
135°	$\lambda/5$	4.8232	0.9662
135°	$\lambda/4$	3.4000	0.9430
135°	$\lambda/3$	1.2399	0.7574
135°	$\lambda/2$	0.4556	0.1459
135°	λ	0.3999	0.1525
120°	$\lambda/40$	13.3635	0.9997
120°	$\lambda/20$	12.2927	0.9990
120°	$\lambda/10$	9.7435	0.9940
120°	$\lambda/8$	7.9050	0.9863
120°	$\lambda/5$	3.5485	0.9206
120°	$\lambda/4$	1.3707	0.7063
120°	$\lambda/3$	0.4537	0.3401
120°	$\lambda/2$	0.3767	0.1481
120°	λ	0.6735	0.2035

105°	$\lambda/40$	14.3587	0.9997
105°	$\lambda/20$	12.9495	0.9984
105°	$\lambda/10$	9.3382	0.9921
105°	$\lambda/8$	7.0680	0.9806
105°	$\lambda/5$	2.2844	0.8607
105°	$\lambda/4$	0.9570	0.5119
105°	$\lambda/3$	0.7117	0.0783
105°	$\lambda/2$	0.4327	0.1277
105°	λ	0.6122	0.0460
90°	$\lambda/40$	14.6786	0.9999
90°	$\lambda/20$	13.0730	0.9982
90°	$\lambda/10$	8.9484	0.9921
90°	$\lambda/8$	7.0290	0.9812
90°	$\lambda/5$	2.2409	0.8081
90°	$\lambda/4$	0.7158	0.3398
90°	$\lambda/3$	0.4812	0.1085
90°	$\lambda/2$	0.5383	0.1166
90°	λ	0.7828	0.0754

Table7.1 (continued)

Note that $\rho_{(\frac{\lambda}{N},flat)}$ i.e the correlation coefficient of the scattered field patterns of a rough surface with a roughness standard deviation value of $\frac{\lambda}{N}$ and a flat surface for a given incidence angle is actually a complex value. What we are interested in is it's magnitude value, therefore it's magnitude values are given in Table7.1.

In order to see whether the scattered field peak loss fits to the Ament's Formula or Boithias formula, we should plot the scattered field peak values versus the standard deviation of surface roughness for each incidence angle using Table7.1.

It is also important to see the correlation of a rough surface scattered field pattern with that of a flat surface, given an incidence angle. The correlation coefficient of rough surface scattered field patterns with a flat surface is expected to decrease as surface roughness increases. For each incidence angle, we should calculate and plot the correlation coefficient magnitude of rough surface scattered field patterns with a flat surface, to have a better understanding of the pattern change with respect to surface roughness.

Case 1: Angle of incidence $\cong 180^{\circ}$, *Peak value of the scattered field = L(*λ*)*

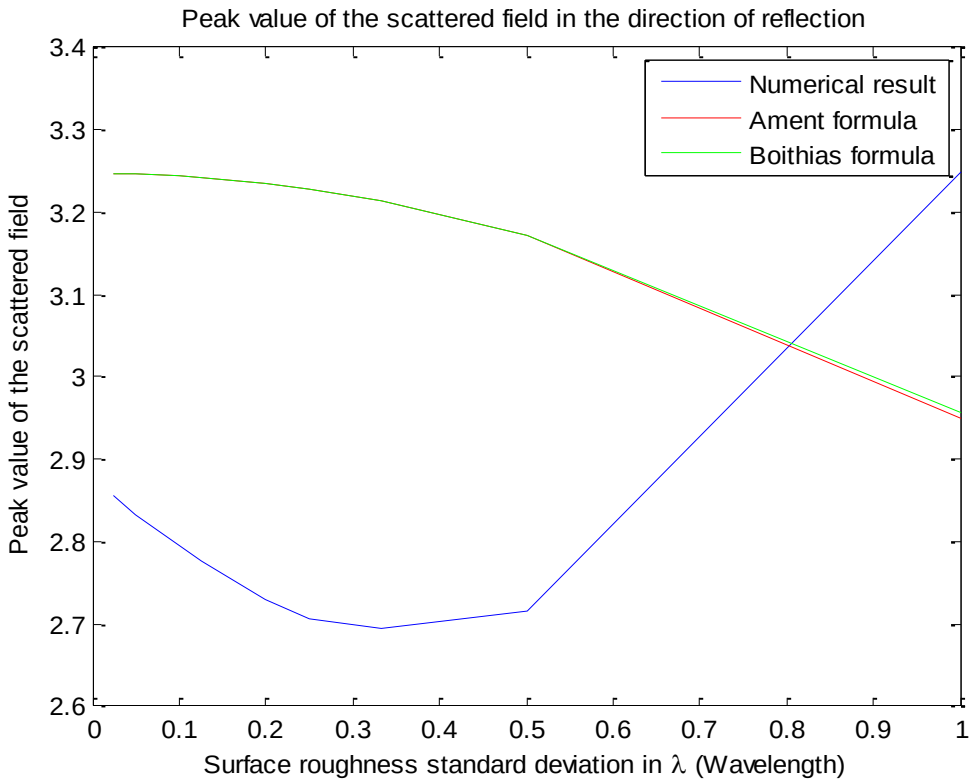

Figure7.27: Peak power decay w.r.t surface roughness

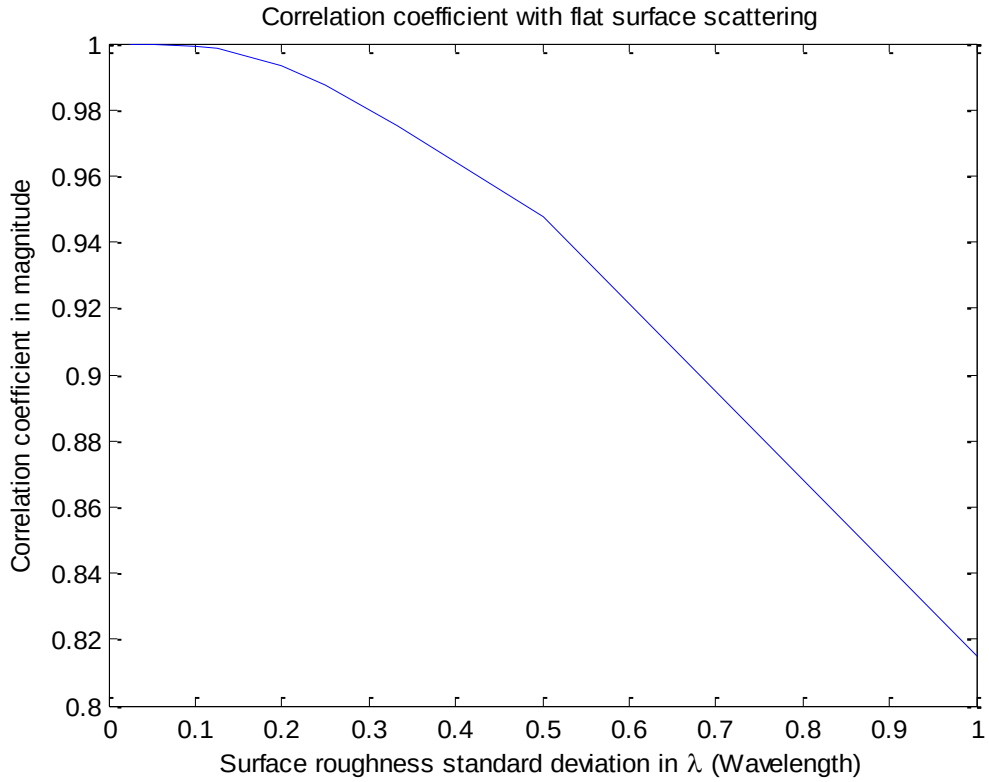

Figure7.28: Correlation coefficient w.r.t surface roughness

Case 2: Angle of incidence $\cong 165^{\circ}$, *Peak value of the scattered field = L(λ)*

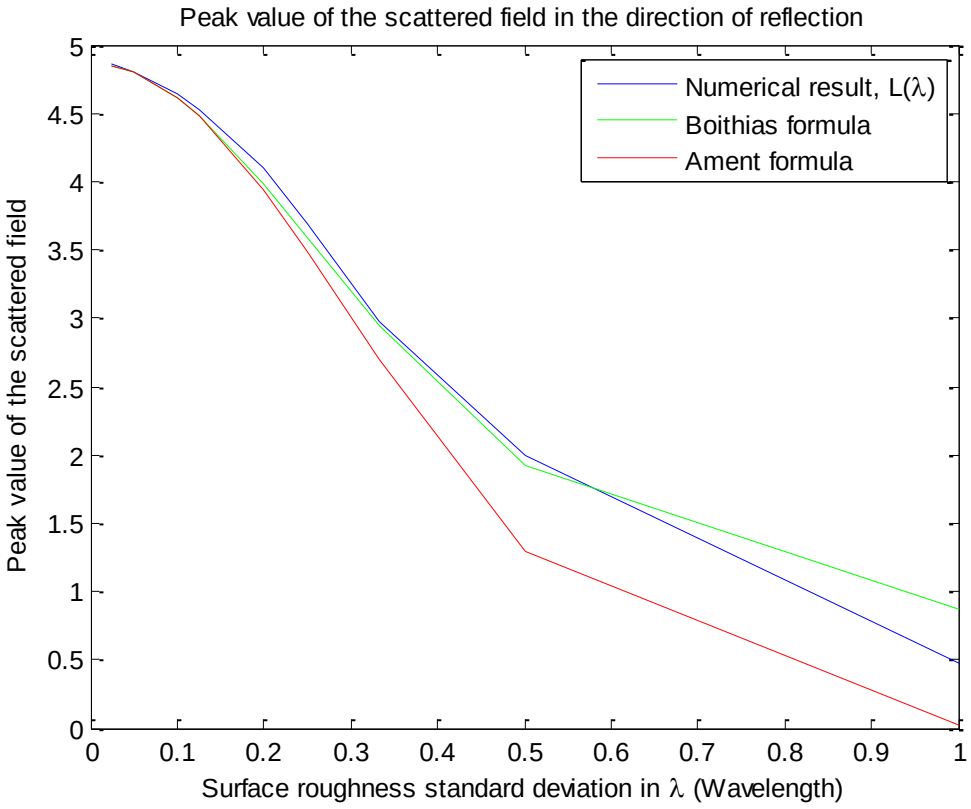

Figure7.29: Peak power decay w.r.t surface roughness

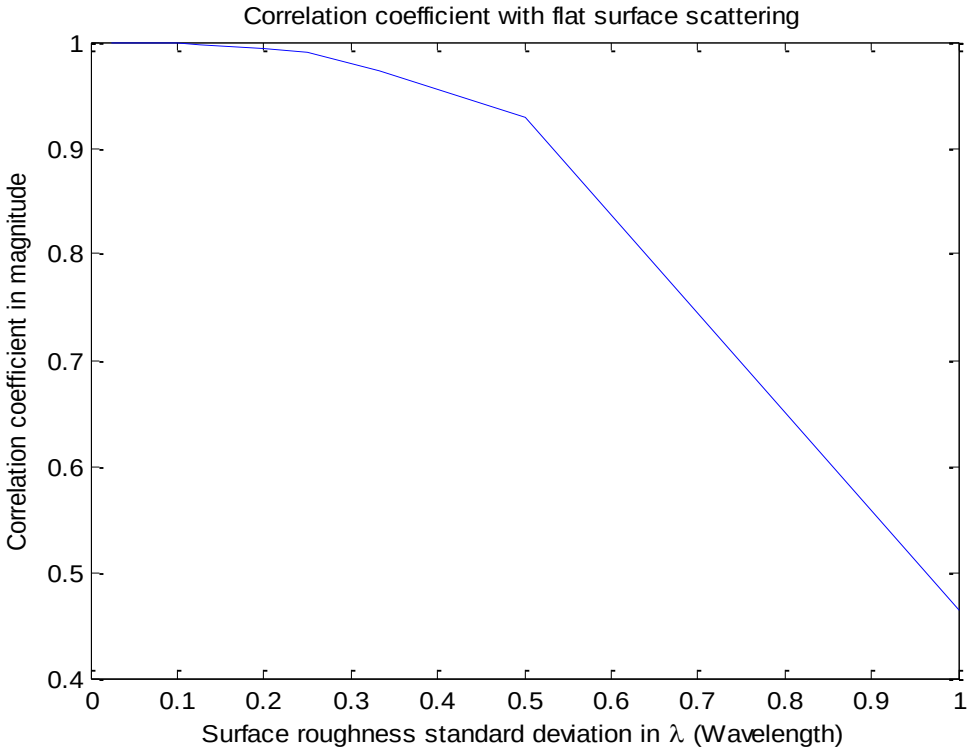

Figure7.30: Correlation coefficient w.r.t surface roughness

Case 3: Angle of incidence $\cong 150^{\circ}$, *Peak value of the scattered field = L(λ)*

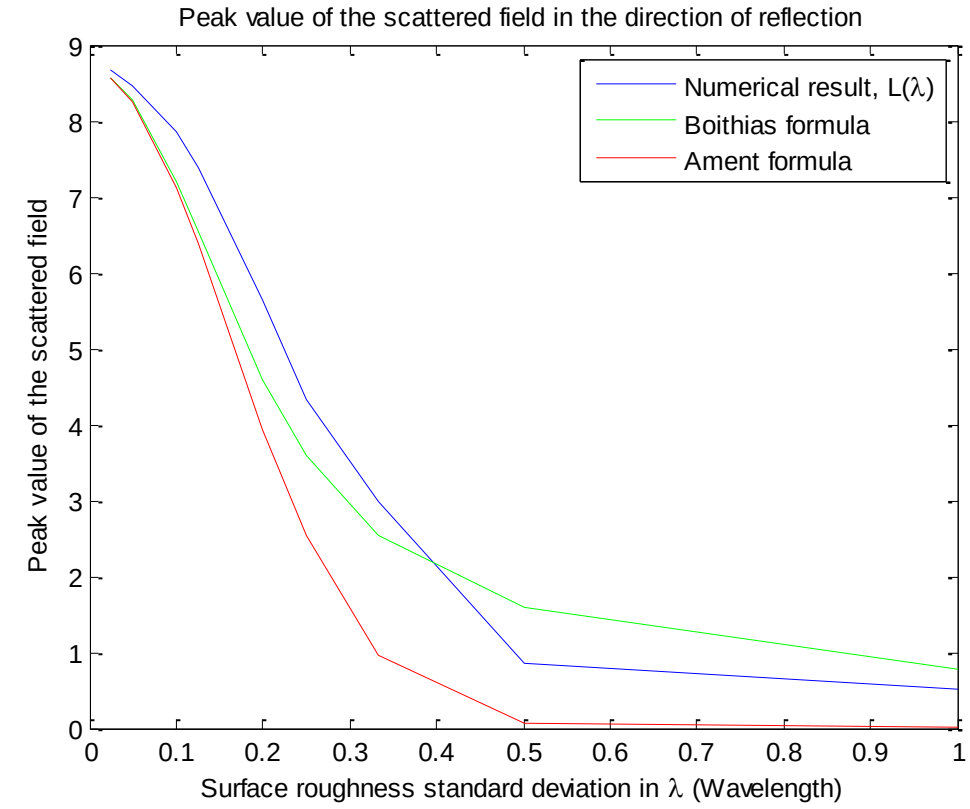

Figure7.31: Peak power decay w.r.t surface roughness

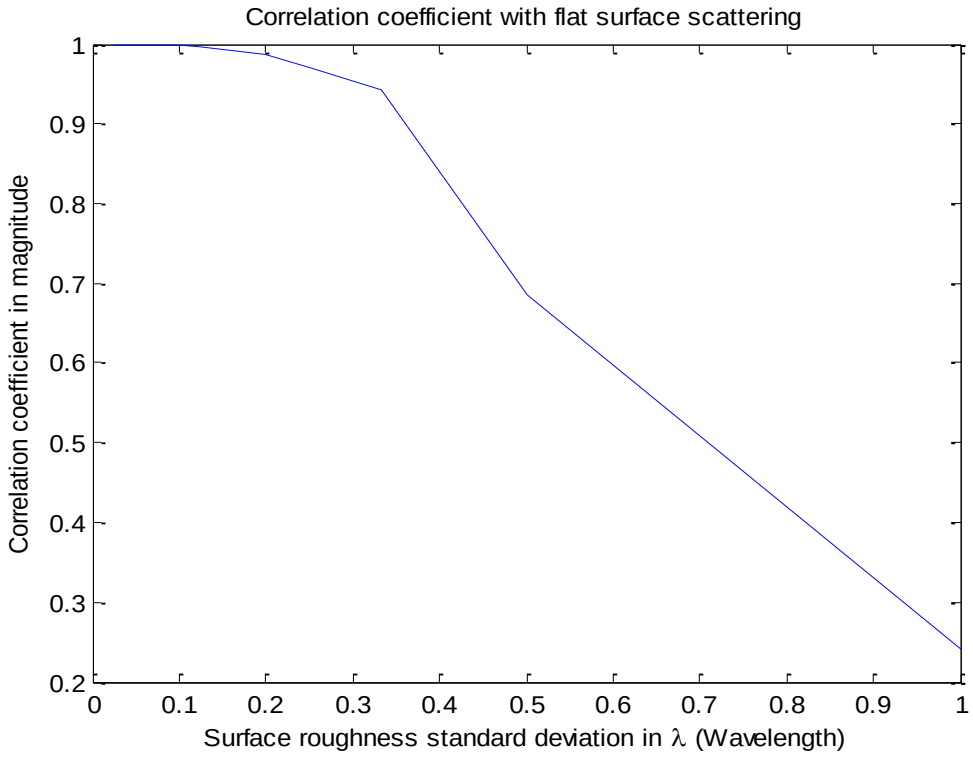

Figure7.32: Correlation coefficient w.r.t surface roughness

Case 4: Angle of incidence $\cong 135^{\circ}$, *Peak value of the scattered field = L(λ)*

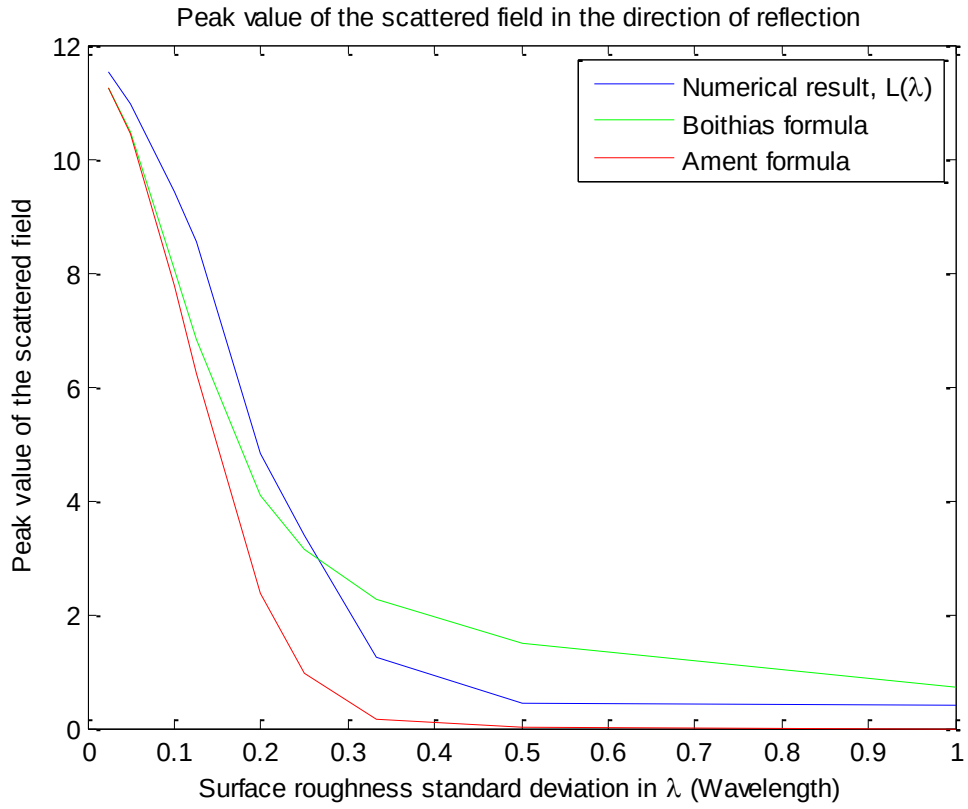

Figure7.33: Peak power decay w.r.t surface roughness

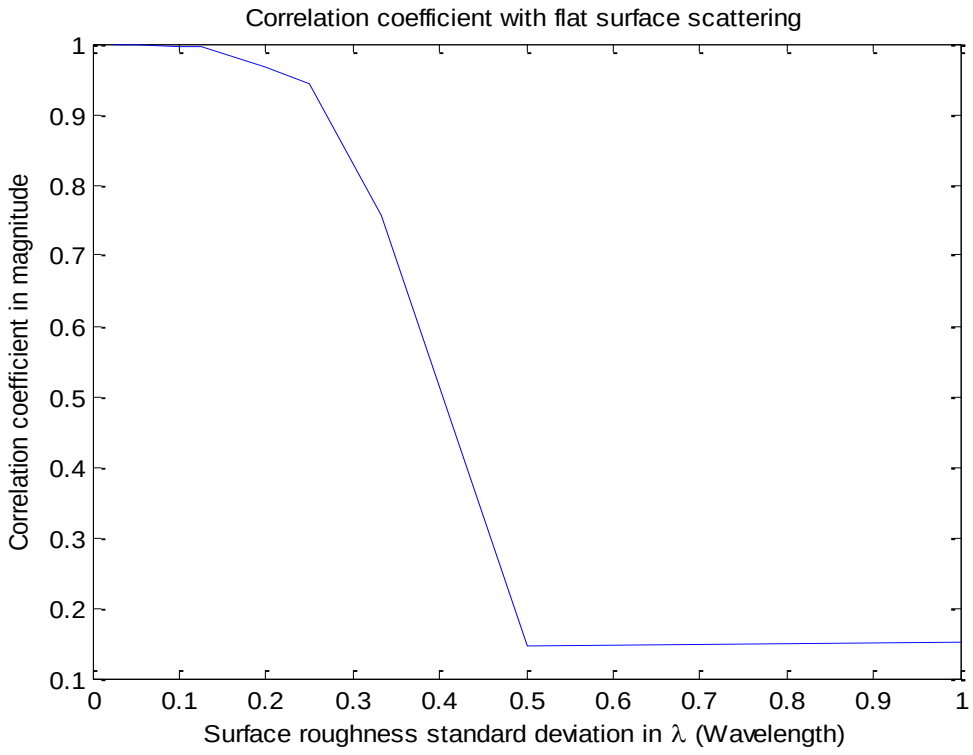

Figure7.34: Correlation coefficient w.r.t surface roughness

Case 5: Angle of incidence $\cong 120^{\circ}$, *Peak value of the scattered field = L(λ)*

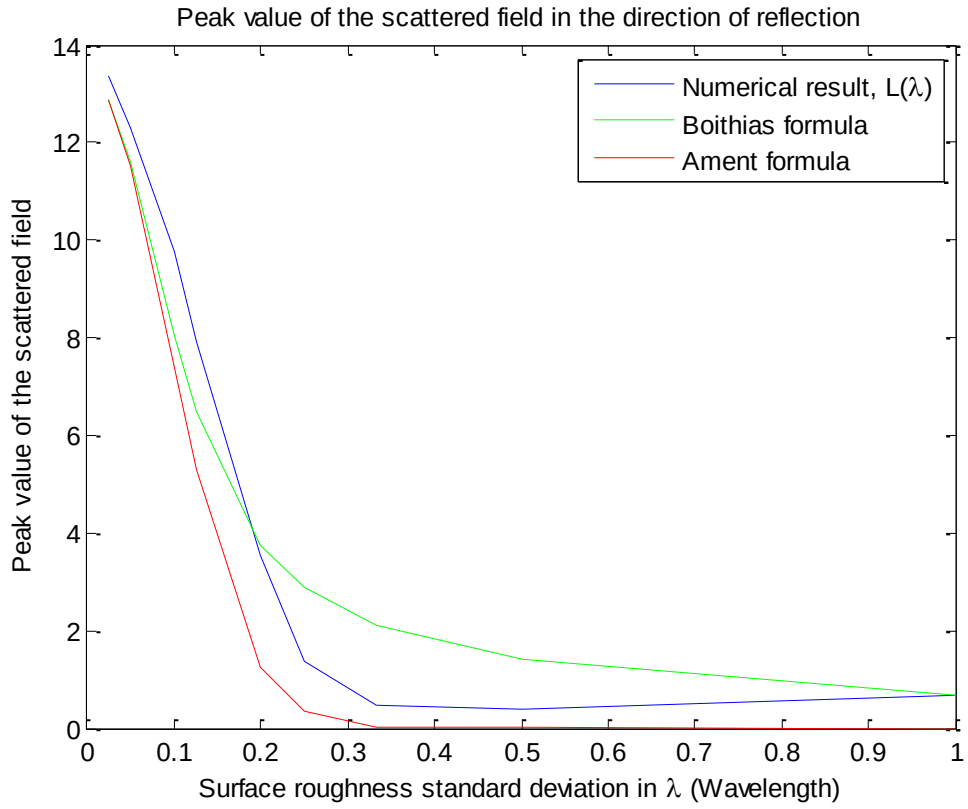

Figure7.35: Peak power decay w.r.t surface roughness

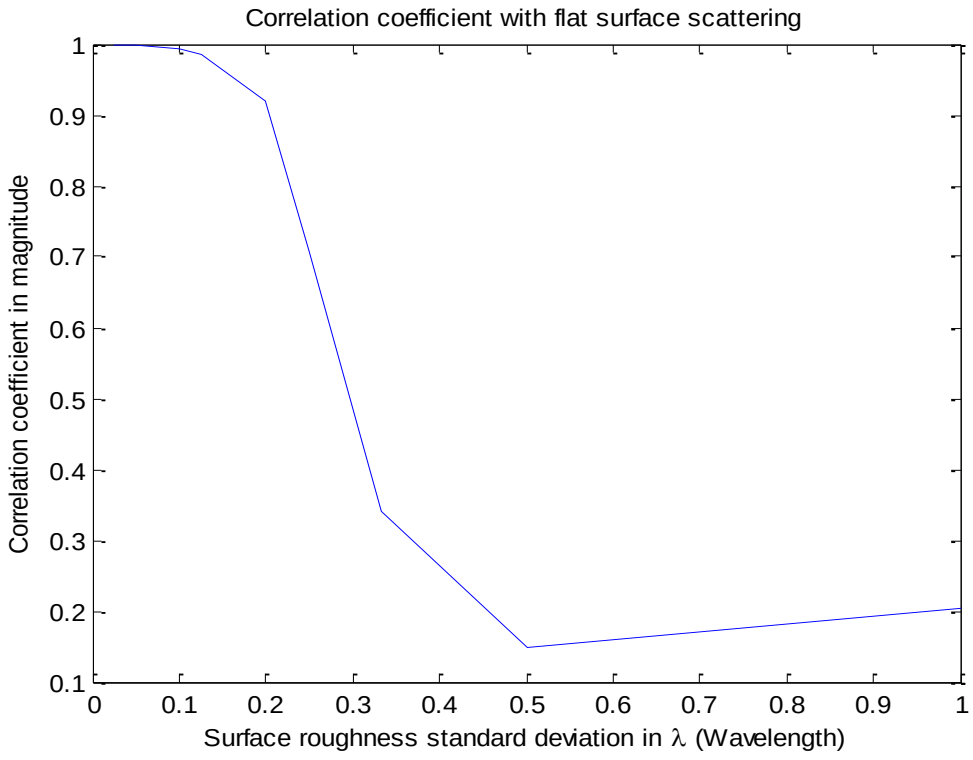

Figure7.36: Correlation coefficient w.r.t surface roughness

Case 6: Angle of incidence $\cong 105^{\circ}$, *Peak value of the scattered field = L(λ)*

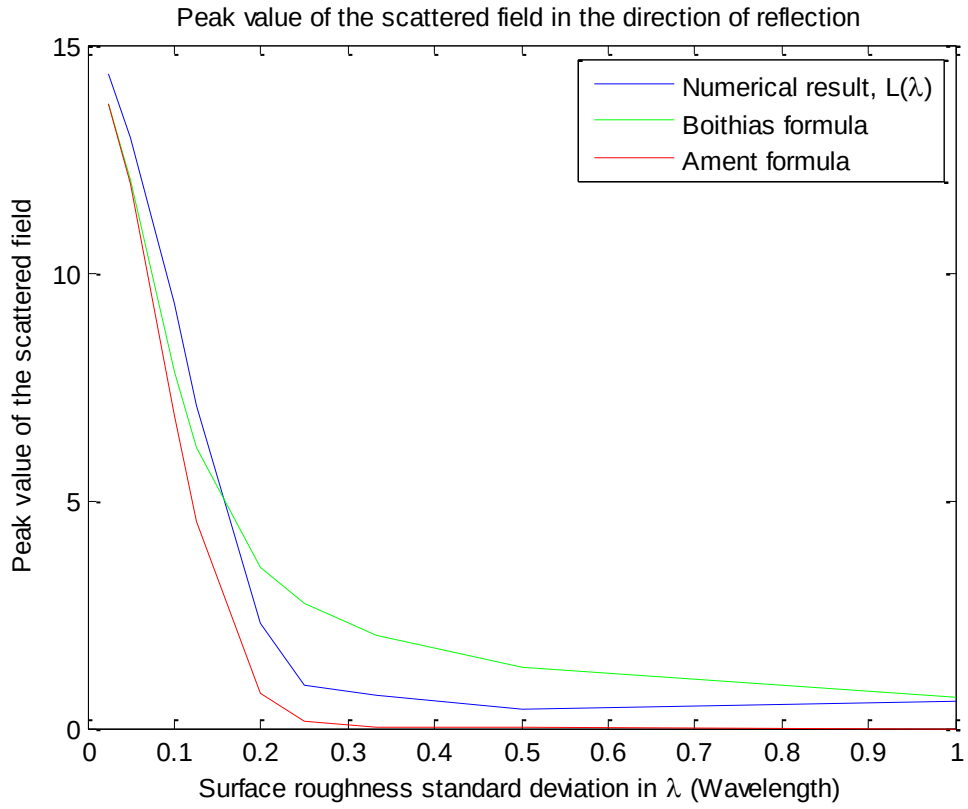

Figure7.37: Peak power decay w.r.t surface roughness

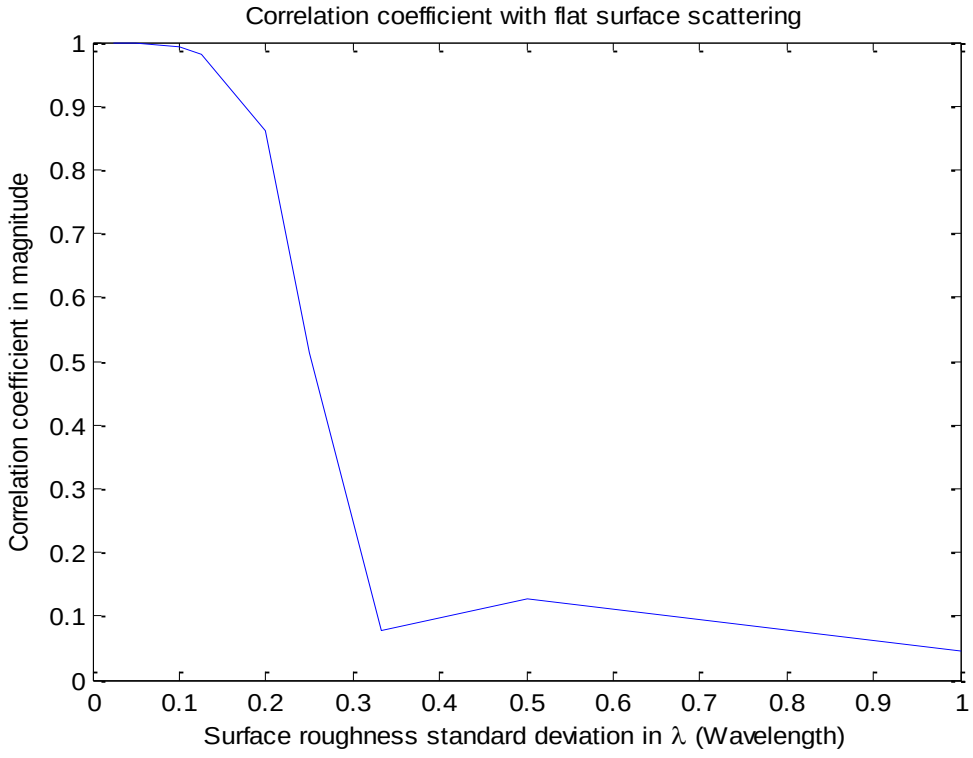

Figure7.38: Correlation coefficient w.r.t surface roughness

Case 7: Angle of incidence $\cong 90^{\circ}$, *Peak value of the scattered field = L(*λ*)*

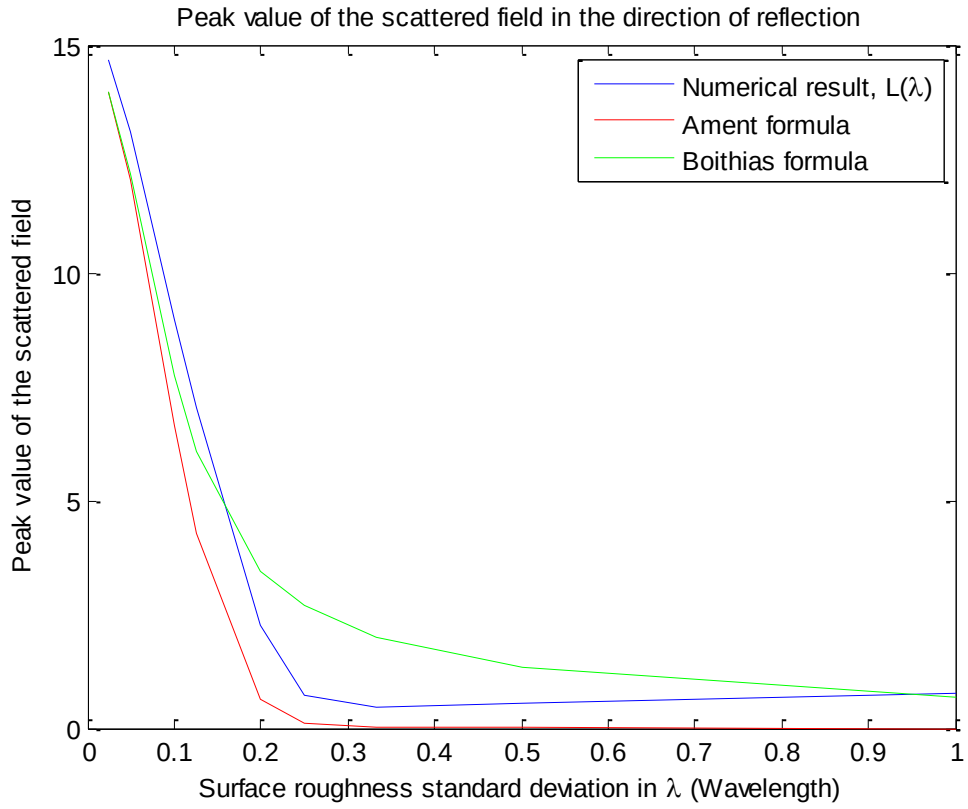

Figure7.39: Peak power decay w.r.t surface roughness

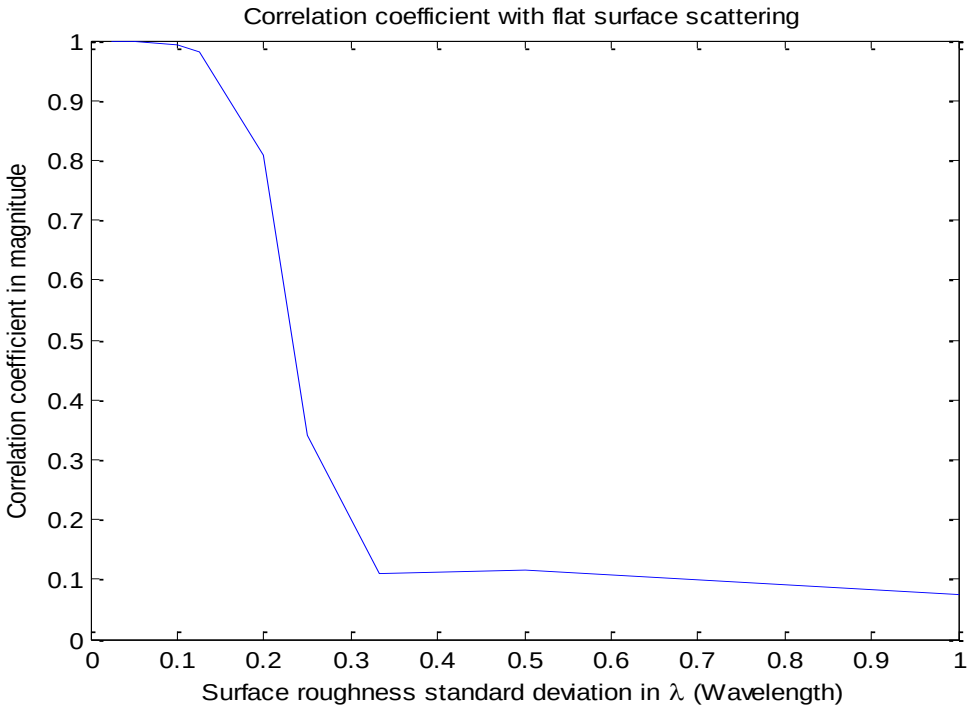

Figure7.40: Correlation coefficient w.r.t surface roughness

All of the investigated patterns show that after a surface roughness of $\frac{\lambda}{2}$, the major lobe of the pattern which is expected to be in the direction of specular reflection, is shifted to another direction and it's amplitude is very sharply reduced. Though this is usually not the case for grazing angles of incidence, an incident field at the grazing angle will produce a scattered field whose pattern is not much affected by the roughness of the surface. If the angle of incidence is more than about 15°, and if the roughness standard deviation is more than λ, the major beam of the scattered field in the specular reflection direction which is 165°, will be shifted to another direction and it's amplitude will be sharply reduced such that it cannot be distinguished from the minor lobes of the pattern, therefore analyzing a rough surface scattering problem for surfaces with roughness standard deviation more than λ, only has meaning if the incidence angle is small enough to be considered as a grazing angle.

As the surface roughness increases, the correlation coefficient of the flat and rough surface scattered field patterns decreases as expected. Some small amount of random increase may occur due to randomness of the surface only after the surface becomes very rough.

For incident fields at a grazing angle, the surface roughness does not affect the scattered field pattern very much, however this is valid up to some roughness level, let us further investigate, up to which roughness level and incidence angle, the scattered field pattern is not distorted for grazing incidence angles. This time we increase the surface roughness standard deviation value up to 5λ to have a better understanding of the effect of surface roughness on pattern distortion of grazingly incident fields. Calculating the correlation coefficient between flat and rough surface patterns is an effective way of measuring distortion and it's graph is indicated for each case.

Case 8: Angle of incidence $\cong 179.5^{\circ}$, *Peak value of the scattered field = L(*λ*)*

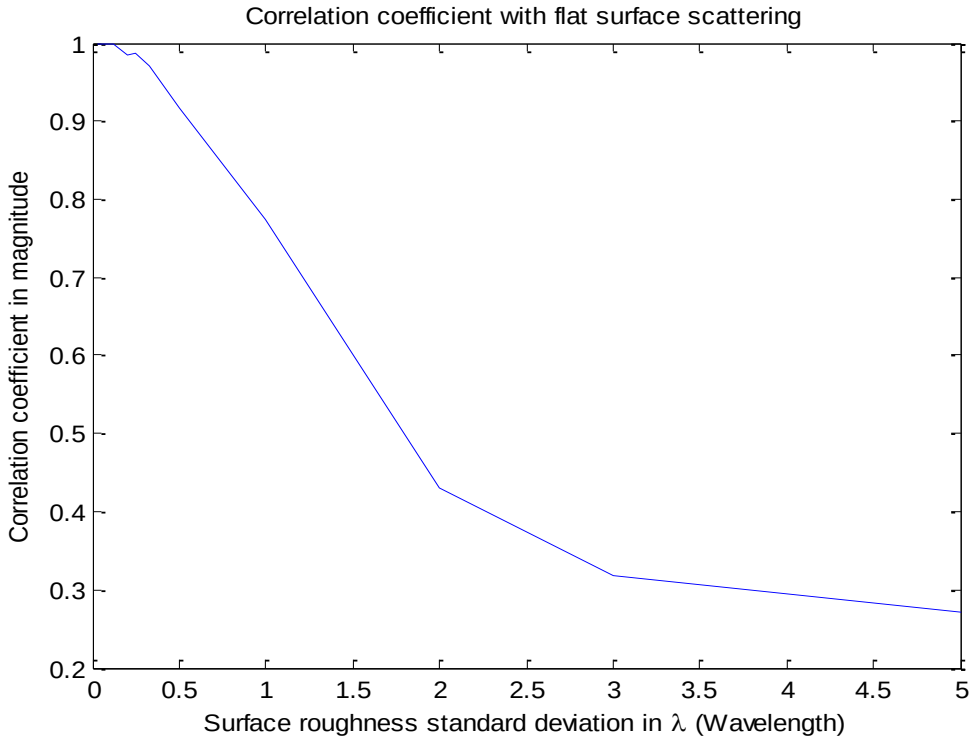

Figure7.41: Correlation coefficient w.r.t surface roughness (grazing angle incidence)

Case 9: Angle of incidence $\cong 172^{\circ}$, *Peak value of the scattered field = L(*λ*)*

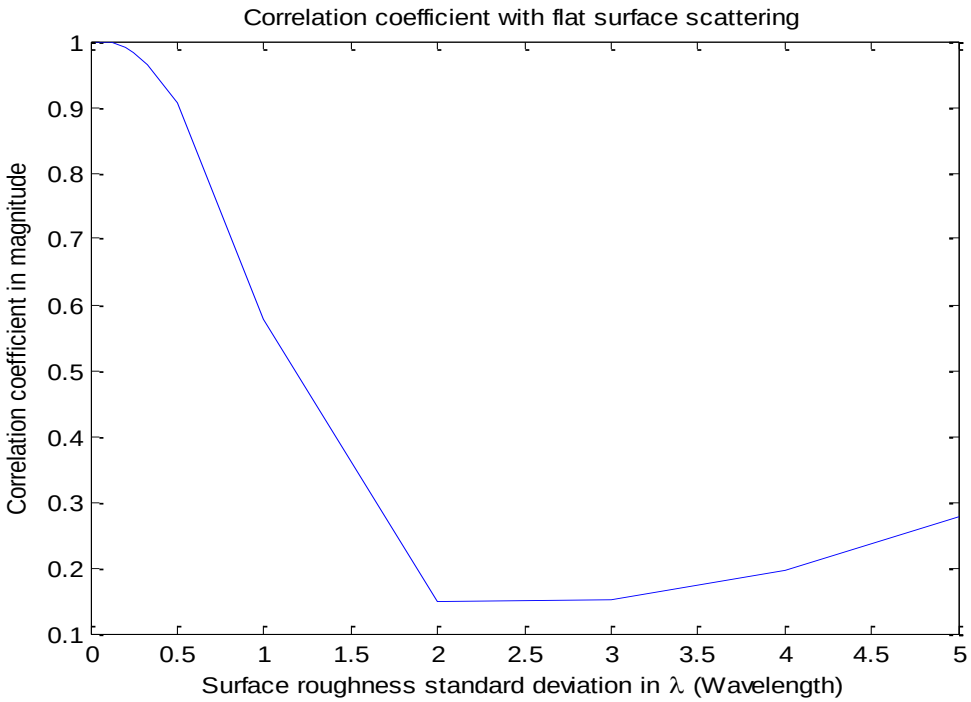

Figure7.42: Correlation coefficient w.r.t surface roughness (grazing angle incidence)

Case 10: Angle of incidence $\cong 165^{\circ}$, *Peak value of the scattered field = L(*λ*)*

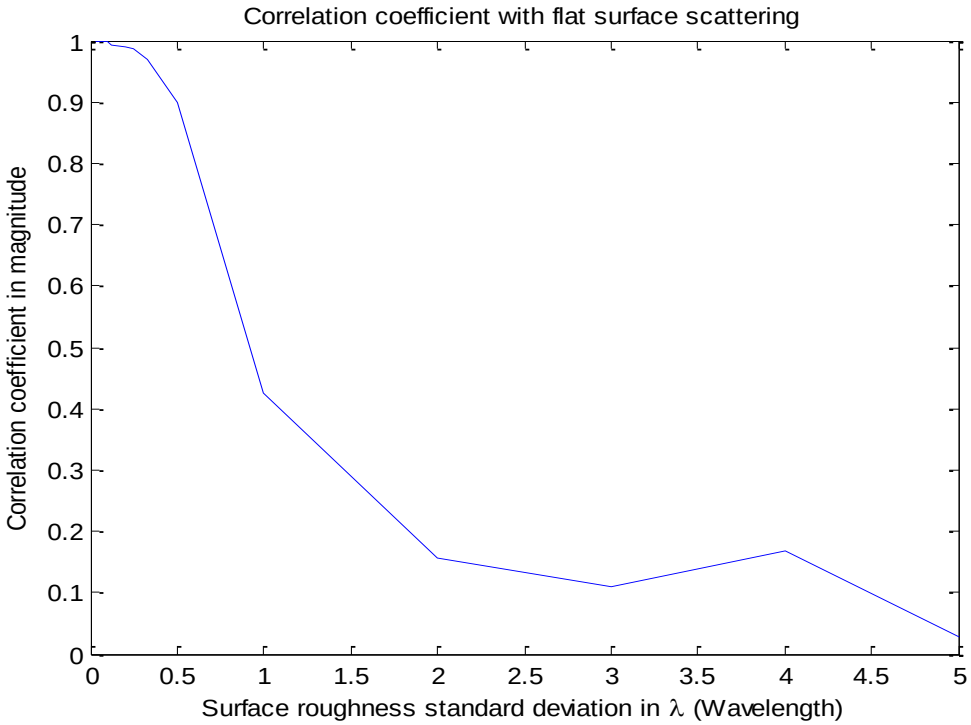

Figure7.43: Correlation coefficient w.r.t surface roughness (grazing angle incidence)

The Boithias' formula seems a little more accurate than Ament's formula for

$180^{\circ} \leq \phi_i \leq 135^{\circ}$, but the Ament's formula is a little more accurate than the Boithias' formula for $135^{\circ} \leq \phi_i \leq 90^{\circ}$, however the two formulas yield different amount of errors for different angles of incidence, so there is no definite answer of which of them should be used instead of the other. Usually both formulas yield an accurate result, so either of them can be used. As the roughness standard deviation value approaches and goes beyond λ , the numerical results converges to the Boithias' formula, however, beyond λ the rough surface problem is not worth to investigate as the pattern is almost completely distorted and the major lobe is lost, this can be verified by checking the correlation coefficient with the pattern of a flat surface. Therefore convergence of the numerical results to the Boithias' formula does not have much importance for us.

Summary:

- As the surface roughness increases the peak value of the pattern's major lobe is reduced.

- A rough surface scattered field pattern is usually completely distorted after a roughness standard deviation value of λ. And will not bear much information.

-Usually both the Ament's formula and the Boithias' formula can be used for approximate analytical results, their accuracy depends on the angle of incidence and the roughness of the surface and either of them may yield greater error than the other depending on the surface roughness and the angle of incidence.

- Correlation coefficients of rough surface scattered field patterns with that of a flat surface scattered field pattern, both at a specific incidence angle, can be calculated to check the distortion in the rough surface scattered field pattern. Usually a correlation coefficient below 0.3 means that the pattern is completely distorted, and a correlation coefficient value below 0.45 means that the pattern is seriously distorted. Above a correlation coefficient value of 0.7 there is not a serious distortion in the pattern.

-When the incident wave comes at a grazing angle, the scattered field pattern will not be significantly affected from the roughness of the surface, unless the change in surface roughness is large.

CHAPTER 8

CONCLUSION

The roughness of a given surface has a significant effect on the far field pattern of the scattered field. As the surface roughness increases, the scattered field pattern becomes more distorted. For small surface roughness values, the shape of the scattered field pattern is not affected considerably but the peak value of the pattern experiences a considerable decrease. For higher levels of surface roughness, the scattered field pattern is almost completely distorted and the actual major lobe of the pattern that exists for the flat surface scattering case is totally diminished. It is important to determine the critical roughness levels for each incidence angle that causes complete distortion in the pattern. We have done this job in the last chapter and tabulated the results for different roughness levels and for each incidence angle. This table can be expanded with the expansion of surface roughness values and incidence angle values into a much greater set of values. But the included results in this thesis is enough to give a valuable insight to the reader about the topic.

All of the results obtained in chapter 7 are the mean results of 100 different measurements. Large number of measurements is necessary to provide certainty since the rough surfaces are all randomly generated. The certainty obtained in the results is a direct consequence of the central limit theorem. We should find the mean pattern of many different scattered field patterns in the far field to increase accuracy in measurements.

As the surface roughness increases, the peak value of the scattered field pattern decreases. This relation was already proven and analyzed by Ament and Boithias, but their useful mathematical formulations about this relation were not exact and can be erroneous for some angles of incidence. In this thesis we have checked the accuracy of these formulations and we have stated our own computed values. Our results are compared with these two formulas.

Based on the results and figures given in chapter 7, it is not clear to say whether Ament's formula or Boithias' formula is more accurate. Both of them become more accurate with respect to each other for different angles of incidence and for different surface roughness values. In general, both of the formulas yield accurate results for lower surface roughness values. However when the standard deviation value of the surface roughness becomes comparable to the wavelength, the accuracy of these two formulas may decrease and their accuracy can be examined with the numerical results given in this thesis. There is no point in comparing the two formulas for surface roughness standard deviation values of more than a wavelength (λ) as the scattered field pattern becomes completely distorted for such roughness levels and bears almost no information.

For the grazing angle incidence case, the scattered field pattern is not much affected by the roughness of the surface up to a standard deviation value of surface roughness of λ .

Above this level of roughness however, the scattered field pattern starts to distort and for roughness standard deviation values of 2λ or 3λ, the pattern becomes almost completely

distorted. For the grazing angle incidence case, the distortion rate is the smallest. The distortion rate is the largest in the normal incidence case. The table given in chapter 7 indicates the amount of distortion for each roughness level in the grazing angle case and for other cases as well.

The Ament's formula and the Boithias' formula are both not very accurate for the grazing angle incidence case and the scattered field pattern is not very much affected by the surface roughness for the grazing angle incidence case. The case of grazing angle incidence can be seperately investigated in detail in the future.

As a measure of distortion in the scattered field pattern we have used the correlation coefficient of a rough surface scattered field pattern with a flat surface scattered field pattern. For different surface roughness values, we have checked the correlation coefficient value and we have concluded that above a correlation coefficient value of 0.7 the pattern is not seriously distorted. But a correlation coefficient value below 0.45 indicates a serious distortion in the scattered field pattern. If the correlation coefficient value is above 0.5, then the major lobe of the scattered field pattern and the angle of incidence is usually detectable. If the correlation coefficient value is below 0.35, then the major lobe of the scattered field pattern and the angle of incidence is usually not detectable. Measuring the correlation coefficient of rough and flat surface scattered field patterns is a useful and accurate method for checking pattern distortion. But some other methods may also be used to measure far field pattern distortion.

REFERENCES

[1] Constantine A.Balanis, Advanced Engineering Electromagnetics,1989 edition, by John Wiley & Sons, pages 2-120.

[2] Jean Pierre Berenger, A Perfectly Matched Layer For The Absorption Of Electromagnetic Waves, Journal Of Computational Physics 114 (1994), pages 185-200.

[**3**] http://www.mathworks.com/help/pde/index.html , MATLAB Partial Differential Equation (PDE) Toolbox, last accessed date: 21 December 2012.

[**4**] http://en.wikipedia.org/wiki/Normal_distribution , last accessed date 14 December 2012.

[**5**] Matthew N.O.Sadiku, Numerical Techniques In Electromagnetics With MATLAB, Third Edition, pages 235-245 and 379-435.

[**6**] Ozlem Ozgun, Mustafa Kuzuoglu, Near-field performance analysis of locally-conformal perfectly matched absorbers via Monte Carlo simulations, Journal of Computational Physics, vol. 227, no. 2, pp. 1225-1245, 2007.

[**7**] Shree K.Nayar, Katsushi Ikeuchi, Takeo Kanade, Surface Reflection: Physical and Geometrical Perspectives, IEEE Transactions on pattern analysis and machine intelligence, vol. 13, no. 7, July 1991.

[**8**] J. N.Reddy, An Introduction To The Finite Element Method, Mc Graw –Hill International Editions, Mathematics and Statistics Series (1984) , pages 194-220.

[**9**] Jin Au Kong, Electromagnetic Wave Theory (1986) , Chapters 1-2.

[10] Kevin Krause, Application Of The Finite Element Method To Random Rough Surface Scattering With Neumann Boundary Conditions, MSc. Thesis, University Of Washington, pages 1-13.

[**11**] Simon N. Chandler-Wilde, Peter Monk, The PML For Rough Surface Scattering, ScienceDirect Applied Numerical Mathematics, Applied Numerical Mathematics 59 (2009) 2131-2154, www.elsevier.com/locate/apnum

[**12**] N.C Bruce, J.C Danity, Multiple scattering from random rough surfaces using the Kirchoff approximation, Journal of modern optics, 1991, vol. 38, no. 3, pp. 579-590 .

[**13**] Ozlem Ozgun, Mustafa Kuzuoglu, Monte Carlo –Based Characteristic Basis Finite-Element Method for Numerical Analysis of Scattering From Objects On/Above Rough Sea Surfaces, IEEE Transactions on GeoScience and Remote Sensing, vol. 50, no. 3, pp. 769-783, 2012.